INVESTIGATION OF THE DETERMINANTS OF THERMAL STABILITY OF THE NITRILE HYDRATASE FROM *Geobacillus pallidus* RAPc8

By:

John Maina Kianja

A dissertation submitted in fulfilment of the requirements for the degree of Master of Science in Medical Biochemistry in the Department of Integrative and Biomedical Sciences

UNIVERSITY OF CAPE TOWN

September 2016.

Supervisor: Prof. B. T. Sewell

Abstract

The mechanisms of thermal stability have been a long studied subject for many years with the aim of enhancing thermal stability of protein molecules to enhance their application in industry. The nitrile hydratases group of enzymes catalyse the hydrolysis of nitriles to amides using an exothermic catalytic mechanism. Understanding and applying specific amino acid residue mutations at specific regions in protein structures has been important for engineering of thermal stability into these often tetrameric thermolabile nitrile hydratases currently used in industry globally. At the near atomic level, the interatomic interaction(s) between specific amino acid residues governs the structure and function of nitrile hydratases. This study investigated several possible interactions responsible for conferring thermal stability to several thermostability-enhanced nitrile hydratase composite mutants generated from the wild type *Geobacillus pallidus* RAPc8 nitrile hydratase (NHase), namely: L103S+Y127N+F36L+D4G, M43K+T150A+S169R and D96E+D167V+M188V each labelled as 9E, 9C and 8C respectively. The composite mutants were previously developed using error-prone PCR of the wild type nitrile hydratase genes coding for the alpha and beta subunits from *Geobacillus pallidus* RAPc8. These composite mutants presented an opportunity to understand intramolecular thermostabilising mechanisms in this nitrile hydratase. Each individual mutation found in the composite mutants, was separately introduced into the DNA coding for the *Geobacillus pallidus* RAPc8 NHase by site directed mutagenesis. These individual mutants were over-expressed from *E. coli* and purified for further study. Using activity assays and protein melting curves, their individual thermal stability contributions were determined and represented as the difference in free energy of thermal unfolding (change in Gibbs free energy) of the single and composite mutants relative to the wild type nitrile hydratase. The measured residual activity following thermal inactivation was used together with the Arrhenius equation and a three parameter non-linear fit to determine the free energy of thermal unfolding. The change in Gibbs free energy resulting from each thermostabilising mechanism coupled to the analysis of their crystal structures was used to suggest the contributing mechanisms.

This study found that intersubunit interactions through hydrogen bonds and salt bridges are especially important for contributing towards thermal stability of tetrameric nitrile hydratases. Hydrophobic interaction through the formation of a water shell around hydrophobic side-chains and packing of hydrophobic side-chains was also observed to contribute to thermal stability. These results suggest a path towards rational design and

engineering of thermostabilising mutations into nitrile hydratases. Increased thermostability would improve their large scale application in industry by allowing these enzymes to be more active for longer at higher temperatures and decrease the cost of amide production.

Acknowledgements

I would like to thank God and my family for the motivation, the drive, social, psychological and financial support in conducting this study.

I would also like to thank my supervisor, laboratory staff and student members of the Structural Biology Research Unit (SBRU) and Centre for Imaging and Analysis (CIA) at the University of Cape Town for the continued sharing of advice and ideas that have been instrumental in completion of this work.

I would also like to thank the coffee farmers for the continued supply of copious quantities of stimulants consumed during the study.

I acknowledge the partial financial assistance of the NRF via the grant holder linked bursary granted towards me for this study.

Thank you all.

Keywords and Phrases

Amide

Catalysis

Cation-π

Crystal Structure

Geobacillus pallidus RAPc8

Hydrogen bond

Hydrophilic interaction

Hydrophobic interaction

Intrasubunit

Intermediate State

Intersubunit

Nitrile

Ping pong bi bi mechanism

Salt bridge

Thermal stability

Thermolabile

Declaration

I declare that the thesis titled "**INVESTIGATION OF THE DETERMINANTS OF THERMAL STABILITY OF THE NITRILE HYDRATASE FROM *Geobacillus pallidus* RAPc8"** is my own work and has not been submitted for any degree or examination in any other higher educational institution and all sources used and/or quoted in this thesis have been indicated and acknowledged by complete references.

John Maina Kianja

Signed by candidate

Signature Removed

Signed: … …. 6th September 2016.

List of Abbreviations

°C	degrees Celsius
B. smithii	*Bacillus smithii*
C. testosteroni	*Comamonas testosteroni*
CFE	cell free extract
CIA	Centre for Imaging and Analysis
DNA	Deoxyribonucleic acid
DTT	dithiothreitol
EC	Enzyme Classification
F-T	flow through
G	Gibbs free energy
G. pallidus	*Geobacillus pallidus*
HIC	hydrophobic interaction chromatography
HPLC	high performance liquid chromatography
IEX	ion exchange chromatography
IPTG	isopropyl thiogalactopyranoside
K	Kelvin
kDa	kilo Dalton
MCC	Mitsubishi Chemical Corporation
NHase	nitrile hydratase
NIH	National Institutes of Health
OD	optical density
OXD	Aldoxime dehydratase
P. thermophila	*Pseudonocardia thermophile*
P. putida	*Pseudomonas putida*
P. chlororaphis	*Pseudomonas chlororaphis*
P. aeruginosa	*Pseudomonas aeruginosa*
PDB	protein data bank
QHP	anion exchange chromatography
R. rhodochrous	*Rhodococcus rhodochrous*
R. erythropolis	*Rhodococcus erythropolis*
RBI	Reed Business Information
RFU	relative fluorescence units

S200	Sephadex 200
SBRU	Structural Biology Research Unit
SDM	site directed mutagenesis
SDM-PCR	site directed mutagenesis polymerase chain reaction
SDS-PAGE	sodium dodecyl sulphate polyacrylamide gel electrophoresis
SEC	size exclusion chromatography
T_m	melting temperature
TRIS	tris(hydroxymethyl)aminomethane
UCT	University of Cape Town
WT	Wild-type

Table of Contents

List of Figures, Tables and Equations

CHAPTER 1:

NITRILE AND AMIDE CATALYSING ENZYMES

Introduction

Enzymes that show activity on nitriles have been studied for more than three decades. The nitrile hydratases (E.C. 4.2.1.84) convert nitriles to amides and were first isolated from *Arthrobacter* sp. J-1 using acetonitrile as a substrate (Asano *et al*., 1980) and then in the nitrile utilising *Pseudomonas chlororaphis* B23 assayed using isobutyronitrile, acrylonitrile and acetonitrile as substrates (Asano *et al.,* 1982b). Additional nitrile hydratases (NHases) have been described such as the NHase from the actinomycete *Brevibacterium sp.* R312 which showed catalysis of the hydration of propionitrile to propionamide (Nagasawa *et al*., 1986; Nishiyama *et al*., 1991), the NHase from *R. rhodochrous* J1 which catalysed hydrolysis of both aliphatic and aromatic nitriles (Nagasawa *et al*., 1990), and the NHase from *Geobacillus pallidus* RAPc8 which preferentially catalysed hydrolysis of acetonitrile and valeronitrile compared to other aliphatic nitriles and the aromatic nitrile *cis,trans* cyclopenteneacetonitrile (Pereira *et al*., 1998).

NHases are important for the biocatalytic industrial production of amides such as acrylamide or nicotinamide, in kilo-ton quantities. The organisms such as *R. rhodochrous* J1 (Kobayashi *et al*., 1990; Nagasawa *et al*., 1990; Kobayashi *et al*., 1993), and *Geobacillus pallidus* RAPc8 (Cowan *et al*., 2003; Makhongela *et al*., 2007; Williamson *et al*., 2010) have been shown to exhibit nitrile hydratase, amidase and nitrilase expression within the same organism. In addition, chaperones are required for synthesis of active properly folded forms of NHase (Nojiri *et al*., 2000; Cameron *et al*., 2005, Zhou *et al*., 2008). Our main focus in this project is the nitrile hydratases and factors that influence their thermal stability. These studies were, in part, facilitated by the use of the *G. pallidus* RAPc8 amidase in the study.

Literature Review

Nitrile Hydratases

Nitrile Hydratases are multimeric enzymes found in a wide range of prokaryotes and archaea (Asano *et al*., 1980; Nagasawa *et al*., 1990; Kobayashi *et al*., 1993); Yamada and

Kobayashi, 1996) and in eukaryotes (Konrad *et al*., 2008; Maron *et al*., 2012). Expression of NHases and nitrilase superfamily enzymes enables their source organisms to utilize nitriles as their sole carbon and/or nitrogen source (Asano *et al*., 1982b; Kobayashi *et al*., 1991). The preferred substrates (*fig*. 1.1) vary across the different NHases from different species with NHases from organisms such as *R. rhodochrous* J1 (Nagasawa *et al*., 1990) preferentially acting on aliphatic nitriles such as acrylonitrile, propionitrile and acetronitrile while other NHases from *R. erythropolis* JCM 2892 preferentially acting on cyclopropylcyanide, *R. erythropolis* N-774 preferentially catalysing the hydration of chloroacetonitrile to its corresponding amide, chloroacetamide (Duran *et al*., 1993) and *G. pallidus* RAPc8 NHase preferentially catalysing the hydration of valeronitrile rather than aromatic nitriles such as benzonitrile and benzylcyanide (Pereira *et al*., 1998). Though different catalytic properties have been observed with different NHases, the key distinguishing factor of NHases from other proteins in the nitrilase superfamily is the conversion of nitriles to amides without the formation of the corresponding carboxylic acid.

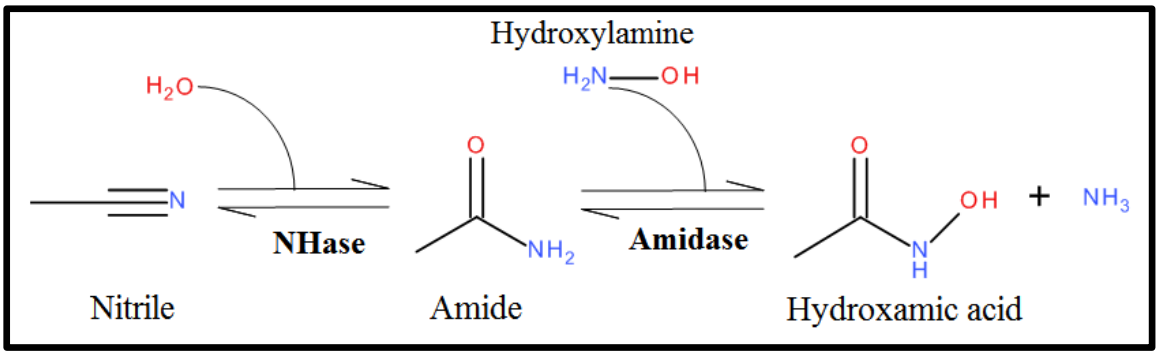

Figure 1.1: The conversion of nitriles to amides catalysed by NHase (Asano *et al*., 1980; Asano *et al*., 1982a; Kobayashi *et al*., 1993; Kato and Asano, 2006). Water is used in the hydrolysis to form the corresponding amide followed by conversion to hydroxamic acid by an amidase via an acyl transfer process. The acyl donor is the amide while the acyl acceptor is hydroxylamine. Ammonia is also released during the amidase catalysis. The image was prepared using Accelrys Draw (BIOVIA, Dassault Systemes).

Importance of NHase and Amides in Industry

Amides are produced using NHases in various industrial settings (Nagasawa and Yamada, 1990). Acrylamide (Asano *et al*., 1982b) is used in its polymerized form, polyacrylamide, as a flocculant in the preliminary steps of water purification (Kurenkov *et al*., 2002) and as polyacrylamide in separation of macromolecules using techniques such as SDS-PAGE (Laemli, 1970). Nicotinamide is produced from nicotinonitrile (3-cyanopyridine), as suggested by Nagasawa *et al*., (1988) and reported by Ghisalba *et al*., (2010), and is then used in nutritional supplements (Lin *et al*., 2004). The NHase from *P. chlororaphis* B23 is used in the production of 5-cyanovaleramide which is in turn used as an intermediate step in production of triazole plant fungicides. This is achieved by using adiponitrile as a substrate for the *P. chlororaphis* B23 NHase (Hann *et al*., 1999).

Global production of amides is at least several hundred thousand tons annually. The company SNF Floerger currently produces over 700,000 tons of acrylamide up from 143,000 tons in 2005 with the major targets of supply being the water and paper industry (SNF Floerger, 2013). Other companies involved in acrylamide production include Kemira Water Solutions with an annual production capacity of about 40,000 tons (RBI ICIS, 2005), the Japanese Mitsubishi Chemical Corporation producing 205,000 tons annually by 2001 (MCC, 2001) and Petro China Daqing Refining and Chemical company producing 170,000 tons per annum amongst 40 other acrylamide producing companies in China (China Jilin, 2013). Senmin South Africa currently produces 20,000 tons of acrylamide (Senmin, 2016). One of the major applications of acrylamide, in its polymerized form, is in water as a flocculant for large scale purification of water. This is due to its adsorption onto the surface of particulate matter suspended in water and its subsequent polymerization into polyacrylamide forming interlinks between the suspended materials. This facilitates coagulation of particulate material in water. It is used in water treatment at municipality level but also in large scale mines for removal of metal ions such as: gold, zinc, silver, uranium and copper, from water.

Other applications of NHase catalysis are in environmental bioremediation. This involves the application of whole cells expressing NHase to catalyse conversion of polluting nitriles in the environment into amides. This can then be coupled with amidase catalysis via whole cells expressing amidase, to convert the amides into their corresponding and less harmful carboxylic acids. Biodegradation of nitriles using multiple microorganisms obtained via culture enrichment has been suggested by Li *et al*., (2007) using aliphatic and aromatic nitriles. The biodegradation of nitriles has also been demonstrated in small scale by Vesela *et al*., (2012) using *R. rhodochrous* PA34 and *R. erythropolis* A4 converting benzonitrile

herbicides into carboxylic acids and amides. These studies suggest the application of microorganisms expressing nitrile catalysing enzymes, especially NHase and in some cases amidase, for bioremediation.

Limitations Associated With NHase Catalysis of Nitriles

Conversion of nitriles using enzymatic methods has several advantages over chemical methods. These are increased production, reduced wastage of raw materials and reduced energy costs. Furthermore, the purity of the product is improved due to reduced contamination hence less purification steps are required for the final amide product.

The NHase group of enzymes consists of both thermolabile and relatively thermostable enzymes. This has been shown via the determination of temperature optima for catalysis on NHases from different organisms such as the relatively thermolabile NHases from: *Rhodococcus sp.* N771 at 303 K (Yamada and Kobayashi, 1996); *P. chlororaphis* B23 at 293 K (Nagasawa *et al*., 1987) and *Brevibacterium sp.* R312 at 298 K amongst others. Other NHases exhibit higher temperature optima such as the NHases from: *P. thermophila* JCM 3095 at 333 K (Yamaki *et al*., 1997) and the NHase from *G. pallidus* RAPc8 at 333 K (Pereira *et al*., 1998).

The drawback with enzymatic hydrolysis of nitriles to amides is that the catalysis is an exothermic process (Yamada and Kobayashi, 1990). This would imply that for efficient catalysis, the reaction chamber needs to be cooled and this translates to higher energy needs due to cooling systems and lower catalytic efficiency due to irreversible thermal denaturation leading to inactivation of NHase if the reaction temperature is too high. Ultimately, thermal denaturation results in decreased yield due to a lower concentration of the active enzyme in the reaction chamber. Despite the high efficiency of enzymatic nitrile catalysis relative to chemical catalysis, once the temperature of the catalysis exceeds the optimum level, irreversible unfolding of the enzyme begins to occur. In this study, the goal is to investigate the structural mechanisms responsible for tolerance to thermal denaturation.

Production of amides is a crucial process whose products are components of many industries. The methods employed in amide production follow one of two paths: chemical methods or enzymatic methods. Presently, the NHase from *R. rhodochrous* J1 is used for the enzymatic industrial production of acrylamide but with difficulty due to the thermolability of NHase (Nagasawa and Yamada, 1990; Yamada and Kobayashi, 1996; Hann *et al*., 1999). Several studies have been made on NHases from organisms such as *R. erythropolis*,

Thiobacillus thioparus, *P. thermophila*, *R. rhodochrous* J1, *G. pallidus*-RAPc8, *B. smithii* and *P. putida* with regard to their enzymatic properties such as enantioselectivity (Fallon *et al*., 1997; Bauer *et al*., 1997); regio-specificity (Gavagan *et al*., 1999; Petrillo *et al*., 2005); chemo-specificity (Black *et al*., 2010) and substrate specificity (Nagasawa *et al*., 1990; Wieser *et al*., 1998) however, few studies have included the investigation of thermal stability determinants which have a major impact on the function and application of the enzyme. Several crystal structures from different NHases have been solved, however; even fewer studies have delved into the structural mechanisms responsible for thermal stability in NHases. Insight on these mechanisms would allow for rationalisation of thermal stability in NHases and also hint at mechanisms that would influence thermal stability of similar proteins.

Structure and Chaperones of NHases

Nitrile hydratases (NHases) can be divided into two groups: Fe type NHases which contain a non-heme Fe^{3+} ion coordinated at the catalytic centre with a claw-setting motif consisting of the residues: **CSLCSCT** (Huang *et al*., 1997; Endo *et al*., 2001) and Co type NHases which contain a non-corrin Co^{3+} ion coordinated at the catalytic centre with a claw setting motif consisting of the amino acid residues: **CTLCSCY** (Miyanaga *et al*., 2001; Hourai *et al*., 2003; Cameron *et al*., 2005). For each type of NHase, a single coordinated metal ion is found per α-β heterodimer (*fig* 1.2). The presence of Fe at the catalytic centre confers a unique ability to Fe type NHases that has not been observed with Co type NHases: light modulated catalysis. This phenomenon has been reported with Fe type NHases in which a nitric oxide molecule was bound to the low spin Fe centre of the NHase from *R. erythropolis* N-771 (Endo *et al*., 1999) which was later observed in the crystal structure of the same organism by Hashimoto *et al*., (2008). The coordinated nitric oxide molecule was dissociated upon irradiation by light which restored activity to the Fe NHase.

The active NHase comprises a higher order multimer of an α-β dimer with a coordinated metal ion at the catalytic centre of each α subunit (*fig.* 1.2). This has been determined for NHases such as: the NHase from *Arthrobacter sp.* J-1 which has 8 α and 8 β subunits with a total molecular mass of approximately 420 kDa (Asano *et al*., 1982a); and the higher molecular weight *R. rhodochrous* J1 NHase which as 10 α and 10 β subunits with a combined total molecular mass of approximately 530 kDa (Kobayashi *et al*., 1991); however the majority of NHases consist of a tetramer comprising of 2 α and 2 β subunits (Huang *et*

al., 1997; Pereira *et al*., 1998; Miyanaga *et al*., 2001; Hashimoto *et al*., 2008). This includes the NHase from *G. pallidus* RAPc8 whose active form consists of an α-β heterotetramer. In this NHase, the active tetramer contains a total of 8 alpha helices and 4 beta strands with the latter organised into 2 beta sheets constituting the α subunit while 9 alpha helices and 6 beta strands constitute the β subunit. The active site of the *G. pallidus* RAPc8 NHase bears a "claw setting" motif consisting of 7 residues along a loop in the enzyme core with the residues **CTLCSCY** numbered from 116 to 122 and is located along a loop as revealed in the crystal structure with PDB code 3HHT (van Wyk, 2008). These residues situated at the catalytic site are organised into a claw setting motif (*fig* 1.2.) in the NHase from *G. pallidus* RAPc8. Other NHases show the same motif such as the Fe NHase from *Rhodococcus sp.* R312 (Huang *et al*., 1997), the NHase from *R. erythropolis* AJ270 (Song *et al*., 2007) and the Co type NHases such as the NHases from *Pseudonocardia thermophila* JCM 3095 (Miyanaga *et al*., 2001), the Co NHase from *Bacillus smithii* (Hourai *et al*., 2003).

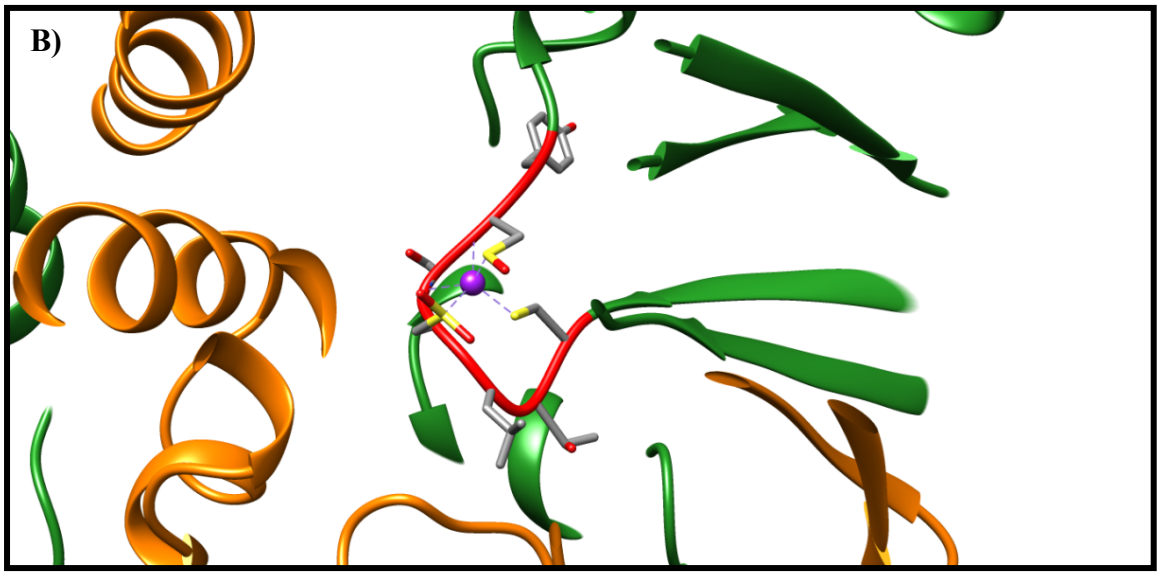

Figure 1.2: A) Ribbon diagram depicting the crystal structure of the WT Co-NHase from *Geobacillus pallidus* RAPc8 (Tsekoa, 2005). The α subunit is coloured in green while the β subunit is coloured in orange. B) An enlarged image of the active site of the WT NHase showing the oxidised Cys and coordinated Co ion (coloured purple). The active site is depicted with a red coloured backbone with the active site residue side chains (CTLCSCY) shown in stick representation. The active site lies between both subunits. The Cys side-chains are coordinated to the Co ion.

NHases that contain Fe or Co at the active site use different chaperones for insertion of the metal centre into the active site after expression of the subunits. Prior to metal insertion, post-translational modification at the active site of two Cys amino acid residues to Cys-sulfenic and Cys-sulfinic acid occur. This allows for the claw setting motif to be set before coordination of the metal centre. For the metal insertion, the Fe type NHases utilise a 47 kDa chaperone (P47K) as suggested by Nojiri *et al*., (1999), while the Co type NHases utilise a 14 kDa chaperone (P14K) as suggested by Wu *et al*., (1997). Interchangeability of the metal ion between Fe NHase and Co type NHase has only been shown with the Fe NHase from *R. erythropolis* N-771 where a Co ion was inserted in the active site of the Fe NHase (Nojiri *et al*., 2000) without the chaperone, resulting in slight but measurable activity. Another exception to the use of the P47K chaperone for metal insertion is the Fe type NHase from *Comamonas testosteroni* Ni1 which does not require a chaperone for insertion of Fe to its active site and its subsequent functional expression (Kuhn *et al*., 2012). This was attributed to the difference in side-chains for residues 76 to 83 of the α subunit of *C. testosteroni* Ni1

NHase allowing for a larger cavity around the active site pocket compared to the α subunit of other Fe type NHases (e.g. *R. erythropolis* N-771) as visualized by comparing the respective crystal structures with PDB codes 4FM4 (Kuhn *et al*., 2012) and 2ZPB (Hashimoto *et al*., 2008). The expression of the Co type NHase chaperone, P14K, has been shown to be important for assembly of the active Co type NHase holoenzyme via introduction of the metal ion to the apoenzyme, when the metal ions are present in the growth medium (Nojiri *et al*., 2000). Further studies by Zhou *et al*., (2008) showed that after the non-post-translationally modified α and β subunits are expressed, the non-modified α subunit is substituted with a modified α subunit. Further details in the same study showed the modified α subunit is organised as a trimer consisting of one α subunit and two P14K chaperone subunits) which after the swap result in release of the two chaperones and the non-modified α subunit and ultimately assembling the active holoenzyme. In the same study, the Co ion in the active site and the post-translationally modified Cys residues in the active site were also shown to be important for maintaining the active form of the tetramer.

The post-translationally modified Cys residues, Cys sulfenic and Cys sulfinic side-chains, are required in their specific oxidised states for NHase activity as shown using the Fe NHase by Murakami *et al*., (2000) and Odaka *et al*., (2001), and later as will be seen in the catalytic mechanism. Thus, for the expression of active NHase, not just the genes for the α and β subunit are required but also the respective chaperones (P47K or P14K) and respective metal ions are required for assembly and maturation of active NHase.

The genes responsible for expression for NHase in their source organisms are found in a gene cluster composed of: NHase regulator 1, NHase regulator 2, NHase α subunit, NHase β subunit, amidase and acyl-CoA synthetase. Some organisms, such as *R. erythropolis* N-771, have an associated aldoxime dehydratase gene (Oxd) within the gene cluster (Kato *et al*., 2000; Kato *et al*., 2004). The Oxd gene has also been shown to exist together with NHase in *Pseudomonas* sp. K-9. The two NHase regulator genes function to regulate active NHase expression and catalysis (Kato *et al*., 2004; Cameron *et al*., 2005; Hashimoto *et al*., 2005).

Proposed Catalytic Mechanisms of NHase

The conversion of nitriles to amides by NHase (*fig.* 1.1) has been proposed to occur by different mechanisms through a cascade of steps involving multiple active site residues. One of the mechanisms is based on time-resolved structure solution of the Fe-NHase crystal structure at different stages of catalysis (Hashimoto *et al*., 2008). An alternative approach to

elucidation of the catalytic mechanism involved a theoretical approach using density functional theory methods (Hopmann, 2014). Both catalytic mechanisms, one supported by density functional theory methods (Hopmann, 2014) and the other by time-resolved crystallography (Hashimoto *et al*., 2008), involve the movement of a nitrile into the catalytic centre above the sixth coordination site of the metal ion, (*fig.* 1.3).

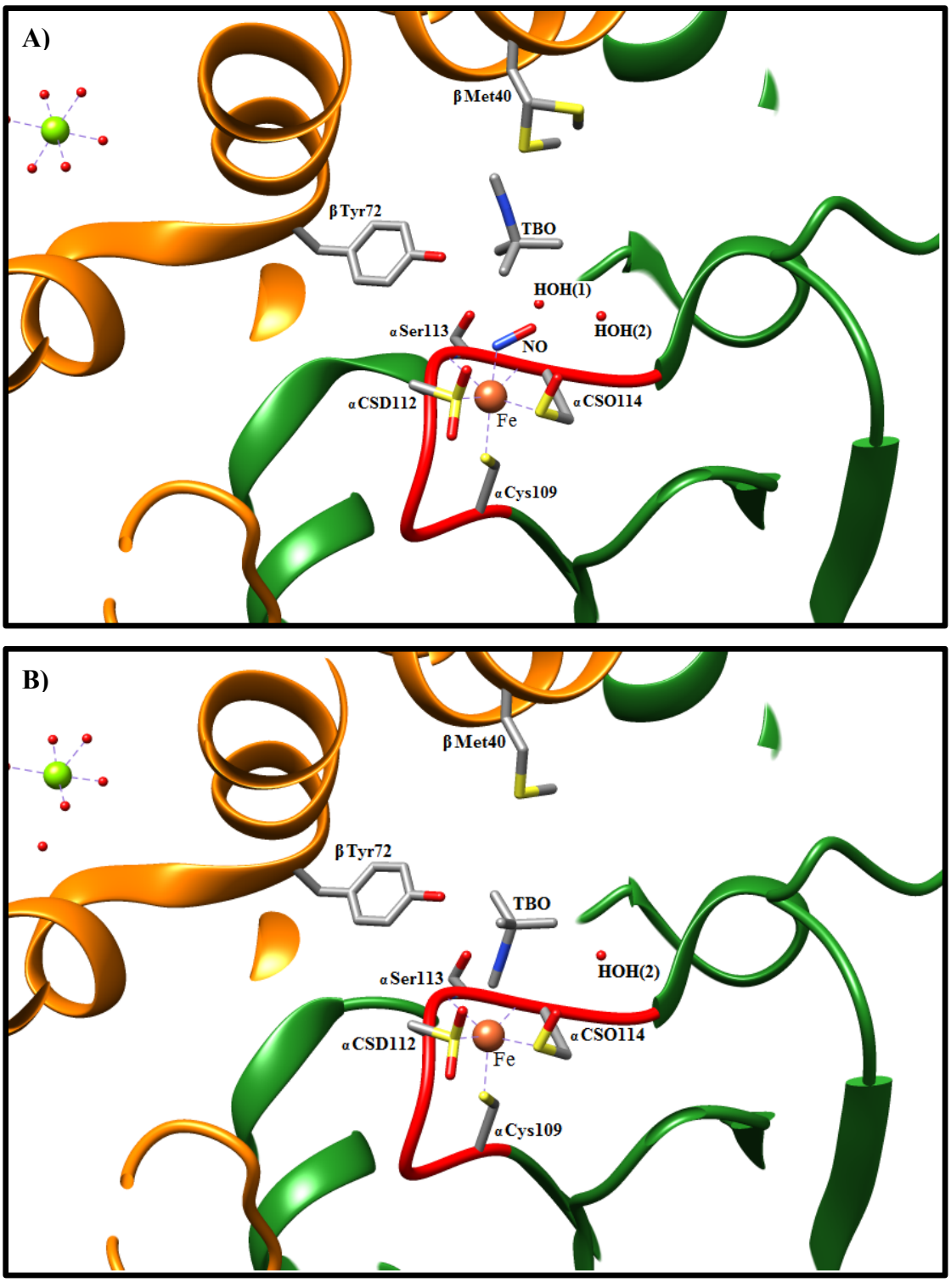

Figure 1.3: A) The initial steps in nitrile hydrolysis by NHase. A nitric oxide molecule (NO) is coordinated to the Fe centre (coloured brown) prior to substrate coordination. The substrate, tert-butylisonitrile labelled as TBO, is above the active site and the side chain of βMet40 is shown in both conformations that allowed the substrate access to the active site. B) The substrate is shown with its orientation reversed relative to its position in image A) shows the importance of the C≡N group of the nitrile coordinating to the metal centre before catalysis. Water molecules are present in the active sites of both images, Hashimoto *et al*., (2008) PDB accession codes: 2ZPF and 2ZPG.

The metal ion and the amino acid residues constituting the claw setting motif (that coordinates the metal ion) have been shown to be important for activity of both Co type and Fe type NHases (Murakami *et al.,* 2000; Nojiri *et al*., 2000; Miyanaga *et al.,* 2004). The crystal structure of *R. erythopolis* with tert-butylisonitrile by Hashimoto *et al*., (2008), suggests that the path the substrate takes on its way to the catalytic site is partially obstructed by the side chain of βMet40 in different conformations (*fig*. 1.3). The level of structural conservation of this residue in NHases from other organisms, as revealed by the superposition of the crystal structures of *Rhodococcus sp.* R312 with PDB code 1AHJ (Huang *et al*., 1997), *P. thermophila* with PDB code 1UGP (Miyanaga *et al*., 2004), *Pseudomonas putida* with PDB code 3QYH (Brodkin *et al*., 2011) and the WT NHase from *G. pallidus* RAPc8 with PDB code 2DPP (Tsekoa, 2005), is relatively low and the function of the corresponding residues in other NHases is yet to be determined. In addition, in the NHase from *P. thermophila*, a bulkier side chain is present (βPhe37) which would reduce the cross-sectional area of the substrate path. Perhaps the residue in other NHases at the position analogous to the position of βMet40 functions to regulate substrate specificity; however this has not been experimentally determined.

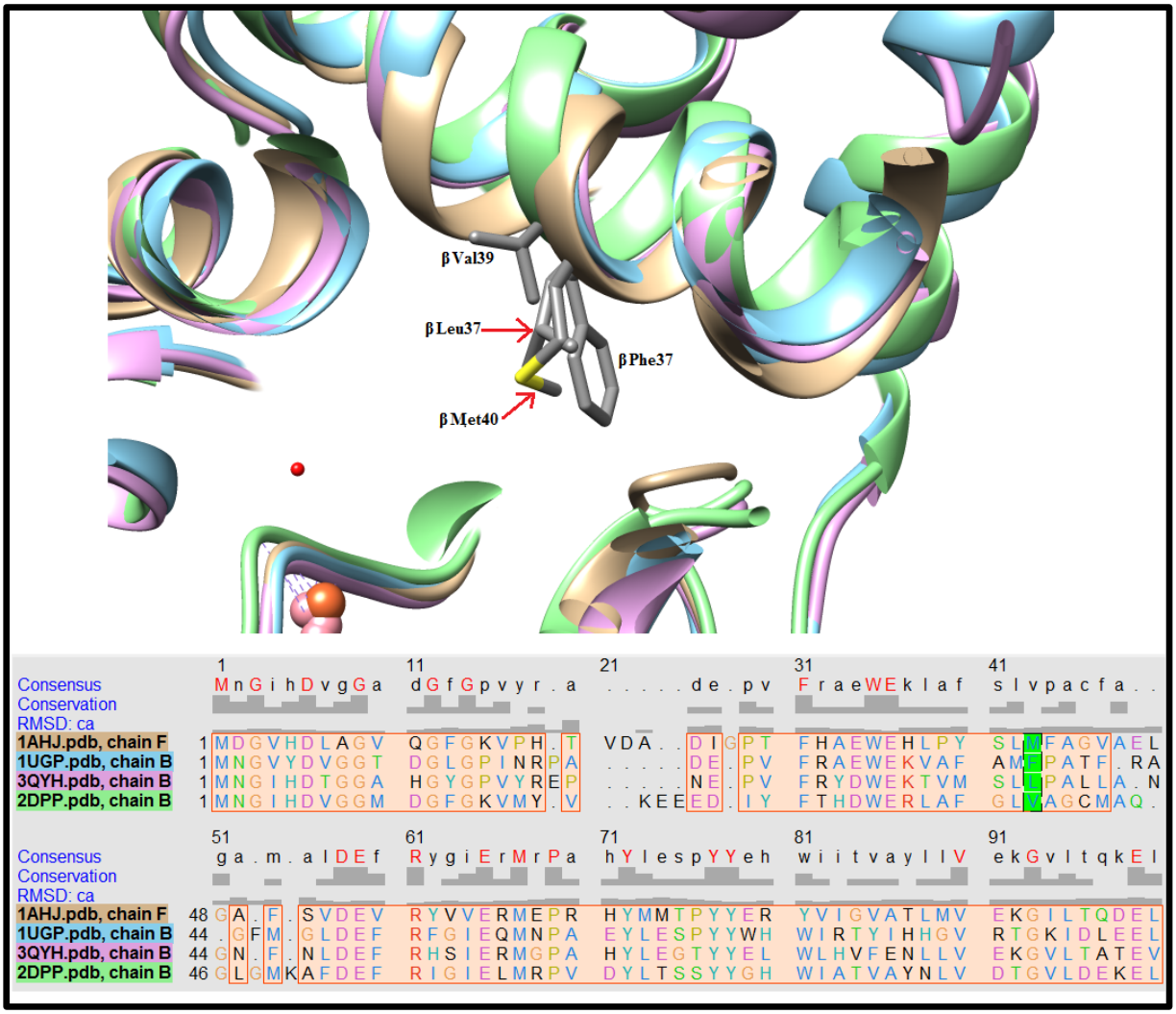

Figure 1.4: Superposition of crystal structures of NHase samples from *Rhodococcus sp*. R312, *P. thermophila*, *Pseudomonas putida* and *G. pallidus* RAPc8 with PDB codes: 1AHJ, 1UGP, 3QYH and 2DPP with their respective side-chains:βMet40, βVal39, βPhe37 and βLeu37 (Huang *et al*., 1997; Miyanaga *et al*., 2004; Brodkin *et al*., 2011; Tsekoa, 2005). The overlapping side-chains have been highlighted in green in the multiple sequence alignment below the superposition of the side-chains.

During catalysis in the *R. erythropolis* NHase, the side chain of βMet40 takes on a new conformation, (*fig*. 1.3 B), to allow the substrate to move to the catalytic site. The nitrile group moves towards the catalytic site, while its cyanide group is pointing away. The side chain of βMet40 reverses its rotation about the Cγ of βMet40 and in the process pushes the cyanide group downwards. As a result the cyanide group of the nitrile is located directly over the 6th coordination site of the metal ion where it displaces the coordinated water molecule, and its side chain fits into the pocket above the cyanide group (*fig* 1.3 B). The presence of a

water molecule at the 6th coordination site has been suggested by both Hashimoto *et al*., (2008) and Hopmann, (2014) using evidence from electron density maps and from theoretical methods. At this point, the differences in the catalytic mechanisms become more pronounced.

Different studies have suggested that it's either the N or the C of the cyanide group that directly coordinates the Fe ion at a distance of about 2.1 Å; however (Hashimoto *et al*., 2008) suggested both may be a possibility. Hopmann, (2014), using theoretical methods, and Martinez *et al.,* (2014) and Yamanaka *et al*., (2015) using crystallography and time-resolved crystallography, suggested that it is the N of the cyanide group that coordinates to the metal ion (*fig.* 1.5 - step 1 and *fig.* 1.6 - step 1). Catalysis was proposed to proceed with the Oδ of Cys114 sulfenic acid side-chain engaging in a nucleophilic attack on the carbon of the cyanide group of the nitrile substrate. On the other hand, Hashimoto *et al*., (2008) suggested that the catalysis proceeds with the O of the Cys114 sulfenic acid side-chain abstracting a proton from an adjacent water molecule, which subsequently engages in a nucleophilic attack on the carbon of the cyanide group. The theoretical approach to the initial nucleophilic attack by the Oδ of Cys114 sulfenic acid side-chain was shown by Hopmann, (2014) to have a lower energy barrier as compared to the alternate mechanism involving the nucleophilic attack by the water molecule. An alternate approach using time-resolved crystallization by Yamanaka *et al.,* (2015) showed the nitrile substrate (pivalonitrile) coordinated to the metal ion at the sixth coordination site through the N atom of the cyanide group. The same coordination site has also been shown by Hashimoto *et al*., (2008) to possess a nitric oxide (NO) molecule coordinated at a distance of 2 Å and also a water molecule in the absence of NO.

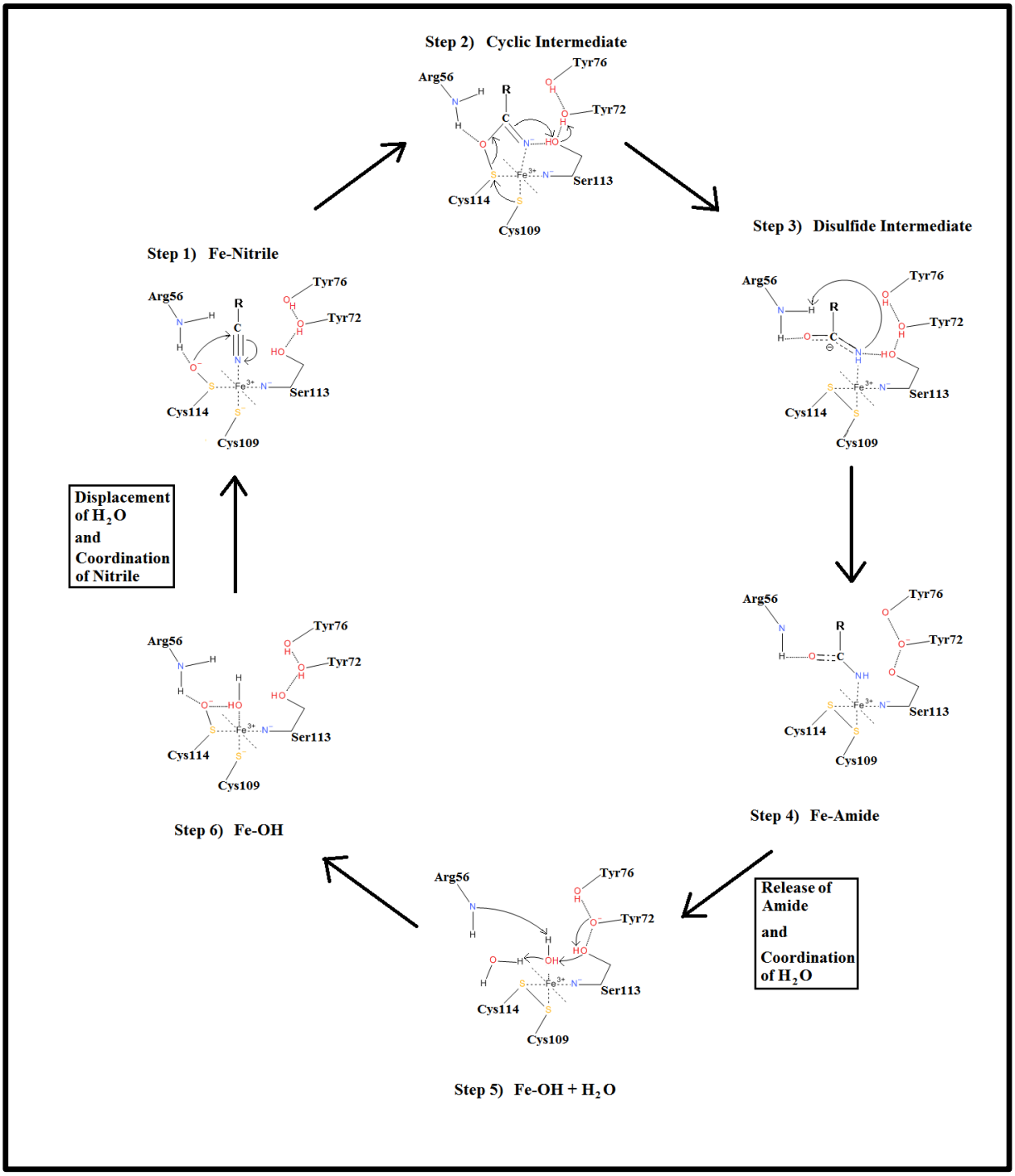

Figure 1.5: The catalytic mechanism of NHase suggested using theoretical methods. The six steps show the nitrile being bound, the cyclic intermediate being formed followed by the disulphide intermediate, the release of the amide, regeneration of the active site and coordination of a water molecule to the metal ion in readiness for the next nitrile molecule to bind (Hopmann, 2014). The image was developed using Accelrys Draw (BIOVIA, Dassault Systemes).

The theoretical approach (Hopmann, 2014) suggested that a cyclic intermediate is formed (*fig*. 1.5 - step 2) which consists of the nitrile coordinated above the metal centre being held by hydrogen bonds with the primary amine of Arg56 and by a bond formed with Oδ of Cys114. The importance of Arg56 in hydrogen bonding has been shown by Piersma *et al*., (2000); its mutation to a Tyr and a Glu completely inactivated the NHase from *Rhodococcus* sp. N-771 while mutation to a Lys led to retention of 1% of activity. The cyclic intermediate is also hydrogen bonded to the OH of Ser113 which is also hydrogen bonded to the OH of Tyr72 which is further hydrogen bonded to the OH of Tyr76. The importance of the conserved Tyr72 in maintaining catalysis has been suggested by Miyanaga *et al*., (2004) where mutagenesis of the Tyr to a Phe resulted in impaired activity in both studies. However, the latter study also showed the inessentiality of Ser113 for catalysis by NHase following a Ser113Ala mutation and measurement using methacrylonitrile as a substrate. Thus, there may be a different amino acid residue side chain involved in hydrogen bonding with the cyclic intermediate. The Ser113 amino acid residue is conserved in both Fe and Co NHases as revealed by structure based alignment of their crystal structures. Additional mutagenesis studies by Miyanaga *et al.,* (2004) on the Co NHase on αT109S showed that the Tyr and Ser residues in Fe type and Co type NHases can be interchanged without impairing catalytic activity at this position respectively. This would suggest that the OH of both residues share the same function: participating in hydrogen bonding. In the same study, an αY114T mutant showed impaired activity in addition to decreased Co ion intake into the active site. Perhaps this residue αY114 may be linked to the inclusion of metal ion by the chaperone and maintenance of the hydrogen bond network at the active site.

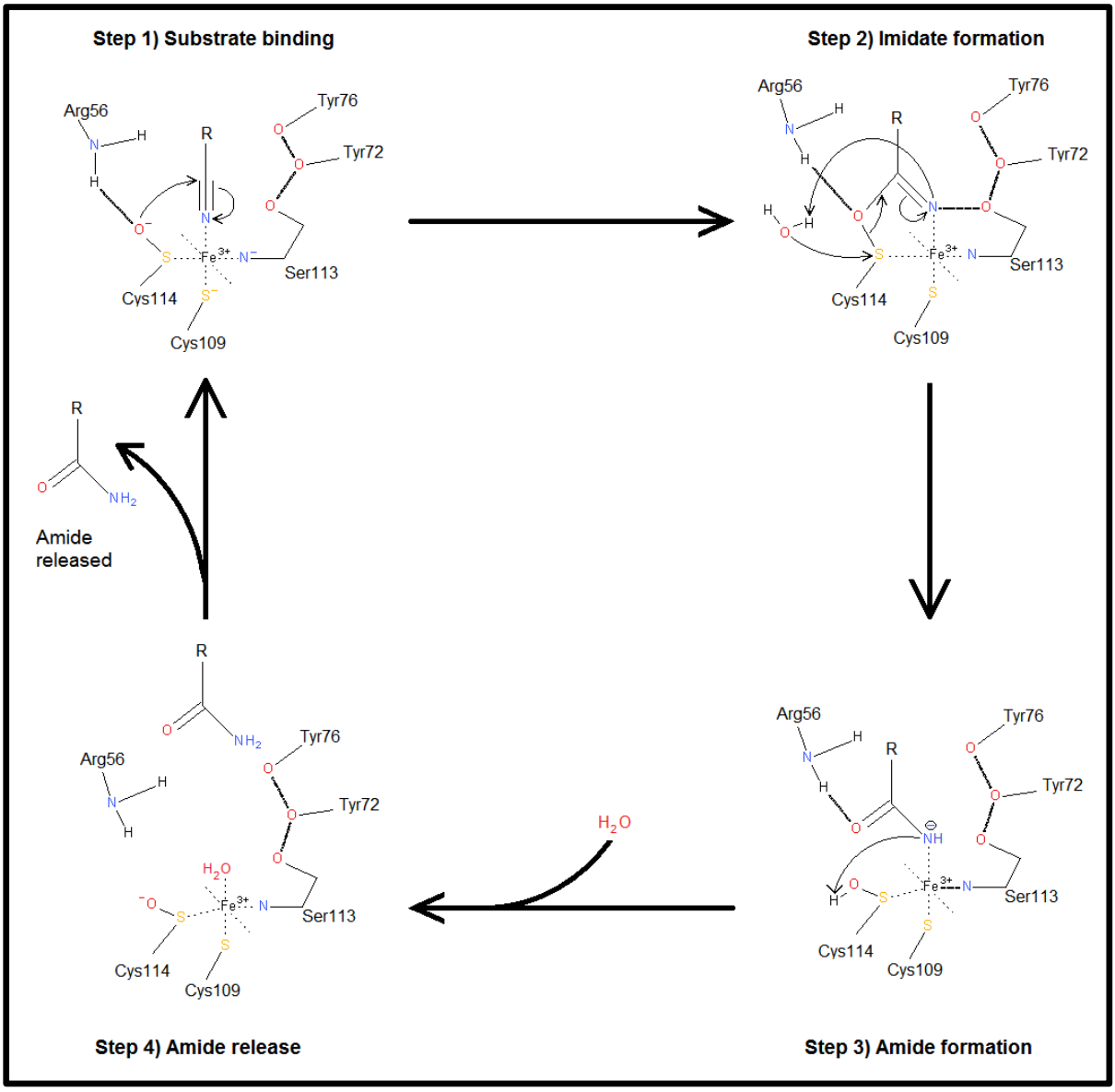

Figure 1.6: The catalytic mechanism of NHase suggested using time-resolved crystallography using the *R. erythropolis* NHase N-771. Following binding of the nitrile, a water molecule is used prior to imidate formation and later on when regenerating the active site for the next nitrile binding. A nucleophilic attack by an activated water molecule completes the formation of amide and regeneration of the Cys114 sulfenic side-chain, (Yamanaka *et al*., 2015). The image was developed using Accelrys Draw (Biovia, Dassault Systemes).

The cyclic intermediate suggested by Hopmann, (2014) is different to that observed by Yamanaka *et al*., (2015) where by the cyclic intermediate consisted of an imidate formed following a nucleophilic attack by the O of the Cys114 sulfenic side-chain thereby linking the

O of the Cys114 sulfenic side-chain and the coordinated substrate (*fig.* 1.6 - step 2). The electron density map at the O of the imidate corresponded to a single O atom and the fitting of the substrate to the electron density map best matched a pivalamide molecule. Hopmann, (2014) by contrast, suggested the formation of a disulphide intermediate (*fig*. 1.5 - step 3) which is formed after Cys109 donates an electron pair to the cyanide carbon then the same Cys109 forms a disulphide bond with Cys114. Part of the disulphide intermediate is also characterized by the N of the cyanide abstracting a proton from the primary amine of Arg56. This results in breaking the hydrogen bond to the hydroxyl of Ser113 resulting in the formation of an amide that is still hydrogen bonded to Arg56 via the carbonyl oxygen of the amide. On the contrary, the disulphide intermediate previously suggested in (*fig.* 1.6 - step 3) has been opposed by Yamanaka *et al.,* (2015) due to the distance between the S atoms of the involved Cys amino acid residues and that the next step would be the release of the amide and regeneration of the active site.

In the same study by Yamanaka *et al.,* (2015), release of the amide and active site regeneration was proposed to occur after a nucleophilic attack by an adjacent activated water molecule onto the S of the Cys114 sulfenic side-chain (*fig.* 1.6 - step 2). This water molecule was shown to replace the O lost by the Cys sulfenic side-chain to the N of the substrate intermediate. The remaining H on the water molecule was abstracted by the N of the substrate intermediate to form an amide. These two events resulted in breaking of the bond of the imidate formed between the sulfenic S and amide O thereby completing the formation of the amide (*fig.* 1.6 - step 3) and leading to the release of the amide (*fig.* 1.6 - step 4). The O from the attacking activated water molecule was also added back to the Cys thiol to regenerate the sulfenic acid side-chain.

The study by Hopmann, (2014) suggested that once the amide is formed, the amide is released (*fig*. 1.5 - step 4) to (*fig*. 1.5 - step 5) and the active site is regenerated in preparation for the next nitrile molecule. Regeneration of the active site requires two water molecules and a cascade of events. The first water molecule moves in place of the amide as it is coordinated at the 6th coordination site of the metal centre and loses a proton to Ser113 (*fig*. 1.5 - step 5). The water molecule then attacks a second water molecule while it loses a proton to Arg56, which now loses the hydrogen-bonded amide. The second water molecule attacks Cys114 thereby breaking the disulphide bond and regenerating the Cys114 sulfenic side-chain. At this point, the first water molecule has obtained the previously lost hydrogen atoms, the Cys114 and Cys109 side-chains are in their reduced state, as required for NHase activity, and the hydrogen bond network between Arg56, the water molecule at the 6th coordination site on the

metal centre, Ser113 and Tyr72 is reformed (*fig*. 1.5 - step 6). The presence of a water molecule at the 6th coordination site has also been shown in the electron density maps with PDB codes: 3HHT (van Wyk, 2008), 1IRE (Miyanaga *et al*., 2001) and a nitric oxide molecule (an inhibitor of Fe-NHase activity) at the same coordination site in the electron density maps depicted in *fig*. 1.3A and *fig*. 1.3B by Hashimoto *et al.,* (2008) and Yamanaka *et al.,* (2015). These cascades of events summed up as sequential and repeated conversion of the nitrile to amide and the regeneration of the active site, facilitate catalysis by NHase.

The rate of catalysis by WT *G. pallidus* RAPc8 NHase at different temperatures has been shown previously (Pereira *et al.,* 1998) to increase as temperature increased until the temperature for catalysis reached the optimum temperature of 333 K. Above this optimum temperature, the rate of catalysis decreased due to thermal unfolding. As shown previously, the active site of the enzyme requires a specific sequence of amino acid residues and their relative spatial arrangement in 3 dimensions, to facilitate the nucleophilic attacks and formation of intermediate states. The interacting groups of the active site side-chains are held in place by hydrogen bonds and coordination interactions involving both the α and β subunits and the metal ion. The potential involvement of ionic interactions in maintaining the active site geometry cannot be ignored due to amine groups such as those of Arg56. In addition, the properly oxidised Cys side-chains (Cys114 sulfenic and Cys109 sulfinic) are also required. Thus the holoenzyme active site geometry and special arrangement must be maintained even at elevated temperatures.

Mutations that would add interactions that enhance the integrity of the structure and maintain the active site geometry would facilitate increases in thermal stability of the enzyme beyond a temperature at which the WT enzyme structure comes apart. This would allow for higher temperatures to be used for catalysis and consequently a higher catalytic rate until the catalytic rate is limited by the rate-limiting step that is independent of temperature. The determination of key elements of this rate limiting step would be a subject of further study to better understand the catalytic mechanism however, at present, enhancement of structural integrity would facilitate the use of higher temperatures for catalysis. Thus the application of thermostabilising mechanisms would be beneficial in ensuring catalysis at elevated temperatures.

Amidases

Amidases (EC 3.5.1.4), are enzymes which catalyse the conversion of amides to their respective carboxylic acids (Brammar and Clarke, 1964; Maestracci *et al*., 1986; Kobayashi, 1993; Fournand and Galzy, 1998). These enzymes, unlike the nitrile hydratases, are classified in the thirteen-member nitrilase super family of enzymes where they occupy 9 out of 13 branches of the nitrilase superfamily (Pace and Brenner, 2001).

Catalysis by amidases can be broad-spectrum or highly specific as evidenced by characterization of catalytic activity of different members in the nitrilase super family (Pace and Brenner, 2001). Amidases (EC 3.1.5.4) from branch 2 of the nitrilase super family, such as the amidases from *R. rhodochrous* J1 (Kobayashi *et al*., 1993), *Rhodococcus sp.* R312 (Fournand *et al*., 1998) and the amidase from *Microbacterium sp.* AJ115 (Doran *et al*., 2004) catalyse conversion of both aromatic and aliphatic amides. The amidase from *Brevibacterium idinium* (Komeda and Asano, 2008) also catalyses the conversion of both aliphatic and aromatic amides such as benzamide, propionamide, butyramide, isobutyramide and cyclohexanecarboxamide. The aliphatic amidases such as the amidase from *G. pallidus* RAPc8 are also classified in the second branch of the nitrilase super family.

Previous studies on the *R. rhodochrous* J1 amidase (Kobayashi *et al*., 1993) showed the capability of acyl transfer using hydroxylamine as a substrate and the quantitation of enzyme activity by measuring the absorbance of the iron-hydroxamic acid complex. This was also shown to occur using the amidase from *Rhodococcus sp.* R312 (Fournand *et al*., 1998) also using hydroxylamine as an acyl acceptor with subsequent measurement of the absorbance of the complex formed between the hydroxamate and $FeCl_3$. Despite the high metal chelating properties of polyamines, viz hydroxylamine HCl, with its associated inactivation of metallo-enzymes such as nitrile hydratase, the above studies also show that amidase retains its activity despite high concentrations of hydroxylamine of around 500mM; perhaps a phenomenon that can be attributed to the lack of a metal centre coordinated within the enzyme as revealed by the crystal structure of the *Geobacillus pallidus* RAPc8 amidase Agarkar *et al*., (2007). Studies on the amidase from *Rhodococcus sp.* 312 (Fournand *et al*., 2001) and on the amidase from *Geobacillus pallidus* RAPc8 amidase by Makhongela *et al*., (2007) have also shown the capability of acyl transfer by amidase and, in addition, the rates of acyl transfer by aromatic and aliphatic amidases using different amides relative to the rate of acyl donation by acetamide. Acyl transfer has been observed in the presence of various

buffer systems by Sharma *et al*., (2012) using the amidase from *Geobacillus pallidus* BTP-5X MTCC 9225.

The crystal structures of other amidases, such as the amidase from *Rhodococcus sp.* N771 (Ohtaki *et al*., 2009), *Pseudmononas aeruginosa* (Andrade *et al*., 2007) and the amidase from *Nesterenkonia sp.* AN1 (Nel *et al*., 2009) and *Geobacillus pallidus* RAPc8 (Kimani *et al.*, 2007) also show the absence of a metal center. In addition, the *P. aeruginosa* crystal structure shows an acyl intermediate and the Nesternkonia *sp.* AN1 crystal structure shows the presence of an amide at the active site. These studies suggest that not only is acyl transfer possible and in different microenvironments facilitated by the different buffer systems, but the amidases studied can utilise hydroxylamine as an acyl acceptor to form the corresponding hydroxamic acid. The organism *Geobacillus pallidus* RAPc8 expressed nitrilase, nitrile hydratase and amidase, and the respective open reading frames encoding these enzymes have been cloned into expression vectors and actively expressed according to Cameron *et al*., (2005) and Williamson *et al*., (2010).

Structure of Amidases

Active amidases are found as dimers, tetramers, octamers and decamers (Komeda and Asano, 2008). Their structures have been determined using X-ray crystallography for the amidase from amidase from *G. pallidus* RAPc8 (Agarkar *et al*., 2007) and *Pseudomonas aeruginosa* (Andrade *et al*., 2007). This has revealed their structure consisting of multiple monomers with each composed of an alpha-beta-beta-alpha fold with a highly conserved catalytic site formed by the residues Glu-Lys-Glu-Cys. These residues and their spatial distribution have been shown to be crucial for amidase activity (Weber *et al*., 2013).

Acyl Transfer Mechanism of aliphatic Amidases

The amidase from *G. pallidus* RAPc8, in addition to catalysis of amides to carboxylic acids, has been shown to have acyl transfer activity from a wide range of amides to hydroxylamine hydrochloride (hydroxylamine HCl) resulting in the formation of the corresponding hydroxamic acid. The hydroxamic acid is then detected following exposure to an acidic iron(iii)chloride solution resulting in formation of a hydroxamic acid-iron(iii)-complex (*fig*. 1.7) (Fournand *et al*., 1998; Kobayashi *et al*., 1993).

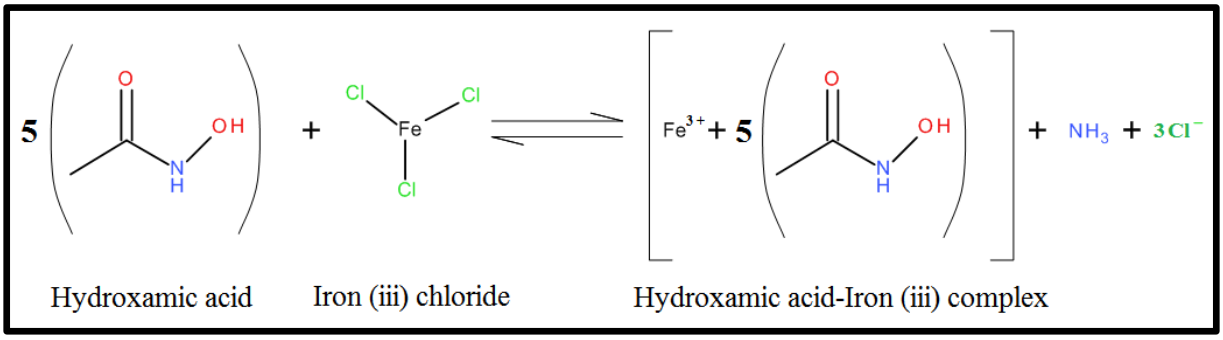

Figure 1.7: The detection of hydroxamic acid using acidic $FeCl_3$ ($FeCl_3$ in 0.1M HCl) which results in formation of a brown coloured hydroxamic acid-Fe complex. It takes 5 parts of hydroxamic acid and one coordinated Fe center to form the complex. The ammonia is a remnant of the previous amidase mediated acyl transfer (*fig.* 1.1) and the Cl ion results from the $FeCl_3$. The absorbance of the brownish coloured complex is then measured at 520nm. The image was done using Accelrys Draw (BIOVIA, Dassault Systemes).

The mechanism involved in the amidase catalysis of amides to their corresponding carboxylic acids is a ping-pong-bi-bi mechanism as suggested by Maestracci *et al*., (1986) and Fournand *et al*., (1998). This mechanism involves an initial binding of the amide to the active site resulting in formation of an acyl donor-enzyme complex. This is then followed by binding of the second substrate, the acyl acceptor (e.g. hydroxylamine), to the acyl donor-enzyme complex. The acyl group is transferred from the amide to the hydroxylamine to form hydroxamic acid which is released from the active site. Farnaud *et* al (1999), Novo *et al.,* (2002), Andrade *et* al (2007) and Weber *et al*., (2013) described further details of the structural mechanism of amidases, with the former three studies showing the importance of the catalytic triad and the fourth study showing the importance of an additional fourth amino acid residue, suggesting that the amidase active site residues consists of the tetrad shown previously. An acyl transfer intermediate has been reported by Andrade *et al* (2007) when using acetamide as an acyl donor and hydroxylamine as an acyl acceptor as visualized in the crystal structure of *P. aeruginosa* with PDB code: 2UXY.

In this study, an acyl transfer assay (hydroxamic acid assay) will be utilised for both the NHase and amidase, from *G. pallidus* RAPc8. The residual activity of WT NHase and various NHase mutants was determined by measuring the acyl transfer mediated by the amidase acting on the amide produced by NHase under saturating conditions of hydroxylamine.

Thermal stability of Proteins

Thermal stability in proteins is the inherent ability of a protein molecule to retain structural integrity and, in applicable cases, retain activity in the event of thermal denaturing conditions characterized by prolonged exposure to elevated denaturing temperatures. This has been observed in different mesophilic, thermophilic, hyperthermophilic and extremophilic organisms whereby the organisms thrive under extremes of heat with their cytosolic macromolecules remaining active as reviewed by Jaenicke *et al*., (1998) and Sadeghi *et al*., (2006) for proteins from both thermophilic and mesophilic organisms). This would imply that these intracellular macromolecules are either intrinsically resistant to thermal unfolding, or have mechanisms that confer resistance to thermal unfolding that are extrinsic to the macromolecules but intrinsic to the organism. An example of the latter is the enhanced stabilisation of RNase A and Lysozyme in the presence of cytosolic osmolytes reported by Santoro *et al*., (1992). These structural intrinsic and extrinsic factors have been employed by organisms in the course of evolution of proteins albeit with some limitations. In the case for thermophilic organisms, intrinsic factors geared towards thermal stability have been facilitated by increases in protein structural rigidity through the use of more structural interactions. However, the limitation associated with increased rigidity is decreased protein flexibility. The balance between protein structural rigidity and flexibility, and the extrinsic factors characterised by the molecular environment around the protein molecule and within its channels, has been key in facilitating the survival of organisms in extreme environments according to Fields, (2001) and Scandurra *et al*., (1998). Thus to understand and apply thermostabilising mechanisms, the intrinsic and extrinsic factors would have to be considered.

Protein structures comprise of tens to hundreds of amino acid residues each with 8 or more covalently attached atoms. This translates to hundreds to thousands of atoms in each protein molecule. The folding of the protein at the ribosome follows the conformation that bears the least steric hindrance with minimum energy in free space (Yonath *et al*., 1983, Ramakrishnan, 2002). The properties of side-chain groups and ligands, their attached hydrophobic or hydrophilic groups and degree of hydrophilicity or hydrophobicity of these groups based on charged groups in the microenvironment has been long thought to be the main contributor to protein structure function. Backbone groups, along the main chain of the protein structure are also involved in hydrogen bonding to side-chain groups. In some cases, the protein will undergo post translational modifications which may include removal of some

residues, addition or removal of functional groups or ions, modification of reduced or oxidised states or enhanced folding by chaperones such as GroEl. As previously described, chaperones are required for posttranslational modifications of NHase: P12K and P14K for the Co-type NHases or P47K for Fe-type NHases (Kim and Oriel, 2000; Murakami *et al*., 2000; Odaka *et al*., 2001; Lu *et al*., 2003; Cameron *et al*., 2005; Zhou *et al*, 2008). These intramolecular interactions and environments determine the properties of the protein molecule, such as, thermal stability (Liu *et al*., 2008), catalysis rate and substrate specificity (Piersma *et al*., 2000; Miyanaga *et al*., 2004; Takarada *et al*., 2006).

Thermal unfolding of proteins is governed by the Gibbs equation for free energy (Atkins and DePaula, 2006), (equation 1). The rate of decrease in activity due to thermal unfolding is determined using the Arrhenius equation (Atkins and DePaula, 2006) (equation 2).

$$\Delta G = \Delta H - T\Delta S$$

Equation 1: The Gibbs free energy equation that describes the relationship between the change in Gibbs free energy (ΔG), the change in enthalpy (ΔH) and the change in entropy (ΔS) at a specific temperature in Kelvin (T) for a thermodynamic system.

$$K = Ae^{-(\frac{E}{RT})}$$

Equation 2: The Arrhenius equation that describes the rate of decrease of a reaction. In our case, the rate is a measured as a decrease in catalysis resulting from thermal unfolding which has its own rate governing the unfolding of the protein molecule from the folded state to unfolded state.

The Gibbs free energy, G, is the energy that is available to do work. This energy is proportional to the sum of the internal energy of the system and work done on the system (enthalpy) minus the product of the change in entropy and temperature in Kelvins, expressed as energy. The work done by the system is negative if the system releases energy and positive if work is done on the system i.e. energy added to the system. Protein structural components that contribute to a change in thermal stability of the whole protein can be thought of as changing the energy of the system. For example, in a case where a thermodynamic system such as a protein molecule in a water bath is heated, the total energy required to break all the interactions maintaining the integrity of the native protein structure is determined by the term

E in equation 2. If a near identical thermodynamic system, such as a protein mutated from the WT form, has an additional bond in its structure, the total energy required for breaking all the interactions in the second thermodynamic system will be the total energy of all the interactions holding the protein molecule in its native folded state including the additional bond. The difference in the two systems will give the energy of the single additional interaction i.e. E_{WT}-E_{mutant}.

The entropy (degrees of freedom) associated with the structural feature at a given temperature results from factors such as protein domain flexibility, number of available binding sites and side-chain conformations, and increasing the number of methylene groups along amino acid side-chains. Increases in entropy lead to a decrease in the intrinsic interaction energy and vice versa (Kumar and Nussinov, 1999). Thus the difference in Gibbs energy required to break a specific interaction within a given protein structure is determined by both the enthalpy of the system and the degrees of freedom of that system at a specific temperature.

Proteins adapted to high temperature environments have structural elements that require a higher amount of energy to unfold. This is observed in the adaptation of thermophiles to high temperature habitats which results in the expression of more thermostable proteins relative to mesophilic organisms. Thus a bacterium such as *Pseudomonas thermophila* JCM3095 has a more thermostable NHase than the mesophilic NHase from *R. rhodochrous*-J1. By adapting the thermostabilising mechanisms in the *P. thermophila* NHase to less thermostable NHases such as the *R. rhodochocus*-J1 NHase (Nagasawa *et al*., 1991), a more thermostable NHase can be obtained which retains the desired thermal stability (Cowan *et al*., 2003). This has also been suggested by Fitter *et al*., (2001) in a study comparing α amylases from mesophilic and thermophilic *Bacillus amyloliquefaciens* and *Bacillus licheniformis*.

Thermostabilising mechanisms in proteins largely depend on the interaction between amino acid side-chain groups in regions that are potentially thermolabile and can be unfolded by breaking the few interactions that maintain the integrity of the local structure. The intrinsic factors within the protein structure can be classified using the interactions involved: hydrogen bonds, salt bridges, cation pi interactions, hydrophobic interaction and packing, the presence of solvent channels, relative position(s) of ligand binding sites within the structure, intersubunit links using hydrogen bonds, and the presence of structural components such as α helices and β sheets . The interactions that have been shown to contribute greatly are hydrogen bonds and salt bridges. Increases in hydrogen bonds and salt bridges have been

reported to increase protein thermal stability in proteins as determined from comparison between mesophilic and thermophilic proteins (Vogt *et al*., 1997; Vogt and Argos, 1997; Sadeghi *et al*., 2006). Of these mechanisms, hydrogen bonding, salt bridges and hydrophobic interaction have been reported to be the strongest having bond energies of approx. -2.2±1.7 kcal/mol when buried in a protein (in a hydrophobic environment), and approx. -1.1±0.7 kcal/mol when exposed (Kumar and Nussinov, 1999; Sheu *et al*., 2003; Gao *et al*., 2009). Gao *et al*., (2009) also showed how the context of a hydrogen bond can influence its energy, with a hydrophobic environment contributing to the largest change in hydrogen bond energy.

Hydrogen Bonds

Hydrogen bonding occurs when an H atom bound to an electronegative atom, such as O, N, S or P, forms a link to another electronegative atom at a distance not exceeding 3.5 Å. This occurs in the bonding pattern: [**donor electronegative atom]—[H atom]—[acceptor electronegative atom]**. In some cases, a water-mediated hydrogen bond can be formed. This occurs when an electronegative atom bonds to one of the H atoms of a nearby water molecule. The remaining H atom of the water molecule bonds with another electronegative atom in the protein structure. This creates a link as follows: **[protein ligand]**—[**water]**—[**protein ligand]**; the link is also referred to as a water bridge.

Hydrogen bonds can be between either side-chain-side-chain, side-chain-protein backbone or protein backbone to protein backbone. The factors influencing hydrogen bonds are listed in Table 1.1.

FACTORS INFLUENCING HYDROGEN BONDS	
Distance between bonding atoms	Kumar *et al*., (2000a)
Bond angle	Kumar *et al*., (2000a)
Electro negativity of interacting atoms	Bosshard and Jelesarov, (2004); Jelesarov and Karshikoff, (2009)
Hydrophobicity or hydrophilicity of the microenvironment	Klotz, (1993); Albeck *et al*., (2000); Sheu *et al*., (2003)
Hydrophobicity of adjacent side-chains	Klotz, 1993; Gao *et al*., 2009
Presence of adjacent hydrogen bonding groups (increases in degrees of freedom)	Kumar *et al*., (2000a), Sheu *et al*., (2003)

Table 1.1: The factors influencing formation of hydrogen bonds in proteins. The factors are related to bond formation and packing such as the interatomic distance, the electronegativity of the interacting groups and the hydrophilic or hydrophobic state of the microenvironment surrounding the microenvironment within 3.5 Å.

The energy of the hydrogen bond is inversely related to the distance between the H atom and the bonded electronegative atom, up to a distance of about 3.5 Å, and is directly related to the hydrophobicity of the surrounding microenvironment (Klotz, 1993; Sheu *et al*., 2003). Through double mutant cycle analysis, Albeck *et al*., (2000) showed the influence of the groups neighbouring a hydrogen bond on the energy of the bond. Later, Gao *et al*., 2009, using a similar approach, showed the changes associated with hydrogen bond energy following substitution of an adjacent smaller and less hydrophobic side-chain with a larger hydrophobic side-chain, resulting in an increase of 1.2 kcal/mol in hydrogen bond energy. This is in agreement with the previous suggestion by Klotz, (1993) that there would be an increase in the hydrogen bond energy in a more hydrophobic environment relative to a hydrophilic environment, and the later suggestion by Sheu *et al*., (2003) that the hydrophobicity of the microenvironment is directly related to the hydrogen bond strength. The presence of a polar medium around the hydrogen bond increases the entropy of the microenvironment thus lowers the energy required to the break hydrogen bonds. This facilitates kinetics of proteins in biological processes and prevents them from being trapped in an irreversible conformation.

The dependence of protein stability on the context in which hydrogen bonds are located in peptides has been investigated in previous studies by eliminating one or both parties involved in the hydrogen bond formation. A study by Gao *et al*., (2009) showed the dependence of unfolding on backbone hydrogen bonds following substitution of the backbone amide to an ester. This resulted in a backbone hydrogen bond being disrupted resulting in decreased thermal stability. Deechongit *et al*., (2004) showed the perturbation of a hydrogen bond in the WW domain (a beta sheet comprising of three anti-parallel beta strands and four loops) to have the greatest effect on protein folding energetics when a hydrogen bond in a hydrophobic environment is disrupted. This outcome combined with the earlier result from Sheu *et al*., (2003), shows the environmental influence on a hydrogen bond and the contribution of backbone hydrogen bonds to protein folding and stability.

The influence of hydrogen bonds on a large scale, with respect to the entire protein structure and its resulting function, is a major aim for thermal stability studies. Kumar *et al*.,

(2000a) described the increased occurrence of side-chain hydrogen bonds in thermophilic proteins relative to their mesophilic homologues. This would indicate that the backbone hydrogen bonds play their role (at least in part) in ensuring structural stability however, the additional links between hydrogen bonded side-chains would provide for a more extensive hydrogen bond network in the thermophilic protein compared to the mesophilic homologue (Kumar *et al*., 2000a). However, the hydrogen bonding network should be sufficiently flexible enough to allow the protein to undergo conformational changes during activity but also retain structural integrity (Fitter *et al*., 2001; Sheu *et al*., 2003). Thus the thermal stability determinants in a given thermophilic protein would be strategically positioned not to inhibit activity.

Salt Bridges

Protein structures are also heavily influenced by salt bridges. The intraprotein electrostatic interactions occur between oppositely charged groups such as between the partially negative O of a carbonyl group from an Asp or Glu residue and the partially positive N of the guanidino group of Arg or a positively charged ammonium e.g. from Lys or His located at a distance not exceeding 4Å (Kumar and Nussinov, 1999). In proteins, this also occurs between other residues with ionisable groups or partially charged groups such as Ser, Thr, Tyr, Asn and Gln when they are in the vicinity of other oppositely charged groups. The stability of a salt bridge is determined by factors which influence the ionisation state of these ionisable groups, their immediate environment, the distance between the interacting groups, the degree of isolation or interconnectedness of the salt bridge network and the presence of nearby non-interconnected salt bridges adjacent to the salt bridge of interest (Kumar *et al*., 2000b). The salt bridge geometry between interacting ionisable groups also influences the entropy and interaction energy of the salt bridge. This is based on the angle at which one ionisable group forms a salt bridge with respect to the other interacting group. Kumar and Nussinov, (1999) and Kumar *et al*., (2000a) describe a criterion for identifying a successful salt bridge based on the angle between two unit vectors which are individually connected to the centroid of their respective partial charges and respective Cα atoms (*fig*. 1.8).

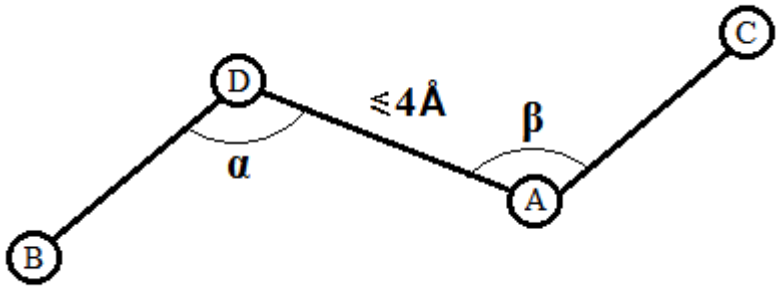

Figure 1.8: The criterion for a favourable salt bridge as described by Kumar *et al*., (2000a). The angle between vectors BD and DA is α while the angle between vector DA and AC is β. Favourable salt bridges are formed when α and β are between 90 and 150° and the distance between interacting groups is less than 4 Å. All other values of these angles would not result in salt bridges considering the unfavourable energies in salt bridges e.g. desolvation penalty.

The pH of the microenvironment influences the strength of the interaction. The protonation states in side-chains are largely determined by the pH of the surrounding solution. Changing the pH alters the protonation or deprotonation of ionisable regions in groups hence at pH extremes, one group loses its charge and the electrostatic interaction is negligible. For example, in the event of low pH conditions, the carbonyl O of an amino acid tends toward protonation and thus breaks its interaction with the NH_3^+ or other partially positive charged group. The reverse also happens in high pH. The ion concentration of the protein solution is also closely tied with the pH of the protein solution whereby the solvation of the protein is altered in different solvent concentrations. A similar concept is used in protein purification using hydrophobic interaction chromatography whereby a hydrophobic interaction between a protein and a hydrophobic ligand (covalently bonded to an inert matrix) is broken by decreasing the ion concentration. By decreasing the ion concentration, the intraprotein interaction sites have fewer degrees of freedom thus more energy is expended on the interaction and vice versa (Klotz, 1993).

The effects of the salt concentration on protein stability have been shown in other studies as well such as the work by Sikkink and Ramirez-Alvarado, (2008) on the effects of negative charges from SO_4^{2-} on amyloid formation. The partial folding of free light chains secreted by B cells was influenced by the salt concentration. An additional term, desolvation penalty, also influences the energy of salt bridge interactions. It is an unfavourable effect (in terms of folding energy) which results from burying a salt bridge in the hydrophobic core of a

protein where it experiences decreased solvation due to the low dielectric property of the surrounding environment. A high desolvation penalty will lead to a decrease in the salt bridge energy (Kumar and Nussinov, 1999; Kumar *et al*., 2000b). The energy contribution from salt bridges can be summarised as the sum of the energy contribution from the opposite charges, the energy decrease arising from the desolvation penalty and the energy resulting from the effect of adjacent charged groups. From the previous study conducted on the *G. pallidus*-RAPc8 NHase variants, the presence of salt bridges, significantly contributes to thermal stability of several mutants e.g. αS169R from the 9C composite NHase mutant; however, the causes of enhanced thermal stability cannot be identified due to the presence of other intramolecular interactions.

Hydrophobic Interactions

The stability of proteins is partially determined by the packing of hydrophobic cores. Hydrophobic cores result from the relatively spatially concentrated occurrence of hydrophobic side-chains on the interior of a protein. The result of this is that water molecules constituting the surrounding environment form a hydrophobic shell by interconnecting with one another thus there are decreased degrees of freedom for the intermolecular bonds of water molecules. This isolates and packs the hydrophobic side-chains in a minimal volume as water molecules associate with polar ligands and not non polar patches.

The force of the shell of water molecules folds the hydrophobic residues in a specific conformation which requires heat energy to unfold. In addition, waters of solvation are needed to pack the hydrophobic core thus in high ionic concentrations, hydrophobic packing decreases due to formation of a relatively weak water shell. Thus less energy has been used to fold the protein structure and it would require less heat energy to unfold. The Hofmeister series shows the ions that favour salting in and out of proteins from solutions. Further, concentrations of various salts and their effect on salting out of amino acids and side-chain groups has been shown previously (Baldwin, 1996). However, the total contribution of hydrophobicity to protein stability is largely dependent on the polarity of the protein solution and the concentration of ions which in turn determine the ionization state of groups on amino acid residues thus determining the formation of hydrogen bonds or salt bridges whose energy would depend on the hydrophobicity of the environment surrounding the interaction. As Atkins and Depaula, (2006) explained it, the strength of hydrophobic interaction is not as a physical interaction similar to hydrogen bonds but rather an indirect effect whereby the

energy of proximal hydrophilic interactions (within less than 3.5 Angstroms as shown above by Kumar *et al*., 2000a) is increased.

Cation-π Interactions

Other interactions less often encountered but still a major contributor to thermal stability are cation pi interactions. These interactions involve the centroid of an electron rich aromatic ring (a cyclic ring of sp2 hybridised carbon atoms of methylene groups such as a Phe, Tyr or Trp aromatic rings) interacting with cations over a range of distances up to 8 Å (Gromiha *et al*., 2006). The cations can be metal ions or positively charged N from amine groups of amino acid residues such as Lys, Arg or His. For example, Matsumura *et al*., (2007) showed a cation pi interaction in the crystal structure of the lipase from *Geobacillus zalihae* T1 whereby a Na^+ ion was observed interacting with the aromatic ring of Phe. An additional study by Prajapati *et al*., (2006) suggested that the measured $\Delta\Delta G^*$ value of cation pi interactions increases with temperature with an average increase of 0.7 kcal/mol up to the T_m of the protein.

Thermal stability in the NHase group of enzymes

Thermal stability studies on NHases have been carried out both *in silico* and *in vitro*. The *in silico* methods employed by Liu *et al*., (2008) using the crystal structures of thermophilic *B. smithii* (PDB code: 1V29) and P. thermophile (PDB code: 1UGQ) suggested the importance of salt bridges in enhancing thermal stability. This was done by examining flexibility of the structure at regions with amino acid side-chains that formed salt bridges under thermal stress. The amino acid residues involved were Asp, Arg and Glu and the work showed that intersubunit salt bridges decreased the fluctuations. In the study by Liu *et al*., (2008), one of the suggested thermostabilising regions (B1) in the β subunit (also referred to as region A3 in a subsequent study using the same NHases by Chen *et al*., (2012) was used to mutate the corresponding region in the mesophilic NHase from *Rhodococcus ruber* TH. The mutation involved replacing Ser-Phe-Ser-Lys with Lys-Phe-Lys-Glu in the β subunit of the *R. ruber* TH NHase and addition of two amino acid residues Asp and Thr at positions 435 and 436 on the C terminus of *R. ruber* TH NHase. These changes facilitated the formation of more salt bridges and resulted in an enhanced thermal stability of the *R. ruber* TH NHase.

Previous studies on the NHase from *Geobacillus pallidus* RAPc8

The NHase from *G. pallidus* RAPc8 was first identified following expression in the organism *G. pallidus* RAPc8 (Pereira *et al*., 1998). In the same study, the optimal growth temperature for the host organism expressing active NHase was determined to be 338 K with an optimal activity temperature of 333 K. Cloning of the genes expressing NHase was done into a pET21a(+) vector (Cameron *et al*., 2005).

In previous studies study by van Wyk, (2008), six NHase thermostability mutants, five containing multiple mutations within each construct and one single mutant αI47S, were discovered via error prone PCR using a polymerase whose fidelity had been decreased using Mn and biased concentration of nucleotides. Some of these NHase mutants, also referred to as composite mutants, contained multiple mutations and were found to be more thermostable than the WT NHase when tested using cell free extract (CFE). This effect was also observed with one mutant, αI47S, which had a single mutation in the α subunit. Three of the most thermostable composite mutants, 9E, 9C and 8C were selected due to their relatively higher thermal stability than the WT NHase. Some of the single mutations within the composite mutants from the previous study by van Wyk, (2008) were developed and confirmed via sequencing while others were developed and confirmed by sequencing as later shown in this study. These NHase mutants: 9E (which contained βL103S, βY127N, βF36L and αD4G mutations), 9C (which contained βM43K, βT150A and αS169R) and 8C (which contained βD96E, βD167V and αM188V) possessed the defining features that would impart thermal stability to NHase. The NHase composite mutants, 9E, 9C and 8C and their respective thermal stabilities expressed as $\Delta\Delta G^*$ values in kJ/mol as measured in the previous study using CFE (van Wyk, 2008), are shown below in Table 1.2.

Composite Mutant NHase	**Previously determined $\Delta\Delta G^*$ for the composite NHase (kJ/mol)**	**α subunit mutations**	**β subunit mutations**
9E	-4.27	αD4G	βL103S
			βY127N
			βF36L
9C	-7.62	αS169R	βM43K
			βT150A
8C	-6.16	αM188V	βD167V
			βD96E

Table 1.2: The $\Delta\Delta G^*$ values of thermal unfolding previously determined for the composite mutant NHases from *G. pallidus* RAPc8 while using CFE and measurement using transmittance of white light (van Wyk, 2008).

In the same previous study by van Wyk, (2008), comparison of the crystal structure of the NHase αI47S mutant, also referred to as variant 7D in the previous study (van Wyk, 2008) with the WT NHase showed the presence of a water-mediated hydrogen bond (*fig*. 1.9 B). The presence of a cluster of hydrophobic side-chains around the hydrogen bond was also observed later (*fig*. 1.9 B). Water-mediated hydrogen bonds have been shown to contribute to thermal stability and the strength of hydrogen bonds has also been shown to increase in the presence of adjacent hydrophobic ligands within hydrogen bonding distance (Klotz *et al*., 1993).

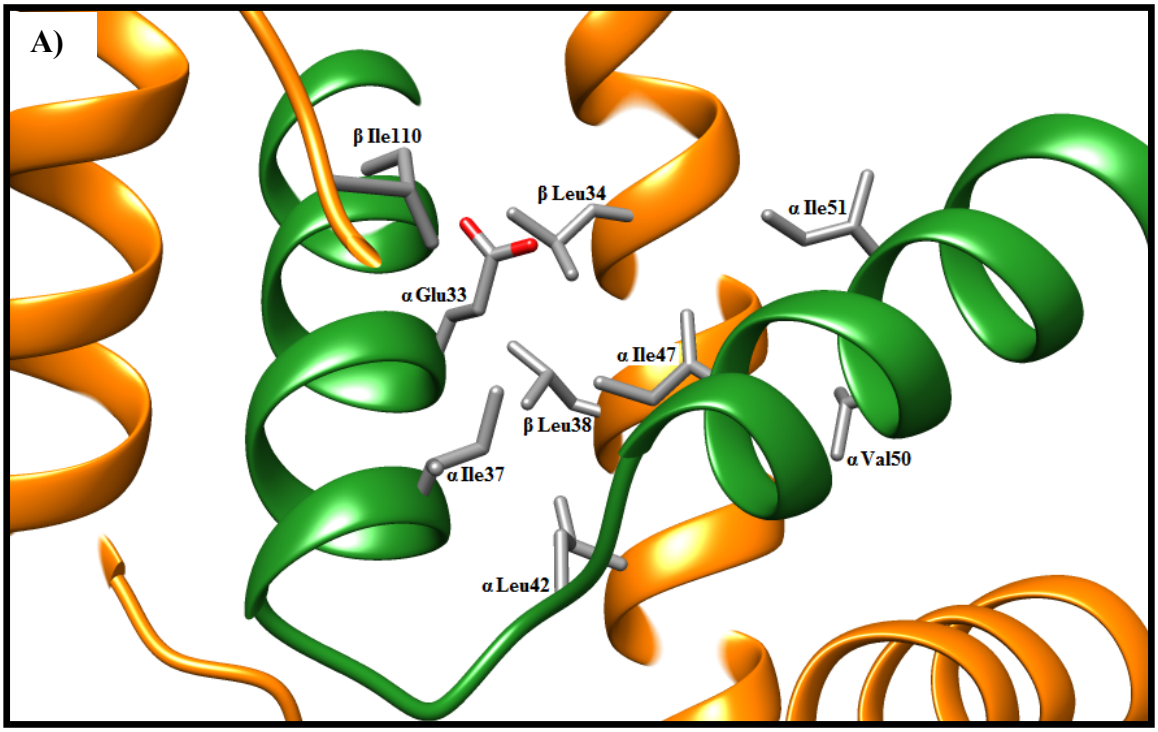

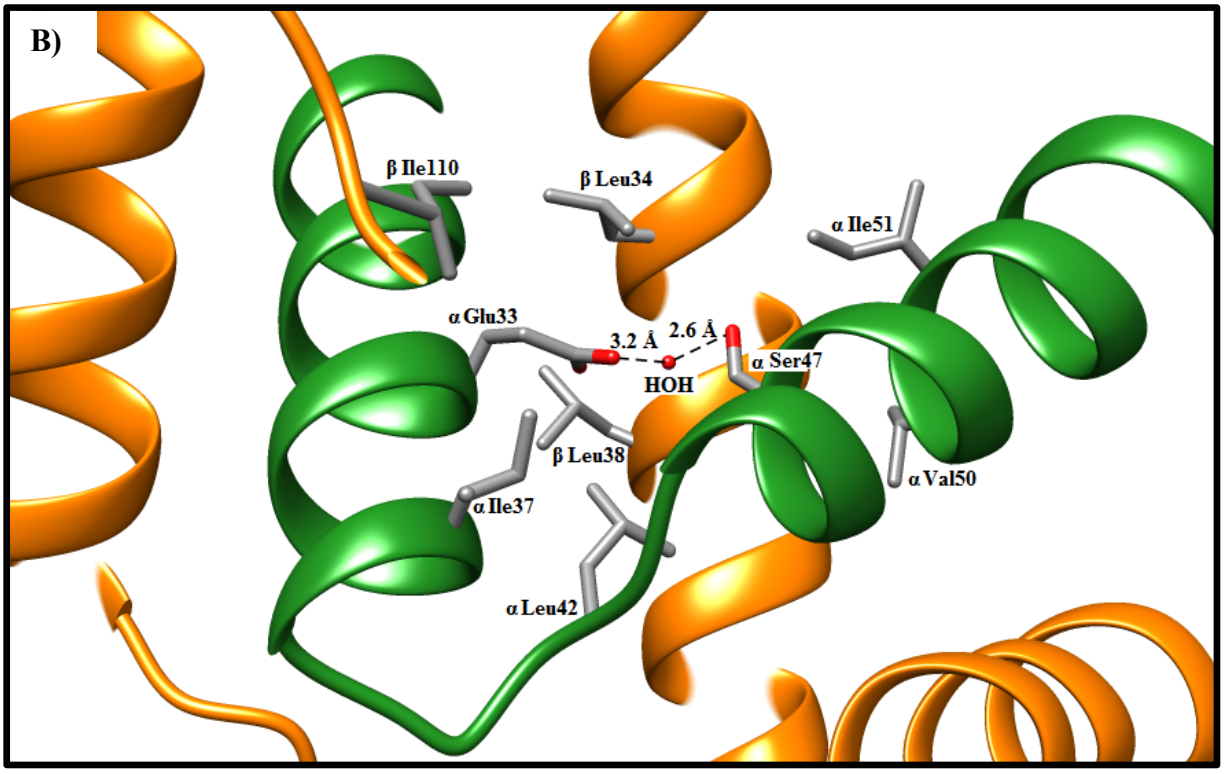

Figure 1.9: A) An image of the crystal structure of the WT NHase showing Ile47 in the α subunit. The α subunit is coloured green while the β subunit is coloured orange. B) An image of the mutation αI47S in the mutant NHase. The single water-mediated hydrogen bond between αGlu33 and αSer47 is in the presence of a cluster of hydrophobic side-chains consisting of αIle37, αLeu42, αLeu38, βIle110, βLeu34, αIle51 and αVal50. This microenvironment of hydrophobic side-chains would reduce the degrees of freedom allowed for hydrogen bond formation (van Wyk, 2008). The image was created using Chimera (Pettersen *et al*., 2004).

Comparison with *R. rhodochrous* J1 NHase Applied in Industry

Industrial production of amides has been accomplished using various NHases such as the NHase from *R. rhodochrous* J1, *P. chlororaphis* B23 and *R. rhodochrous* VKM Ac-1515D amongst others (Hideaki *et al.,* 1994; Yanenko *et al.,* 1998; Watanabe *et al.,* 2010). The *R. rhodochrous* J1 NHase has been used extensively especially for production of acrylamide. The *R. rhodochrous* J1 NHase is available in two forms depending on the inducer. The low molecular weight form has been shown to have an optimum catalysis temperature and pH for catalysis of 313 K and 8.8 respectively, and occurs when over-expressed in the organism using cyclohexanecarboxamide as an inducer (Wieser *et al.,* 1998).

The high molecular weight form has an optimum catalysis temperature and pH of 308 K and 6.65 respectively, and occurs when over-expressed in the organism using urea as an inducer (Nagasawa *et al.,* 1991; Nagasawa *et al.,* 1993).

Due to the absence of a crystal structure in the PDB for this NHase, a homology model built using Genethreader was used to search the PDB for homologous NHase structures and the corresponding positions of amino acids in both the *G. pallidus* RAPc8 and *R. rhodohrous* J1 NHases were compared (Table 1.3). Similarities in the type of mutation can be seen between the NHases of the two organisms, especially in the mutants: αS169R, βD96E and M43K.

Mutations In the *G. pallidus* RAPc8 NHase		**Amino acid residues at the corresponding positions in *R. rhodochrous* J1 NHase**
Composite Mutant	**Single Mutant**	
9E	βL103S	βM99
	βY127N	βT124
	βF36L	βL36
8C	αM188V	αF188
	βD167V	βG164
	βD96E	βD92
9C	αS169R	αS169
	βM43K	βA41
	βT150A	βV147

Table 1.3: A comparison of amino acid mutations in the *G. pallidus* RAPc8 NHase and their corresponding structural positions in the industrial *R. rhodochrous* J1 NHase. The αS169 and βD96 amino acid residues are present in both NHases and the βL36 amino acid residue is present in the βF36L single mutant and the *R. rhodochrous* J1 NHase.

AIMS OF THE STUDY

Following the previous work on the *G. pallidus* RAPc8 composite mutants by (van Wyk, 2008), the thermal stability of composite mutants were determined by isolating individual mutations comprising the composite NHase mutants and determining which mutations were contributing to thermal stability. The crystal structures, in combination with these results, were utilised to determine the possible mechanisms involved. The investigation of elements in the structure of NHase that contribute to thermal stability was achieved via the following specific aims:

1. Measure the thermal stability of WT and composite mutant NHase.

a) Optimise the detection of nitrile catalysis by selected NHases

b) Purify NHase WT, NHase mutants and amidase for use in the study.

c) Optimise the hydroxamic acid assay to enhance detection of NHase activity

d) Measure thermal stability of WT NHase and composite mutants

2. Introduce single amino acid residue mutations into WT NHase and measure thermal stability.

a) Use site directed mutagenesis and sequencing to make single mutants and confirm the mutations.

b) Transform into bacterial expression strains, over express and purify the mutants.

c) Measure thermal stability of single mutants using the optimised hydroxamic acid assay and thermal shift assay.

3. Determine whether thermal stability of the mutants have a cumulative effect.

Determine the $\Delta\Delta G^*$ for each NHase sample, compare and check if the $\Delta\Delta G^*$ values for the single mutants add up to the $\Delta\Delta G^*$ of the composite mutants.

4. Rationalise the contributions to thermal stability using previously determined structures of NHase and the thermal stability results.

CHAPTER 2:

MATERIALS AND EXPERIMENTAL TECHNIQUES

Introduction

The hydration of nitriles to amides by nitrile hydratase followed by an acyl transfer from amides to hydroxylamine to form hydroxamic acids has allowed the development of a two enzyme system comprising of nitrile hydratase and amidase for the measurement of catalysis by the NHase (Kobayashi *et al*., 1993; Fournand *et al*., 1998). This system, albeit modified from early versions, has been coupled with spectrophotometric detection of the end products through the use of a colour reagent, $FeCl_3$ in 0.1 M HCl. This reagent forms a brown coloured Fe-hydroxamic acid complex whose absorbance of light at 520 nm is measured on a spectrophotometer (*fig*. 1. B).

Reagents and bacterial strains

The required salts and solutions such as dithiothreitol, HPLC grade acetonitrile, acetamide, acrylonitrile, acrylamide, hydroxylamine HCl and acetohydroxamic acid were obtained from Sigma-Aldrich. Constructs consisting of the WT and some single mutants of the NHase alpha and beta subunits, and the cobalt NHase chaperone, P14K, cloned into a pET21 vector (van Wyk, 2008) were provided for by Prof. Trevor Sewell (CIA, UCT). Cloning and expression strains of *E. coli*, DH5 alpha and BL21 (DE3) respectively, were obtained from Novagen into which each construct was transformed via the heat shock method. All transformed constructs were stored at 193 K until needed.

Some of the constructs for the randomly generated mutants were generated via error prone PCR and confirmed via sequencing at the sequencing facility at Stellenbosch University (van Wyk, 2008) while others were generated using site directed mutagenesis as described below and using the primers in Table 2.1 and confirmed via sequencing at the same facility.

Protein Determination Techniques

Protein concentration was determined by either of two methods depending on the sample being measured. The total protein concentration of all CFE and partially pure samples

was determined using Bradford assays according to (Bradford, 1976) using BSA for generation of the standard curve. The NHase or amidase sample was diluted serially to different concentrations in triplicate ranging from 1/10 to 1/300. 200 µl of 5 times diluted Bradford reagent was added to 10 µl of sample protein in a 96 well plate. The absorbance of light was measured at 595 nm.

Protein determination was also done using absorbance at 280 nm (A280) measurements. A volume of 2 µl of the purified protein sample (NHase or amidase) was added to a NanoDrop reader and the absorbance at 280 nm was measured. The sequence of the NHase or amidase being measured was uploaded onto ExPASy (Artimo *et al*., 2012) and the protein parameters determined using the ProtParam tool (Gasteiger *et al*., 2003). For this determination method, the computed molecular weight, the absorbance at 280 nm and extinction coefficient was required for each NHase sample.

Site Directed Mutagenesis

Primers were designed using Gene Designer (DNA 2.0), Bioedit (Ibis Biosciences) and DNAMAN (Lynnon Biosoft) (Table 2.1). Synthesis of primers was done at the oligonucleotide synthesis lab at the molecular and cell biology department, UCT. Site directed mutagenesis (SDM) was performed using the WT NHase construct pNH14K using the KAPA HIFI hotstart site directed mutagenesis kit according to the manufacturer's instructions with the following changes: the final concentration of each primer in the reaction mix was 3.2 µM and the concentration of the template was 80 nanograms. A gradient of various annealing temperatures was tested ranging from 328 K to 338 K. The annealing temperature used for the PCR reaction, to generate enough PCR product for downstream applications, was 333 K for a total of 24 cycles. Products from the SDM-PCR were confirmed by visualization on a GBox (Syngene) gel visualizer following electrophoresis on a 1% agarose gel in TAE stained using ethidium bromide (*fig*. 4.2).

NHase Mutant Primer	**Primer Sequence**
Forward βD167V primer	5'-ATA TGC CCG TGT CAA ATA TGG TG -3'
Reverse βD167V primer	5'-CGA GGG AAT CTC GTA TGA CCA G -3'
Forward βF36L primer	5'-GAA AGA CTT GCG CTC GGA CTT GTA G -3'
Reverse βF36L primer	5'-CCA ATC ATG TGT AAA ATA AAT GTC CTC TTC -3'

Forward αM188V primer	5'-GTA CGG AAG GAG TGA CGG AGG AG -3'
Reverse αM188V primer	5'-CTT CAG GTC TTT GCG GCA ATA CC -3'
Forward βT150A primer	5'-GAG AGA ATC AAG GCG AAA AAC ATT C -3'
Reverse βT150A primer	5'-TCC TAC CTT AAA CCG AGG AGA AGC -3'

Table 2.1: A list of forward and reverse site directed mutagenesis primers.

Products from SDM-PCR were digested with DPNI to remove the template DNA from the reaction followed by cleaning of the product via electrophoresis on a 1% agarose gel in TAE to remove fragments of digested template DNA and the PCR mix. The cleaned product was cut out of the gel on a UV box set to a wavelength of 340 nm and the excess gel cleaned using a Bioflux gel cleaning kit according to the manufacturer's instructions and eluted in ultrapure water.

The cleaned product was ligated using T4 ligase (Thermoscientific) overnight at 295 K. Part of the sample was electrophoresed on a 1% agarose gel for a visual confirmation of the construct size followed by transformation into DH5 alpha cells and plating on LB agar with ampicillin/carbenicillin at a final concentration of 100 μg/ml. The plates were incubated at 310 K overnight followed by selection of single colonies. Three single colonies from each construct were inoculated separately into 10 ml LB broth each with ampicillin at a final concentration of 100 μg/ml and incubated at 298 K overnight with shaking at 120 rpm.

Plasmid extractions were performed on each sample using the Bioflux plasmid DNA extraction kit according to the manufacturer's instructions with the following change: the total volume of the bacterial culture prior to pelleting via centrifugation was greater than 8ml. All synthesized constructs were confirmed via sequencing (Appendix 3 and 4) at CAF (Stellenbosch University) and stored in glycerol stocks consisting of separate cultures of *E. coli* cloning strains containing each construct in 10% glycerol at 193 K.
Following this, the constructs were extracted using the Bioflux plasmid DNA extraction kit according to the manufacturer's instructions and transformed into BL21 (DE3) *E. coli* cells and stored at a temperature of 193 K.

Expression of NHase

Starter cultures of each NHase-expressing *E. coli* clones, were prepared in LB broth with 100 µg/ml ampicillin and incubated at 298 K overnight. This was to prevent excessive growth and inactivation of the ampicillin by the β-lactamase. Starter cultures from the overnight incubation were inoculated into 1 litre LB broth with 100 µg/ml ampicillin and incubated for about 2.25 hours at 310 K until the O.D. of the culture measured at 600 nm was about 0.35-0.5. A pre-induction sample was isolated from the culture and stored in 4x sample application buffer. A filter sterilized solution of cobalt chloride was added to a final concentration of 100 µg/ml followed by isopropyl thiogalactopyranoside (IPTG) to a final concentration of 0.4 mM in the 1 litre culture. Induction for NHase expression was done at 310 K for 6-8 hours. Following induction, a post induction sample was obtained in a similar manner as the pre-induction sample, for comparison to the pre-induction sample via SDS-PAGE analysis. The O.D. at 600 nm was also measured after induction.

The cell cultures were centrifuged at 10,000 g on a Beckman-Coulter centrifuge to pellet the cells followed by short term storage (less than 2 months) of cell pellets at 253 K The pre and post induction samples were subjected to SDS-PAGE analysis. This entailed mixing of each pre and post induction sample with 4X sample application buffer (SAB), a subsequent heating at 373 K for 15-20 minutes and electrophoresis on a 10% acrylamide gel at 20 mA together with an appropriate protein molecular weight ladder (New England Biolabs).

Staining of the SDS-PAGE gels was done using either overnight in Coomassie or for 20 minutes in Aqua Stain. Visualisation of gels was done on a ChemiDoc™ XRS+ imaging system (BioRad).

Optimisation of the hydroxamic acid assay

Optimisation of Amidase Catalysed Acyl Transfer

This optimisation allows for determination of the concentration of amidase required for complete catalysis, via acyl transfer, of the acyl group from an amide to hydroxylamine HCl within 30 minutes at 310 K (*fig.* 1 B). A previously purified amidase was prepared at various concentrations: 0.086, 0.1, 0.12, 0.15, 0.2, 0.3 and 0.6 mg/ml in triplicate. To 50 µl of 0.025 M potassium phosphate buffer pH 7.2, 5 mM DTT and a further 50 µl of amidase at each concentration in a 96 well plate, 50 µl of 0.1 M acetamide in 0.025 M potassium phosphate

buffer pH 7.2, 5 mM DTT, was added and incubated at 310 K for 30 minutes. The catalysis was stopped by addition of 50 µl acidified 0.1 M iron(iii)chloride. Measurement of absorbance was done at 520 nm on a Titertek Multiscan MKIII microplate reader or on a FLUOStar Omega microplate reader.

Confirmation of nitrile catalysis

Cell free extract (CFE) containing over expressed NHase was prepared identically as prior to purification. The cell free extract was diluted in 0.025 M potassium phosphate buffer pH 7.2, 5 mM DTT to a total protein concentration of 0.5 mg/ml. A volume of 50 µl of this CFE was added to 50 µl of 0.1M acrylamide in 0.025 M potassium phosphate buffer pH 7.2, 5 mM DTT and allowed to catalyse for 30 minutes at 310 K in Eppendorf tubes. The catalysis by the NHase was stopped by addition of 50 µl of 2 M hydroxylamine HCl in 0.025 M potassium phosphate buffer pH 7.2, 5 mM DTT. A further volume of 10 µl of a previously purified amidase at a concentration of 0.5 mg/ml in 0.025 M potassium phosphate buffer pH 7.2, 5 mM DTT, was added to the reaction and incubated at 310 K for 30 minutes. The catalysis by the amidase was stopped by addition of 50 µl of acidified 0.1 M iron(iii)chloride. Observation of a brown pigment confirmed the catalysis.

Determination of the stoichiometry using the hydroxamic acid assay

A range of dilutions starting from 0 to 400 mM acetamide was prepared in 0.025 M potassium phosphate buffer pH 7.2, 5 mM DTT. A volume of 80 µl of each dilution was aliquoted in triplicate into separate wells on a 96 well plate. For each dilution of acetamide, a volume of 50 µl of buffer consisting of 0.025 M potassium phosphate buffer pH 7.2, 5 mM DTT was added to each well followed by 10 µl of pure and homogenous amidase at a stock concentration of 0.35 mg/ml also prepared in 0.025 M potassium phosphate buffer pH 7.2, 5 mM DTT. The final concentration of amidase was ≈0.02 mg/ml. The reaction mixture was covered in aluminium foil and incubated at 310 K for 30 minutes.

A second set of dilutions starting from 0 to 200 mM acetohydroxamic acid was also prepared in 0.025 M potassium phosphate buffer pH 7.2, 5 mM DTT and a volume of 80 µl of each dilution of acetohydroxamic acid was aliquoted into separate wells in a 96 well plate. An equal volume of 80 µl of 0.025 M potassium phosphate buffer pH 7.2, 5 mM DTT was added to each well. After the 30 minute incubation at 310 K, a volume of 50 µl of 0.1 M

$FeCl_3$ in 0.1 M HCl was added to each well on both plates and the absorbance measured at 520 nm on a FLUOStar Omega multiwall plate reader.

Optimisation of the duration of nitrile catalysis:

Purified NHase at 0.05 mg/ml in 0.025 M potassium phosphate buffer pH 7.2, 5 mM DTT was aliquoted at volumes of 50 µl per well into a 96 well plate in triplicate (Table 2). Each triplicate time point represented a duration of 2.5 minutes of catalysis for each sample. To all wells containing NHase sample, 50 µl of 0.1 M acetamide in 0.025 M potassium phosphate buffer pH 7.2, 5 mM DTT was added and incubated at various temperatures: 298 K, 303 K, 308 K and 313 K for each set of four samples per 96 well plate for the WT NHase and each of three composite mutants: 9E, 8C and 9C. The catalysis was stopped every 2.5 minutes for each set of triplicate samples by adding 50 µl of 2 M hydroxylamine HCl in 0.025 M potassium phosphate buffer pH 7.2, 5 mM DTT. This was done until all time pints were stopped for up to 30 minutes. The 96 well plate was covered using aluminium foil with adhesive to seal around each well. The acyl transfer reaction for the second stage was mediated by adding 10 µl of 0.35 mg/ml amidase in 0.025 M potassium phosphate buffer pH 7.2, 5 mM DTT and incubating at 310 K for 30 minutes. The final concentration of the amidase in the reaction was ≈0.02 mg/ml. Detection was performed by adding 0.1 M $FeCl_3$ in 0.1 M HCl followed by measuring absorbance at 520 nm.

Optimisation of the heat treatment temperature

Purified NHase was prepared to 0.05 mg/ml in 0.025 M potassium phosphate buffer pH 7.2, 5 mM DTT. A total of 5 samples in triplicate were prepared for each purified NHase. For each replicate, 55 µl was aliquoted into 1.5 ml Eppendorf tubes and heat treated at various temperatures (Table 2.2) for up to 40 minutes at 10-minute intervals. From each heat treatment sample, a volume of 50 µl of the NHase samples was allowed to catalyse 50 mM acetronitrile at 298 K for 5-10 minutes in covered 96 well plates. Detection was performed by adding 0.1 M $FeCl_3$ in 0.1 M HCl followed by measuring absorbance at 520 nm.

Hydroxamic Acid Assay

The purified protein sample was diluted to 0.05 mg/ml in 0.025 M potassium phosphate buffer pH 7.2, 5 mM DTT and confirmed by calculating the concentration using

the measured absorbance at 280 nm on a Nano Drop 2000 UV-VIS spectrophotometer (Thermo Scientific), the molecular weight of each dimer and the extinction coefficient for the dimer obtained from ExPASy. Protein determination was also checked for several purified NHase samples using Bradford assays to confirm the protein determination method above done using absorbance at 280 nm, the NHase dimer extinction coefficient and dimer molecular mass. The homogenous protein sample was aspirated into Eppendorf tubes in triplicate with each tube containing 55 µl of sample. This was done for 12 sets of tubes with each set in triplicate. The 12 sets were labelled with the duration of heat treatment for which they will be treated at.

0 min	5 min	10 min	15 min	20 min	25 min	30 min	35 min	40 min	45 min	50 min	55 min
0 min	5 min	10 min	15 min	20 min	25 min	30 min	35 min	40 min	45 min	50 min	55 min
0 min	5 min	10 min	15 min	20 min	25 min	30 min	35 min	40 min	45 min	50 min	55 min
Ctrl s1	Ctrl s1	Ctrl s1	Ctrl 2	Ctrl 2	Ctrl 2	Ctrl 4	Ctrl 4	Ctrl 4			
Ctrl s2	Ctrl s2	Ctrl s2	Ctrl 3	Ctrl 3	Ctrl 3	Ctrl 5	Ctrl 5	Ctrl 5			
0 min	5 min	10 min	15 min	20 min	25 min	30 min	35 min	40 min	45 min	50 min	55 min
0 min	5 min	10 min	15 min	20 min	25 min	30 min	35 min	40 min	45 min	50 min	55 min
0 min	5 min	10 min	15 min	20 min	25 min	30 min	35 min	40 min	45 min	50 min	55 min

Table 2.2: Layout for the hydroxamic acid assay on a 96 well plate. The label "Ctrl s1" represents the negative control for sample 1 while "Ctrl s2" represents the negative control for sample 2. The time points range from time 0 minutes to time 55 minutes indicating the duration of heat treatment of the NHase samples. All measurements were done in triplicate with independently heat treated samples.

The Eppendorf tubes were heat treated in a water bath set at a constant temperature for each of the temperatures: 330 K, 333 K, 334.5K, 336 K and 338 K (57 °C, 60 °C, 61.5 °C, 63 °C and 65 °C) for the durations listed above (Table 2.2) . This was done for different samples depending on the preliminary thermal stability assay carried out during optimisation. Following heat treatment, the samples were quenched in an ice bath at 273 K for >10 minutes then centrifuged for 7 seconds at 8000 g and incubated again on ice immediately. A volume

of 50 µl was aspirated from each tube to a respective well in a 96 well plate. This was done for all the triplicate samples and time points.

A further volume of 50 µl of each sample was included in the controls in triplicate. A volume of 0.1 M acetonitrile in 0.025 M potassium phosphate buffer pH 7.2, 5 mm DTT, was added to each well using a multichannel pipette. Five sets of controls each with 4 wells were added. The controls were as follows:

Control s1 or s2	Control 2	Control 3	Control 4	Control 5
50 µl sample + 50 µl buffer	50 µl of substrate + 50 µl buffer	50 µl of acetamide + 50 µl of buffer	100 µl of buffer	100ul acetohydroxamic Acid + 50 ul buffer

Table 2.3: The controls used during the hydroxamic acid assay. Each control was done in triplicate. The controls represented as s1 and s2 represent the negative controls for each NHase sample assayed within the same 96 well microplate. Control 2 tested for contamination of the substrate, control 3 tested the activity of amidase, control 4 tested the buffer alone and control 5 tested the detection using acetohydroxamic acid and $FeCl_3$ (positive control).

The 96 well microplate was covered using an adhesive layered aluminium foil which also sealed around each well with adhesive. The plate with the samples was incubated at 298 K (25 °C) for 5 minutes for the samples: βD167V, αM188V, βF36L and βT150A; and 10 minutes for all remaining nitrile hydratase samples. Following incubation, a volume of 50 µl of 2 M hydroxylamine in 0.025 M potassium phosphate buffer, 5 mM DTT, was added to each well to stop the catalysis of acetonitrile by the nitrile hydratase sample. A volume of 10 µl of amidase diluted to a stock concentration of 0.35 mg/ml in 0.025 M potassium phosphate buffer pH 7.2, 5 mM DTT, was added to each well resulting in a final concentration of ≈0.02 mg/ml. The 96 well plate was covered as before and incubated for another 30 minutes at 310 K (37 °C). This was followed by addition of 50 µl of acidic 0.1 M iron (iii) chloride to each well to stop the amidase catalysis and form a brown coloured Fe-hydroxamic acid complex. Measurement of the colour intensity was done on a FLUOStar Omega microplate reader

(BMG Labtech) at 520 nm. Data was recorded using the MARS data analysis program (BMG Labtech) and stored in Microsoft excel format.

Thermal Shift Assay

Measurement of NHase thermal denaturation using the Sypro orange assay

The purified NHase samples were utilised in this assay. Each of the samples was prepared to a final concentration of 0.1 or 0.2 mg/ml with Sypro orange diluted to 1:2500 or 1:1250 respectively in a total buffer volume 50 µl. The reactions were heat treated from a temperature range of 293 K to 368 K. Fluorescence was measured throughout the thermal cycle and the melting temperatures (Tm) determined by taking the first derivative of the observed change in fluorescence. All reactions were done in triplicate.

CHAPTER 3:

PROTEIN PURIFICATION

Introduction

The cloning of the NHase genes was performed onto a pET21a(+) vector without the addition of amino acid residue tags that would aid in purification. The subsequent generation of composite and single mutants was done via site directed mutagenesis on the same vector. Thus all the NHase constructs used did not possess tags e.g. His tags that would aid in protein purification. Consequently the purification strategy was done by exploiting the properties inherent to NHase such as: the exposure of the hydrophobic core in the presence of high ammonium sulphate concentration for phenyl sepharose chromatography, the distribution and magnitude of charges on the surface of the NHase tetramer for anion exchange chromatography and the physical dimensions and molecular mass of the tetramer for SEC chromatography. All these properties were refined from insight obtained from previous purifications of the *G. pallidus* RAPc8 NHase and the purifications carried out in this study.

Overview of the Purification Strategy

The expression of amidase was done according to (Agarkar *et al*, 2007). The purification of the NHase was similar to the amidase except for three changes: there was no heat treatment throughout the purification strategy due to the nature of the experiment measuring thermal denaturation of NHase, the ammonium sulphate precipitation was done at 20% ammonium sulphate at 273 K and the binding to the phenyl sepharose column was done at 1 M ammonium sulphate. The preliminary steps in purification of NHase followed the steps: sonication of the cell pellet, clarification by centrifugation and ammonium sulphate precipitation. This was then followed by the chromatographic steps: phenyl sepharose chromatography, anion exchange chromatography, and size exclusion (SEC) chromatography. Some of the chromatographic stages were done repeatedly at each step for each protein and analysed using SDS-PAGE using a 10% gel. The desired fractions were then pooled and fractionated on the next chromatographic step

Preliminary Purification

The expression of each NHase sample was achieved following inoculation into and induction in Lysogeny broth (10 grams tryptone, 5 grams yeast extract and 5 grams sodium chloride per litre of broth) + 100 μg/ml ampicillin/carbenicillin at 310 K for 6-8 hours. Cells were pelleted via centrifugation at 10,000 g for 10 minutes and washed once using 0.025 M potassium phosphate buffer pH 7.2. The cell pellets were frozen at 253 K for at least 2 hours or until sonication.

Cell lysis was done via sonication on an ice bath at a power rating of 39 Watts on a Misonix 3000 sonicator for 8 minutes at 15 second on/off intervals. Cell lysate was clarified via centrifugation at 10,000 g for 15 minutes to obtain the cell free extract. An ammonium sulphate precipitation was performed using a final concentration of 20% ammonium sulphate followed by clarification at 15000 g for 30 minutes. Only the supernatant for the amidase expression was subjected to heat treatment at 318 K for 2 minutes followed by centrifugation at 15000 g for 30 minutes. The supernatant from the nitrile hydratase expression was not subjected to heat treatment.

Chromatographic Steps for Purification

Phenyl Sepharose Chromatography

The supernatant was passed through a 0.45 μM followed by a 0.22 μM filter prior to application onto a phenyl sepharose column (GE Life Sciences) previously equilibrated using 1.7 M ammonium sulphate in 0.05 M potassium phosphate buffer pH 7.2, 5 mM DTT, for the amidase expression sample. For the nitrile hydratase expression sample, the phenyl sepharose column was previously equilibrated using 1.0 M ammonium sulphate in 0.05 M potassium phosphate buffer pH 7.2, 5 mM DTT. A total of 60 fractions were collected at 2 minute intervals using a decreasing linear gradient of ammonium sulphate using 0.05 M potassium phosphate buffer pH 7.2, 5 mM DTT at a flow rate of 2.5 ml per minute.

The fractions were analysed using SDS-PAGE. The peak fractions were pooled and total protein concentration was determined via Bradford assays using BSA as a standard.

Anion Exchange Chromatography

The pooled fraction was buffer exchanged and concentrated using 0.025 M potassium phosphate buffer pH 7.2, 5 mM DTT on a nitrogen pressured Amicon system using a 10 kDa

membrane (Millipore) and applied onto a QHP anion exchange column (GE Life Sciences) previously equilibrated using 0.025 M Tris(hydroxymethyl)aminomethane (TRIS) buffer pH 7.2, 5 mM DTT. A total of 60 fractions were collected using a linear increasing gradient up to 1 M sodium chloride in 0.025 M TRIS buffer pH 7.2, 5 mM DTT, at a flow rate of 2.5 ml per minute. The fractions were analysed using SDS-PAGE. The fractions corresponding to the appropriate molecular size (about 30 kDa) were pooled and the total protein concentration was determined using Bradford assays and BSA as a standard.

Size Exclusion Chromatography

The pooled sample from anion exchange chromatography was concentrated down to a volume of 0.5 ml and applied onto a Sephadex 200 (S200) column (GE Life Sciences) previously equilibrated using 0.025 M potassium phosphate buffer pH 7.2, 5 mM DTT, at 277 K. 80 fractions were collected at a flow rate of 0.5 ml per minute. The fractions were analysed using SDS-PAGE and the fractions with the desired band were pooled and tested for activity. The total protein concentration was also determined using Bradford assays.
The purified protein was stored in multiple aliquots in volumes of approximately 300 µl at 193 K (-80 °C) in 0.025 M potassium phosphate buffer pH 7.2, 10 mM DTT 15% glycerol, until when needed for assays. All purified NHase samples were electrophoresed on a 10% gel and visualised following overnight staining in Coomassie stain *fig*. 3.6.

Indophenol Blue Assay

Preparation of detection reagents

Phenolic alcohol was prepared by dissolving 1 gram of phenol into 95% ethanol to a final volume of 100 ml. The sodium nitroprusside solution was prepared by dissolving 0.1 grams of solid nitroprusside in distilled water to a final volume of 20 ml. The alkaline complexing reagent was prepared by dissolving 10 grams of trisodium citrate and 0.5 grams sodium hydroxide in distilled water to a final volume of 50 ml. The oxidising solution was prepared by adding 1 part of sodium hypochlorite (NaOCl) to 4 parts of the alkaline complexing reagent.

Assay method

An ammonia standard curve was prepared ranging from 0 to 10 mM using ammonium chloride in 0.025 M potassium phosphate buffer pH 7.2, 5 mM DTT.

A 1 ml reaction volume containing various triplicate dilutions of the amidase (1/100, 1/200, 1/500) and acrylamide at a final concentration of 10 mM was incubated for 30 minutes at 310 K. The reaction was stopped following addition of the detection reagents: 40 µl of phenolic alcohol, 40 µl of sodium nitroprusside and 100 µl of the oxidising solution. Following addition of the detection reagents, the solution was incubated in the dark for 30 minutes. A volume of 100 µl was dispensed into a microplate and absorbance measured at 620 nm using a Titertek Multiskan MKII microplate reader.

Data Capture and Analysis

The absorbance readings were recorded using Ascent Software version 2.6 and MARS Data Analysis software. The measured activity for each NHase sample was analysed using a three parameter non-linear fit on Sigma Plot version 11 and Microsoft Excel 2010. Crystal structures and electron density maps were analysed using UCSF Chimera version 1.10.2 (Pettersen *et al*., 2004), WinCoot version 0.7.2.1 (Emsley *et al*., 2010), CCP4 suite of programs version 6.3.0 and Phenix version 1.8.2-1309 (Adams *et al*., 2010).

Results of Protein Purification

Overview of purification of *Geobacillus pallidus* RAPc8 NHase samples

Purification of all the NHase samples was followed by the purification of the amidase. The ammonium sulphate precipitation step was omitted from analysis due to high background levels of ammonium sulphate (>20% ammonium sulphate) which interfered with analysis when using SDS-PAGE. No activity was detected during the anion exchange chromatography stage. NHase did not show activity in the presence of 0.025 M TRIS buffer pH 7.2 with 5 mM DTT but regained activity after buffer exchanging into 0.025 M potassium phosphate buffer pH 7.2 with 5 mM DTT. The CFE from NHase expression did not exhibit activity when the cells were sonicated in 0.025 M TRIS buffer pH 7.2 with 5 mM DTT and tested using the hydroxamic acid assay. In addition, for all samples, the pooled and concentrated sample from anion exchange was divided into four quantities each about 330 µl. Each aliquot was then taken to the next step, SEC chromatography and fractionated using 80 fractions. The

fractions corresponding to the amidase were pooled together, concentrated in 0.025 M potassium phosphate buffer pH 7.2 with 5 mM DTT and stored at 193 K. Samples from each step of purification, excluding the ammonium sulphate precipitation step, were analysed using SDS-PAGE (Laemli, 1970). Gel intensities were analysed using Image J (NIH) and Microsoft Excel (Vincent *et al*., 1997; Taylor *et al*., 2013) with added imaging capability using the ChemiDoc™ XRS+ imaging system (BioRad).

Protein Purification Chromatograms and SDS-PAGE Analysis

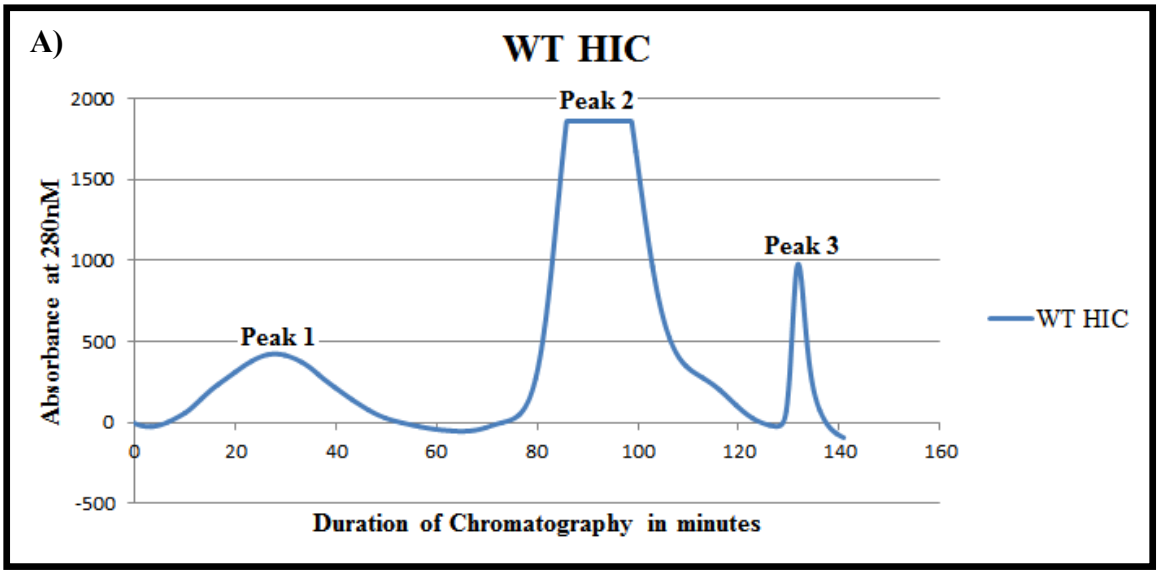

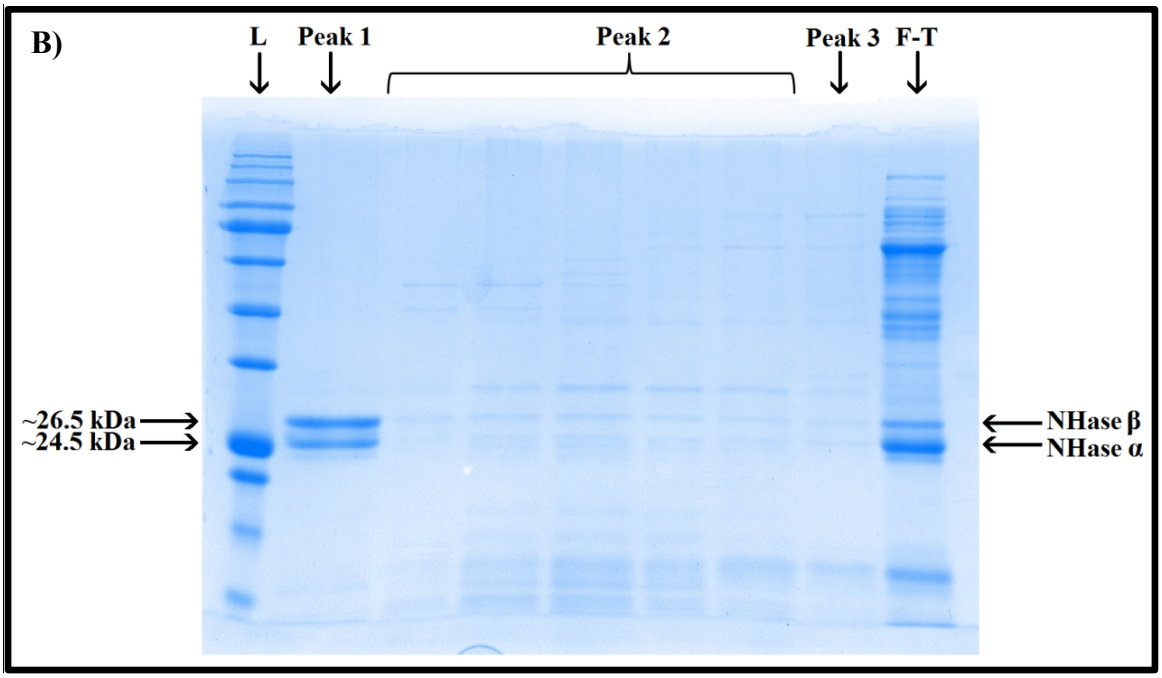

Figure 3.1: A) Phenyl sepharose chromatography elution profile of WT NHase showing multiple peaks (Peak 1, 2 and 3) with elution from 1 M to 0 M ammonium sulphate in 0.05 M potassium phosphate buffer pH 7.2, 5 mM DTT. The graph values are absorbance measurements done at 280 nm. B) The fractions from the phenyl sepharose chromatography purification step from Peak 1, Peak 2, Peak 3, and the flow through were visualized after electrophoresis on 10% SDS-PAGE gel and stained using Coomassie stain. The NHase dimer can be seen as a double band corresponding to 26.5 kDa and 24.5 kDa for the β and the α subunit respectively, the protein molecular weight ladder is labelled as "L" and the flow through fraction is labelled as "F-T". Peak 1 was taken to the next purification step.

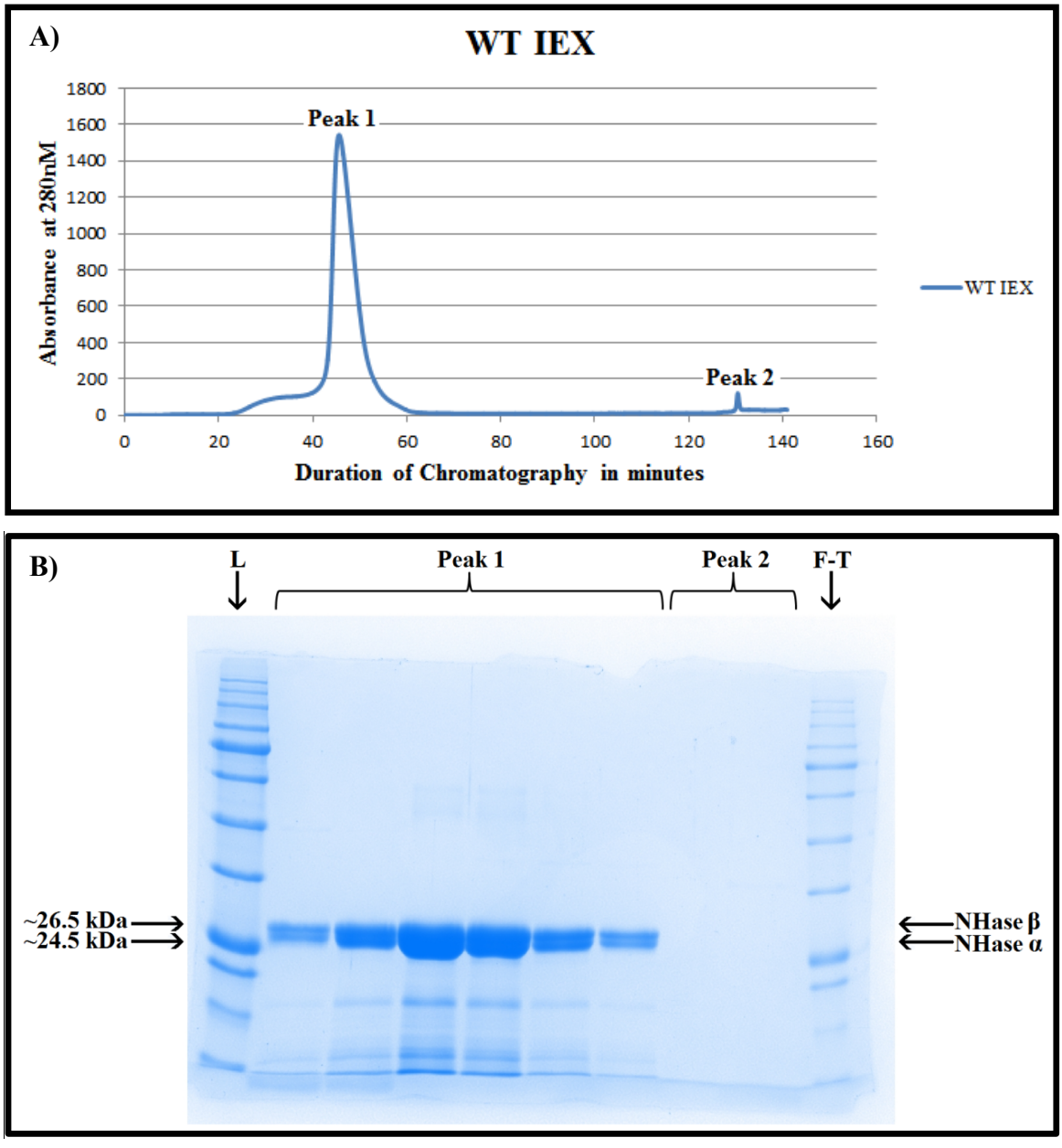

Figure 3.2: A) Anion exchange (IEX) chromatography elution profile of WT NHase from 0 M to 1 M NaCl in 0.025 M potassium phosphate buffer pH 7.2, 5 mM DTT. The graph indicates absorbance at 280 nm with Peak 1 being more prominent than Peak 2. B) Visualization of fractions from Peak 1 and Peak 2 from the anion exchange chromatography purification step and the flow through following electrophoresis on 10% SDS-PAGE gel and staining using Coomassie. The NHase dimer can be seen as a double band corresponding to 26.5 kDa and 24.5 kDa for the β and the α subunit respectively, the flow through fraction is labelled as "F-T" and the protein molecular weight ladder labelled as "L". Peak 1 was taken to the next purification step.

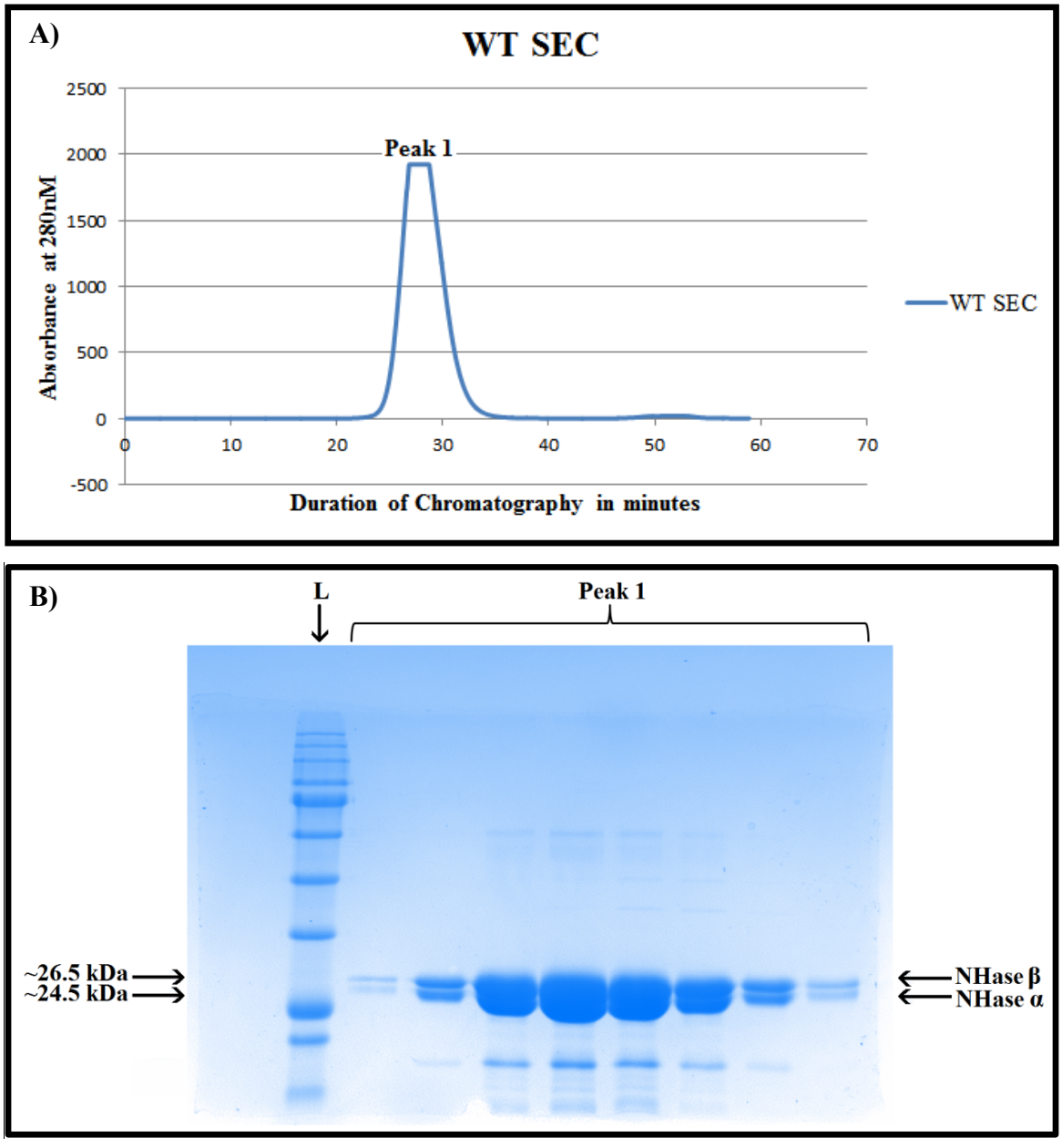

Figure 3.3: A) Size exclusion chromatography elution profile of WT NHase in 0.025 M potassium phosphate buffer pH 7.2, 5 mM DTT showing the absorbance values at 280 nm during elution. B) Visualization of fractions from the SEC chromatography purification step for fractions comprising Peak 1 in fig. 3 A), and the flow through following electrophoresis on 10% SDS-PAGE gel and staining using Coomassie. The protein molecular weight ladder is labelled as "L". The NHase dimer can be seen as a double band corresponding to 26.5 kDa and 24.5 kDa for the β and the α subunit respectively. Peak 1 was used stored at 193 K and used for NHase assays.

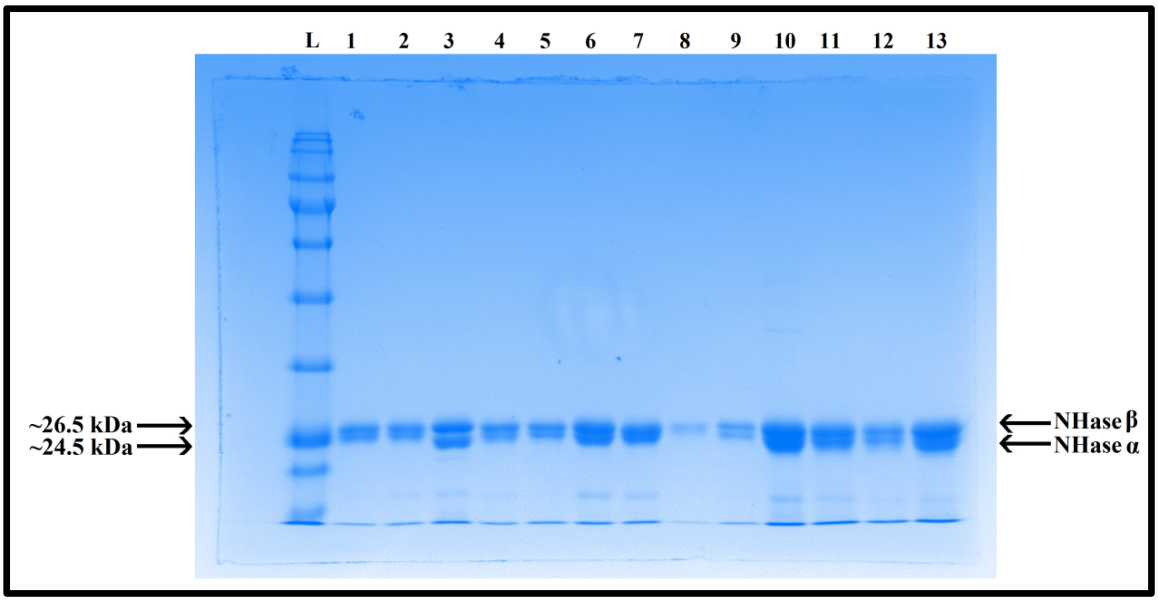

Figure 3.4: Visualization of all purified NHase samples in this study on a 10% SDS-PAGE gel following overnight staining in Coomassie stain. The lane labelled "L" is the protein molecular weight ladder. The lanes labelled as L, 1, 2, 3, 4, 5, 6, 7, 8, 9, 10, 11, 12, 13 represent the protein molecular weight ladder and the samples: WT NHase, 8C, 9E, 9C, βL103S, βY127N, αS169R, βD96E, βM43K, βD167V, αM188V, βF36L and βT150A respectively.

Protein Purification Tables using Densitometry

The purity was calculated using the integrated intensity of the bands corresponding to NHase divided by the integrated intensity resulting from the initial total load after subtracting the background signal. The fraction was then expressed as a percentage. The yield was calculated

by dividing the total protein at each step by the total protein in the initial cell free extract step. Samples from the QHP step were pooled, concentrated and stored in 4 separate aliquots for each construct in 15% glycerol. One aliquot from QHP was carried forward and applied onto SEC using loading volume of ≈330 µl. The total quantity of protein needed for one complete hydroxamic acid assay in a 96 well plate was ≈0.2 mg for each NHase construct. The total volumes for the SEC step were not recorded because not all QHP aliquots were applied onto SEC. Final protein purity was estimated using SDS-PAGE (*fig.* 3.4).

Table 3.1: Purification table for the WT NHase. The ammonium sulphate precipitation and phenyl sepharose chromatography steps eliminated most of the contaminants. Other proteins previously applied on the communal QHP column may have eluted with the NHase

Purification Table for WT NHase						
Fraction Step	**Volume (ml)**	**Concentration (mg/ml)**	**Total Protein (mg)**	**Band Intensity**	**Calculated Purity (%)**	**Yield (%)**
Cell Free Extract	**24**	**9.6**	**230.4**	**34283**	**0**	**100**
20% ammonium sulphate precipitation	**-**	**-**	**-**	**-**	**-**	**-**
Phenyl Sepharose	**44**	**0.9**	**39.6**	**10658**	**98.5**	**17.2**
QHP	**37.5**	**0.8**	**30**	**12241**	**96.6**	**13.0**
SEC	**-**	**5.2**	**-**	**5590**	**99**	-

thus lowering the purity however, this was clarified with SEC. The final estimated purity was 99%.

Purification Table for 9E NHase composite mutant						
Fraction Step	**Volume (ml)**	**Concentration (mg/ml)**	**Total Protein (mg)**	**Band Intensity**	**Calculated Purity (%)**	**Yield (%)**
Cell Free Extract	**35**	**26.2**	**917**	**30138**	**0**	**100**
20% ammonium sulphate precipitation	**-**	**-**	**-**	**-**	**-**	**-**
Phenyl Sepharose	**42.5**	**13.2**	**561**	**30728**	**86.9**	**61.2**
QHP 1	31	6.6	205.0	30693	87.8	-

QHP 2	50	0.9	45	16998	94.4	-
QHP (averaged)	**81**	**3.1**	**250**	**22240**	**91.9**	**27.3**
SEC	**-**	**20.1**	**-**	**9856**	**96.9**	-

Table 3.2: Purification table for the 9E composite mutant NHase. The expression of this construct was the highest albeit with high quantity of unwanted contaminants resulting in a final purity of 96.9%. The multiple QHP steps (QHP1 and QHP2) indicate separate chromatographic steps which were eventually pooled together to form the QHP averaged stage of purification.

Purification Table for 8C NHase composite mutant						
Fraction Step	**Volume (ml)**	**Concentration (mg/ml)**	**Total Protein (mg)**	**Band Intensity**	**Calculated Purity (%)**	**Yield (%)**
Cell Free Extract	**34.5**	**22.2**	**765.9**	**51574**	**0**	**100**
20% ammonium sulphate precipitation	**-**	**-**	**-**	**-**	**-**	**-**
Phenyl Sepharose	**50.5**	**5.2**	**262.6**	**23699**	**90.8**	**23.4**
QHP 1	31	2.1	65.1	23260	91.6	-
QHP 2	50	0.9	45	17791	98.3	-
QHP (averaged)	**81**	**1.4**	**110.1**	**19884**	**95.7**	**14.4**
SEC	**-**	**9.1**	**-**	**4961**	**97.5**	-

Table 3.3: Purification table for the 8C composite mutant NHase. The QHP 1 and QHP 2 chromatographic steps were pooled to form the QHP averaged step which was further clarified using SEC. Final purity was estimated at 97.5%.

Purification Table for 9C NHase composite mutant						
Fraction Step	**Volume (ml)**	**Concentration (mg/ml)**	**Total Protein (mg)**	**Band Intensity**	**Calculated Purity (%)**	**Yield (%)**
Cell Free Extract	**31.5**	**22.4**	**705.6**	**64362**	**0**	**100**
20% ammonium sulphate precipitation	-	-	-	-	-	-
Phenyl Sepharose 1	42.5	1.5	63.8	13962	93.1	-
Phenyl Sepharose 2	41	0.3	12.3	8842	96.4	-
Phenyl Sepharose 3	45	1.4	63	14059	94.3	-
Phenyl Sepharose (averaged)	**128.5**	**1.1**	**139.1**	**12362**	**94.6**	**19.7**
QHP 1	31	0.9	27.9	11643	98.9	-
QHP 2	50	0.2	10	4885	97.3	-
QHP (averaged)	**81**	**0.5**	**37.9**	**7472**	**97.9**	**5.4**
SEC	**-**	**7.2**	**-**	**5315**	**98.3**	-

Table 3.4: Purification table for the 9C composite mutant NHase. This purification utilised multiple chromatographic steps for each stage of purification i.e. Phenyl sepharose 1, 2 and 3 for the HIC stage and QHP 1 and QHP 2 for the IEX stage. Purity was estimated at 98.3%

Purification Table for βD167V NHase mutant						
Fraction Step	**Volume (ml)**	**Concentration (mg/ml)**	**Total Protein (mg)**	**Band Intensity**	**Calculated Purity (%)**	**Yield (%)**
Cell Free Extract	**26**	**26.6**	**691.6**	**113786**	**0**	**100**
20% ammonium sulphate precipitation	-	-	-	-	-	-
Phenyl Sepharose	**44.5**	**10.6**	**471.7**	**32939**	**72.0**	**68.2**
QHP	**37**	**3.2**	**118.4**	**24093**	**91.1**	**17.1**
SEC	-	**24.7**	-	**9730**	**97.8**	-

Table 3.5: Purification table for the βD167V single mutant NHase. The ammonium sulphate precipitation and phenyl sepharose chromatography steps (HIC stage) doing the bulk of the

purification. No multiple chromatographic steps were done for this sample. The final estimated purity attained was 97.8%.

Purification Table for αM188V NHase mutant						
Fraction Step	**Volume (ml)**	**Concentration (mg/ml)**	**Total Protein (mg)**	**Band Intensity**	**Calculated Purity (%)**	**Yield (%)**
Cell Free Extract	**28**	**14.5**	**406**	**101439**	**0**	**100**
20% ammonium sulphate precipitation	**-**	**-**	**-**	**-**	**-**	**-**
Phenyl Sepharose	**39.5**	**4.7**	**186.8**	**23185**	**89.6**	**46.0**
QHP	**44**	**3.6**	**158.4**	**18666**	**93.5**	**39.0**
SEC	**-**	**25**	**-**	**14085**	**94.8**	**-**

Table 3.6: Purification table for the αM188V single mutant NHase. Ammonium sulphate precipitation and HIC took the bulk of contaminants from the protein sample. The final estimated purity was 94.8% without additional chromatographic steps.

Purification Table for βF36L NHase mutant						
Fraction Step	**Volume (ml)**	**Concentration (mg/ml)**	**Total Protein (mg)**	**Band Intensity**	**Calculated Purity (%)**	**Yield (%)**
Cell Free Extract	**30**	**8.2**	**246**	**113317**	**0**	**100**
20% ammonium sulphate precipitation	**-**	**-**	**-**	**-**	**-**	**-**
Phenyl Sepharose	**48**	**4**	**192**	**25667**	**82.8**	**78.0**
QHP	**44**	**3.4**	**149.6**	**24082**	**84.0**	**60.8**
SEC	**-**	**30.9**	**-**	**13311**	**99.0**	**-**

Table 3.7: Purification table for the βF36L single mutant NHase. Multiple chromatographic steps were not done for this sample. The final estimated purity was 99%.

Purification Table for βT150A NHase mutant						
Fraction Step	**Volume (ml)**	**Concentration (mg/ml)**	**Total Protein (mg)**	**Band Intensity**	**Calculated Purity (%)**	**Yield (%)**
Cell Free Extract	**32**	**6**	**192**	**124333**	**0**	**100**
20% ammonium sulphate precipitation	**-**	**-**	**-**	**-**	**-**	**-**
Phenyl Sepharose 1	42	3.9	163.8	14442	94.6	-
Phenyl Sepharose 2	29	3.9	113.1	29794	48.0	-
Phenyl Sepharose (averaged)	**71**	**3.9**	**143.1**	**20712**	**75.6**	**74.5**
QHP 1	31	1.1	34.1	22320	88.9	-
QHP 2	18.5	1	18.5	11196	89.4	-
QHP (averaged)	**49.5**	**1.1**	**52.6**	**18163**	**89.1**	**27.4**
SEC	**-**	**17.9**	**-**	**5288**	**98.8**	-

Table 3.8: Purification table for the βT150A single mutant NHase. Multiple chromatographic steps, phenyl sepharose 1 and 2 for HIC and QHP 1 and 2 for IEX were done for this sample. The final estimated purity was at 98.8%.

Purification Table for αS169R NHase mutant						
Fraction Step	**Volume (ml)**	**Concentration (mg/ml)**	**Total Protein (mg)**	**Band Intensity**	**Calculated Purity (%)**	**Yield (%)**
Cell Free Extract	**30**	**5.5**	**165**	**57656**	**0**	**100**
20% ammonium sulphate precipitation	**-**	**-**	**-**	**-**	**-**	**-**
Phenyl Sepharose 1	99	0.9	89.1	12519	92.9	-
Phenyl Sepharose 2	6.5	0.9	5.85	11232	94.5	-
Phenyl Sepharose (averaged)	**105.5**	**0.9**	**95.0**	**12440**	**93.0**	**57.5**
QHP 1	31	1.5	46.5	14174	97.2	-
QHP 2	62.5	0.3	18.8	4625.8	92.7	-
QHP (averaged)	**93.5**	**0.7**	**65.25**	**7792**	**94.1**	**39.5**
SEC	**-**	**9.5**	**-**	**8629**	**95.4**	-

Table 3.9: Purification table for the αS169R single mutant NHase. Multiple chromatographic steps were utilised at each stage of purification i.e. HIC used 2 phenyl sepharose chromatographic steps while IEX used two QHP chromatographic steps. Final estimated purity was 95.4%.

Purification Table for βD96E NHase mutant						
Fraction Step	**Volume (ml)**	**Concentration (mg/ml)**	**Total Protein (mg)**	**Band Intensity**	**Calculated Purity (%)**	**Yield (%)**
Cell Free Extract	**24**	**10.7**	**256.8**	**51826**	**0**	**100**
20% ammonium sulphate precipitation	**-**	**-**	**-**	**-**	**-**	**-**
Phenyl Sepharose	**40**	**0.8**	**32**	**13105**	**97.9**	**12.5**
QHP 1	12.5	1	12.5	6508	98.5	-
QHP 2	12.5	0.3	3.75	5163	96.3	-
QHP 3	12.5	1	12.5	14064	97.0	-
QHP (averaged)	**37.5**	**0.8**	**28.8**	**8578**	**97.3**	**11.2**
SEC	**-**	**2.4**	**-**	**1169**	**99**	-

Table 3.10: Purification table for the βD96E single mutant NHase. The IEX stage of purification utilised multiple chromatographic steps i.e. QHP 1, 2 and 3. Final estimated purity was 99%.

Purification Table for βM43K NHase mutant						
Fraction Step	**Volume (ml)**	**Concentration (mg/ml)**	**Total Protein (mg)**	**Band Intensity**	**Calculated Purity (%)**	**Yield (%)**
Cell Free Extract	**27.5**	**9.3**	**255.8**	**39130**	**0**	**100**
20% ammonium sulphate precipitation	**-**	**-**	**-**	**-**	**-**	**-**
Phenyl Sepharose 1	42.5	0.9	38.3	10579	98.8	-
Phenyl Sepharose 2	39.5	0.5	19.8	6138	91.6	-
Phenyl Sepharose (averaged)	**82**	**0.7**	**58**	**8440**	**95.3**	**22.7**
QHP 1	37.5	0.8	30	7817	98.9	-
QHP 2	37.5	0.3	11.25	3775	100	-
QHP (averaged)	**75**	**0.6**	**41.25**	**5796**	**99.5**	**16.1**
SEC	**-**	**3.2**	**-**	**3085**	**99**	**-**

Table 3.11: Purification table for the βM43K single mutant NHase. Multiple purification steps were used at each stage of purification with the HIC stage having two phenyl sepharose steps and the IEX stage having two QHP steps. The final estimated purity was 99%.

Purification Table for βL103S NHase mutant						
Fraction Step	**Volume (ml)**	**Concentration (mg/ml)**	**Total Protein (mg)**	**Band Intensity**	**Calculated Purity (%)**	**Yield (%)**
Cell Free Extract	**32**	**23.2**	**742.4**	**108471**	**0**	**100**
20% ammonium sulphate precipitation	**-**	**-**	**-**	**-**	**-**	**-**
Phenyl Sepharose	**42**	**3.2**	**134.4**	**22192**	**95.7**	**18.1**
QHP 1	49.5	1.3	64.35	19404	92.4	-
QHP 2	32	0.4	12.8	6169	91.8	-
QHP (averaged)	**81.5**	**0.9**	**77.2**	**14208**	**92.2**	**10.4**
SEC	**-**	**16**	**-**	**4923**	**98.6**	-

Table 3.12: Purification table for the βL103S single mutant NHase. The HIC stage utilised two phenyl sepharose chromatographic steps. The ammonium sulphate and phenyl sepharose chromatography steps attained a purity of 95% however, in the pursuit of attaining higher purity, other contaminating proteins from a previous chromatographic step may have eluted during the QHP chromatography step resulting in a decreased purity which was then corrected using SEC. The final estimated purity was 98.6%.

Purification Table for βY127N NHase mutant						
Fraction Step	**Volume (ml)**	**Concentration (mg/ml)**	**Total Protein (mg)**	**Band Intensity**	**Calculated Purity (%)**	**Yield (%)**
Cell Free Extract	**32**	**18.6**	**595.2**	**117107**	**0**	**100**
20% ammonium sulphate precipitation	**-**	**-**	**-**	**-**	**-**	**-**
Phenyl Sepharose	**45**	**2.9**	**130.5**	**18926**	**92.4**	**21.9**
QHP 1	49.5	0.3	14.9	14725	96.4	-
QHP 2	32	0.8	25.6	4700	95.0	-
QHP (averaged)	**81.5**	**0.5**	**40.4**	**10789**	**95.9**	**6.8**
SEC	**-**	**10.5**	**-**	**10382**	**95.0**	-

Table 3.13: Purification table for the βY127N single mutant NHase. The HIC stage utilised two phenyl sepharose chromatography steps. This stage together with the ammonium sulphate precipitation stage attained an estimated purity of 92.4% and the final estimated purity was at 95% with a possibility of a slight contamination from the column beds resulting from a previous chromatographic step.

Purification table of *Geobacillus pallidus* RAPc8 Amidase:						
STEP	**Total protein**	**Total activity**	**Specific activity**	**Yield %**	**Fold purification**	**Purity**
CFE	**468.0**	**21243.2**	**45.4**	**100.0**	**1.0**	**0.0**
Heat Treatment	**191.4**	**66761.5**	**348.9**	**40.9**	**7.7**	**11.8**
20 % Ammonium sulphate precipitation	**-**	**-**	**-**	**-**	**-**	**-**
Phenyl Sepharose	**32.8**	**(71942.5)**	**2194.4**	**7.0**	**48.3**	**74.1**
QHP	**19.0**	**52068.0**	**2743.7**	**4.1**	**60.5**	**92.6**
SEC	**7.1**	**20999.6**	**2963.2**	**1.5**	**65.3**	**99**

Table 3.14: Purification table for the WT amidase. Multiple full scale purifications were done for this amidase to amass sufficient amidase for the hydroxamic acid assay. The activity measurements were done using the indophenol blue assay and the measured activity indicated

in parenthesis was done after dialysis thus contained background quantities of dissolved ammonia. No assays were done on the ammonium sulphate precipitation step due to high levels (1.7 M) of ammonium sulphate in the amidase solution. The final attained purity was 99%.

CHAPTER 4:

BIOCHEMICAL CHARACTERIZATION AND THERMAL INACTIVATION

Introduction

Thermal denaturation of NHase has been attempted previously using CFE. In the course of thermal unfolding, proteins have been proposed to undergo a two-state model of thermal unfolding, often characterized by a decreasing parameter representative of active properly folded protein. In this study, the decreasing parameter was the proportion of residual activity measured via absorbance following detection of an acyl transfer assay. The observed thermal denaturation of proteins can be represented graphically by plotting the free energy state of the protein against temperature.

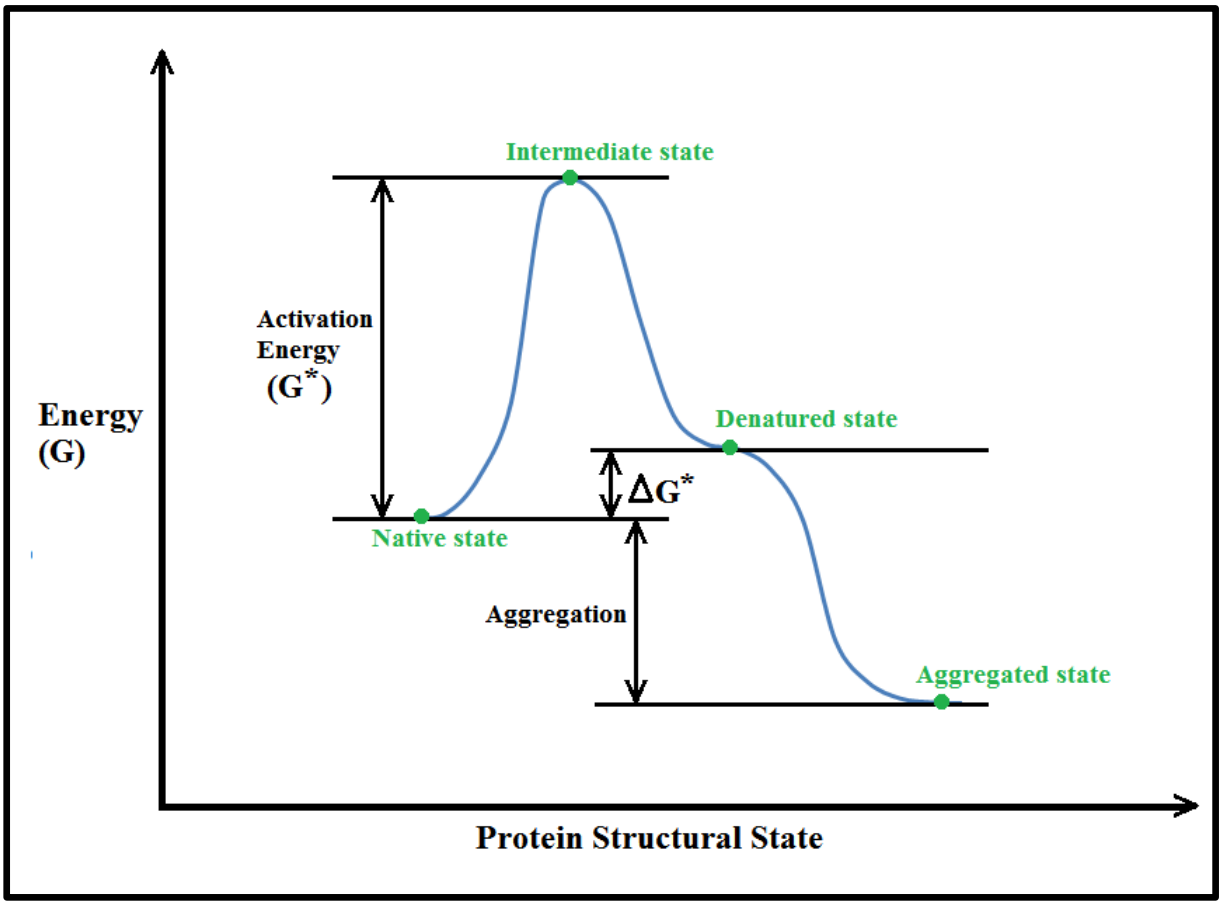

Figure 4.1: The curve representing the change in free energy of a molecule as it transits from the folded state to its unfolded state following provision of energy to the folded molecule (Bischof *et al*., 2006). As energy is supplied to the molecule, the structure unfolds as an increasing number of interactions are broken until it reaches the peak of the intermediate state then onwards to the denatured state and finally to the aggregated state. The energy of activation of key interest in this study is the activation energy, G^*.

The thermal unfolding of proteins can be described using the Arrhenius equation where by the relationship between temperature in Kelvin and the rate of decrease of active protein is represented as:

$$K = Ae^{-(\frac{E}{RT})} \qquad \text{(Equation: 3)}$$

Taking the natural logarithm on both sides of the equation gives:

$$\ln(K) = -\frac{E}{RT} + \ln(A) \qquad \text{(Equation: 4)}$$

Rearranging to make E the subject of the formula gives:

$$E = RT(\ln(K) + \ln(A)) \qquad \text{(Equation: 5)}$$

The E represents the activation energy while K represents the rate of deactivation. The change in energy ΔG^* required to thermally unfold a molecule is represented by "E" while the difference in ΔG^* between any two populations of molecules under comparison gives the amount of energy that each respective population requires to be denatured by heat. Thus when comparing the WT protein to a mutant protein, the difference in energy required to thermally unfold the population of mutant protein molecules compared to the WT population is given by:

$$\Delta\Delta G^* = \Delta G^*_{wt} - \Delta G^*_{mut} \qquad \text{(Equation: 6)}$$

Thermal denaturation previously proposed to follow a two-state model where a specific protein will unfold from its folded state to an unfolded state without any stable intermediate state (scheme 4.1). This model has two rate constants that describe the forward rate of thermal unfolding and the reverse rate of folding back to the folded state from the unfolded state. The ΔG^* for this model is calculated using equation (5) with K being the overall rate of unfolding from the folded to unfolded state.

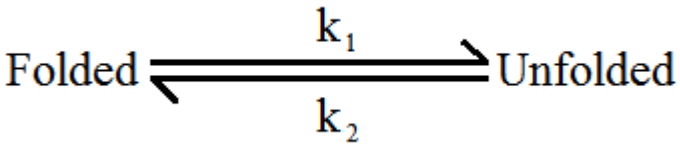

Scheme 4.1: The thermal unfolding of a protein from its folded to unfolded state without a partially unfolded intermediate step.

$$\Delta G^* = -RT\ln k \qquad \text{(Equation: 7)}$$

Where: $k=k_1/k_2$

R=the universal gas constant 8.31446 kJ/mol/Kelvin

T=the temperature in kelvin

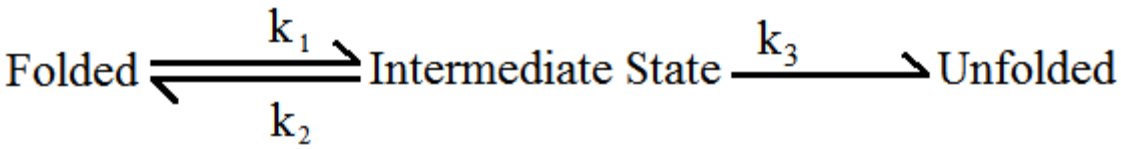

Scheme 4.2: The thermal unfolding of a protein molecule that has a stable intermediate partially unfolded state. The overall rate of unfolding, k, is given by: $k=(k_1*k_3)/(k_2+k_3)$ taking into account all three rates k1, k2 and k3, according to Sterner and Liebel, (2001).

$$y = y_0 + A * \exp(-\alpha x) \qquad \text{(Equation: 8)}$$

Where: y=the measured parameter (absorbance)

y_0=a constant that accounts for the baseline

α=the rate of decrease

x=the varying term of measurement e.g. time

A=constant describing the magnitude of the exponential decrease of exp(-αx).

This has been criticized by Aymard and Belarbi, (2000) and Sterner and Liebl, (2001) as being applicable to small proteins with a single domain but not for large multi-domain proteins. For larger proteins, both authors proposed that an additional intermediate state may be present (Scheme: 4.2) and the former suggested multiple intermediate states may be present each with its respective forward and reverse rates to the irreversible unfolded state and to the folded state respectively. In the event of one intermediate state being present, the measured parameter (which in our case is absorbance resulting from catalysis) depicting the thermal denaturation would follow an exponential decrease representing a transition from the folded state to intermediate and finally to the unfolded state. An additional term, y_o, added to the exponent term would account for the shift in baseline values as the absorbance approached baseline (equation 6).

In the event of having mixed populations of thermally unfolding proteins, each protein would have its exponential rate of decrease and the total observed decrease would be a sum of the individual rates for each component in the population in addition to the y_o term to account for the baseline (equation 7). Thus the bi-exponetial equation governing the observed decreasing sum of rates of two proteins in the same thermal unfolding environment would be as shown below:

$$y = y_0 + \mathrm{A} * e\exp(-\alpha x) + \mathrm{B} * e\exp(-\beta x) \quad \text{(Equation: 9)}$$

The fitting of exponential equations to data has been shown to describe thermal denaturation better than linear fits by Aymard and Belarbi, (2000) resulting in near perfect R squared values. The results presented herein utilised the single exponential equation to fit the data (equation 6). Each enzyme population that is unfolding from the mixture of intermediate states is represented by a decreasing exponential term whose rate of decrease is the "-a" term with progressive increases in heat treatment represented by the "x" term in the above equation.

Results

In-silico analysis of NHase and Amidase parameters:

NHase and Amidase Protein Parameters Determined *In-Silico*			
Sample	**Computed Molecular Weight**	**Extinction coefficient**	**Number of amino acids**
NHase α subunit	24.575 kDa	36440	216
NHase β subunit	26.416 kDa	42860	229
Amidase	38.596 kDa	56840	348

Table 4.1: The NHase and amidase protein parameters determined using the online tool ExPASy available at: http://web.expasy.org/protparam/ using the WT NHase sequence as input. The NHase β subunit has a larger molecular weight of ≈26.4 kDa compared to the α subunit which is at ≈24.6 kDa. The amidase has a molecular weight of ≈38.6 kDa. The summed extinction coefficient representing a tetramer with two α and two β subunits is used when calculating the protein concentration using the absorbance at 280 nm.

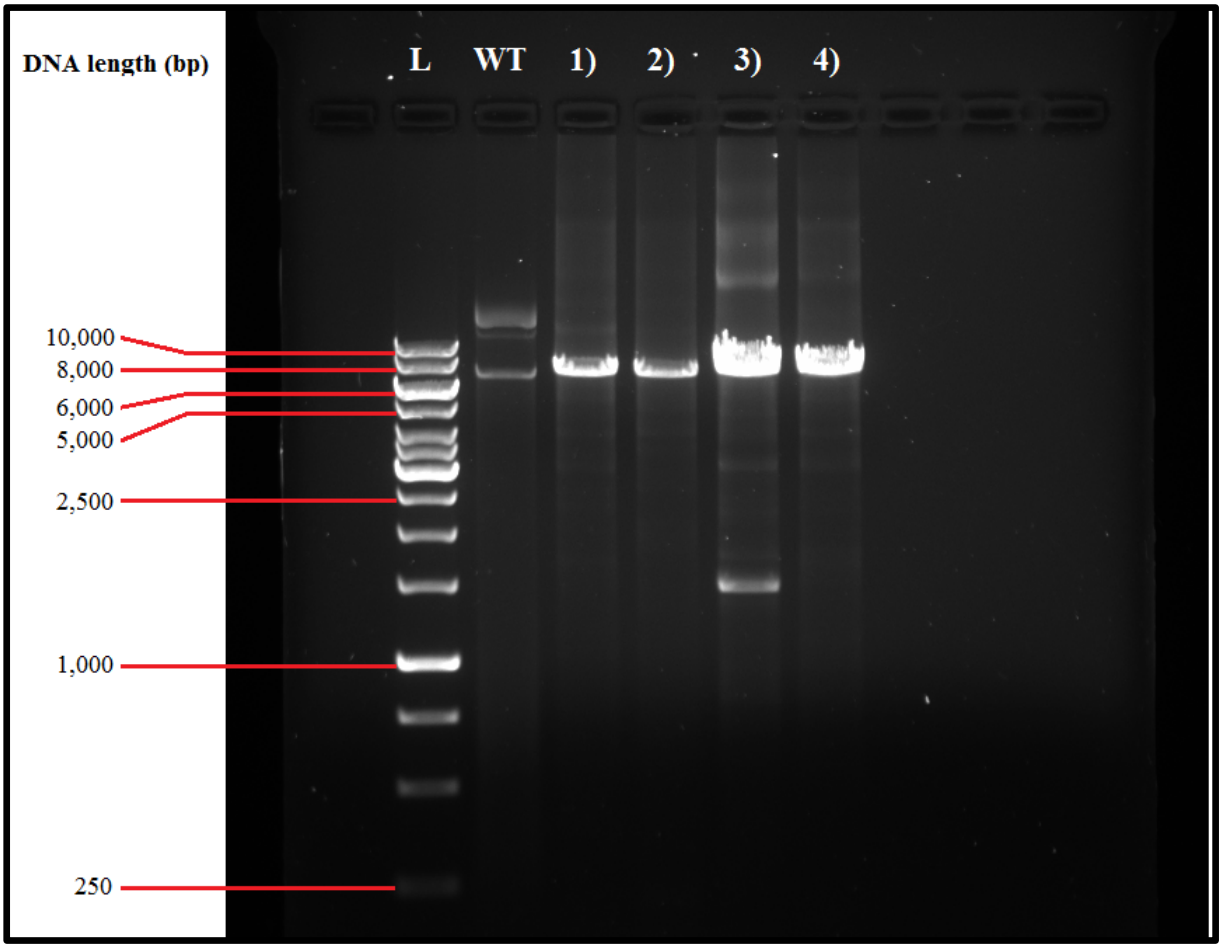

Figure 4.2: A 1% agarose gel for visualization of the SDM-PCR product from four NHase mutants. The lanes are labelled as L, WT, 1), 2), 3) and 4) representing the 1 kB ladder, the WT, βD167V, βF36L αM188V and βT150A NHase samples respectively. The molecular weight of the bands closely corresponds to the construct size of 7176 bp. The circular WT plasmid was electrophoresed to check if the sample had not degraded after storage in type 1 water at 253 K. If so, long indistinct smears would be observed along the lane instead of distinct bands corresponding to the correct molecular mass.

Protein determination standard curve using Bradford Assay

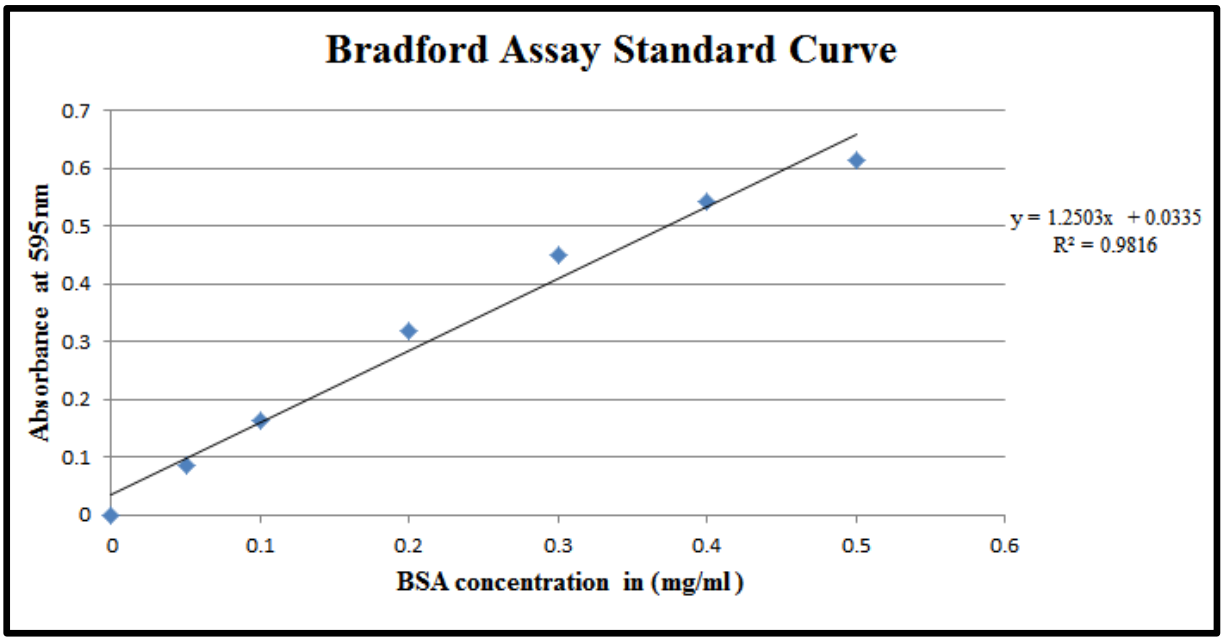

Figure 4.3: A standard curve for the Bradford assay plotting the measured absorbance at 595 nm against protein concentration ranging from 0 mg/ml to 0.5 mg/ml of BSA prepared in 0.025 M potassium phosphate buffer pH 7.2, 5 mM DTT. The linear equation describing the data is shown on the right hand side of the graph with an R squared value >0.98.

Suggestion of expression of NHase WT and mutants using SDS-PAGE

This was done using each NHase sample comparing the pre- and post-induction expression of NHase using IPTG at 0.4 mM concentration.

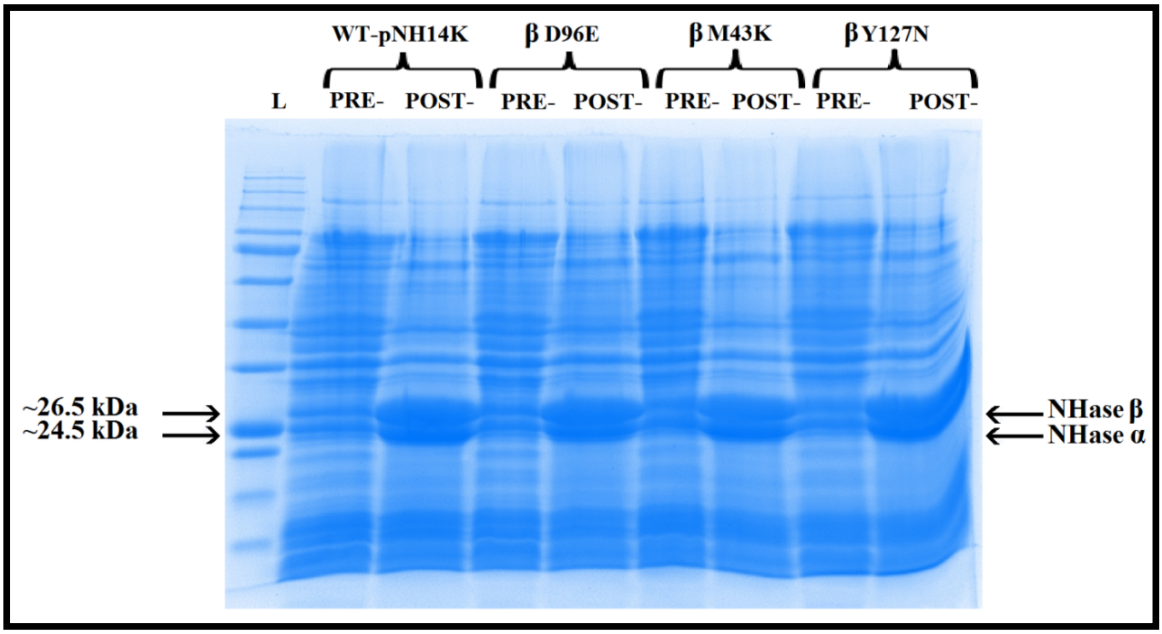

Figure 4.4: Visualization of a 10% SDS-PAGE gel showing the differences between pre- and post- induction for the samples: WT NHase, βD96E, βM43K and βY127N. The two bands indicated with arrows at approximately 26.5 kDa and 24.5 kDa represent the NHase β and α subunits respectively. The lane loaded with the protein ladder is indicated with "L".

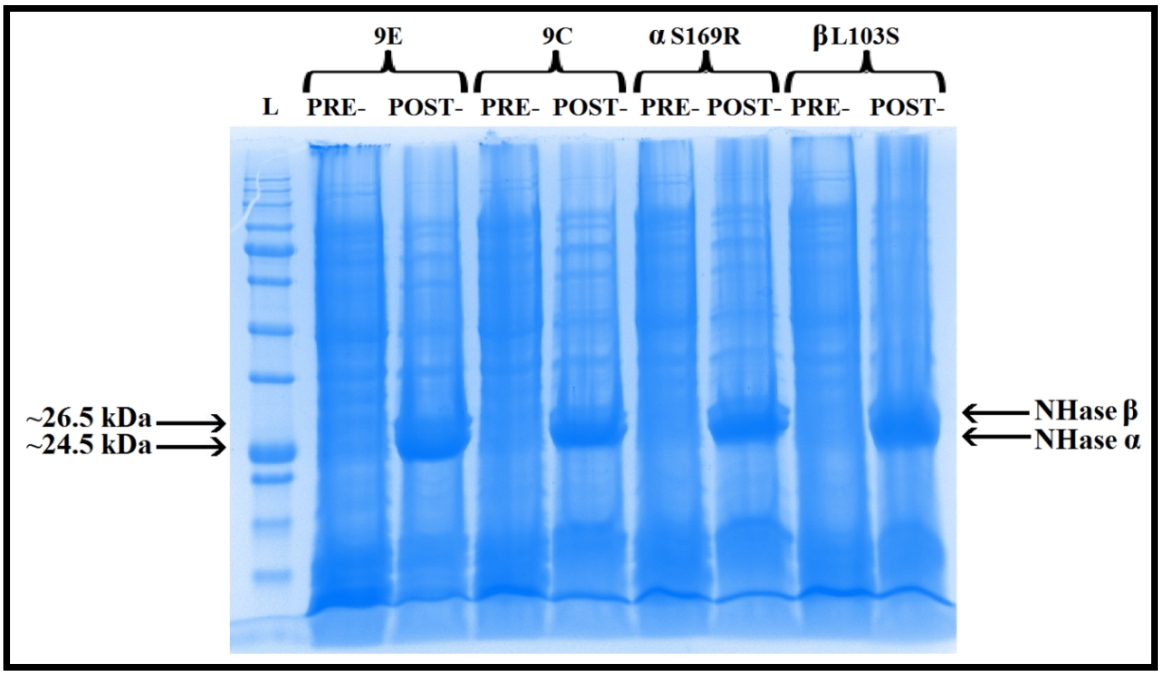

Figure 4.5: An SDS-PAGE gel showing the differences between pre- and post- induction for the samples: 9E, 9C, αS169R and βL103S. The two bands indicated with arrows at

approximately 26.5 kDa and 24.5 kDa represent the NHase β and α subunits respectively. The lane loaded with the protein ladder is indicated with "L".

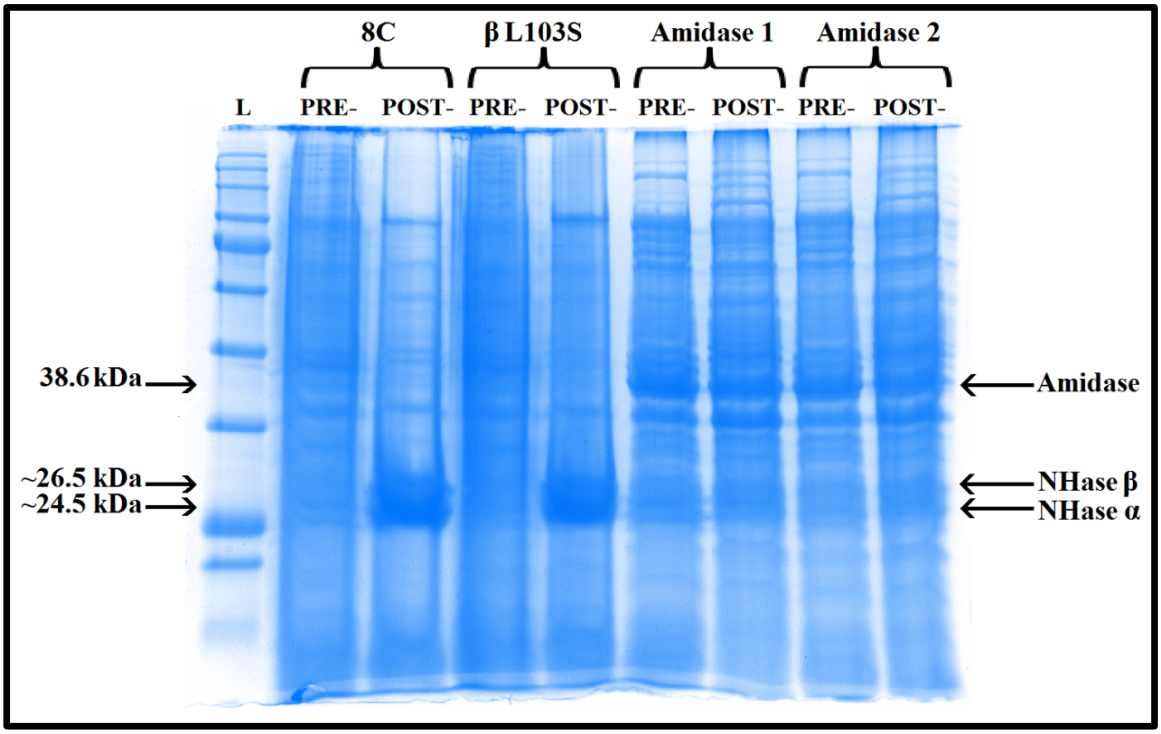

Figure 4.6: An SDS-PAGE gel showing the differences between pre- and post- induction for the samples: 8C, βL103S and two amidase expressions. The pre- and post- induction amidase bands seem similar due to dilution of the post-induction amidase samples. The banding pattern differs due to the use of expression strains from different suppliers. The two bands indicated with arrows at approximately 26.5 kDa and 24.5 kDa represent the NHase β and α subunits respectively while the amidase band corresponds to approximately 38.6 kDa. The lane loaded with the protein ladder is indicated with "L".

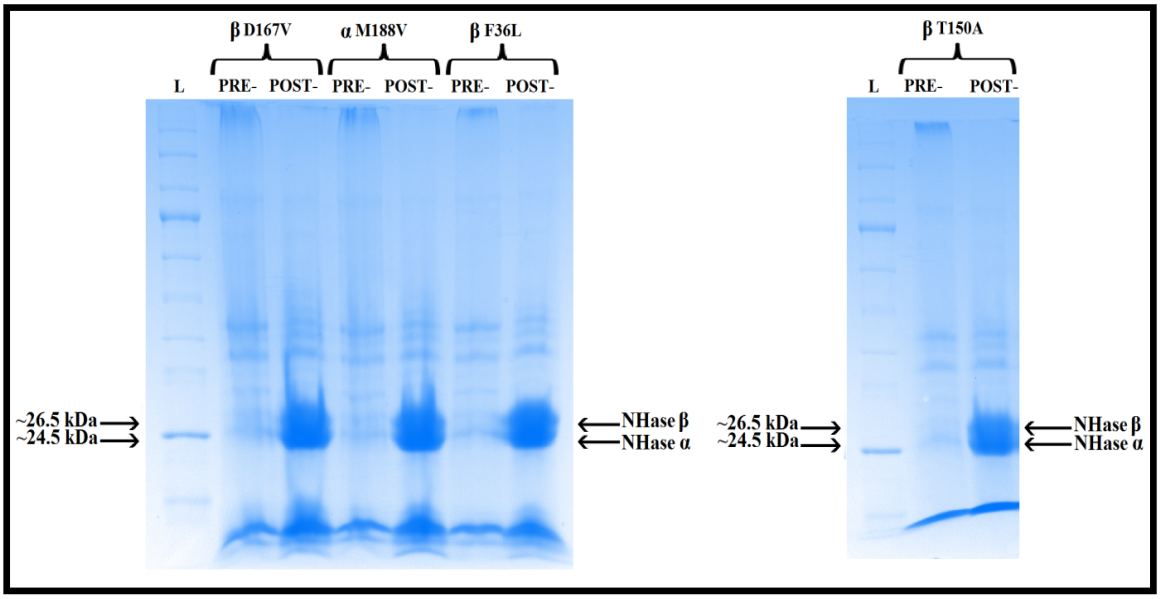

Figure 4.7: An SDS-PAGE gel showing the differences between pre- and post- induction for the samples: βD167V, αM188V, βF36L and βT150A. The two bands indicated with arrows at approximately 26.5 kDa and 24.5 kDa represent the NHase β and α subunits respectively. The lane loaded with the protein ladder is indicated with "L".

Optimisation of the Hydroxamic Acid Assay

Optimisation of Amidase Catalysed Acyl Transfer

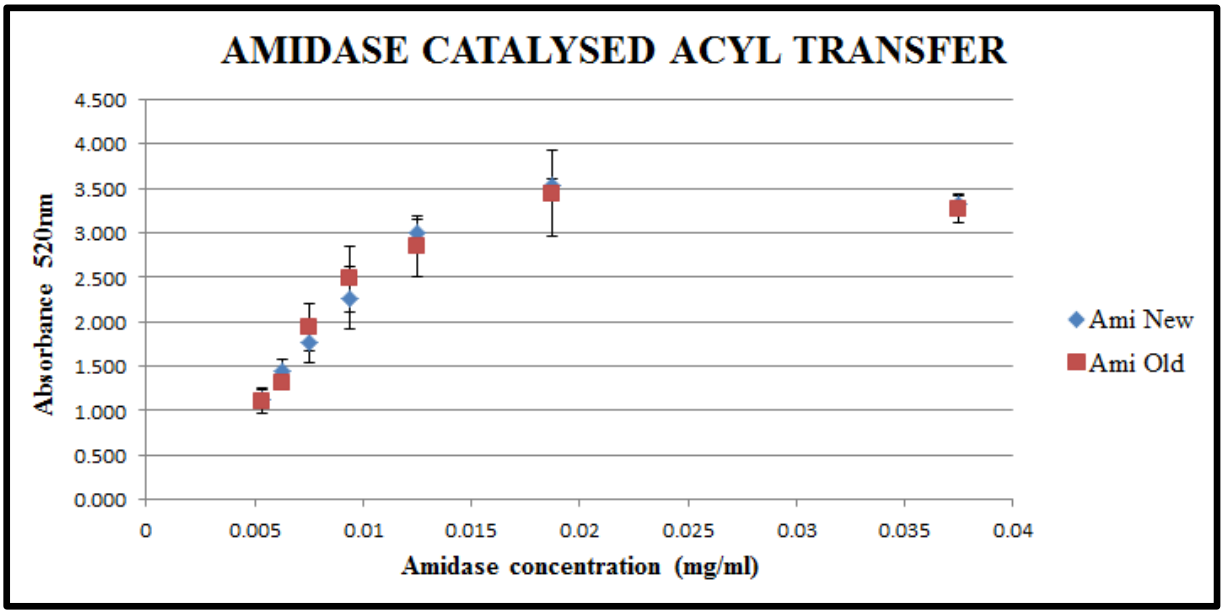

Figure 4.8: A graph depicting acyl transfer by amidase using acetamide and hydroxylamine as a substrate. The final concentration of amidase in the reaction ranged from 0.05 to 0.6 mg/ml and the acetamide concentration was 50 mM in 0.025 M potassium phosphate buffer

pH 7.2, 5 mM DTT at the start of all the reactions at each concentration. The incubation period was 30 minutes at 310 K. The amidase profile plotted in red represents the catalysis of a previously purified and stored *G. pallidus* RAPc8 amidase that had been stored at 193 K for 3 years. The catalysis profile of another amidase sample, which was purified and stored using the same purification strategy as the previous amidase sample, is plotted in blue. The rates of catalysis are identical considering the experimental error. A final amidase concentration of ≥0.02 mg/ml in a 160 µl reaction is required for complete acyl transfer at 310 K within 30 minutes

Confirmation of nitrile catalysis by NHase

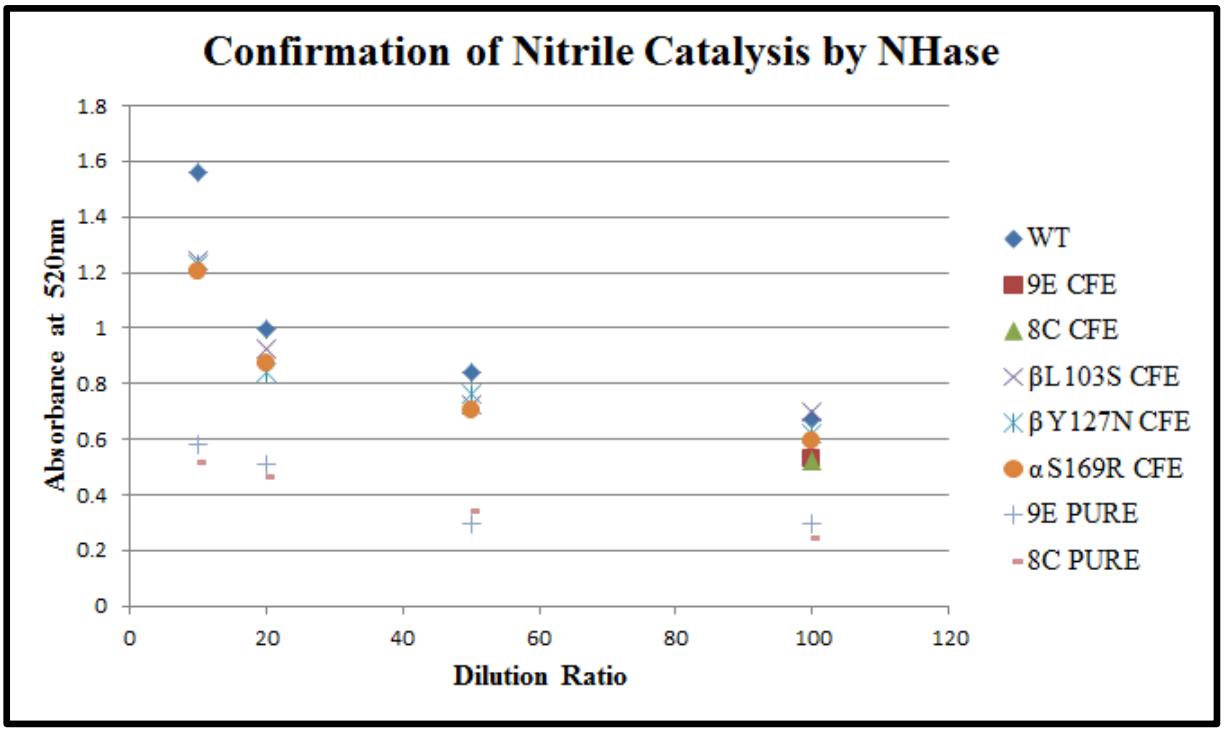

Figure 4.9: Nitrile catalysis exhibited by different NHase samples. The samples selected were: the WT NHase, two composite: mutants 9E and 8C, and three single single mutants: βL103S, βY127N and αS169R. This was tested using acrylonitrile at a final concentration of 50 mM and using different concentrations of NHase using CFE and purified samples to show that the expressed NHases catalysed the nitriles. The assay used was the hydroxamic acid assay.

	DILUTION RATIO			
SAMPLE	**10**	**20**	**50**	**100**
WT NHase CFE	1.6	1	0.8	0.7
9E CFE	-	-	-	0.5
8C CFE	-	-	-	0.5
βL103S CFE	1.2	0.9	0.7	0.7
βY127N CFE	1.2	0.8	0.7	0.6
αS169R CFE	1.2	0.9	0.7	0.6
9E PURE	0.6	0.5	0.3	0.3
8C PURE	0.5	0.5	0.3	0.3

Table 4.2: The observed absorbance values using the hydroxamic acid assay for confirmation of nitrile catalysis by different NHase samples: both cell free extract and purified samples. The assay used was the hydroxamic acid assay.

Determination of Stoichiometry of the Amidase Catalysed Acyl Transfer

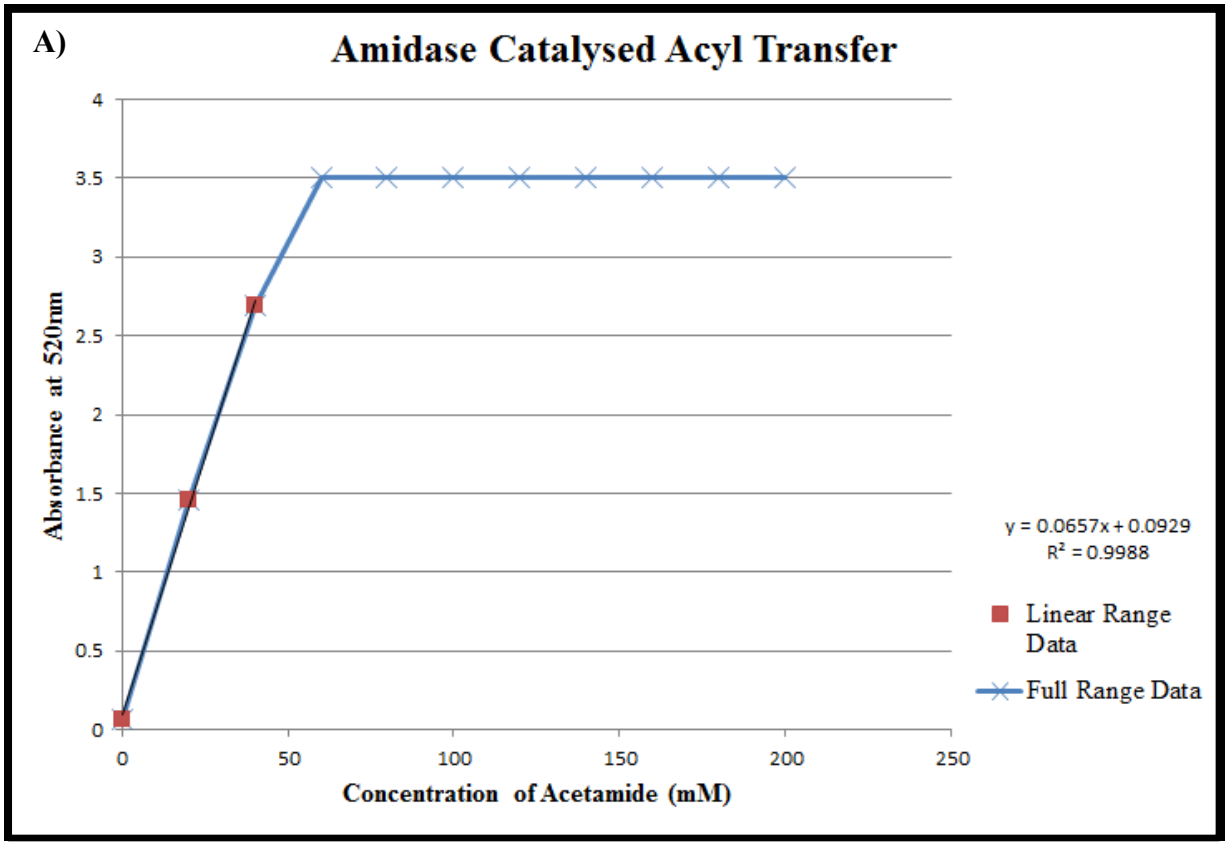

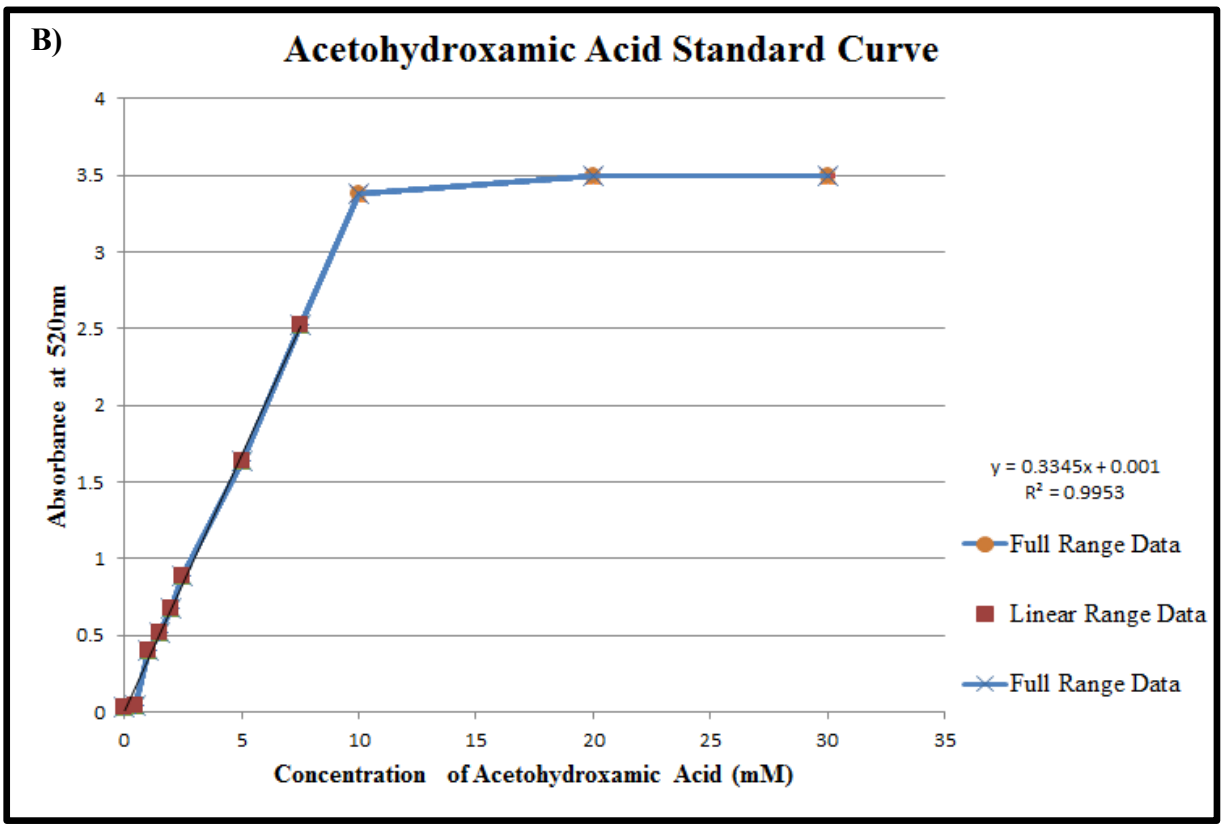

Figure 4.10: A) The catalysis of amidase using the final concentration of ≈0.02 mg/ml testing the substrate concentration from 0 to 200 mM acetamide. B) A standard curve for acetohydroxamic acid ranging from 0 to 100 mM. The quantity of detection reagent (acidic $FeCl_3$) added to both was identical. The linear range for the amidase catalysed acyl transfer was from 0 mM to 50 mM acetamide and the linear range for acetohydroxamic acid was from 0 mM to 10 mM. All substrates and enzyme concentrations were made in potassium phosphate buffer pH 7.2, 5 mM DTT.

Optimisation of Catalysis by NHase

Optimisation of the NHase Incubation Temperature

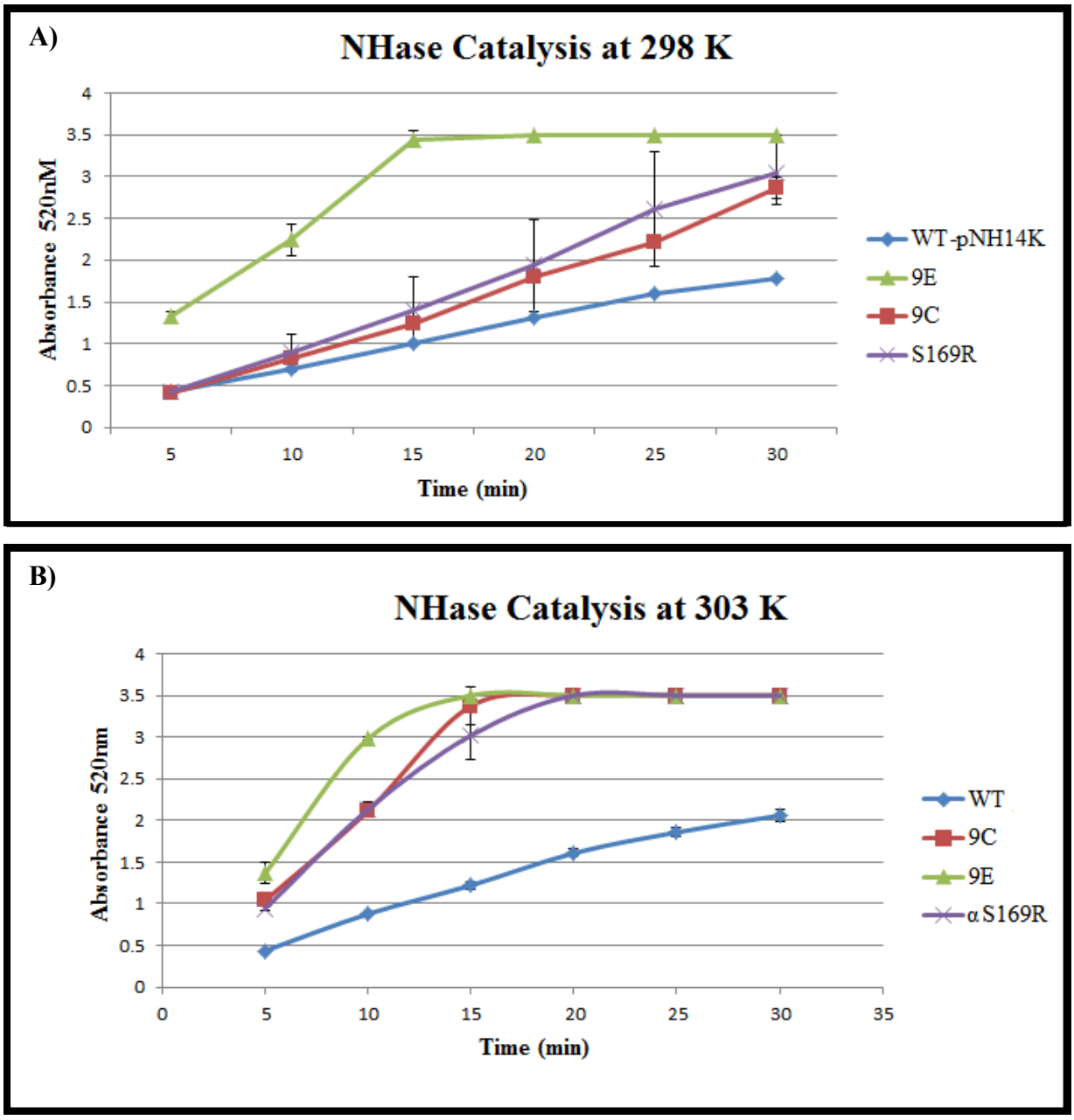

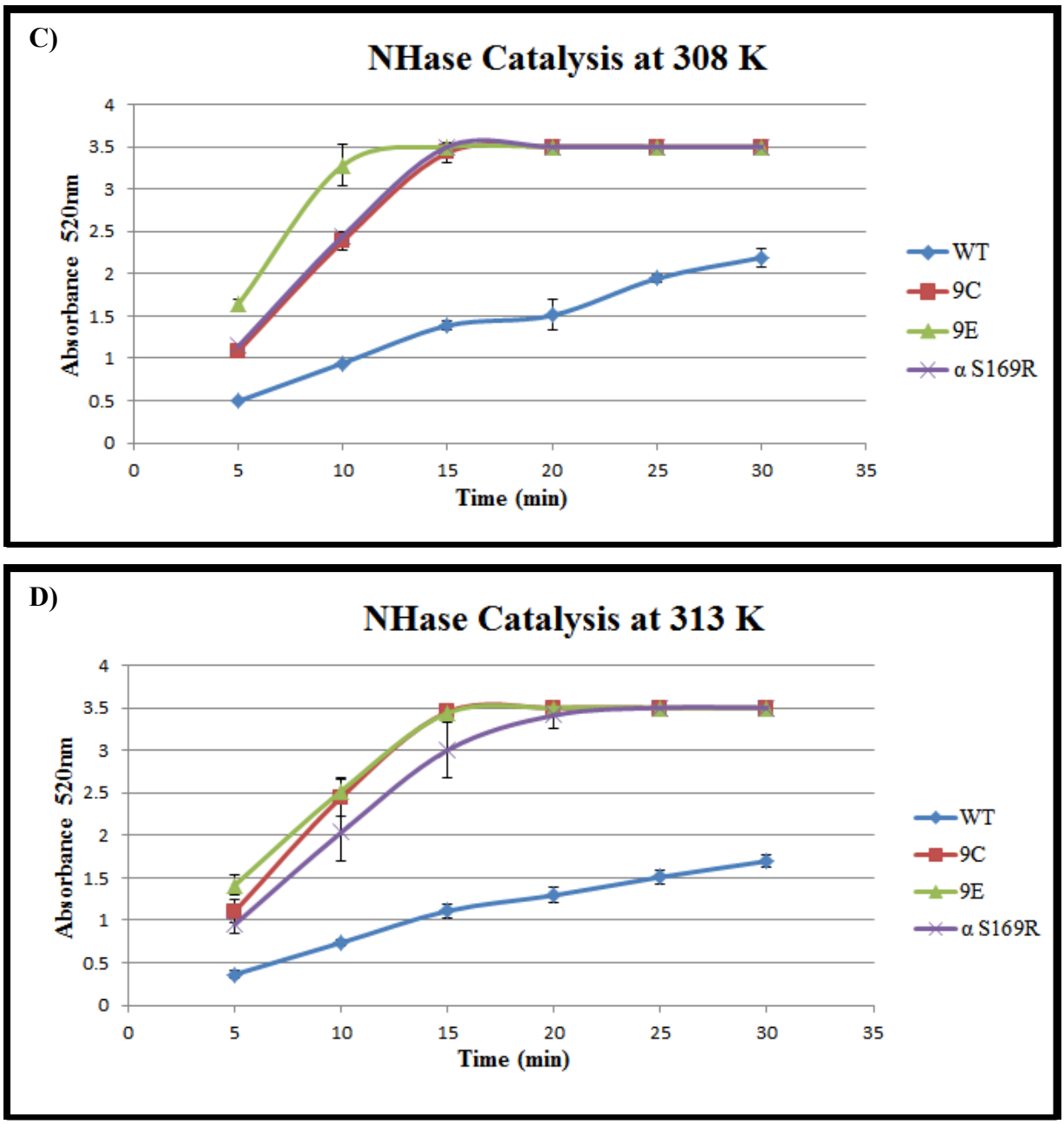

Figure 4.11: Catalysis by different NHase samples as a function of time. Graph A) shows catalysis at 298 K; graph B) shows catalysis at 303 K; graph C) shows catalysis 308 K and graph D) shows catalysis at 313 K, with all assays done over a period of 30 minutes. At the time period between 5 and 15 minutes, the catalysis is still within the linear range using acetamide as the acyl donor in all reactions following catalysis of 50 mM acetonitrile by NHase at equal protein concentration of 0.05 mg/ml.

Optimisation of the NHase Duration of Catalysis

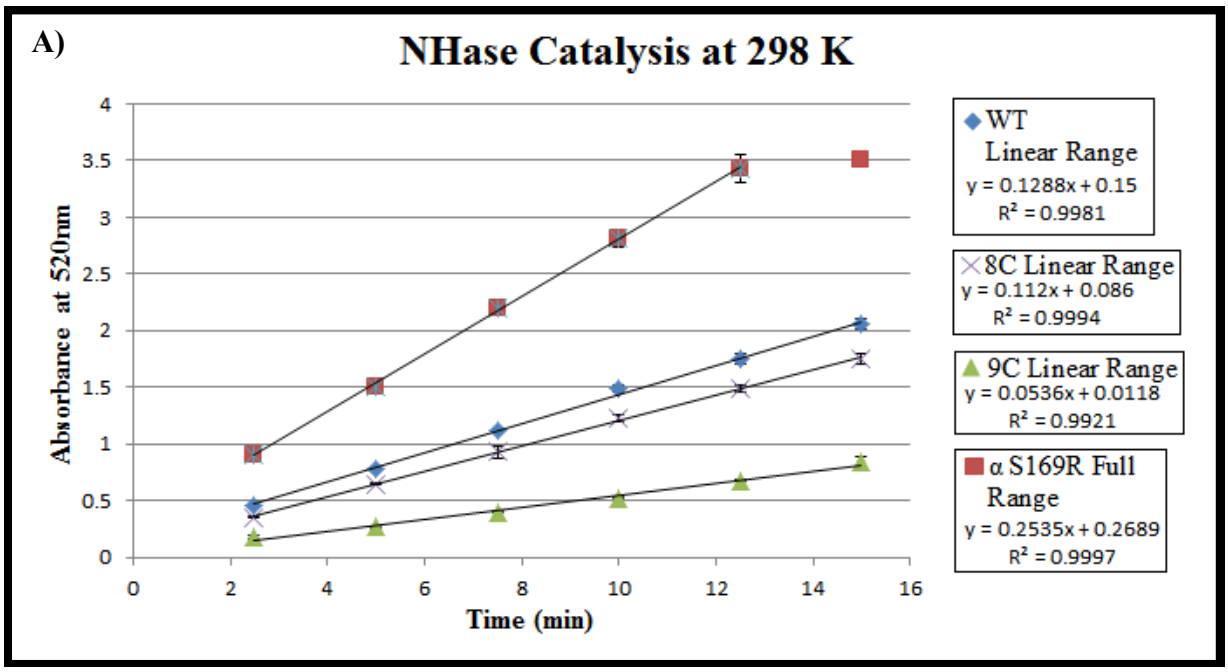

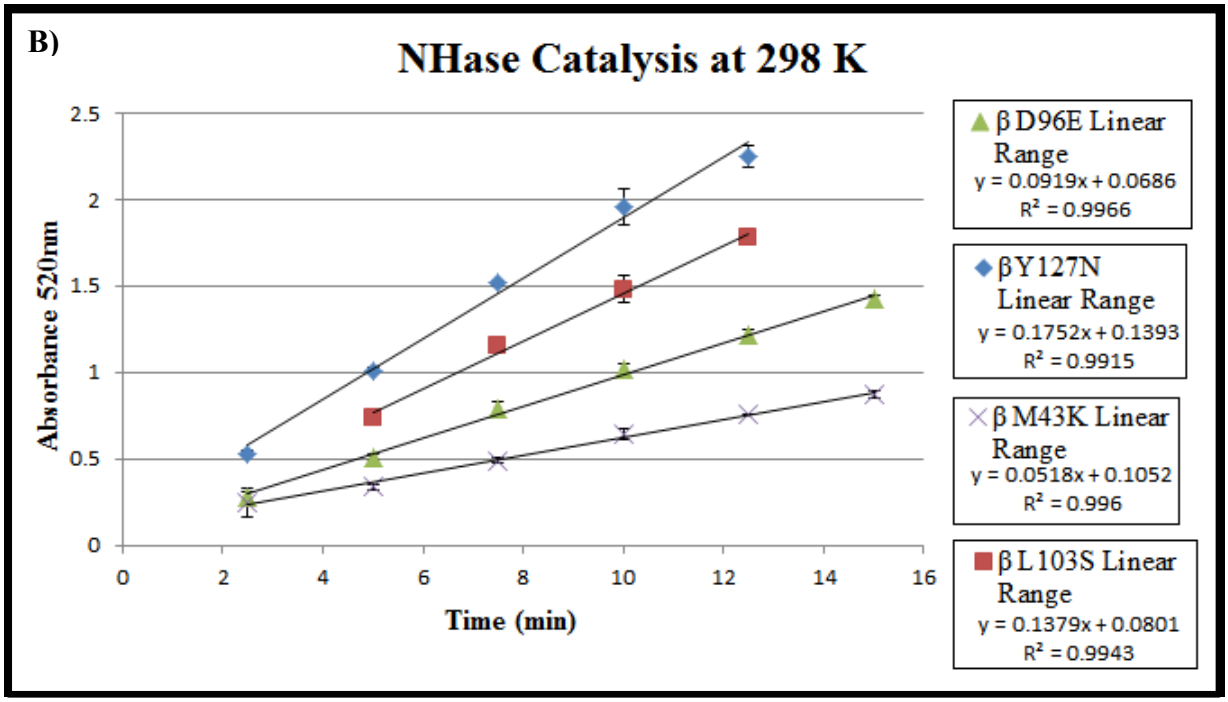

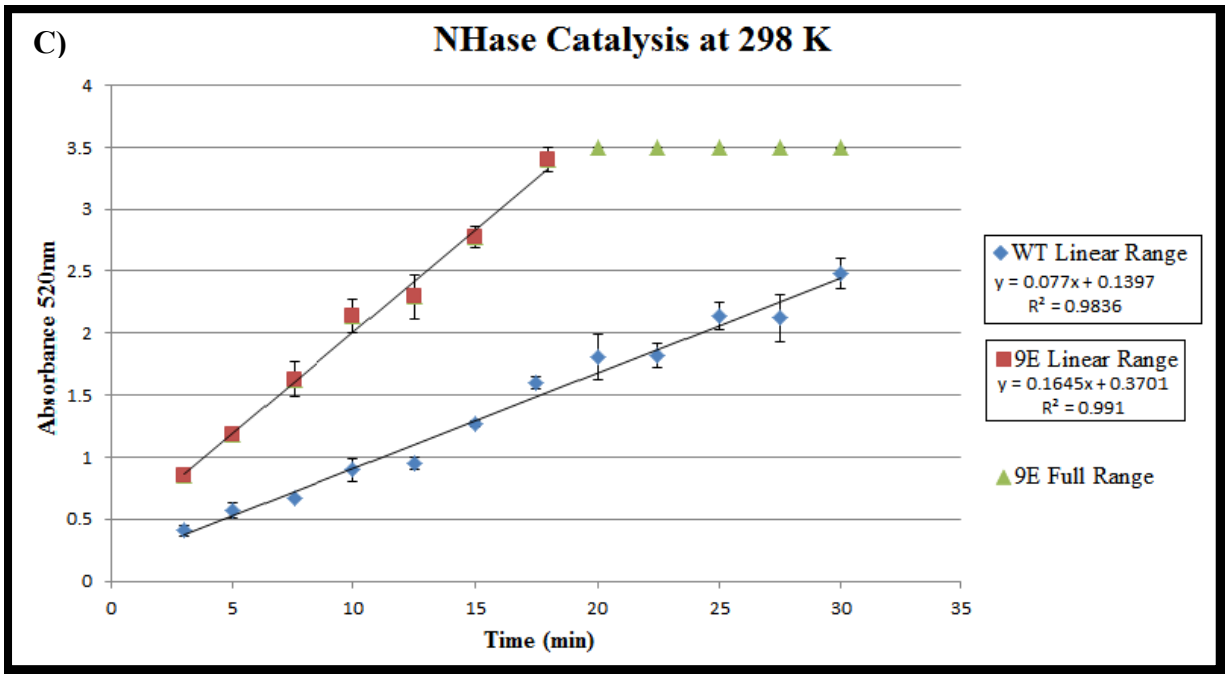

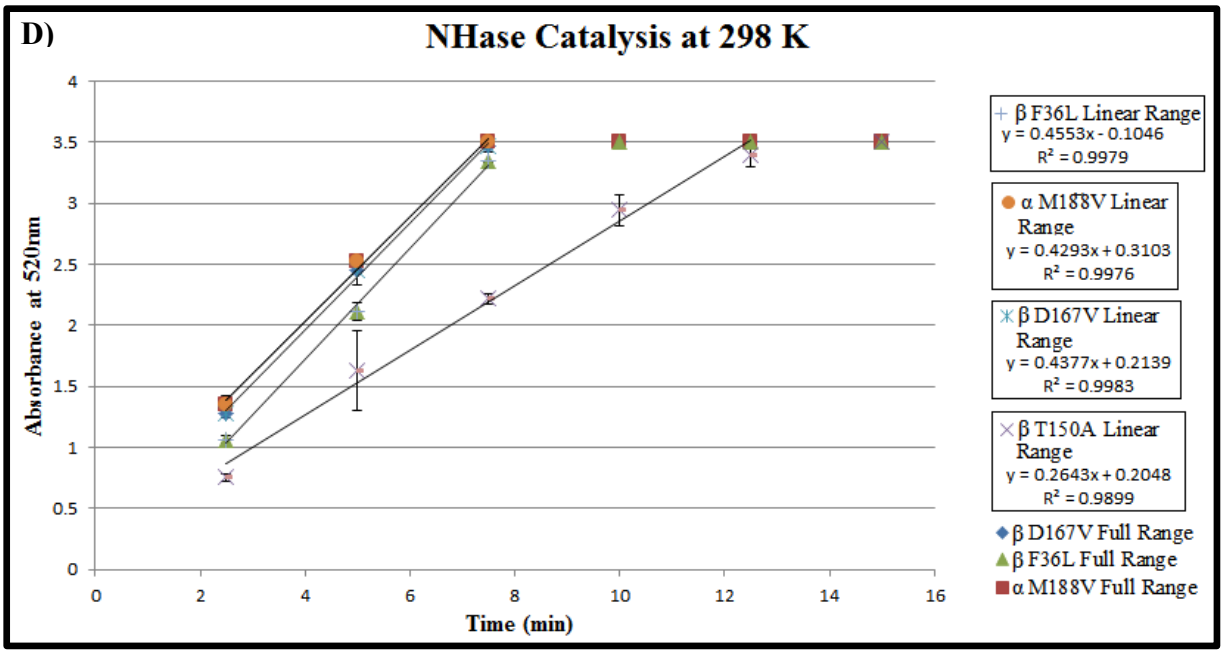

Figure 4.12: Catalysis by NHase at 298 K measured from 2.5 minutes to 15 minutes depicted in graphs A), B) and D). The catalysis observed in graph C) was extended up to 30 minutes using the WT NHase and one chosen composite mutant, 9E. Acetonitrile was used as a substrate at equal protein concentration of 0.05 mg/ml for all NHase samples and acetonitrile at a final concentration of 50 mM. All reaction substrates and protein dilutions were done in 0.025 M potassium phosphate buffer pH 7.2, 5 mM DTT.

Optimisation of the Heat Treatment Temperature

A)

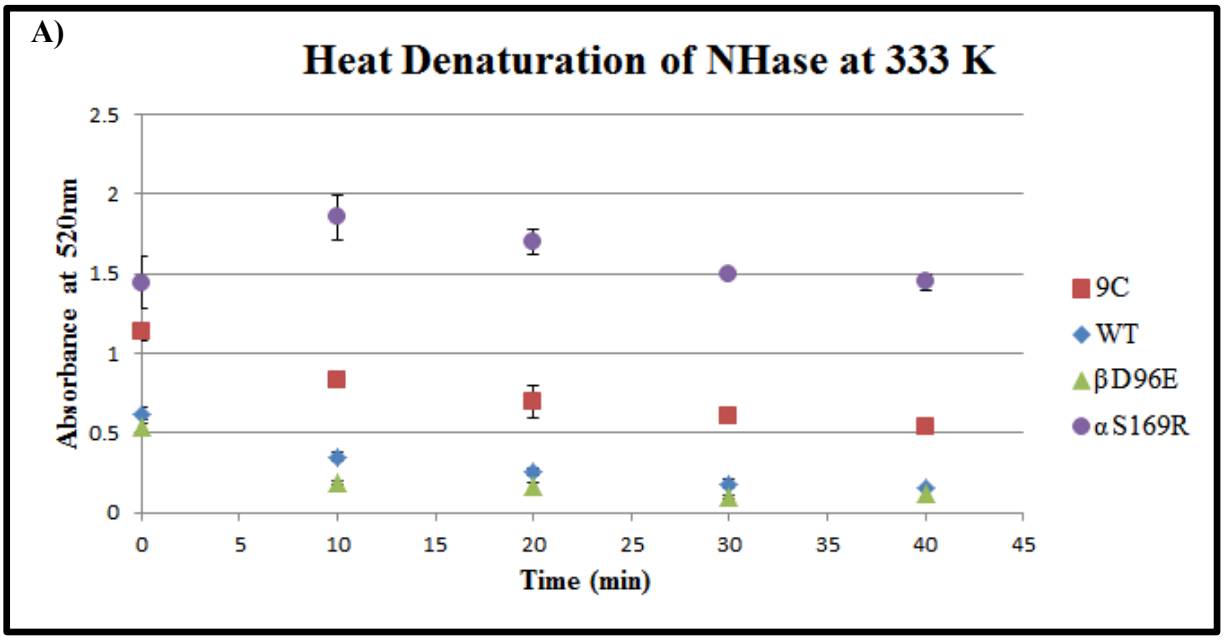

B)

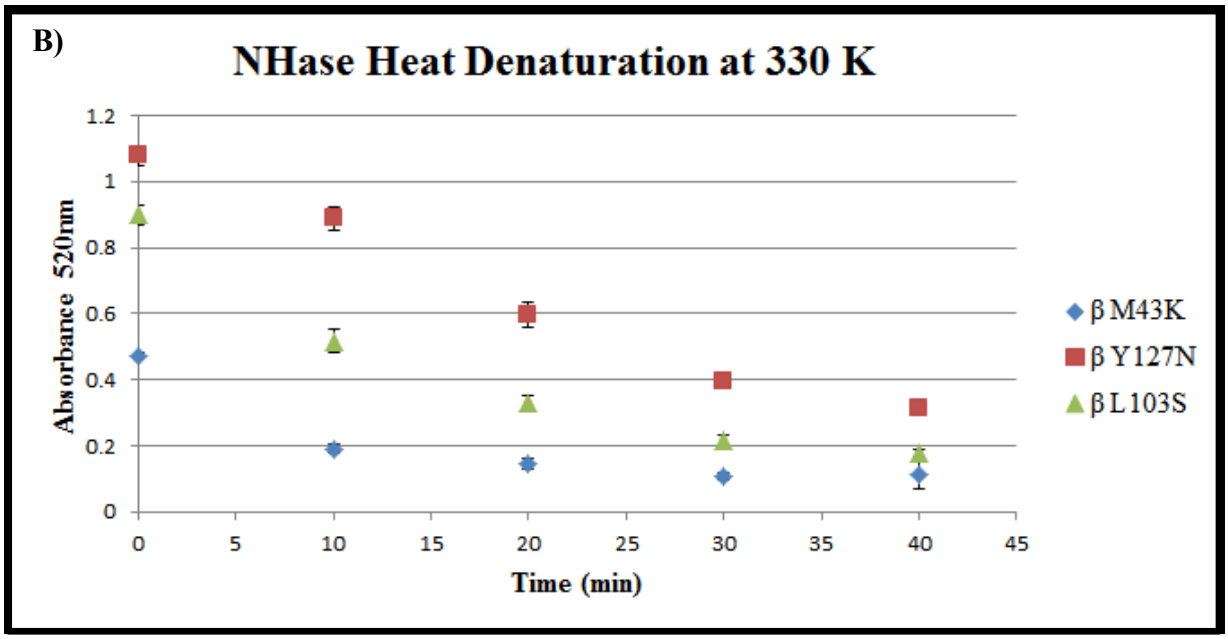

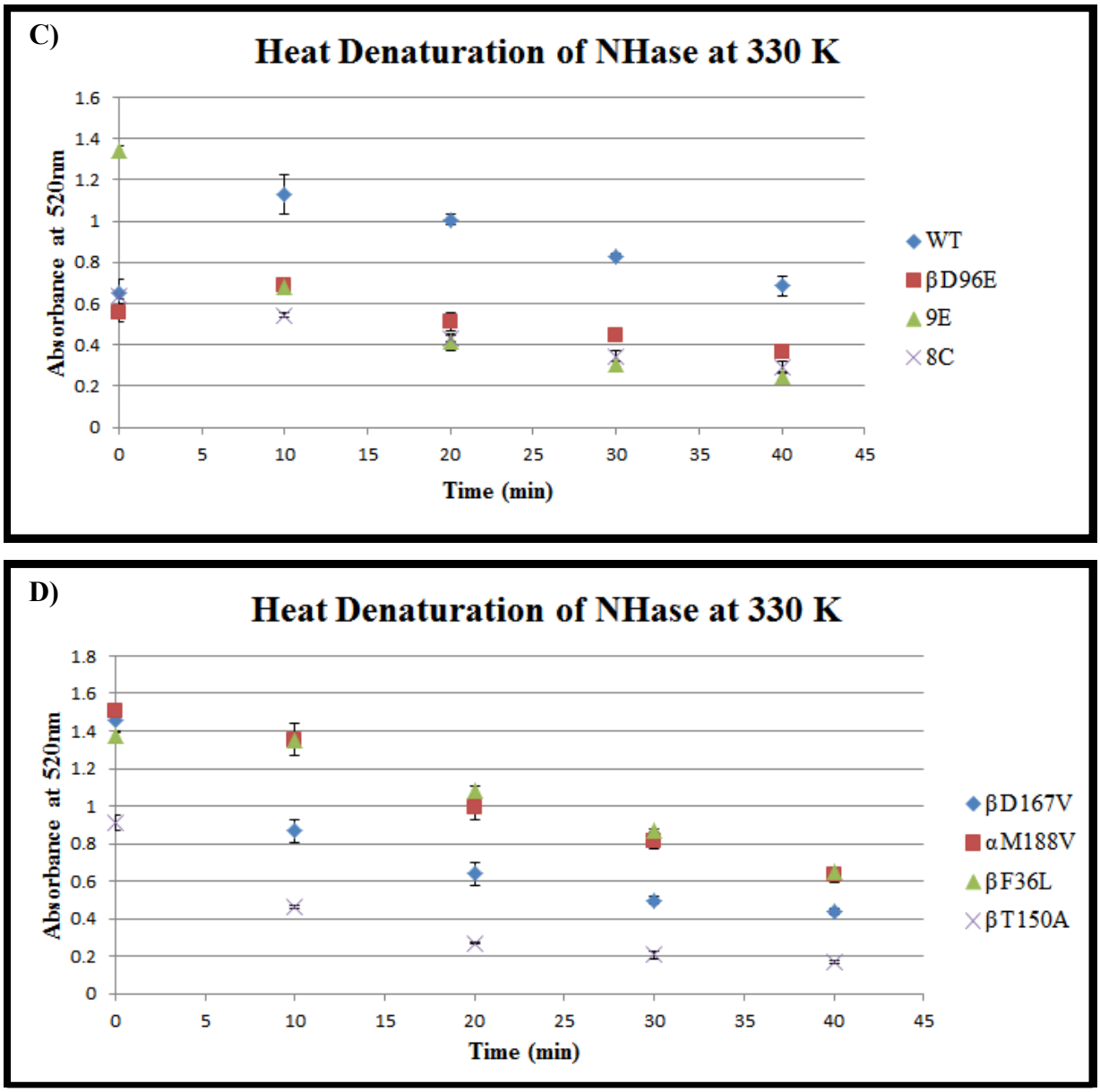

Figure 4.13: A preliminary thermal denaturation of different NHases at 330 K or 333 K and using the previously optimised conditions of temperature, substrate concentration and duration of catalysis. All NHase samples were prepared in 0.025 M potassium phosphate buffer pH 7.2, 5 mM DTT to a final concentration of 0.05 mg/ml. The measured absorbance of catalysis was plotted against the duration of heat treatment at the indicated temperature. This was performed for all the NHase samples under study to determine the temperature required for complete thermal unfolding. Some of the NHase samples such as WT, 9E and S169R showed a slight increase in activity which is discussed further below.

Measurement of Thermal Denaturation using the Hydroxamic Acid Assay

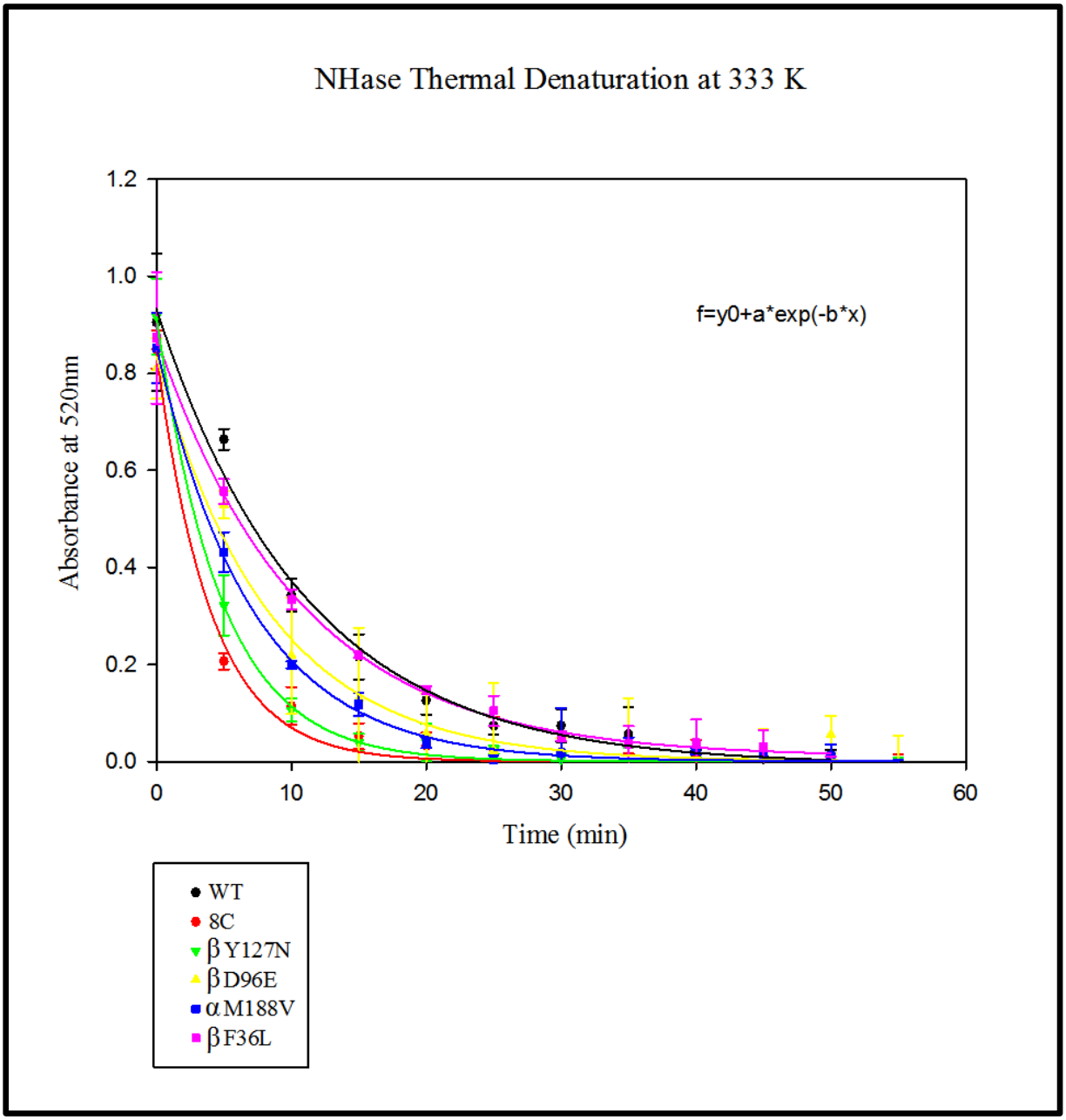

Figure 4.14: Thermal denaturation of the NHase samples WT, βY127N, βD96E, αM188V, βF36L and the composite mutant 8C at 333 K. The concentration of acetonitrile was 50 mM and was catalysed using the optimised conditions by NHase samples heat treated for up to 55 minutes. The non-linear equation for the fit of the data is indicated on the graph. The absorbance resulting from detection of the catalysis was plotted against the duration of heat treatment for up to 55 minutes.

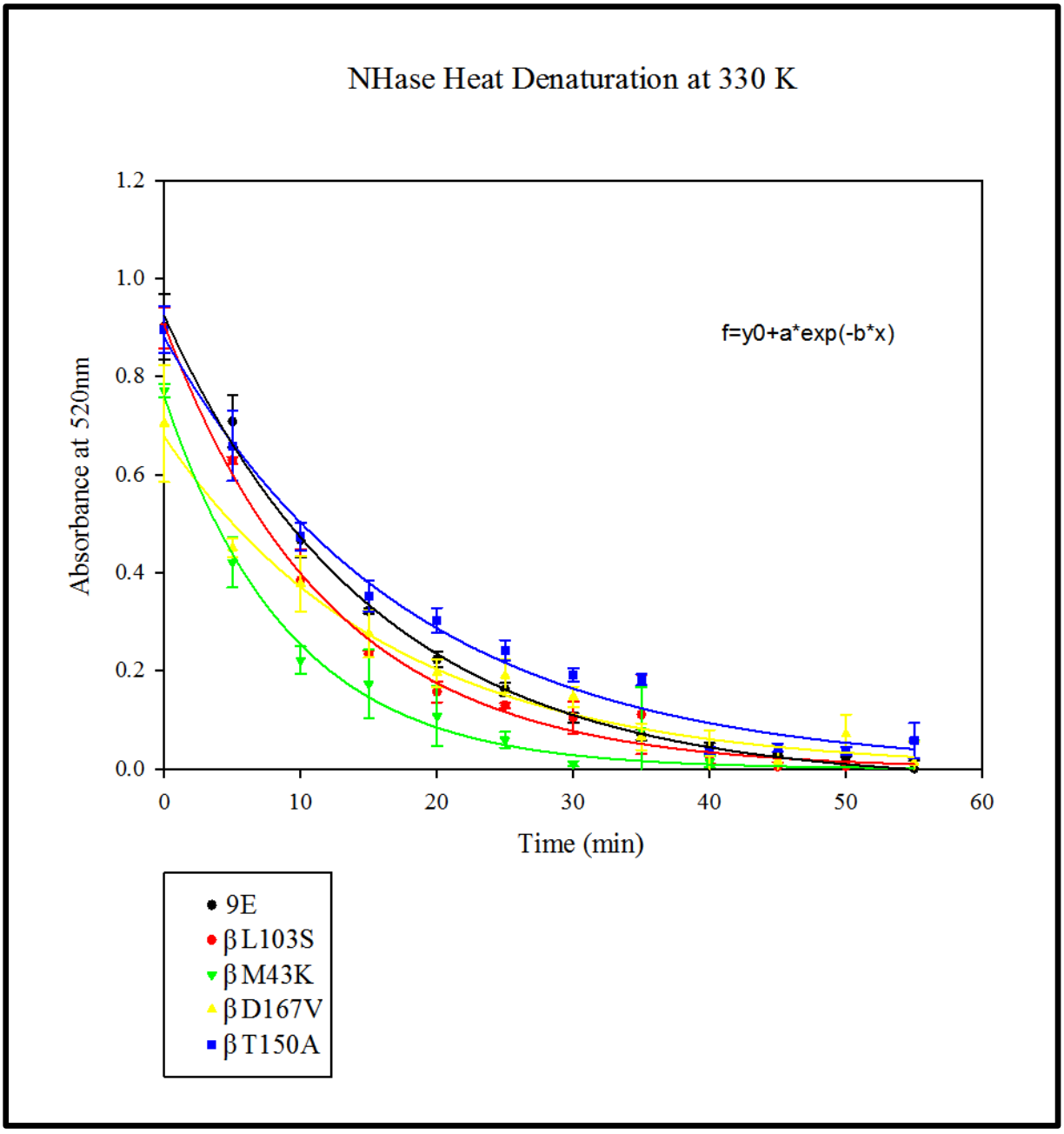

Figure 4.15: Thermal denaturation of the NHase samples βL103S, βM43K, βD167V, βT150A and the composite mutant 9E at 330 K. The concentration of acetonitrile was 50 mM and was catalysed using the optimised conditions by NHase samples heat treated for up to 55 minutes. The non-linear equation for the fit of the data is indicated on the graph. The absorbance resulting from detection of the catalysis was plotted against the duration of heat treatment for up to 55 minutes.

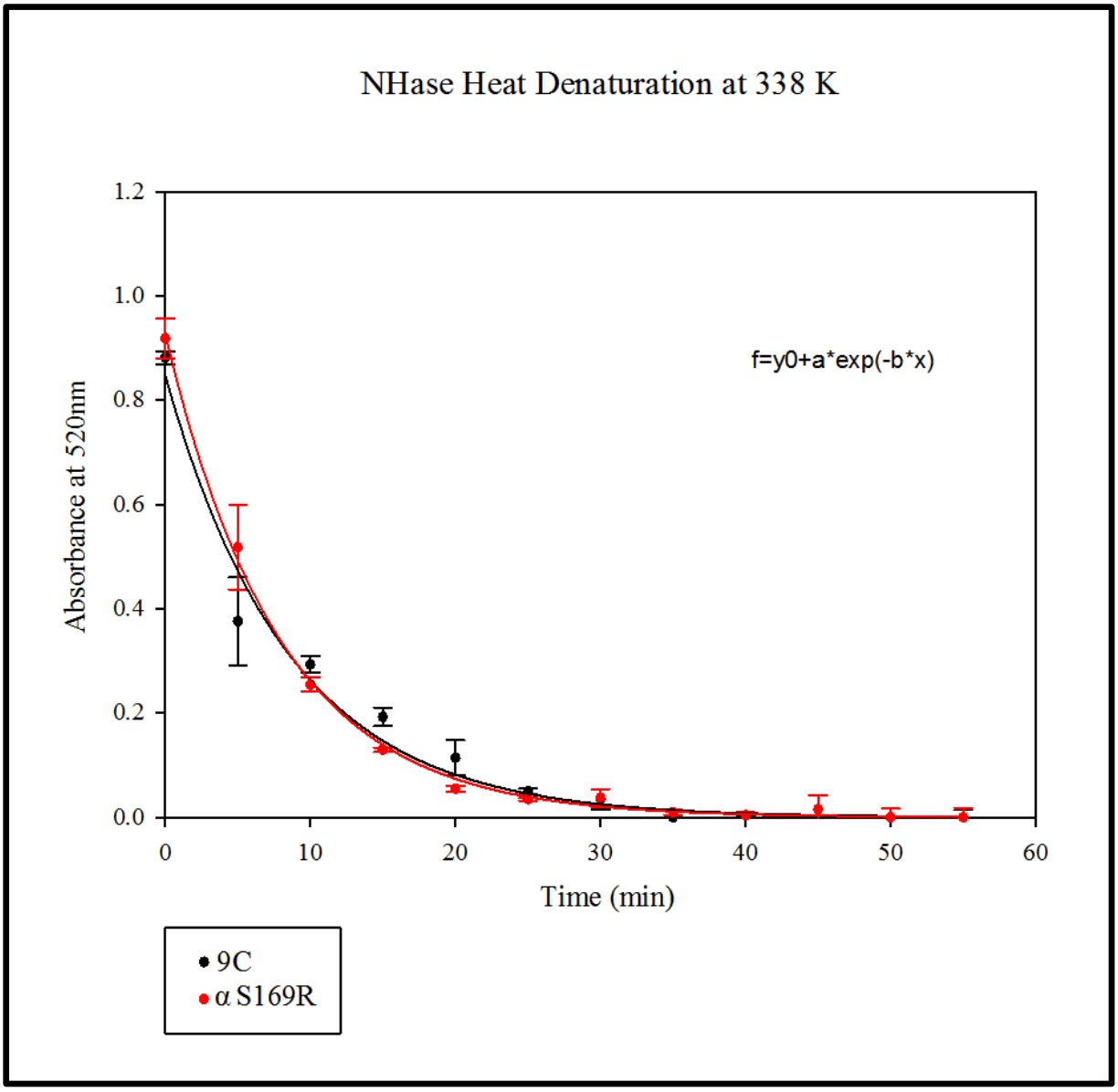

Figure 4.16: Thermal denaturation of the composite 9C NHase mutant and αS169R single NHase mutant at 338 K. The concentration of acetonitrile was 50 mM and was catalysed using the optimised conditions by NHase samples heat treated for up to 55 minutes. The non-linear equation for the fit of the data is indicated on the graph. The absorbance resulting from detection of the catalysis was plotted against the duration of heat treatment for up to 55 minutes.

Table of non-linear fit Constants, ΔG^* and $\Delta\Delta G^*$ Values							
Sample Name	**b value**	**y_0 value**	**a value**	**Temp (K)**	**Graph R^2**	**ΔG^* kJ/mol**	**$\Delta\Delta G^*$ kJ/mol**
WT NHase	0.0926	0.0949	0.9339	333	0.9895	-6.39872	0
9E	0.1325	0.0989	0.9018	333	0.9968	-5.30987	-1.08885
βL103S	0.0821	0.1003	0.9058	330	0.9911	-6.58747	0.188745
βY127N	0.3381	0.1135	0.8858	333	0.9979	-2.66669	-3.73204
βF36L	0.0911	0.1268	0.871	333	0.9977	-6.25088	-0.14784
8C	0.2491	0.1511	0.8431	333	0.9879	-3.3757	-3.02302
βD167V	0.0602	0.296	0.6771	330	0.98	-6.64033	0.241607
αM188V	0.1412	0.1481	0.8549	333	0.9975	-4.98592	-1.4128
βD96E	0.1196	0.19	0.8337	333	0.9837	-5.37607	-1.02265
9C	0.1169	0.1189	0.8475	338	0.979	-5.5671	-0.83162
βM43K	0.1097	0.2283	0.7596	330	0.9845	-5.30932	-1.08941
αS169R	0.1264	0.0817	0.9267	338	0.9981	-5.59859	-0.80013
βT150A	0.056	0.1044	0.8796	330	0.9861	-7.55666	1.157942

Table 4.3: The constants determined from the non-linear fit of the absorbance readings resulting from thermal denaturation of different NHase samples. The constants are labelled as used in the equations in the previously shown graphs. The R squared for the fit, the calculated ΔG^* values and $\Delta\Delta G^*$ values are shown calculated using the rate determined from equation 6 using the "b value" in the table as the rate of exponential decrease (in the equation, the b value is negative). The negative $\Delta\Delta G^*$ values indicate samples that are more thermostable than the WT NHase while the positive $\Delta\Delta G^*$ values indicate samples that are less thermostable than WT NHase. The universal gas constant used was, **R=8.31446 J/mol/K.**

Thermal Shift Assay NHase Melting Temperatures

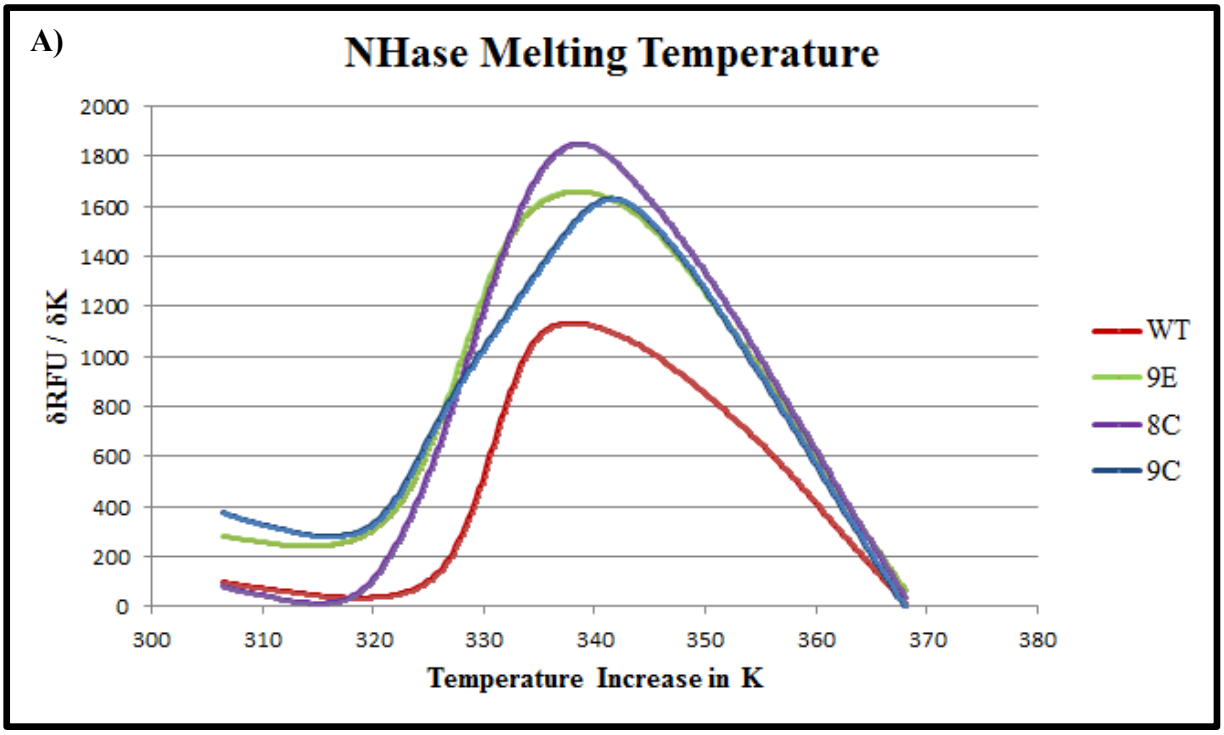

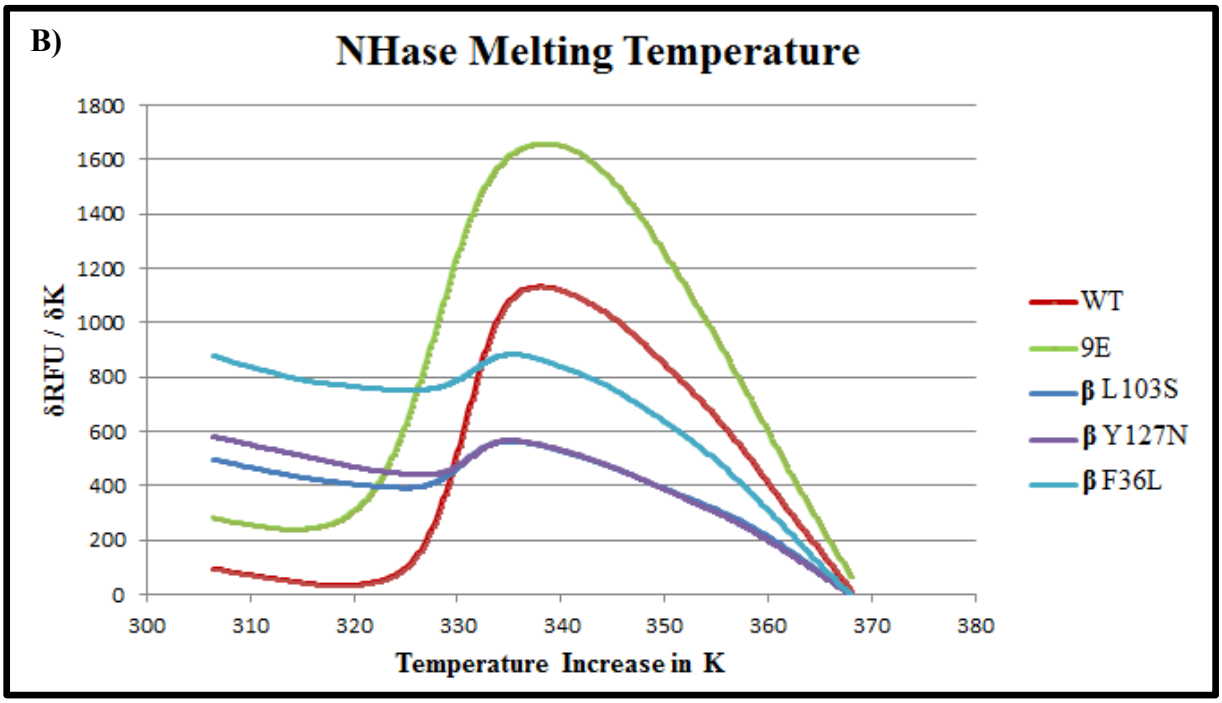

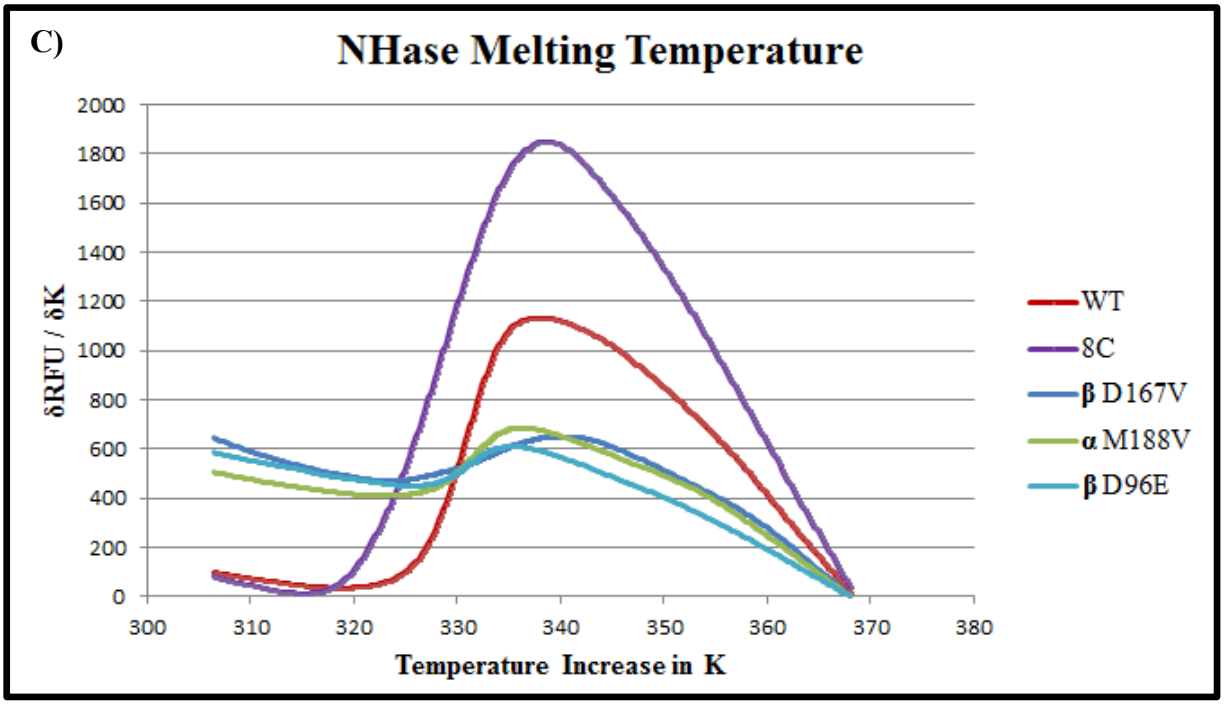

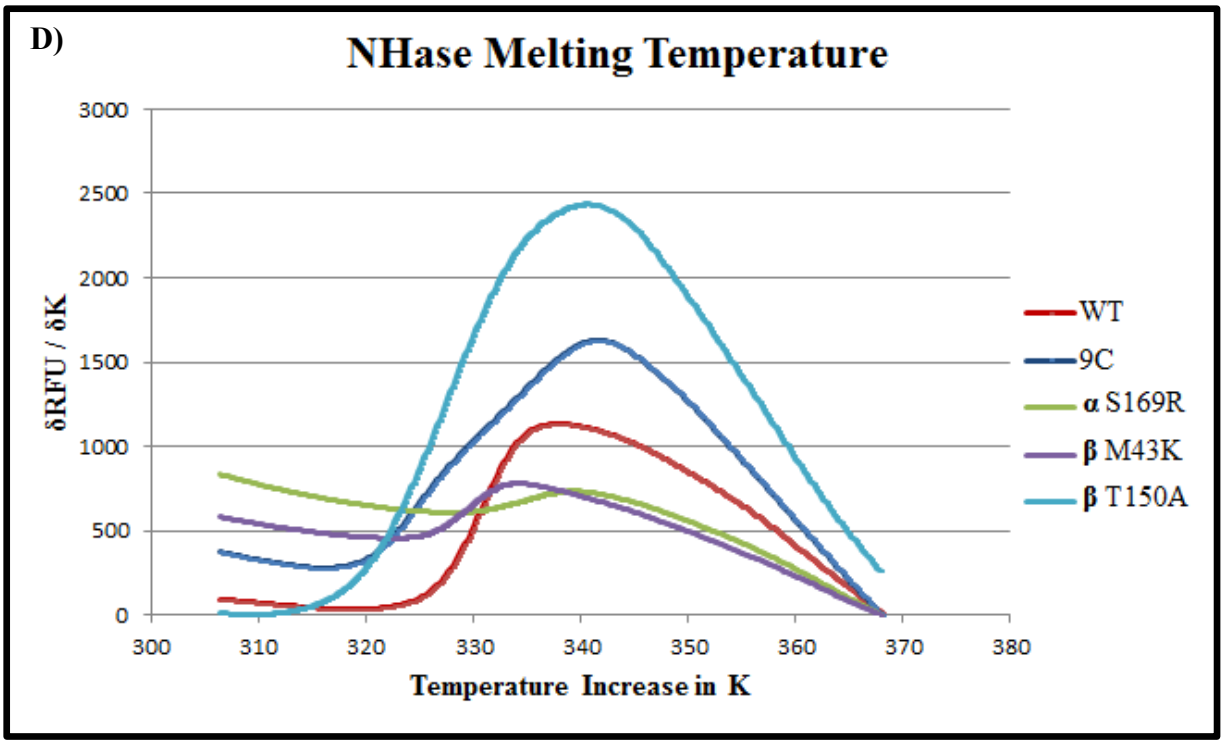

Figure 4.17: Thermal shift graphs depicting the fluorescence (RFU) plotted against increasing temperature. A) Plot of the WT NHase together with the three NHase mutants: 9E, 8C and 9C. B) Plot of the WT NHase together with the 9E NHase mutant and the single NHase mutants: βL103S, βY127N and βF36L C) Plot of the WT NHase together with the 8C NHase mutant and the single NHase mutants: βD167V, αM188V and βD96E. D) Plot of the

WT NHase together with the 9C NHase mutant and the single NHase mutants: αS169R, βM43K and βT150A.

Sample	Melting Temp (K)
WT NHase	330.7
9E	328.6
βL103S	330.4
βY127N	331.3
βF36L	331.5
8C	328.9
βD167V	332.7
αM188V	331.4
βD96E	331
9C	324.9
βM43K	329.2
αS169R	334.5
βT150A	324.1

Table 4.4: The melting temperatures of all the different NHase samples measured using the thermal shift assay in 0.025 M potassium phosphate buffer pH 7.2, 5 mM DTT without any salt in solution. Some of the mutants seem more thermostable than the WT NHase in the presence of buffer only such as the αS169R, βD96E, αM188V, βD167V, βF36L and βY127N NHase mutants.

CHAPTER 5:

DISCUSSION

Heat energy has been shown to influence the activity of enzymes and their structural integrity with a profound effect on the intramolecular interactions linking various domains and structural artefacts of the enzyme at elevated temperatures (Atkins and DePaula, 2006; Garrett and Grisham, 2010). The structural features that contribute to thermal stability of NHase in this study are influenced by three main features: hydrogen bonding, salt bridges and hydrophobic packing. The position of the hydrogen bonds and/or salt bridges has to be within 3.5 Å and not sterically strained. The location of hydrogen bonds and salt bridges, if the interactions are adjacent to a hydrophobic e.g. an aromatic ring from Phe or cluster of hydrophobic side-chains or adjacent to a solvent exposed area, can influence the energy of the hydrophilic interaction. Location next to hydrophobic side-chains or microenvironment would make the hydrophilic interaction stronger while location next to a hydrophilic microenvironment would make the hydrophilic interaction weaker. Hydrophobic packing tends to form a water shell which excludes water molecules and ions away from hydrophobic groups or side-chains. The strength of this water shell can reinforce the rigidity of protein structures in the event of thermal denaturing conditions.

Different stabilities of proteins have been reported when the protein is assayed in the presence of other molecules such as osmolytes, free amino acids, free ions and salts as discussed above (Santoro *et al*., 1992). Thus different thermal stabilities would be measured when proteins are assayed in different buffer conditions (in the presence of substrates compared with in the absence of substrate for the hydroxamic acid assay and thermal shift assay respectively). This would influence the solute and solvent microenvironment around the thermostabilising mutation and give different thermal stabilities. In this study, we examined and compared the thermal denaturation of NHase WT and mutants by measuring the residual activity of the purified enzyme after heat treatment. This was measured using optimised conditions for catalysis and acetonitrile as a substrate.

Catalysis by NHase

The determination of conditions required for catalysis by NHase in this study was crucial due to the nature of the measurement of thermal stability, that is, determining the rate of decrease of residual activity of NHase as function of time at a specific temperature. The optimisation of catalysis facilitated the measurement of residual activity. The first step entailed determining whether NHase was synthesized using the transgenic expression system: *E. coli* BL21(DE3), (*fig* 4.4, *fig* 4.5, *fig*. 4.6 and *fig*. 4.7). Protein determination using Bradford assays was done on all subsequent CFE and semi pure protein samples using a similar standard curve with R-squared value > 0.98 (*fig* 4.3). Confirmation of expression was then followed by checking whether the expressed NHase was not only active but also producing the amide product as shown in previous studies by Makhongela *et al*., (2007) using a substrate that is highly efficient for the acyl transfer catalysis by amidase (*fig*. 4.8, *fig*. 4.9 and Table 4.2). Following confirmation of expression and nitrile catalysis of acrylonitrile using CFE, all NHase samples were purified (Chapter, 3) and catalysis was confirmed using purified NHase. The amidase was previously purified to be used with all NHase assays (Table 3.14).

The conditions of the catalysis using purified NHase were optimised using acetonitrile. These were the temperature of incubation which was done using the WT NHase and the composite NHase mutants: 9E, 8C and 9C, for four different temperatures: 298 K, 303 K, 308 K and 313 K for varying durations of time ranging from 2.5 minutes to 30 minutes at 2.5 minute intervals (*fig* 4.11). This was to determine the temperature at which the catalysis by NHase increased linearly with time. The catalysis rate at 298 K was selected due to the length of the linear range which facilitated accurate measurement using the hydroxamic acid assay and also to reduce evaporation of reaction components especially the nitrile substrate (*fig* 4.12). Higher temperatures were likely to have a relatively short linear range and higher rate of evaporation of the volatile substrate. Furthermore higher temperatures increased the risk of thermal denaturation of the enzyme. The possibility of evaporation was countered by covering the reaction plates with aluminium foil with adhesive which sealed around each reaction well. The aluminium foil also facilitated even conduction of heat during incubation. The stoichiometry of the acyl transfer was also determined using the optimised conditions in order to allow quantitation of the units of NHase using the hydroxamic acid assay (*fig* 4.10). From the stoichiometry determination, one Fe-hydroxamic acid complex consisted of 5

acetohydroxamic acid molecules coordinated to one Fe centre which is also in agreement with previous determination according to Taylor *et al*., (1998) and Andrieux *et al*., (2014).

The protein concentration used for catalysis was determined by comparing catalysis profiles of various concentrations. The 0.05 mg/ml concentration of NHase was selected because of the reaction velocity, the potential for having the least interference in measurement of absorbance due to thermal unfolding and the accuracy of measurement i.e. 0.05 mg/ml concentration is the lowest concentration that can be accurately measured using a Bradford assay (*fig*. 4.3) and A280 protein determination techniques coupled to the use of protein extinction coefficients (Table 4.1) without having to dilute further. The interference of high protein concentrations with absorbance readings for catalysis was observed following the formation of a white precipitate of NHase after heat treatment. The absorbance of the Fe-hydroxamic acid complex at 520 nm is specific to the complex however white suspensions will also absorb any wavelength within the visible light range thus interfere with the accuracy of measurement. To add to this, the absolute and relative concentrations of the many different components in CFE such as other expressed proteins and macromolecule complexes cannot be accurately determined. This is, in part, the reason for shifting to using purified proteins for the hydroxamic acid assay as opposed to using NHase in CFE.

The optimisation of the duration of incubation was done after the determination of the optimal incubation temperature (*fig*. 4.11). This duration of incubation varied because some mutants catalysed at different rates compared to the WT NHase. The residual activity of NHase was meant to be as a result of thermal denaturation not because of decreased catalytic efficiency due to a mutation which blocked the substrate channel and thus impaired access of the nitrile substrate to the active site. Thus the optimisation of the duration of incubation was made to ensure that the catalysis by NHase was in the linear range (*fig*. 4.12). This would allow normalization across different NHase samples which would mean that the observed decrease in catalysis characterised by residual activity, would be solely because of thermal denaturation and not decreased catalytic efficiency by NHase or amidase.

The acyl transfer by amidase was confirmed and optimised to ensure that the quantity of amidase used in the reaction managed to catalyse the conversion of all the amide produced by the NHase to the corresponding hydroxamic acid. This was to ensure that the decrease in NHase activity that was measured was because of thermal denaturation and not inactivity by amidase viz, acyl transfer to hydroxylamine. The choice of substrate catalysed by NHase was also to produce an amide which has been shown in previous studies with the *Rhodococcus sp.* R312 amidase (Fournand *et al*., 1998a; Fournand *et al*., 1998b) and with the *Geobacillus*

pallidus RAPc8 amidase used in this study) to be the most efficient for acyl transfer (Makhongela *et al*., 2007).

The temperature and duration of heat treatment of NHase was done to ensure complete thermal unfolding of the intermediate state(s) of NHase and decrease the likelihood of reverse folding from the intermediate state. This optimisation also hinted at the possibility of multiple intermediate states present during thermal unfolding of NHase with the intermediate states being catalytically active as seen with the thermal denaturation curves of WT NHase and αS169R (*fig*. 4.13) whereby an increase in catalysis was observed. The event of proteins regaining activity after thermal denaturation following reversible folding back into the active state has been previously reported on the protein transthyretin by Kim *et al*., (2000) and the lipase from *B. subtilis* by Rajakumara *et al*., (2007). Perhaps, multiple stable intermediate states of NHase exist following heat treatment at temperatures lower than their melting temperature (Tm) but have not been reported as of this writing.

In brief, the hydroxamic acid assay optimisation facilitated the application of the following catalysis conditions for determining of the rate of thermal denaturation by measuring residual activity:

1. Heat treatment at a specific temperature for unfolding the purified NHase.
2. Catalysis of a specific nitrile by heat treated NHase at a specific protein concentration, at a specific incubation temperature, for a specific duration within the linear range of NHase catalysis.
3. Catalysis by amidase to completion at a specific temperature that did not adversely impair measurement of catalysis.
4. Detection and measurement of the products of residual activity at a specific wavelength (520 nm) which also maximised the signal to noise ratio, i.e., by not measuring other wavelengths which would interfere with measurement, and comparing the observed absorbance values to background values.

The thermal stability of the composites and single mutant NHases was determined using the Arrhenius equation using a non-linear fit of the data. Comparisons of the different rates of thermal inactivation between the composite mutants and their constituent single mutants were done together with the WT NHase. Structural analysis facilitated determination of the possible mechanisms involved. In this chapter, all NHase mutants are referred to using single letter amino acid codes representing the NHase single mutants e.g. βL103S NHase mutant, while the individual mutations are referred to using three letter amino acid codes e.g. βLeu103 and βSer103 representing a leucine amino acid residue and serine amino acid

residue respectively, in the β subunit at positions 103 in the WT NHase and single mutant NHase, respectively. In addition, images showing the electron density around each amino acid in this study are shown in addition to their corresponding ribbon diagrams. This was done to facilitate visualization of each mutation in its structural context with sufficient depth of field in the view.

Structural Analysis of the 9E *G. pallidus*-RAPc8 NHase crystal structure

The crystal structure of the 9E variant (van Wyk, 2008) was used to interpret the result. This structure bears three mutations, βL103S, βY127N and βF36L which were shown using the hydroxamic acid assay to influence its thermal stability as previously shown (*fig*. 5.1 and Table 4.3). The βY127N mutant contributed to thermal stability while the βL103S mutant did not. The thermal stability of the βF36L mutant was comparable to the WT NHase. In the results, the $\Delta\Delta G^*$ values for the single mutants βL103S, βY127N and βF36L are +0.2 kJ/mol, -3.7 kJ/mol and -0.1 kJ/mol respectively. When the energy contribution from the single mutants is combined the total $\Delta\Delta G^*$ value is -3.6 kJ/mol while the measured $\Delta\Delta G^*$ value of the 9E NHase mutant is -1.1 kJ/mol. This would suggest that the βY127N mutation contributes the most to the thermal stability of the 9E NHase mutant. The remaining single mutant αD4G which was not observed in the crystal structure is likely to have made the 9E NHase mutant more thermolabile. This could be in part due to the location of the αD4G mutant in a highly flexible region that is exposed to the solvent. The βL103S mutation, which is exposed to the solvent, provides little contribution to the thermal stability of the 9E NHase mutant.

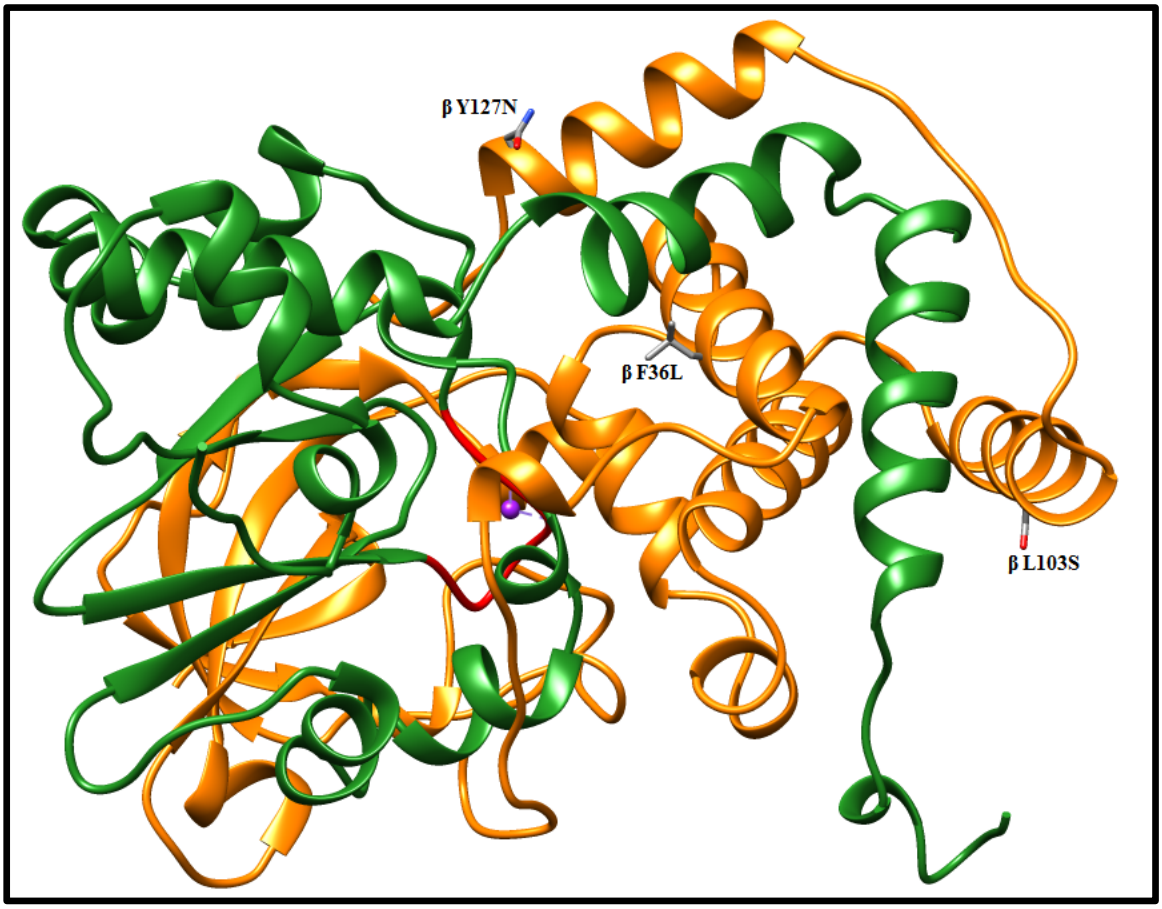

Figure 5.1: The three mutations visualized in the crystal structure of the NHase from *G. pallidus* RAPc8 9E mutant: βL103S, βY127N and βF36L. The α subunit is coloured green while the β subunit is coloured orange. The active site coordinated Co ion is coloured purple with the red coloured main chain bearing the active site residues described earlier in the text. The images were visualised using Chimera (Pettersen *et al*., 2004).

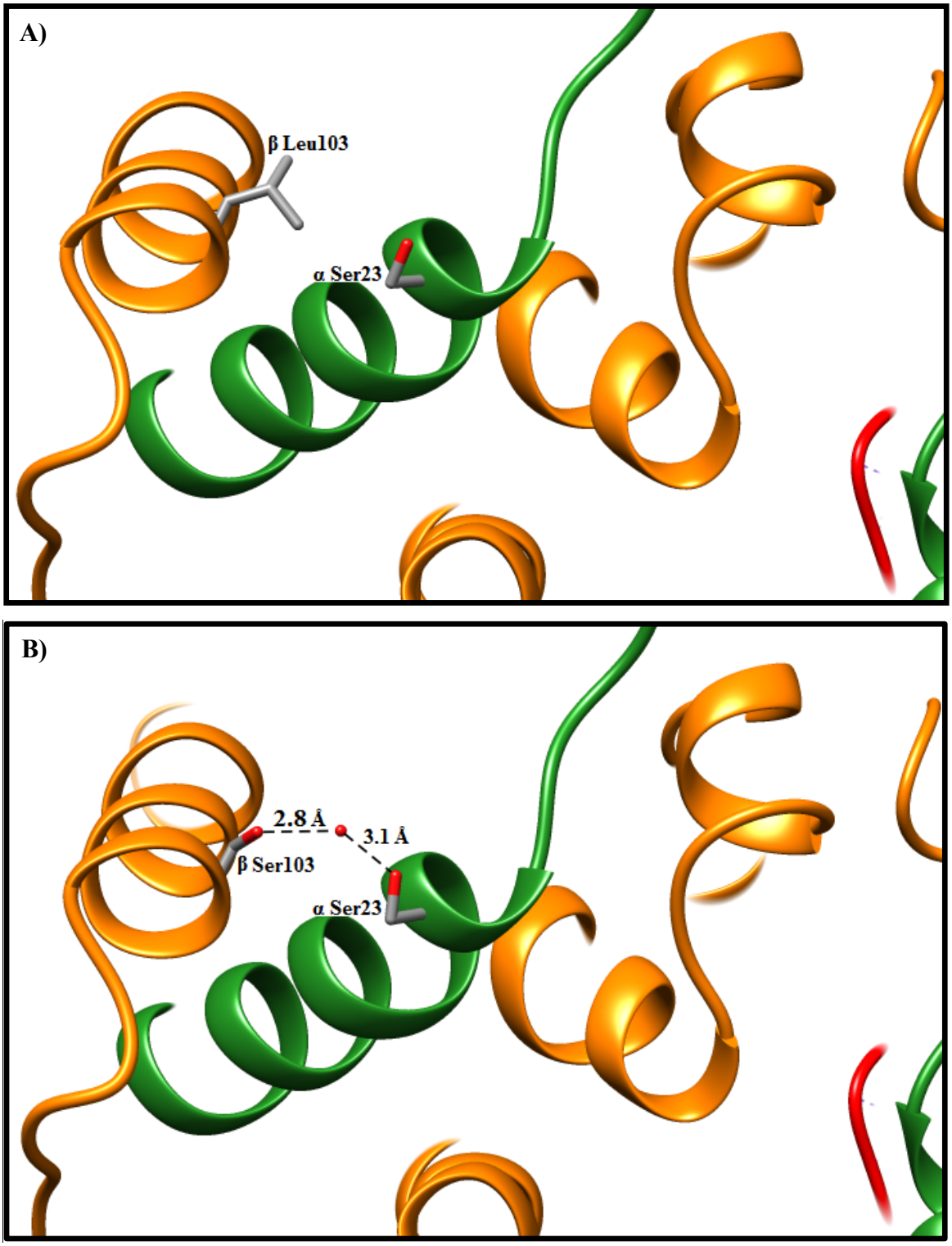
A)
β Leu103
α Ser23
B)
2.8 Å
3.1 Å
β Ser103
α Ser23

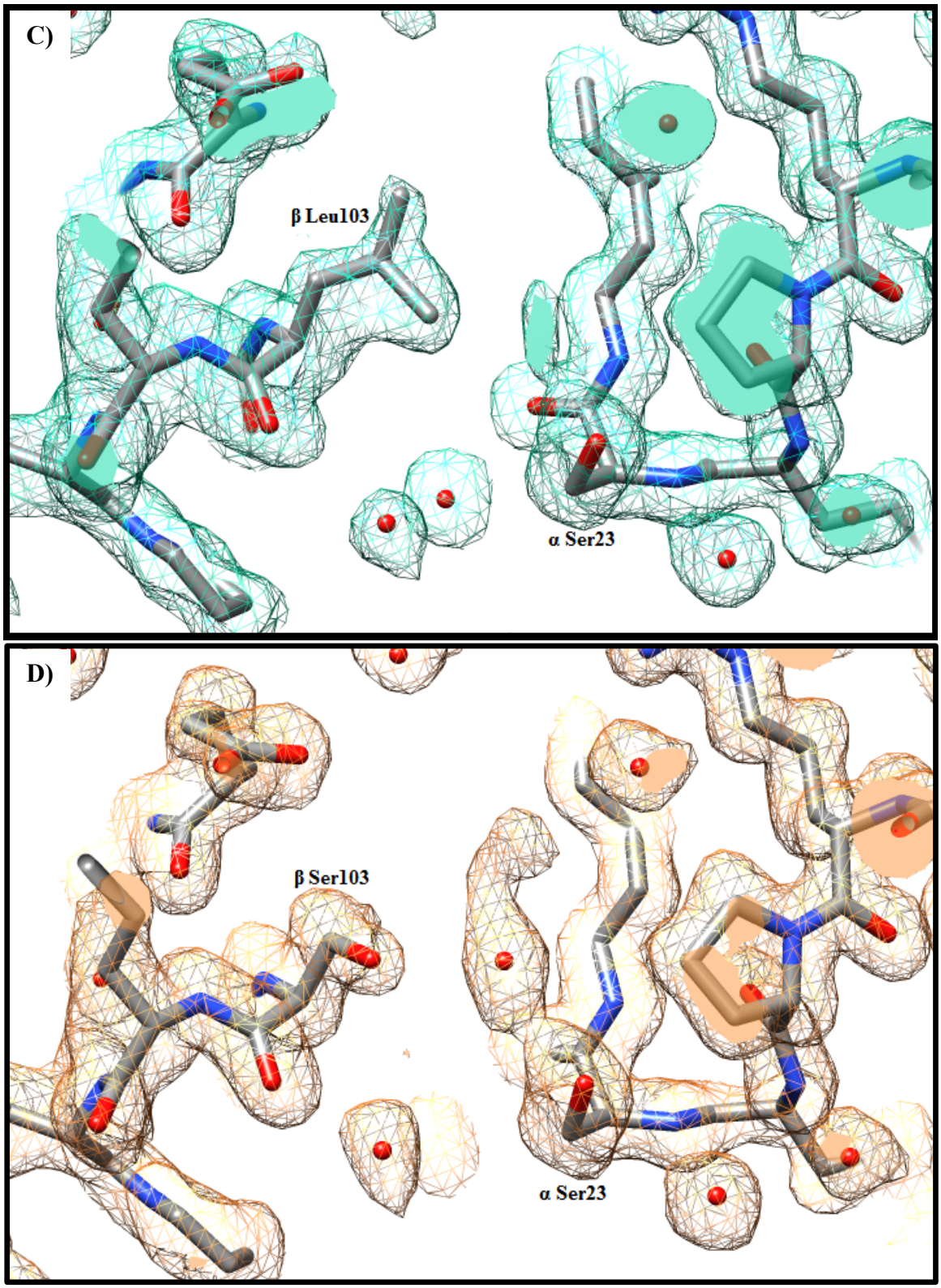

Figure 5.2: The WT NHase variant A) compared with the βL103S mutation in the 9E NHase variant B). Images C) and D) show the electron density maps and the protein mutation sites of the WT NHase and βL103S NHase mutant respectively. The α subunit is coloured green while the β subunit is coloured orange. The residue βSer103 in the crystal structure of the mutant forms a water-mediated hydrogen bond with αSer23 and an adjacent water molecule

(coloured red) at distances of 2.8 Å and 3.1 Å between both hydrogen bond acceptors. In the WT structure, B), no hydrogen bonds are formed due to the absence of hydrogen bond acceptor groups in the βLeu103 side-chain.

The βL103S NHase mutant possesses a βSer103 residue which is hydrogen bonded to an adjacent water molecule (*fig*. 5.2 B). Specifically, the Oγ of the OH group of βSer103 accepts and forms a water-mediated hydrogen bond at a distance of 2.9 Å with the H of an adjacent water molecule. The remaining H of the same water molecule forms a hydrogen bond with the Oγ of αSer23. There are no other acceptor groups in at less than 3.5 Å to form any hydrogen bonds. The residues βSer103 and αSer23 are exposed to the solvent hence accessible to freely available water molecules. The crystal structure of the WT *G. pallidus*-RAPc8 NHase does not have any hydrogen accepting side-chain atoms located on the side-chain of βLeu103 (*fig*. 5.2 A). The electron density around βLeu103 and αSer23 and βSer103 and αSer23 in the images of the WT NHase and the βL103S NHase mutant respectively (*fig*. 5.2 C and D) is well defined.

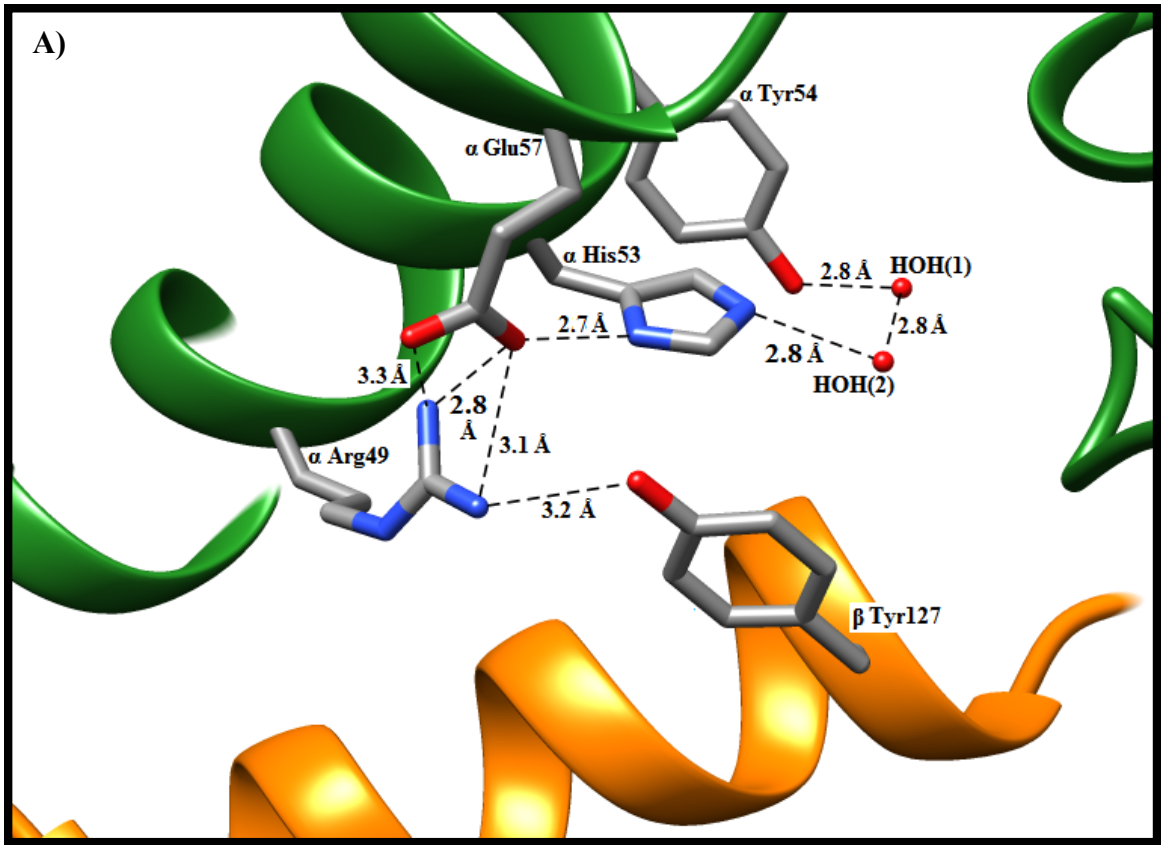

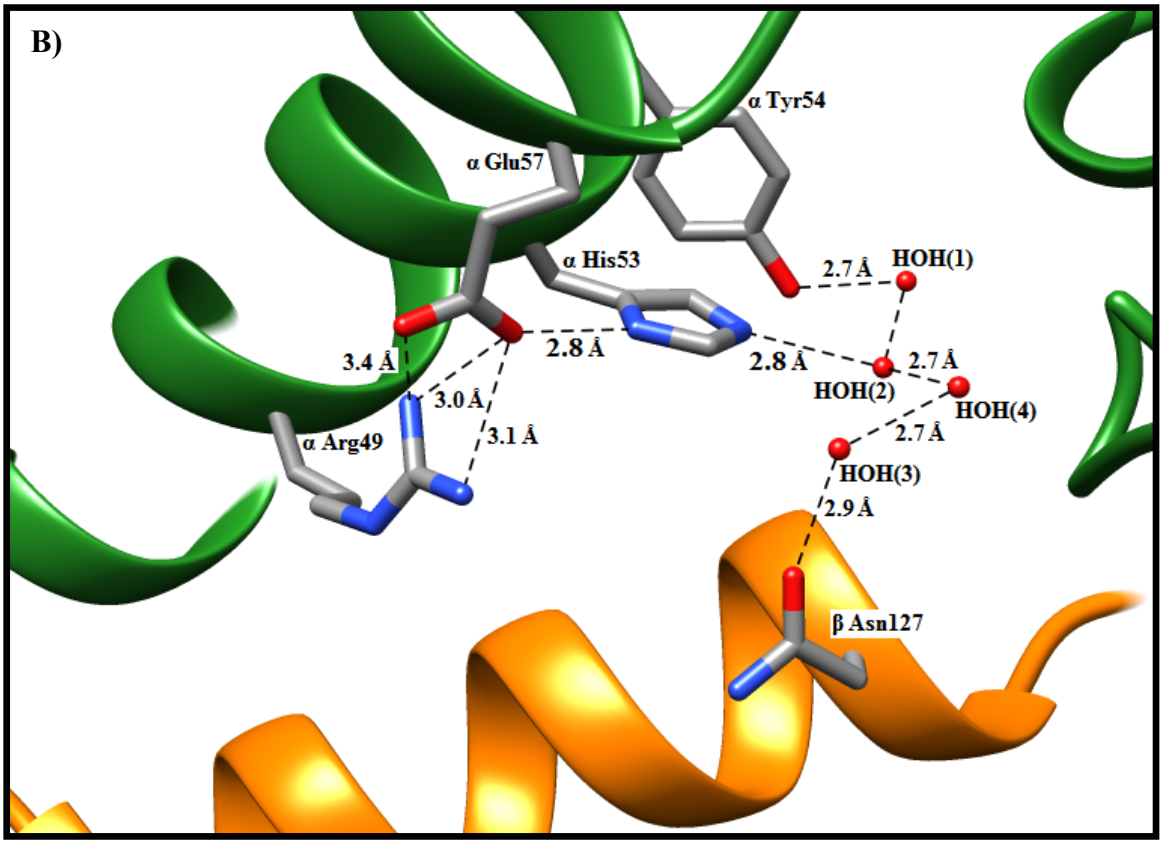
B)
α Tyr54
α Glu57
α His53
2.7 Å
HOH(1)
3.4 Å
2.8 Å
2.8 Å
2.7 Å
HOH(2)
HOH(4)
3.0 Å
3.1 Å
2.7 Å
α Arg49
HOH(3)
2.9 Å
β Asn127

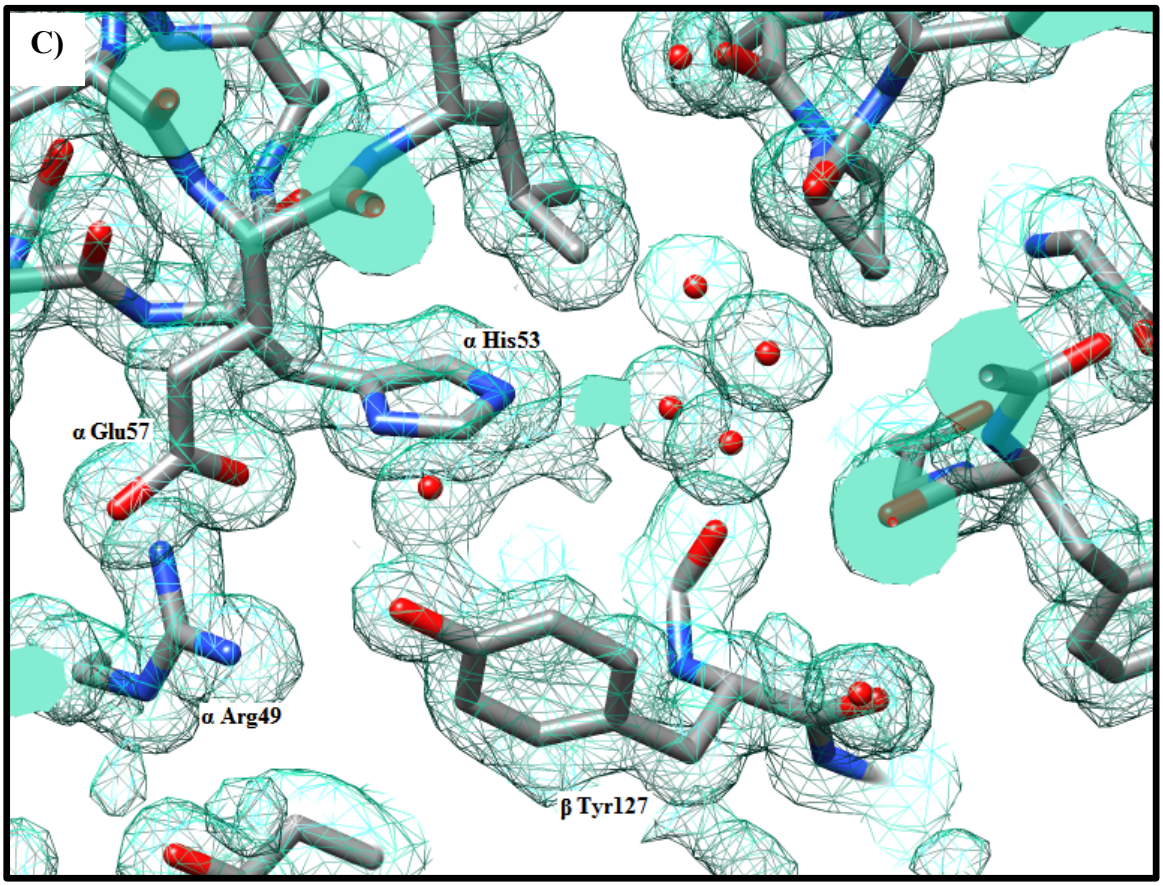
C)
α His53
α Glu57
α Arg49
β Tyr127

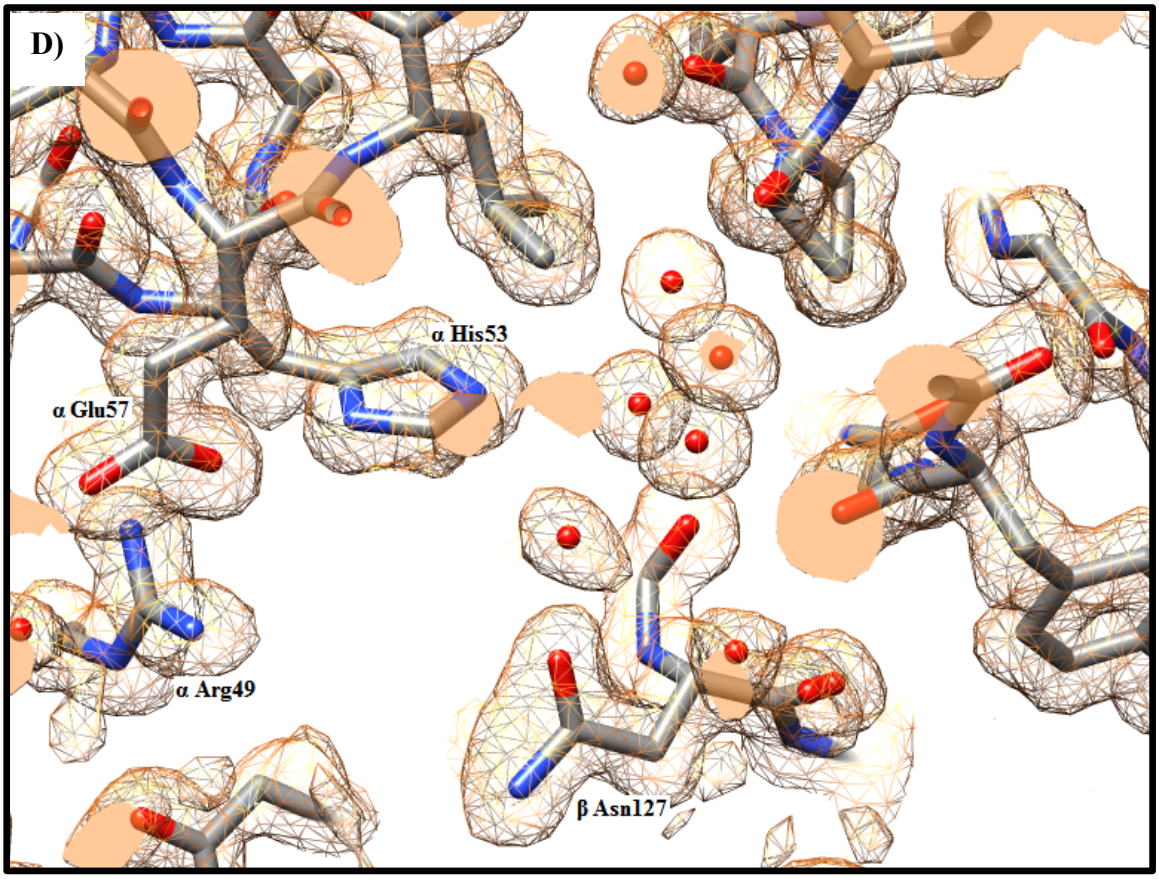

Figure 5.3: The WT NHase variant A) compared with the βY127N mutation in the 9E NHase variant B). Images C) and D) show the electron density maps and the protein mutation sites of the WT NHase and βY127N NHase mutant respectively. In both images A) and B), the α subunit is coloured green while the β subunit is coloured orange. The crystal structure of the mutant shows the water molecules involved in formation of a water bridge with αH53. In the WT NHase crystal structure, the O in the OH group of βTyr127 donates a hydrogen bond to Oε1 of αE57. The hydrogen bond of the mutant appears straight due to the overhead view of the hydrogen bond.

In the WT crystal structure, βTyr127 is hydrogen bonded to αArg49 (*fig.* 5.3 A) at a distance of 3.2 Å. The side-chains of αArg49 and αGlu57 are also hydrogen bonded to one another at distances of 3.3 Å and 2.8 Å in addition to the electrostatic interaction between the amine N and carbonyl O of both αArg49 and αGlu57. The side-chain of αHis53 is hydrogen bonded to αGlu57 and a water molecule (the HOH(2) in *fig.* 5.3 A) at 2.8 Å which is in turn hydrogen bonded to another water molecule (the HOH(1) in *fig.* 5.3 A) at 2.8 Å followed by a hydrogen bond to the OH of αTyr54.This network of hydrogen bonds is exhibited in both of the crystal structures of the WT NHase and 9E composite NHase mutant. The other

difference between the 9E composite NHase mutant and WT NHase besides presence of the βY127N mutation, is the presence of three water molecules in the 9E composite structure which adds to the hydrogen bond network interacting with βAsn127. The three water molecules labelled as HOH(3), HOH(4) and HOH(5) in (*fig*. 5.3 B) facilitate the connection between the α and β subunit. The electron density around βTyr127 and βAsn127 in the images of the WT NHase and the βY127N NHase mutant respectively (*fig*. 5.3 C and D) is well defined. In addition, the electron density around the interacting water molecules and side-chains is also well defined. An increase in inter subunit interactions have been shown to increase the energy required to break the subunit in our results and in other proteins such as a super oxide dismutase from *Potentilla atrosanguinea* as reported by (Kumar *et al*., 2012) and visualised in the crystal structure 2Q2L by Yogavel *et al*., (2008).

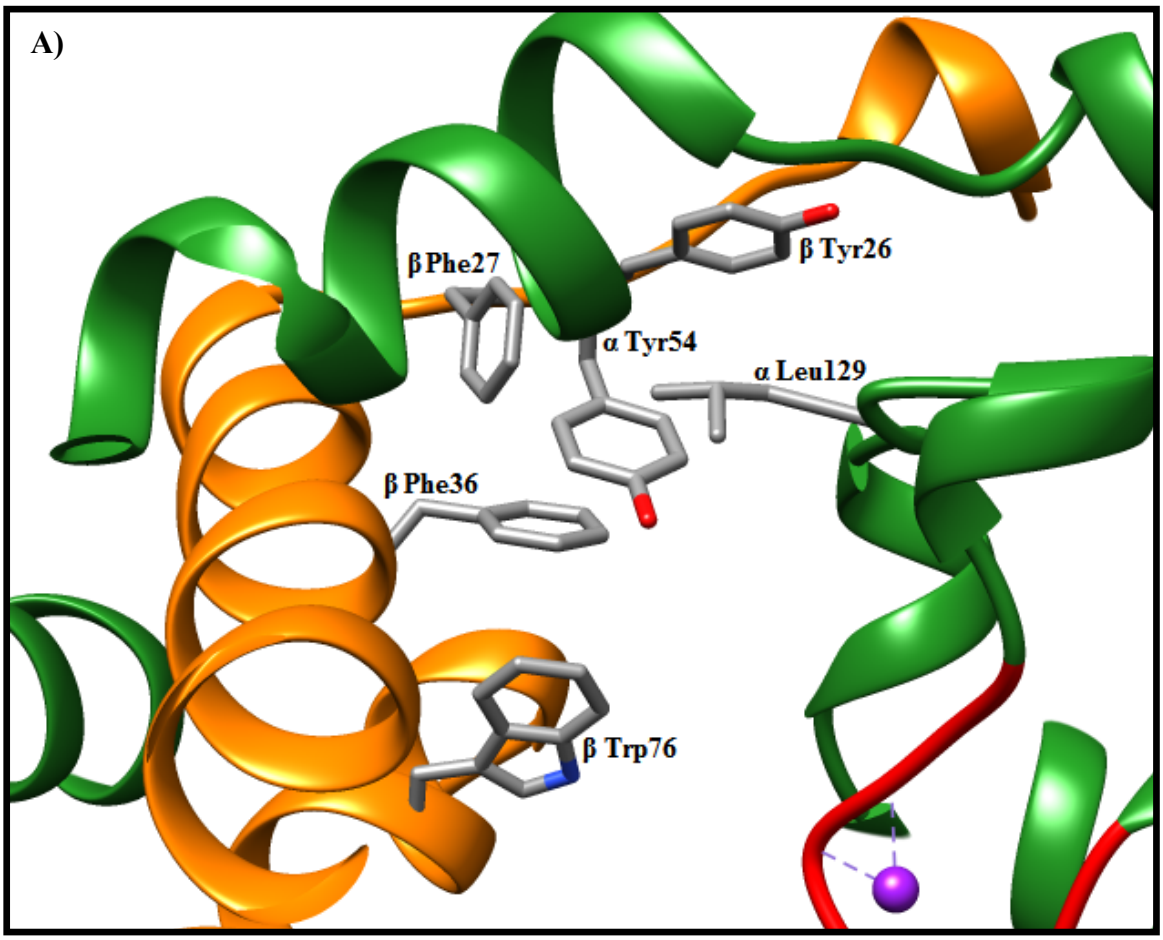

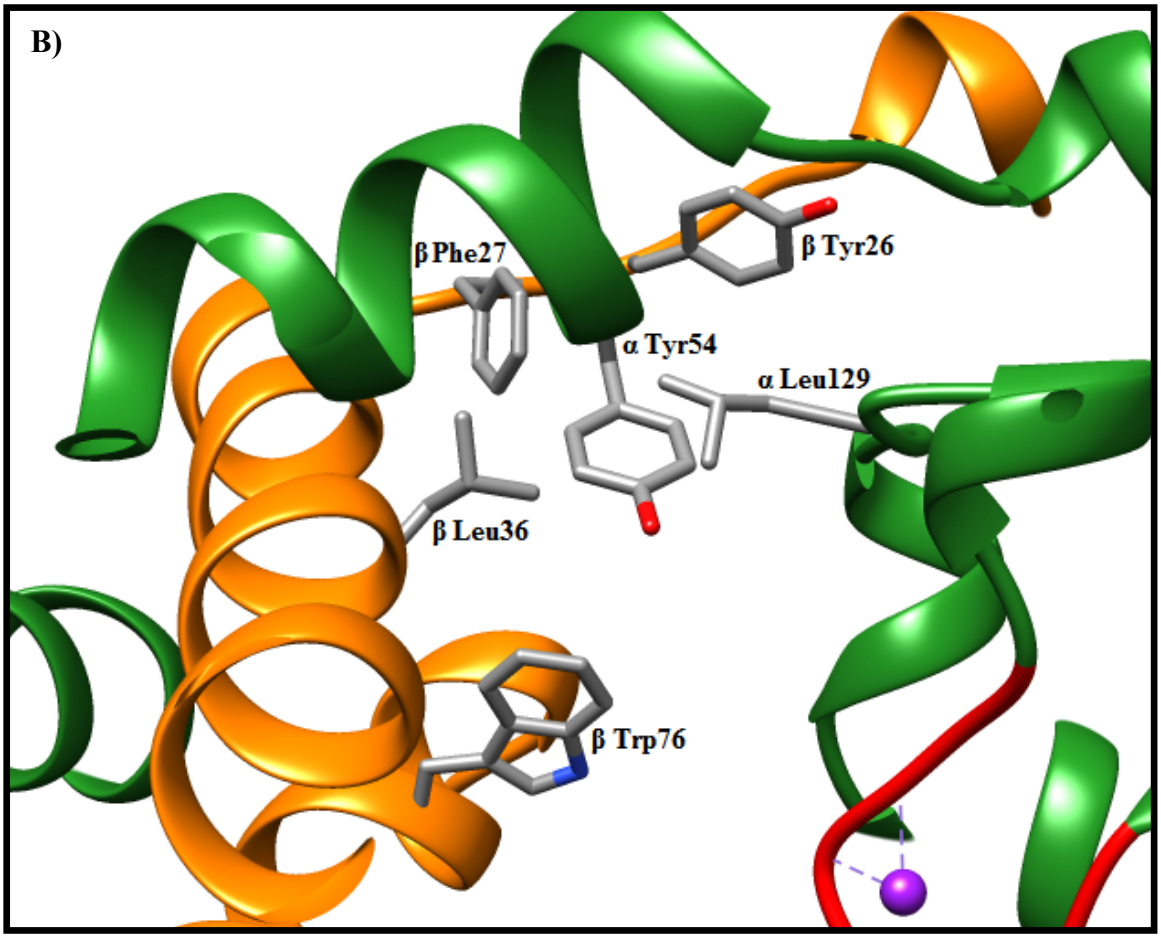
B)
β Phe27
β Tyr26
α Tyr54
α Leu129
β Leu36
β Trp76

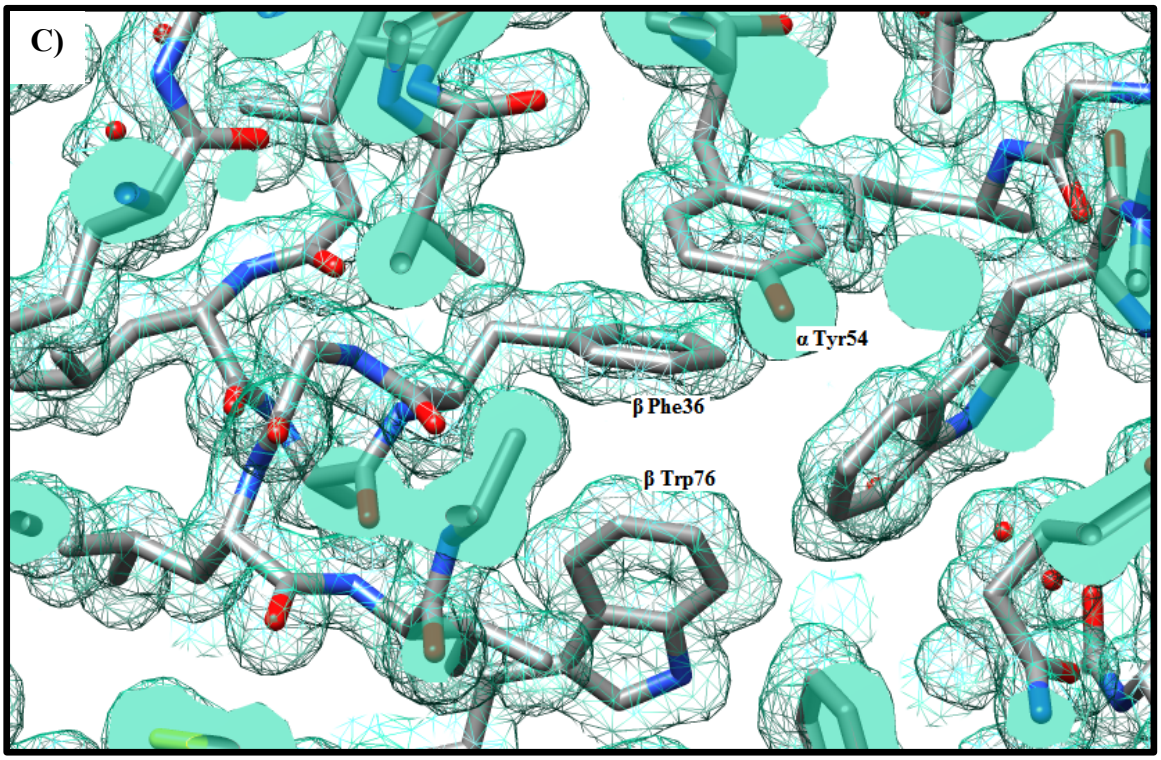
C)
α Tyr54
β Phe36
β Trp76

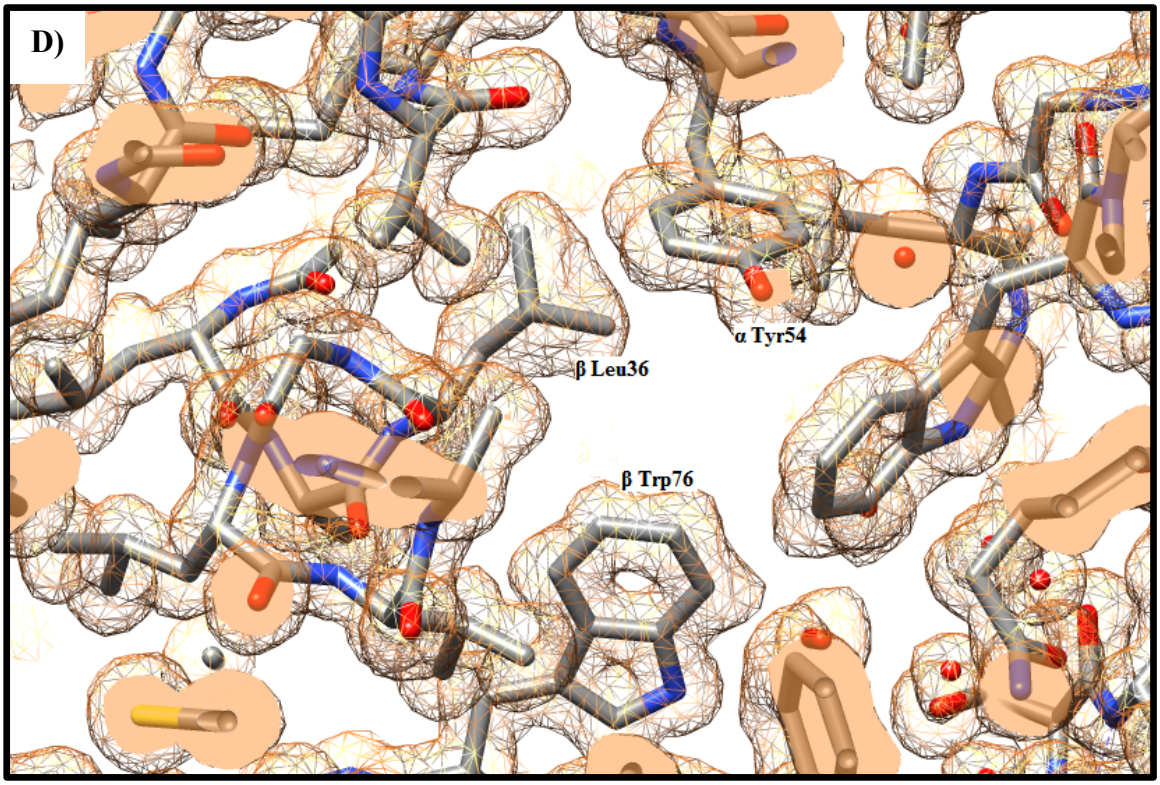

Figure 5.4: The WT NHase variant A) compared with the βF36L mutation in the 9E NHase variant B). Images C) and D) show the electron density maps and the protein mutation sites of the WT NHase and βF36L NHase mutant respectively. The α subunit is coloured green while the β subunit is coloured orange. The aromatic hydrophobic side-chain of βPhe36 fills the hydrophobic cavity better than βLeu36 and may interact with the aromatic ring of αTyr54 in the WT NHase. The other residues in the hydrophobic cavity are displayed.

The observed ΔΔG* of the βF36L mutant is similar to the WT (Table 4.3). The βF36L mutation changes the hydrophobic packing in that part of the enzyme and also breaks the interaction between the hydrophobic ring of βPhe36 and the ring of αTyr54 (*fig.* 5.4 B). In the WT NHase (WT NHase), the hydrophobic aromatic rings are at their closest, 4 Å apart and the indole system of βTrp76 forms a "wall" which is part of the hydrophobic cluster (*fig.* 5.4 A). The amino acid side-chains present in the cluster of hydrophobic side-chains are: αLeu129, αTyr54, βTyr26, βPhe27 and βTrp76 with βPhe36 in WT NHase or βLeu36 in the mutant. The ring of βPhe27 adjacent to βLeu36 may also contribute to the packing. The presence of the hydrophobic side-chains is in between both α and β subunits. The aromatic ring of βPhe36 fills the hydrophobic volume. The cluster of hydrophobic residues moves slightly inwards in the hydrophobic cavity. The electron density around βPhe36 in the image of the WT NHase (*fig.* 5.4 C) is well defined. However, the electron density around the

βLeu36 side-chain (*fig*. 5.4 D) suggests the βLeu side-chain is more mobile than the βPhe side-chain in the WT NHase at position 36. This suggests that when the βPhe was mutated to βLeu, the βLeu side-chain does not fill the hydrophobic cavity left behind as before in the WT NHase.

Structural Analysis of the 9C *G. pallidus*-RAPc8 NHase crystal structure

The 9C NHase composite mutant bears three mutations: αS169R, βM43K and βT150A whereby the first mutation is in the α subunit and the latter two are in the β subunit (*fig*. 5.5). The results from the hydroxamic acid assay (Table. 4.2) show that the $\Delta\Delta G^*$ values of the 9C NHase mutant and the three single NHase mutants αS169R, βM43K and βT150A are: -0.83 kJ/mol, -0.8 kJ/mol, -1.1 kJ/mol and +1.2 kJ/mol respectively. The sum of the $\Delta\Delta G^*$ of the single mutants is -0.73 kJ/mol. Thus the contribution by the single mutants adds up to within 0.1 kJ/mol of the $\Delta\Delta G^*$ of the 9C NHase mutant. The greatest contribution seems to be from βM43K and αS169R mutations which both mediate more inter-subunit interlinks in an environment with decreased degrees of freedom due to adjacent hydrophobic side-chains.

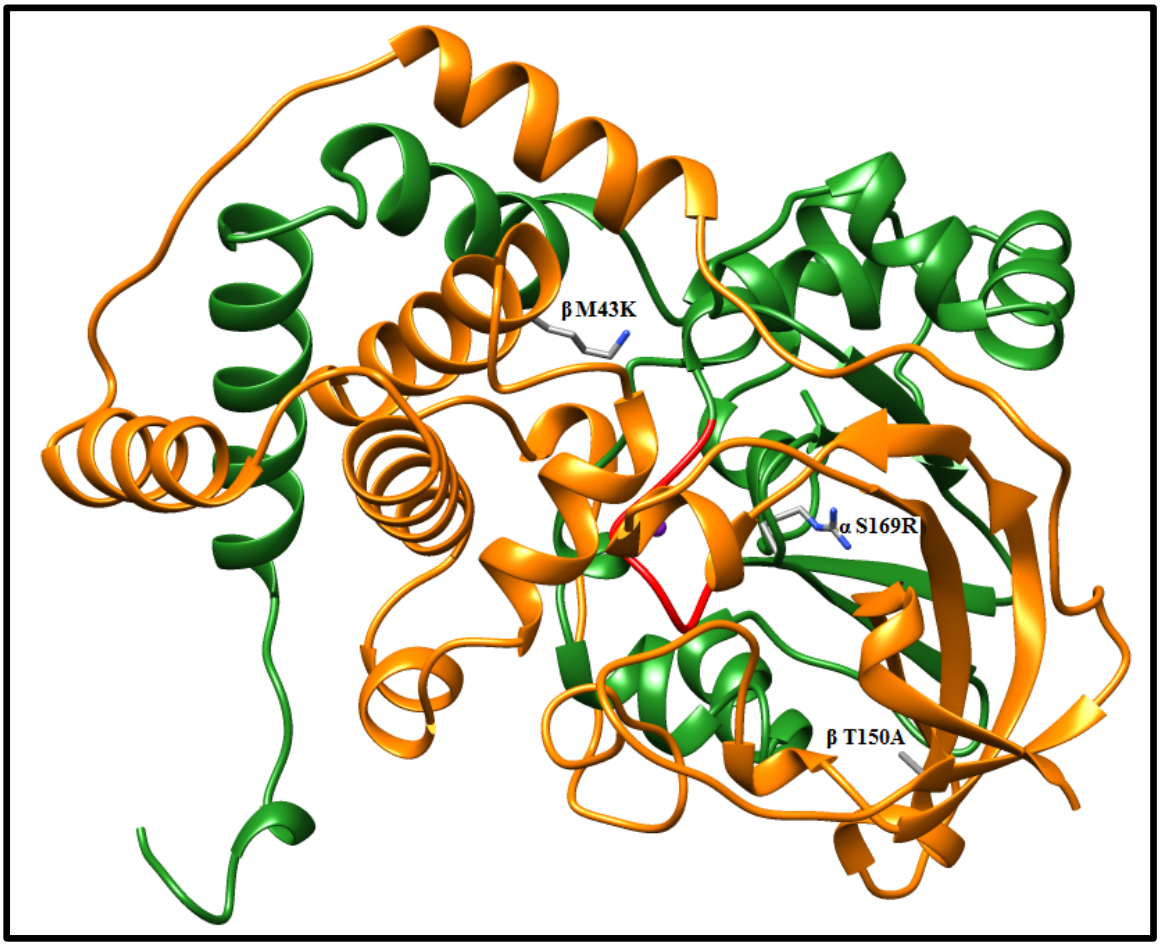

Figure 5.5: The crystal structure of the 9C composite mutant showing the locations of the three mutations: αS169R, βM43K and βT150A. The α subunit is coloured green while the β subunit is coloured orange. The main chain of the active site is coloured red with the low spin cobalt ion, partly obscured by an alpha helix, is coloured purple. The side-chains of the mutations are coloured by element: red represents oxygen; blue represents nitrogen while grey represents the carbon atoms and their bonds.

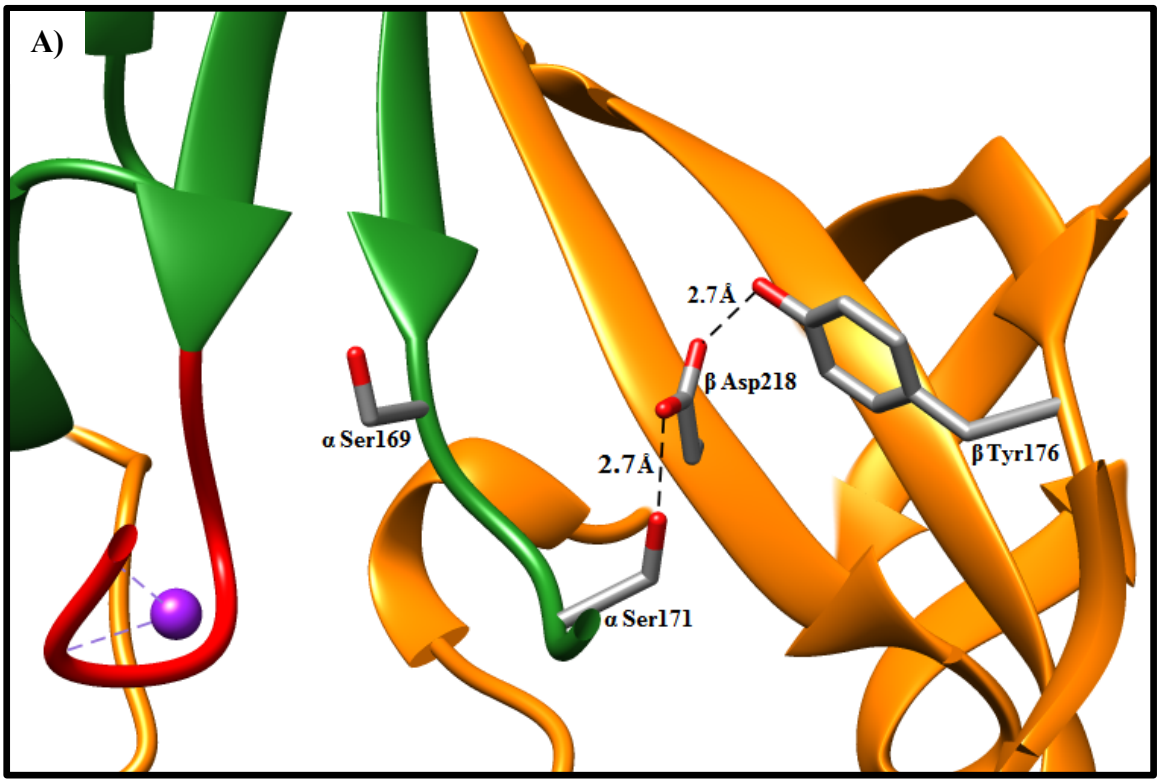

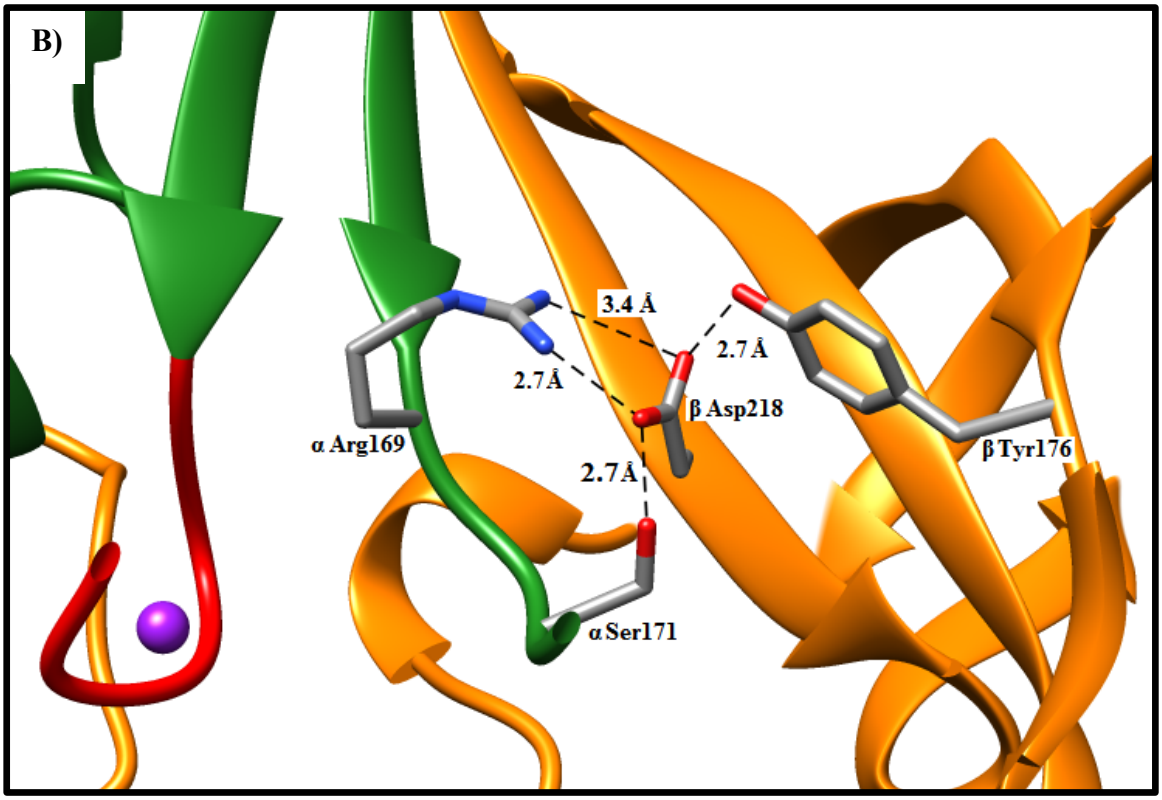
B)
3.4 Å
2.7Å
2.7 Å
2.7Å
α Arg169
β Asp218
β Tyr176
α Ser171

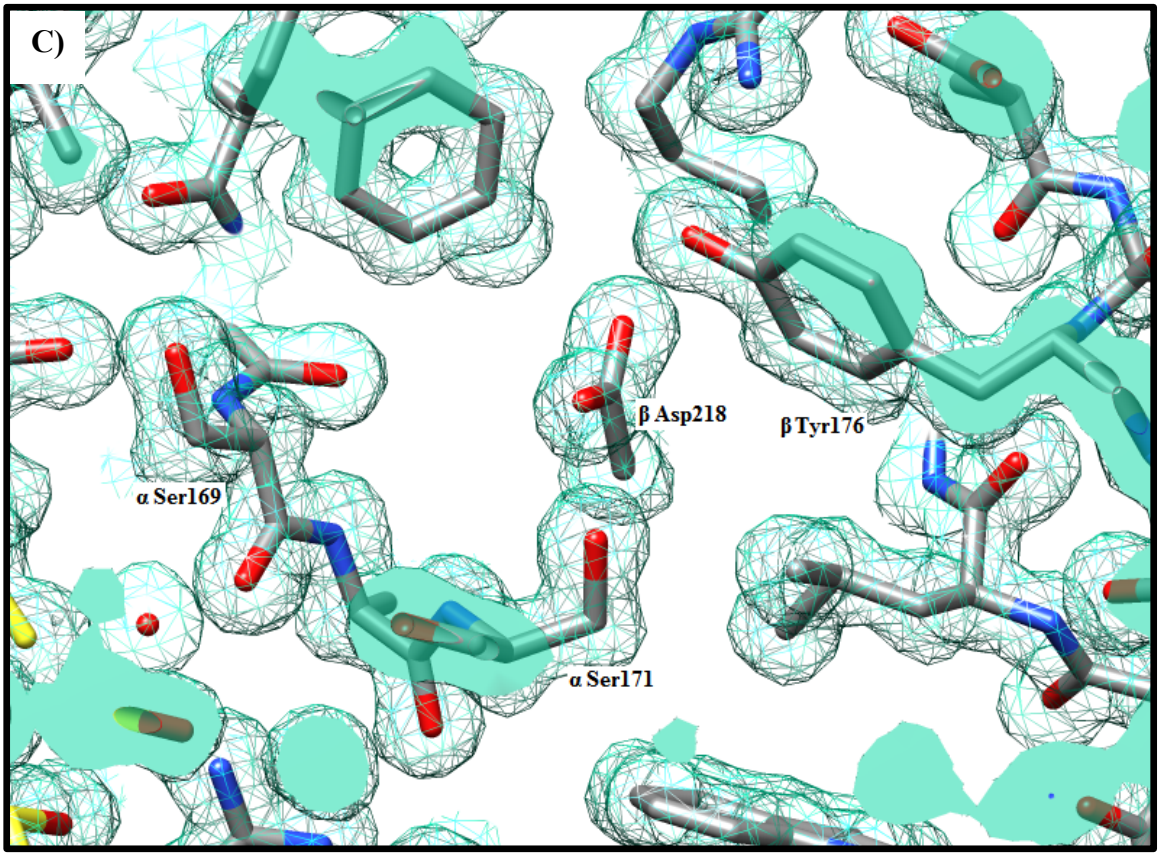
C)
β Asp218
β Tyr176
α Ser169
α Ser171

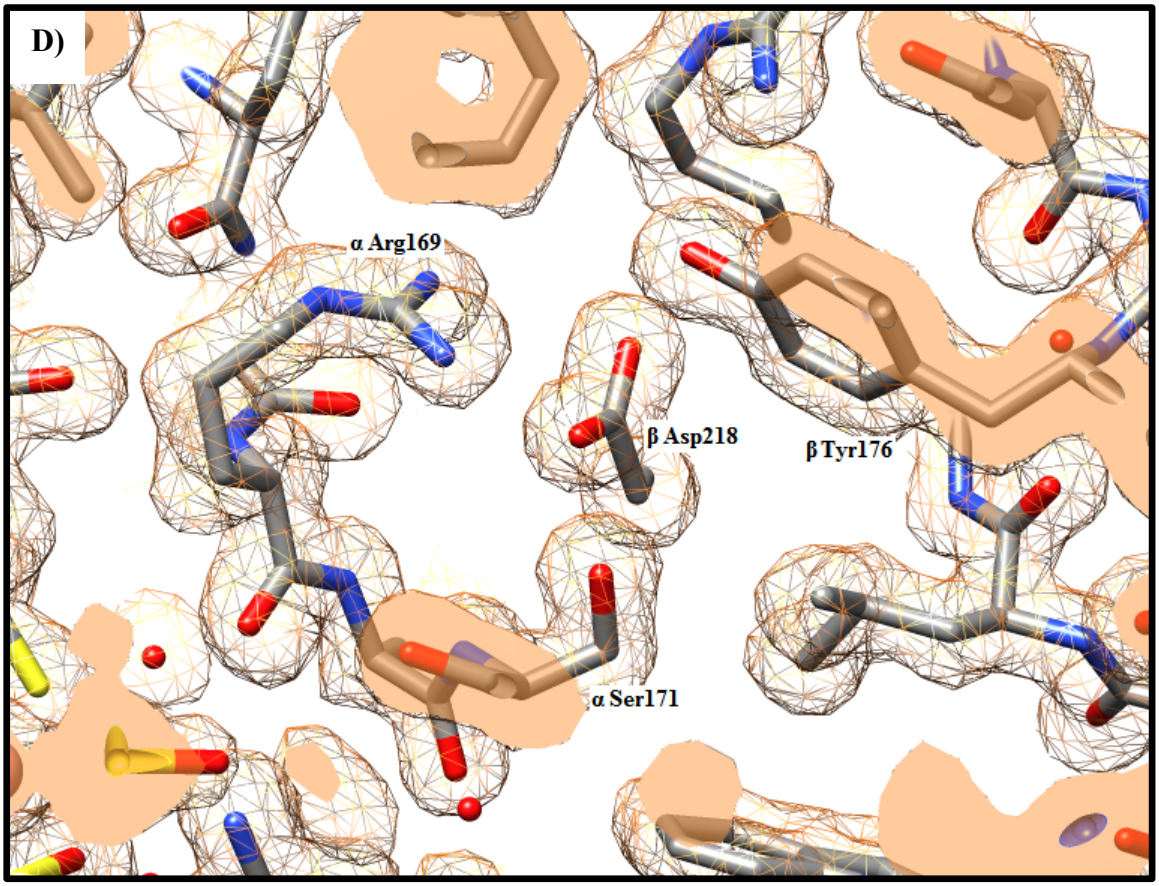

Figure 5.6: A) The WT NHase variant A) compared with the αS169R mutation in the 9C NHase variant B). Images C) and D) show the electron density maps and the protein mutation sites of the WT NHase and αS169R NHase mutant respectively. The αS169R mutation from the 9C composite NHase mutant. The α subunit is coloured green while the β subunit is coloured orange. The presence of other amino acid side-chains, αSer71, βAsp218 and βTyr76, which are hydrogen bonded to the αArg169 side-chain can be seen coloured by element.

The αS169R mutation is located in between both α and β subunits (*fig.* 5.6 B). The interaction between both subunits is facilitated by the salt bridge formed by the guanidino group of αArg169 and the carbonyl O atoms of αSer171 and βAsp218. In the WT NHase, the Oγ of αSer169 is seen pointing towards the main chain of αVal115 within a distance of less than 3.5 Å. Being within hydrogen bonding distance and the apparent direction of the side-chain of αSer169, this would suggest it forms a hydrogen bond with the main chain of αVal115. The side-chains Oγ of αSer171, Oδ1 and Oδ2 of βAsp218 and the OH of βTyr176 are interlinked via hydrogen bonding to another as depicted in the crystal structure of WT NHase (*fig.* 5.6 A). In the crystal structure depicting the αS169R mutation (*fig* 5.6 B), the

side-chain of αArg169 in the mutant NHase is facing the opposite direction compared to the side-chain of αSer169 in the WT NHase. The side-chain amines of αArg169 form two interactions with Oδ1 and Oδ2 of βAsp218 (*fig.* 5.6 B) at distances of 2.8 Å and 3.4 Å respectively. The electron density around αSer169 and αArg169 in the images of the WT NHase and the βS169R NHase mutant respectively (*fig.* 5.6 C and D) is well defined suggesting these side-chains have limited flexibility and maintained the interactions during elevated temperatures.

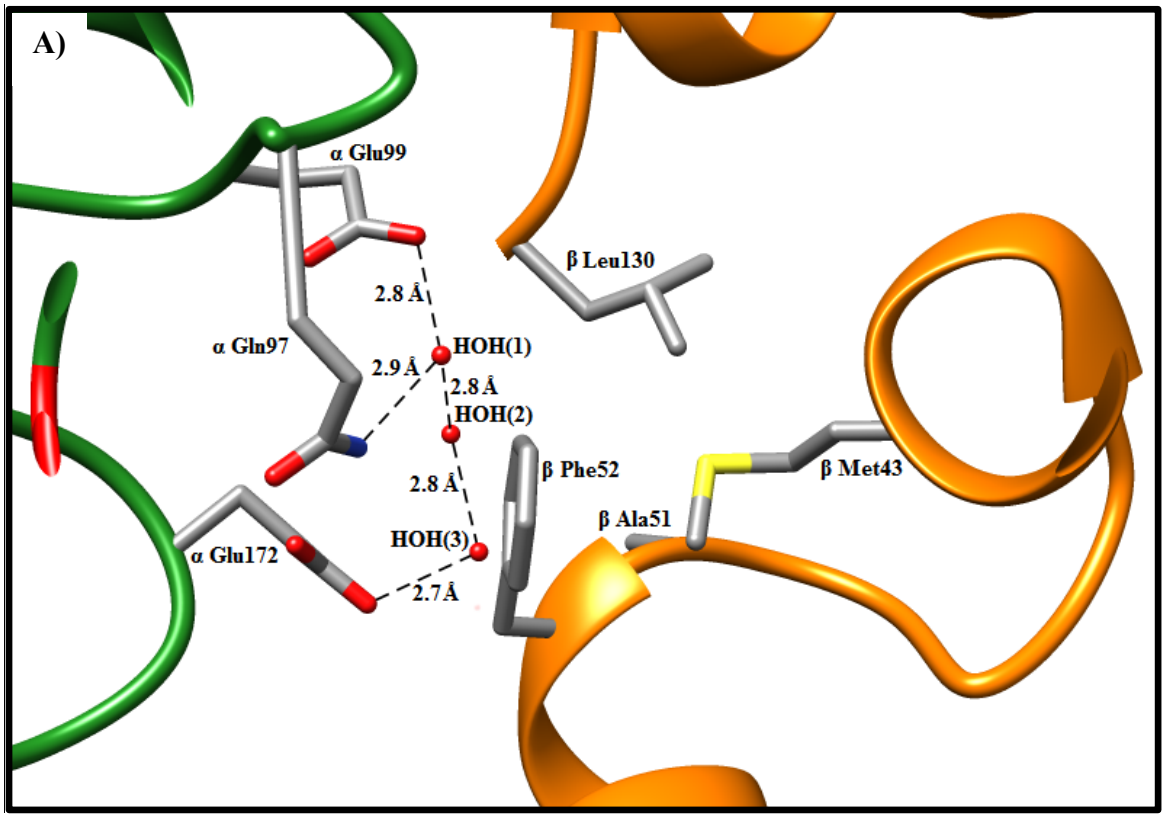

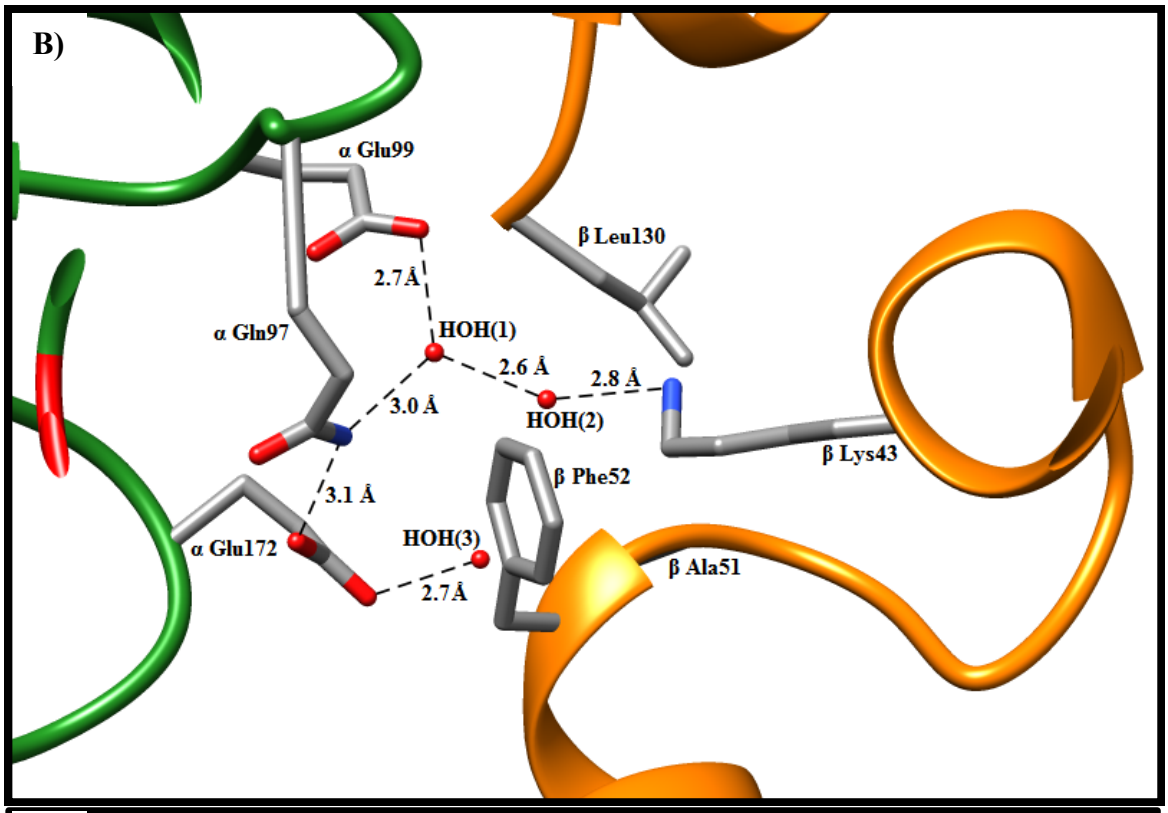
B)
α Glu99
β Leu130
2.7Å
α Gln97
HOH(1)
2.6 Å
2.8 Å
3.0 Å
HOH(2)
β Lys43
β Phe52
3.1 Å
HOH(3)
α Glu172
β Ala51
2.7Å

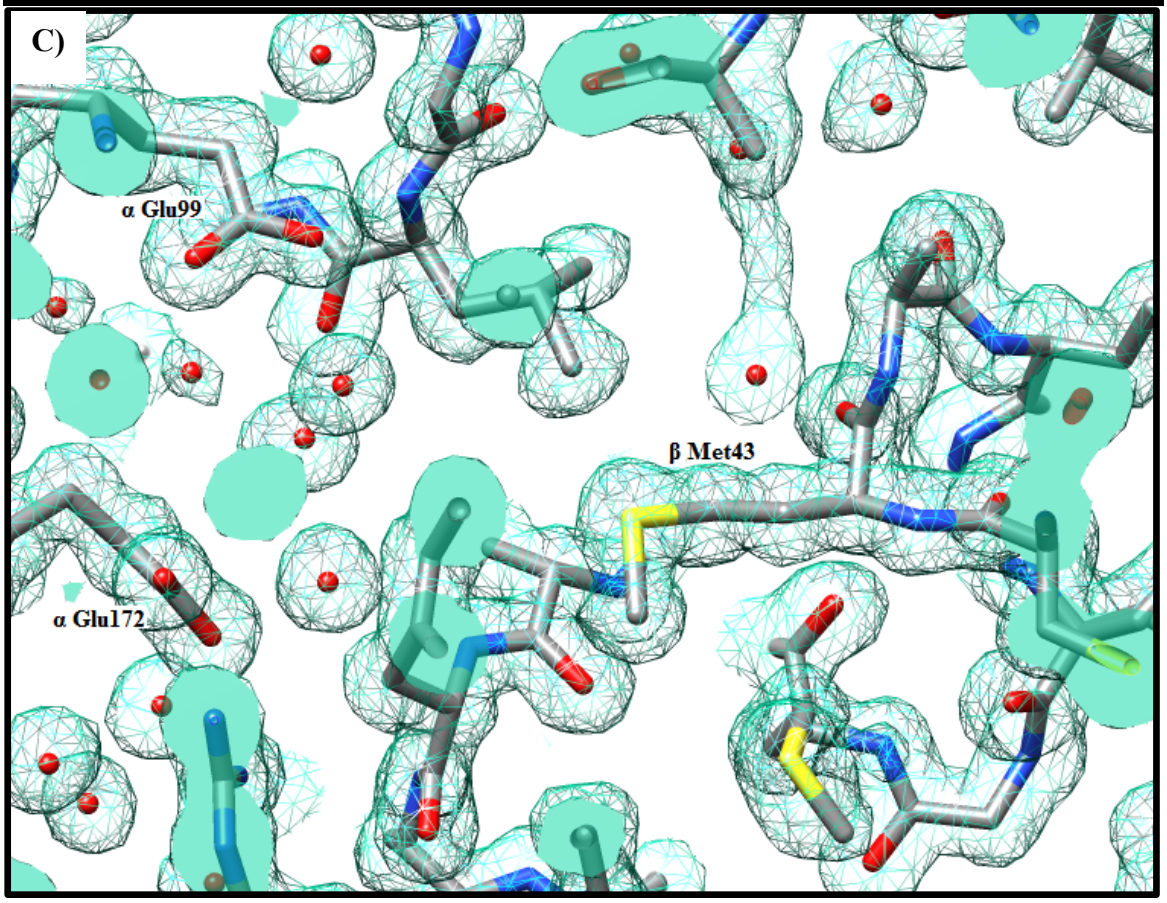
C)
α Glu99
β Met43
α Glu172

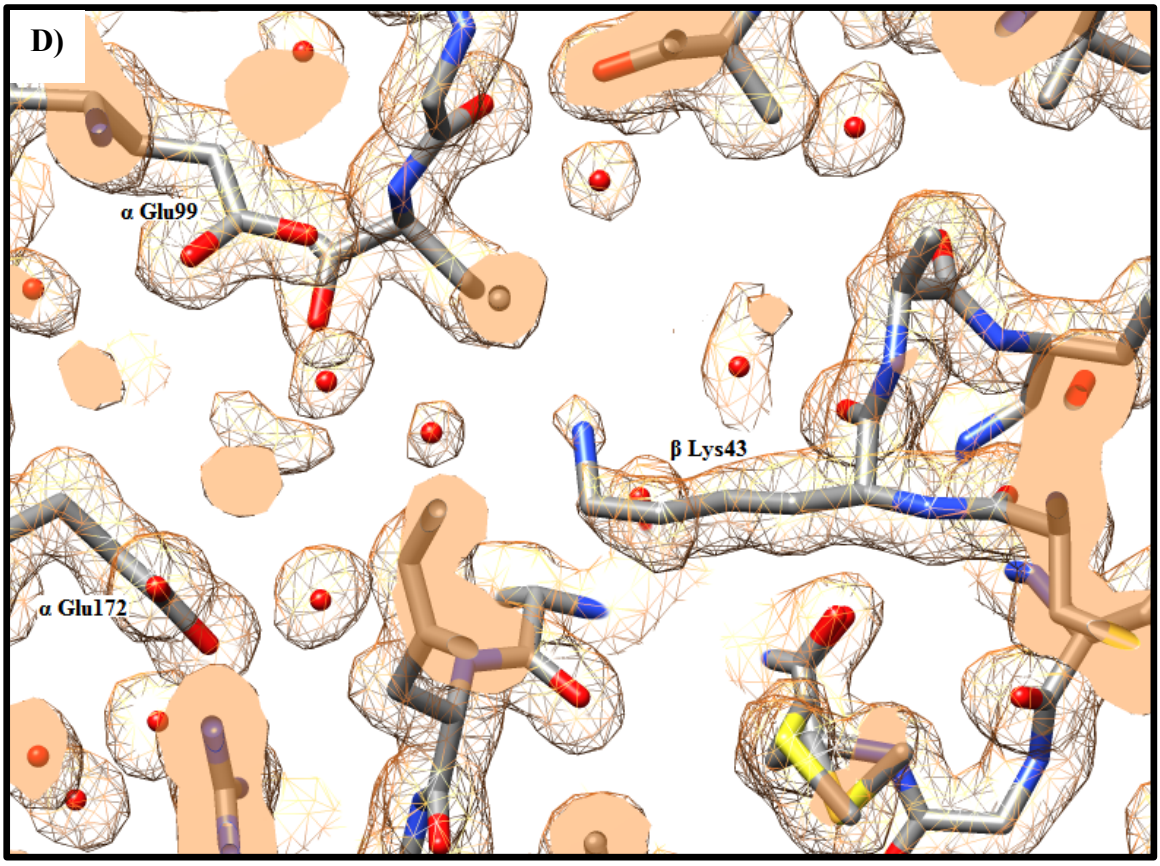

Figure 5.7: A) The WT NHase variant A) compared with the βM43K mutation in the 9C NHase variant B). Images C) and D) show the electron density maps and the protein mutation sites of the WT NHase and βM43K NHase mutant respectively. The crystal structures of the WT NHase with the α subunit coloured green while the β subunit is coloured orange. The hydrogen bonded side-chains of αGlu99 αGln97 and αGlu172 are present in both A) and B) whereby they are hydrogen bonded with two water molecules labelled as HOH(1) and HOH(3). The βPhe52 side-chain is shown situated perpendicularly to the plane of the hydrogen bond network between αGln97 and βLys43.

The βM43K mutation is located between the core and the periphery of NHase (*fig*. 5.7 A). The WT NHase crystal structure shows a βMet residue at position 43 in the β subunit while the crystal structure of the 9C composite mutant shows a βLys residue in the same position. In A) the βMet43 is seen clustering with the hydrophobic side-chains of βAla51, βLeu130 and the aromatic ring of βPhe52 inclined away from the hydrophilic side-chains of αGlu99, αGln97 and αGlu172. The S of the thioether in βMet43 in WT NHase is not observed interacting with any other side-chain at a distance of less than 3.5 Å. A network of hydrogen bonds consisting of HOH(1), HOH(2) and HOH(3) is observed interacting via hydrogen bonding with αGlu99, αGln97 and αGlu172, (*fig*. 5.7 A and B). The presence of the

hydrophobic side-chains of βPhe52 and βLeu130 reduce the degrees of freedom allowed for the hydrophilic side-chains to interact. The βM43K mutation resulted in a higher measured thermal stability of the βM43K mutant relative to WT NHase (Table. 4.3); however, their absolute rates of catalysis at 298 K were different with the WT NHase showing a higher catalytic rate (*fig*. 4.12).

The observed difference in catalytic rate could be attributed to two effects: the oxidation of the catalytic Cys sulfenic side-chain which has been shown to be important for NHase activity (Hashimoto *et al*., 2008; Hopmann, 2014) or obstruction of the substrate pathway to the active site. The latter was observed by a nearby placed amino acid residue, βMet40, by Hashimoto *et al*., (2008) in an Fe-NHase. The side-chain of βMet40 had to swing open to allow the substrate access to the active site. This was determined by measuring the occupancies of the side-chain of βMet40 while the substrate was in transit to the active site. Normalizing for both rates of catalysis would suggest that the βM43K mutant contributes to thermal stability but has a reduced catalytic rate as measured and reported in the velocity vs rate assay (*fig*. 4.12). The electron density around βMet43 in the image of the WT NHase (*fig*. 5.7 C) is well defined. However, the electron density around βLys43 is poorly defined (*fig*. 5.7 D). This suggests that the βMet43 side-chain destabilises this part of the enzyme but could facilitate increased access of the substrate to the active site.

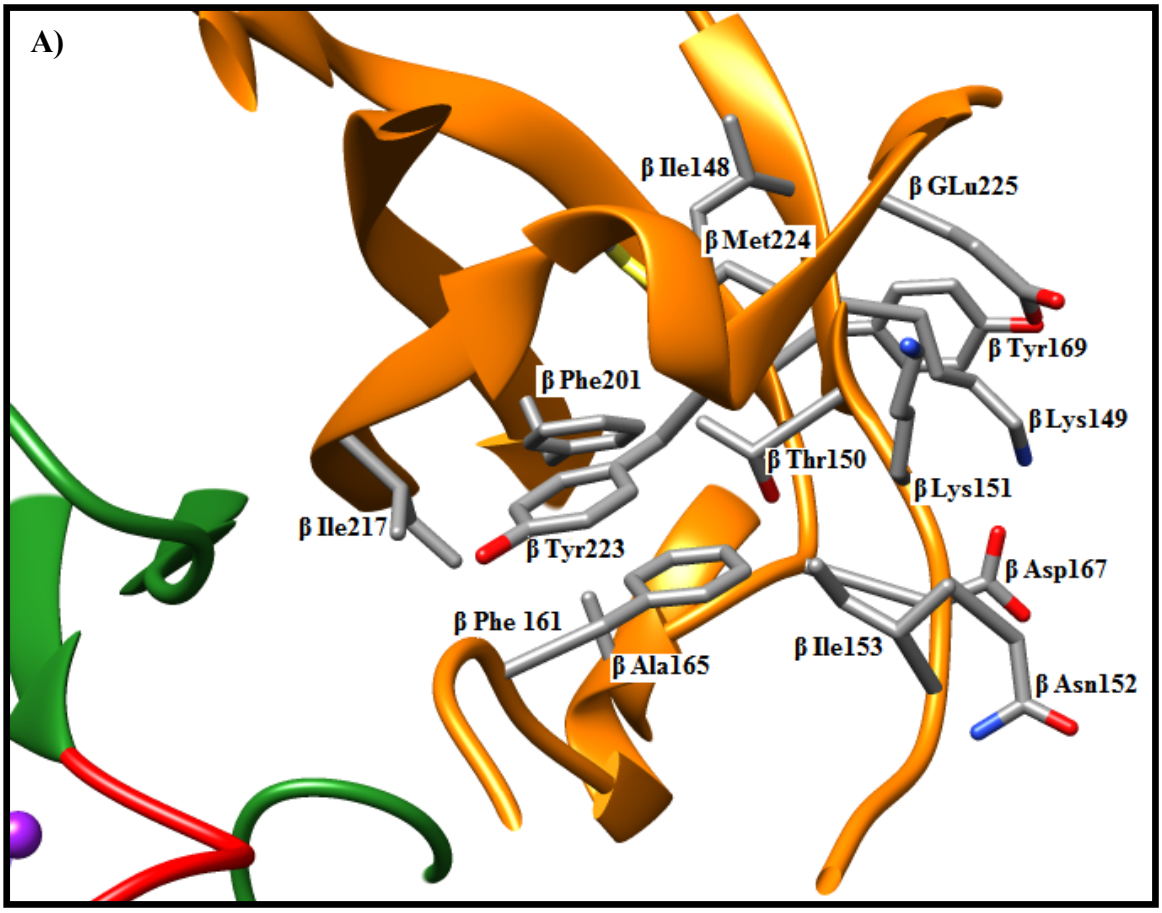
A)
β Ile148
β GLu225
β Met224
β Tyr169
β Phe201
β Lys149
β Thr150
β Lys151
β Ile217
β Tyr223
β Asp167
β Phe 161
β Ile153
β Ala165
β Asn152

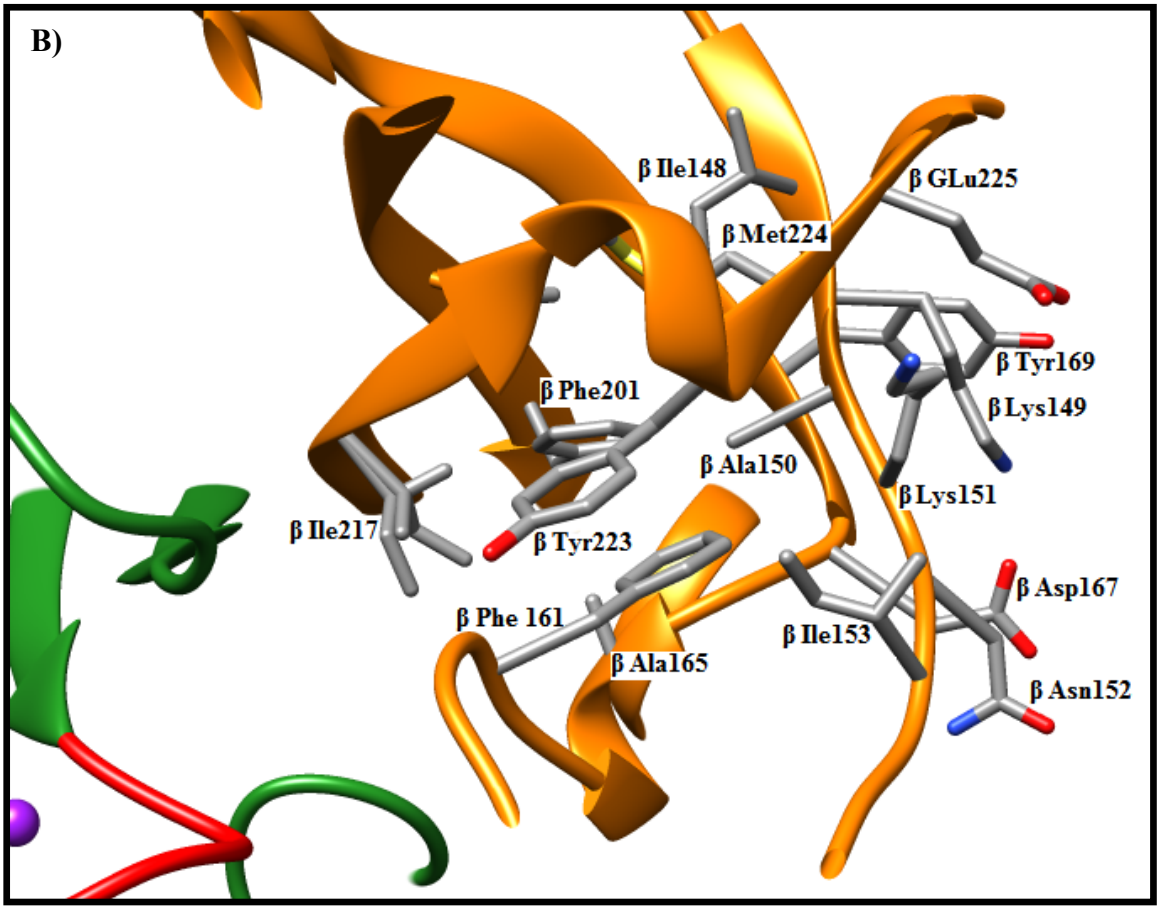
B)
β Ile148
β GLu225
β Met224
β Tyr169
β Phe201
β Lys149
β Ala150
β Lys151
β Ile217
β Tyr223
β Asp167
β Phe 161
β Ile153
β Ala165
β Asn152

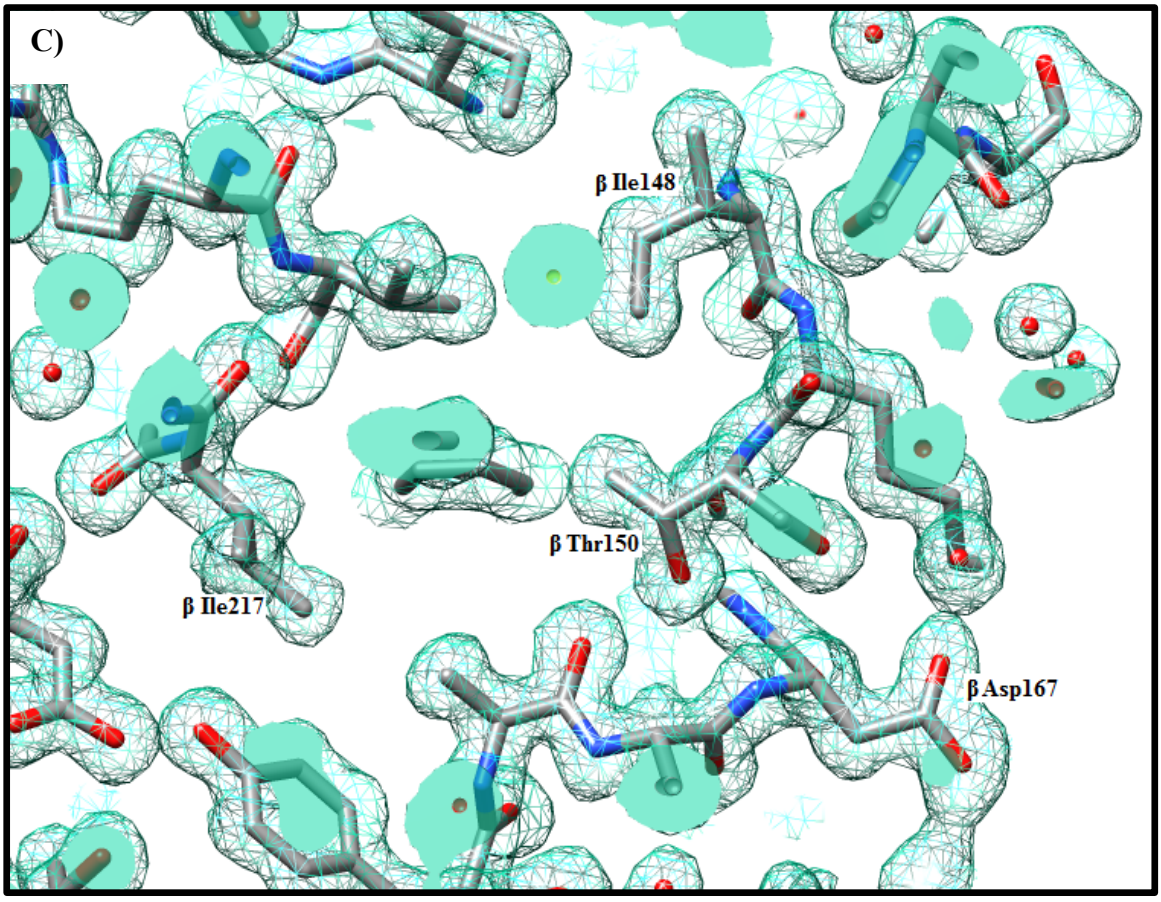
C)
β Ile148
β Thr150
β Ile217
βAsp167

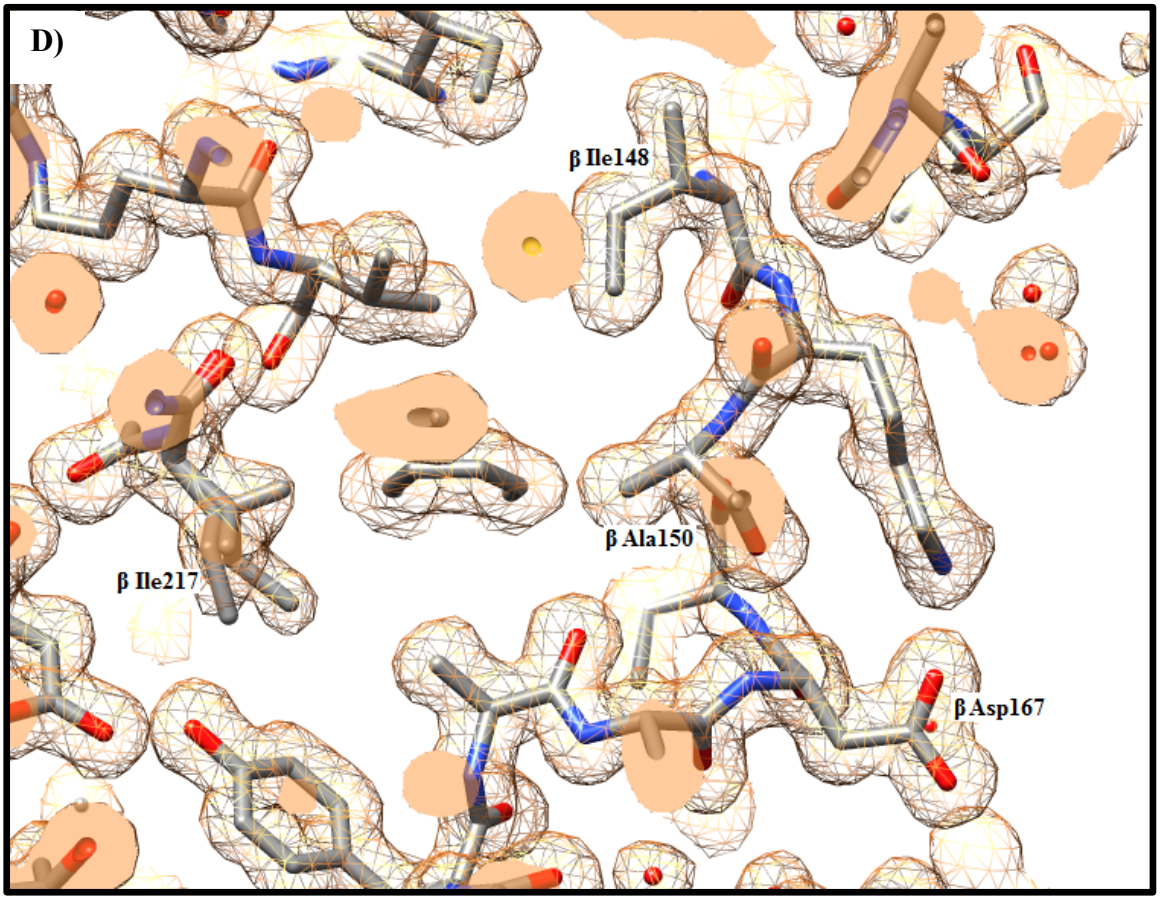
D)
β Ile148
β Ala150
β Ile217
βAsp167

Figure 5.8: A) The WT NHase variant A) compared with the βT150A mutation in the 9C NHase variant B). Images C) and D) show the electron density maps and the protein mutation sites of the WT NHase and βT150A NHase mutant respectively. The α subunit is coloured green while the β subunit is coloured orange in both images. The cluster of hydrophobic side-chains: βIle48, βMet224, βPhe201, βPhe161, βAla165 and βIle153 are seen clustering together while the hydrophilic side-chains of βGlu225, βTyr169, βLys149, βAsp167, βAsn152 and the OH of βTyr223 are all pointing away from the cluster of hydrophobic side-chains in both A) and B). The βLys149 side-chain takes different conformations in image A) and B).

The βT150A mutant is a component of the 9C NHase mutant. The mutant is an intra-subunit mutation located on the periphery of the NHase structure (*fig*. 5.8 B). In the crystal structure of the WT NHase, βThr150 makes a 2.7 Å hydrogen bond to the backbone carbonyl of βAla165. A shift in the backbone allows βLys149 to interact with the carbonyl of βLys 167 via hydrogen bonding. The shift of the backbone causes the hydrogen bond in the WT NHase between βLys149 and βTyr169 to transfer and link βLys149 with βAsp167 in the 9C mutant NHase. The electron density around βThr150 in the images of the WT NHase (*fig*. 5.8 C) and βAla150 (*fig*. 5.8 D) is well defined. The observed decrease in thermal stability of the βT150A single mutant relative to WT NHase would suggest that the interference of the hydrogen bond network adjacent to the mutation site resulted in the decreased thermal stability.

Structural Analysis of the 8C *G. pallidus*-RAPc8 NHase crystal structure

The 8C composite mutant contains three mutations, all within the β subunit: βD96E, βM188V, βD167V (*fig*. 5.9).

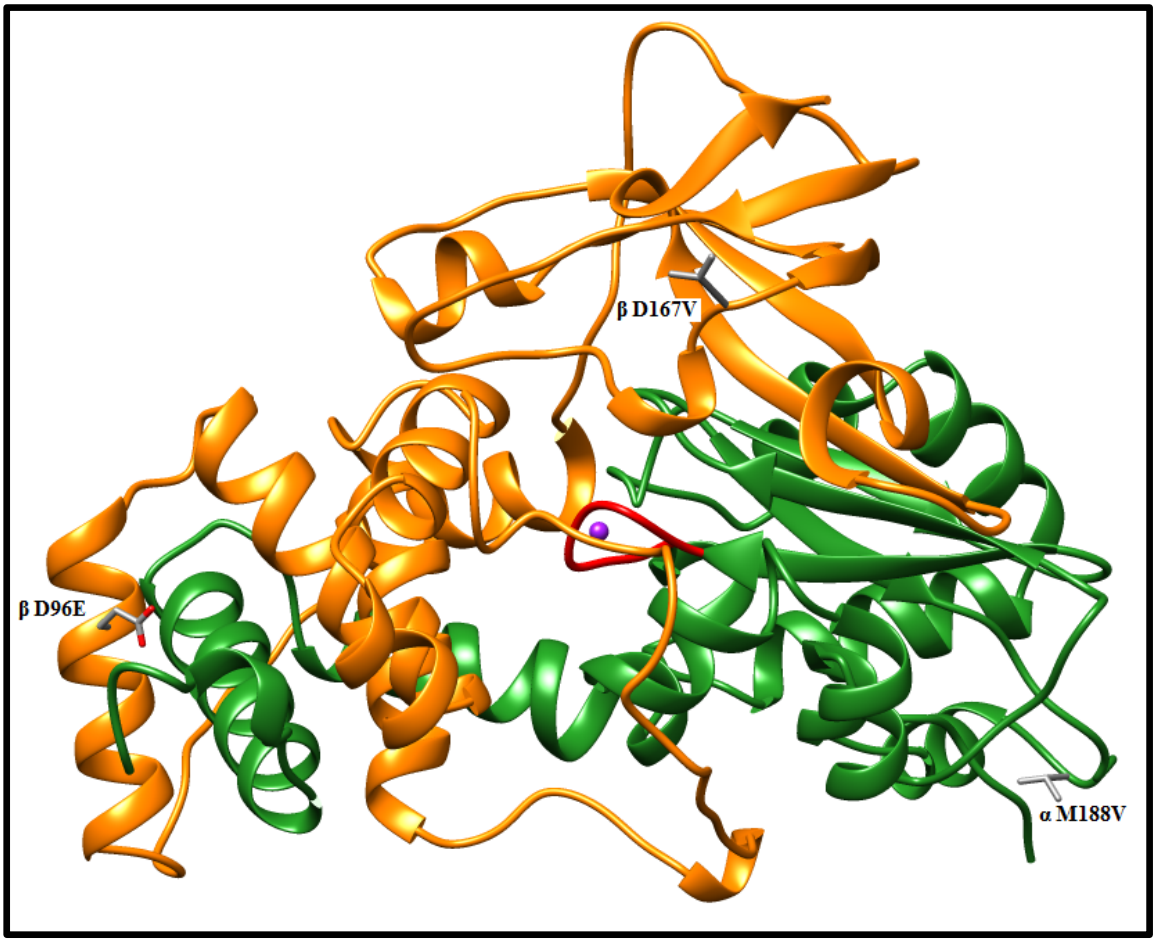

Figure 5.9: The crystal structure of the 8C NHase composite mutant containing three mutations: βD96E, αM188V, βD167V. The α subunit is coloured green while the β subunit is coloured orange. The main chain along the active site is coloured red while the low spin cobalt ion is coloured purple. The side-chains of the mutations are coloured by element: red represents oxygen while grey represents the carbon atoms and their bonds.

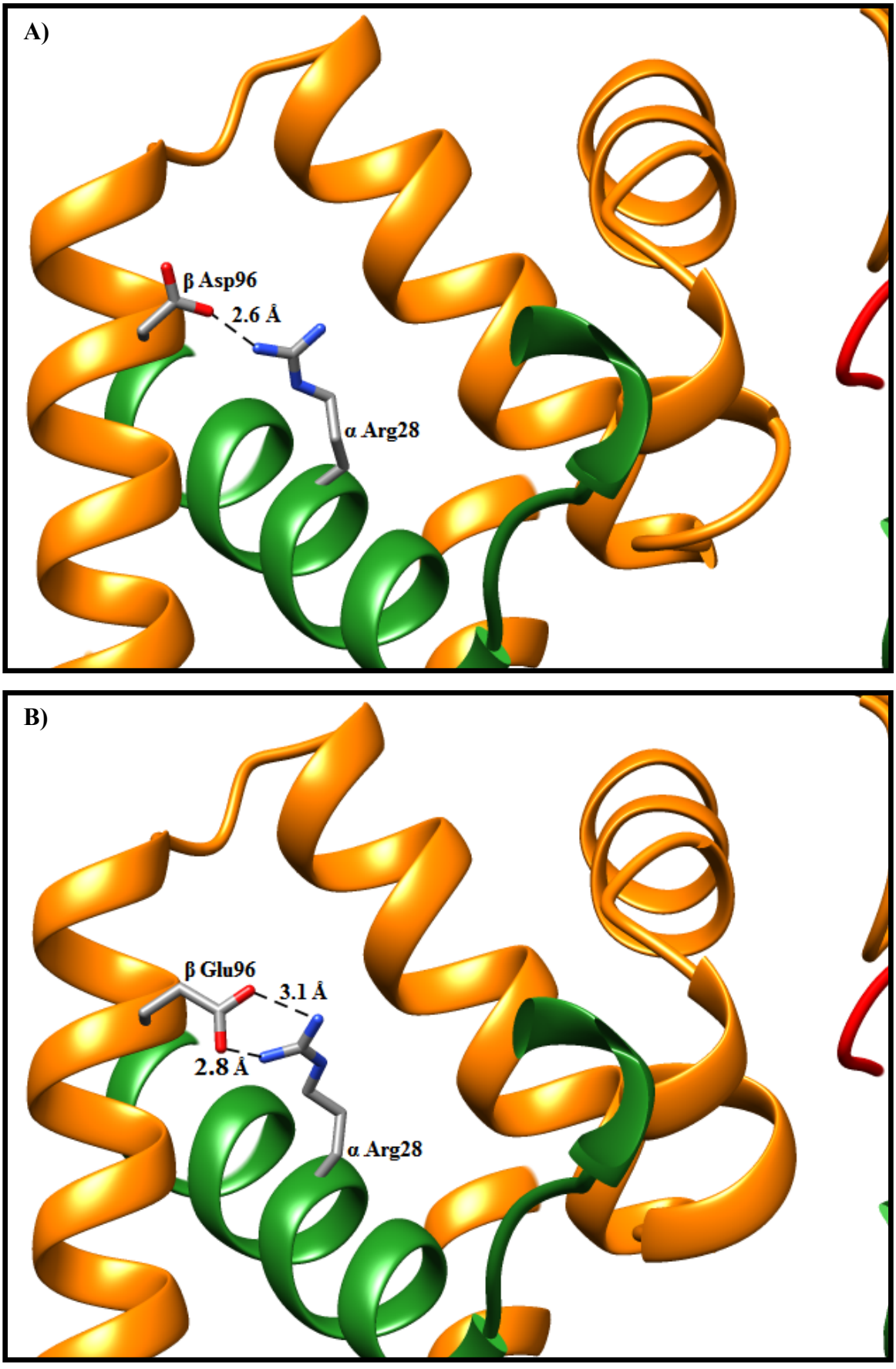
A)
β Asp96
2.6 Å
α Arg28
B)
β Glu96
3.1 Å
2.8 Å
α Arg28

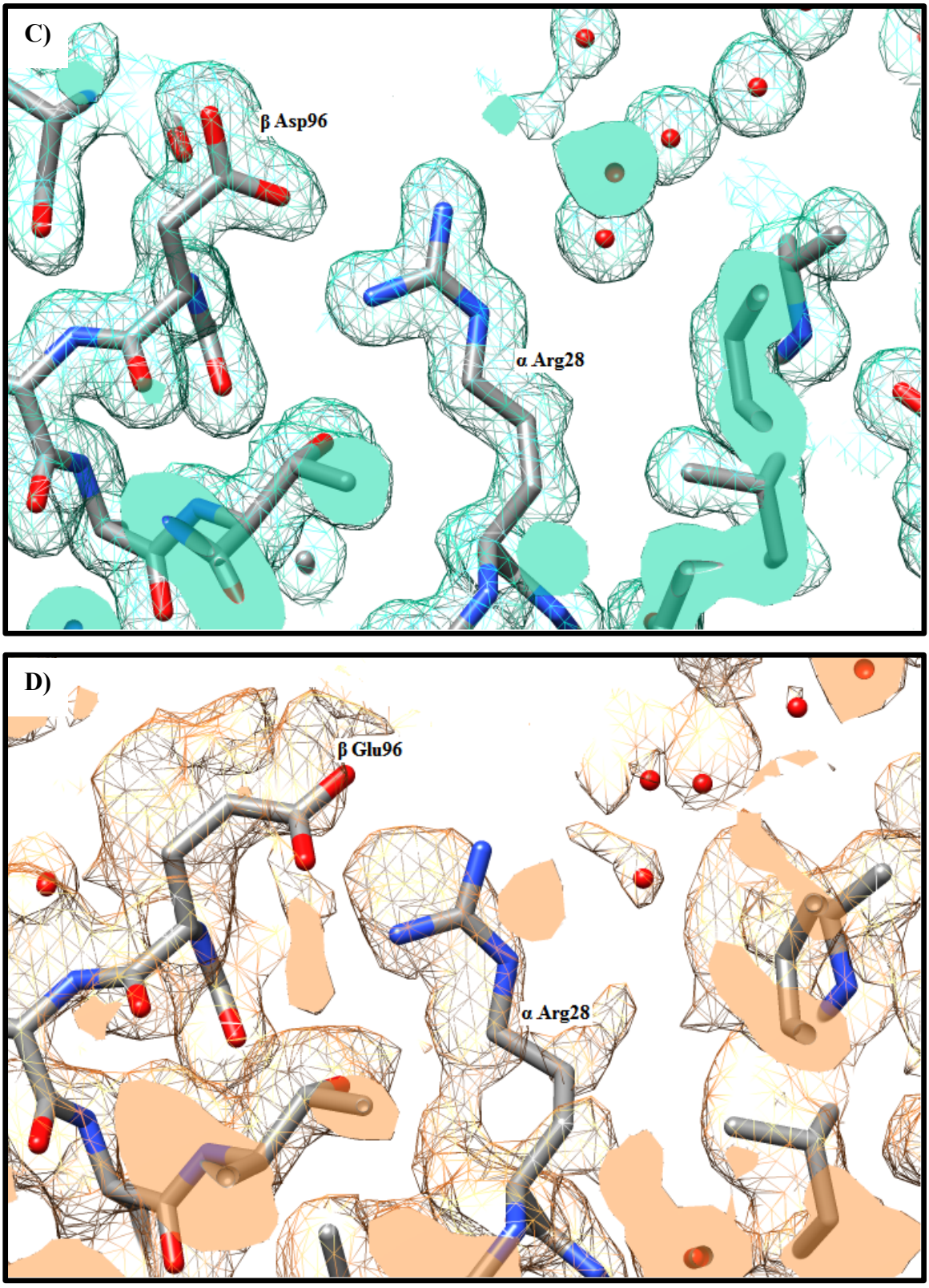

Figure 5.10: A) The WT NHase variant A) compared with the βD96E mutation in the 8C NHase variant B). Images C) and D) show the electron density maps and the protein mutation sites of the WT NHase and βD96E NHase mutant respectively. In both images, the α subunit is coloured green while the β subunit is coloured orange. The βAsp96 in A) and the βGlu96

in B) are depicted with the targeted interacting residue βArg28 shown in stick representation in both crystal structures. The additional hydrogen bond in the mutant adds an interlink between the α and β subunits.

The βD96E single mutant has a $\Delta\Delta G^*$ energy of -1.02 kJ/mol which is similar to the $\Delta\Delta G^*$ energy of the other inter-subunit mutation βM43K (Table 4.3). The location of the βD96E mutation is between the subunits (*fig*. 5.10 B). The βAsp96 side-chain in the WT NHase forms a single hydrogen bond and salt bridge with αArg28 at a distance of 2.6 Å (*fig*. 5.10 A). The electron density around βAsp96 and αArg28 in the image of the WT NHase (*fig*. 5.10 C) is well defined. On the other hand, the poor electron density around βGlu96 and αArg28 in the image of the 8C NHase mutant could have resulted from the crystallisation or data collection. However, fitting the side-chains in the best possible manner using iterative restrained refinements shows that both side-chain ends are facing one another likely resulting from an interaction between the two side-chains in the βD96E mutant when compared to the corresponding image of the WT NHase (*fig*. 5.10 D and C, respectively). In the crystal structure depicting the mutation at this position, two hydrogen bonds are likely formed between both the carbonyl O of βGlu96 and the guanidino group of αArg28 at 2.8 Å and 3.1 Å (*fig*. 5.10 B). In addition, there are shifts in the backbone surrounding these residues which would imply that the structure around this region is influenced by the interactions of βGlu96 and αArg28. The proximity of opposite charges of the guanidino group of αArg28 and the carbonyl O of βAsp96 would also contribute to the energy required to break the interaction between the side-chains of βGlu96 and αArg28. Thus the energy required to unfold the single mutant βD96E is higher relative to WT NHase as shown in table 4.3.

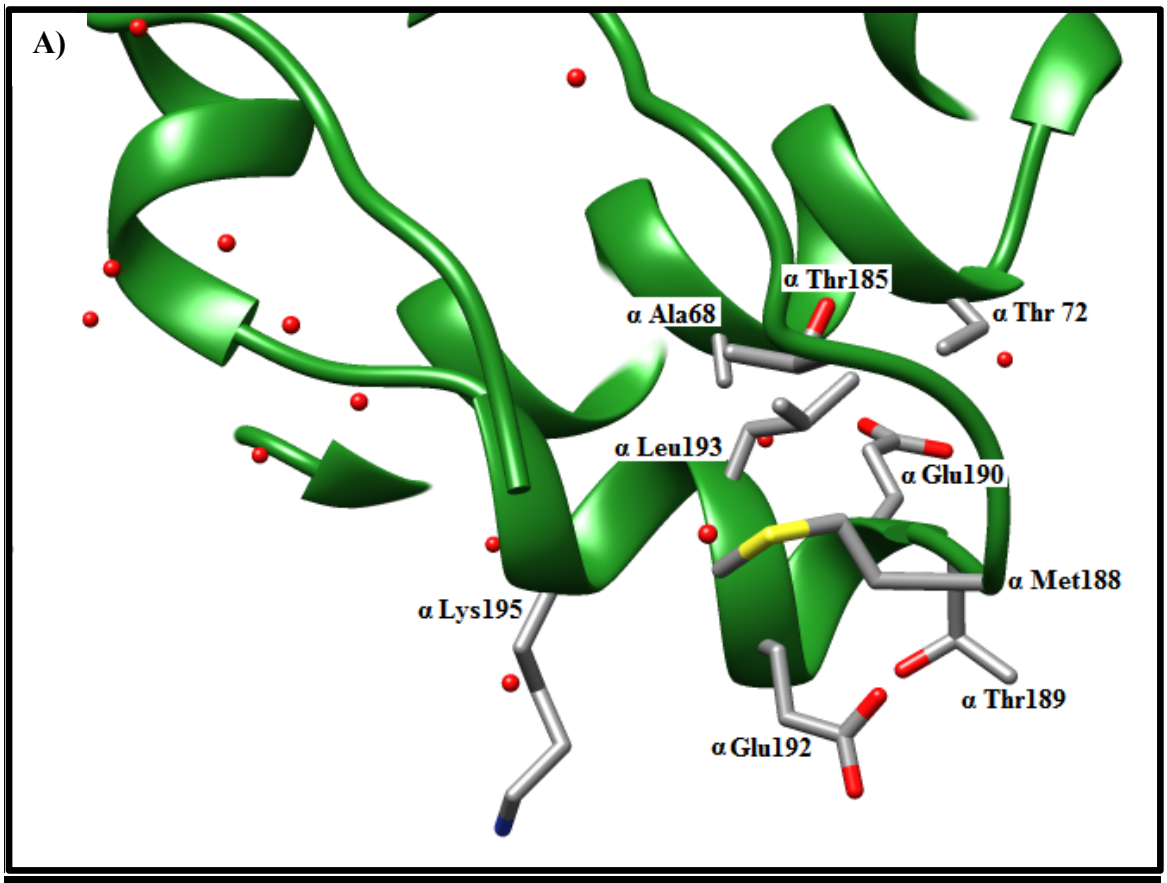
A)
α Thr185
α Ala68
α Thr 72
α Leu193
α Glu190
α Met188
α Lys195
α Thr189
α Glu192

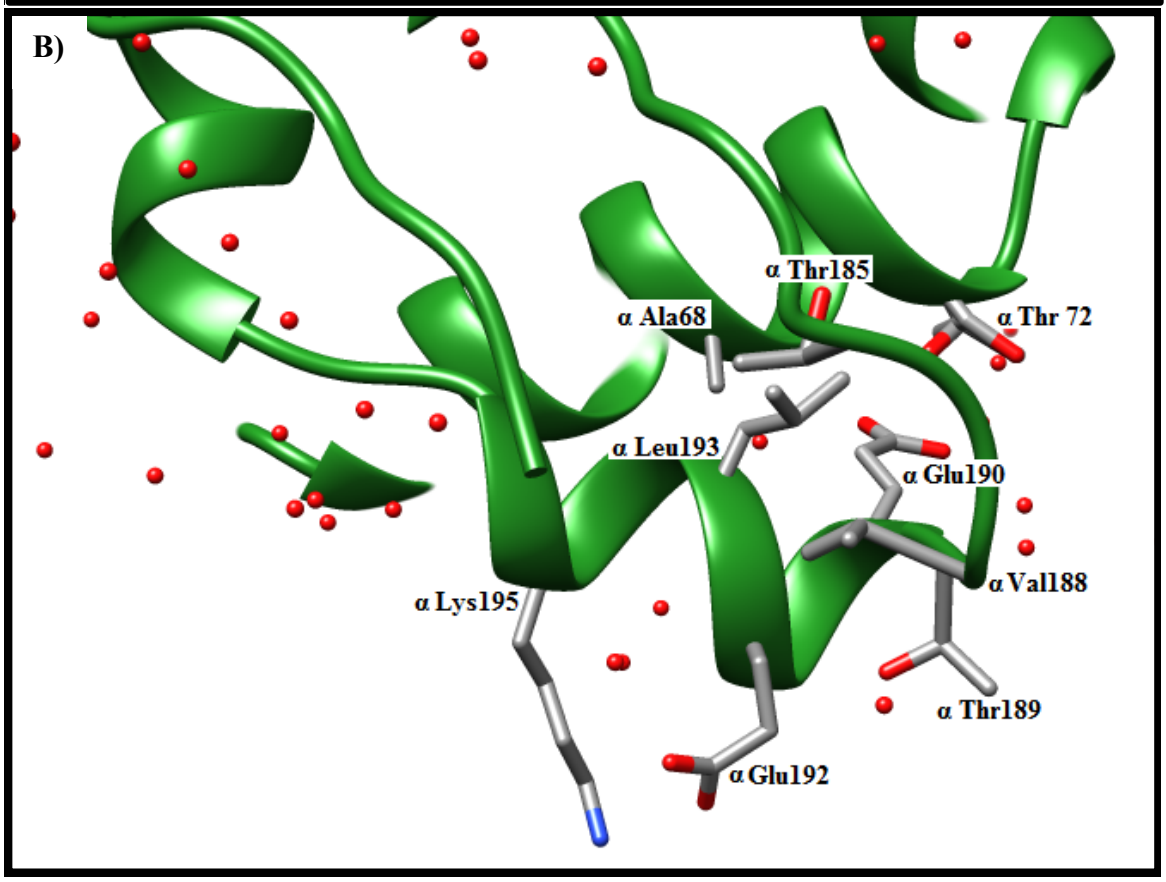
B)
α Thr185
α Ala68
α Thr 72
α Leu193
α Glu190
α Val188
α Lys195
α Thr189
α Glu192

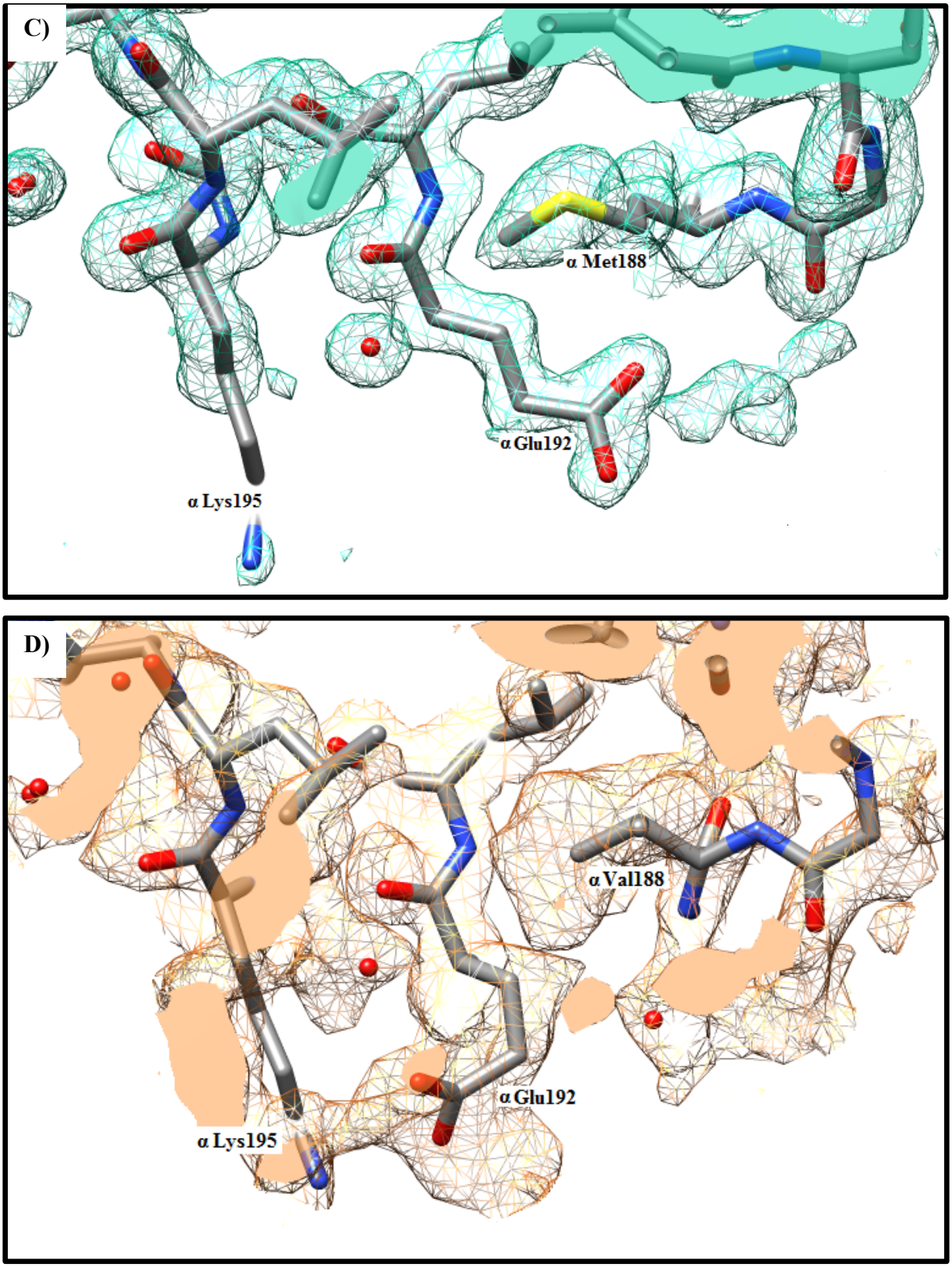

Figure 5.11: A) The WT NHase variant A) compared with the αM188V mutation in the 8C NHase variant B). Images C) and D) show the electron density maps and the protein mutation sites of the WT NHase and αM188V NHase mutant respectively. The hydrophobic side-chains of αVal188, αLeu193 and αAla68 are shown clustered together separately from the

side-chains of αThr185, αThr189, αThr72 and αGlu190. Additional side-chains not shown above in A) and B) but are adjacent to the hydrophobic side-chains are: αLeu196 and αPro211. Water molecules (coloured red) are excluded from the cluster of hydrophobic side-chains. The hydrophilic side-chains of αGlu190, αGlu192, αThr72, αThr185 and αThr189 are pointing away from the cluster of hydrophobic side-chains.

The measured $\Delta\Delta G^*$ of the αM188V NHase single mutant was -1.4 kJ/mol higher than the WT NHase (Table 4.3). The αM188V mutation is an intra-subunit mutation located in the α subunit (*fig.* 5.11 B). The WT NHase has a Met at position 188 which is closely packed with αGlu192 and αThr185. The side-chains of αGlu190 and αThr189 are pointing away from the cluster of hydrophobic side-chains consisting of: αLeu193, αVal188 and αAla68. The OH of αThr185 is also pointing away while its methyl group is adjacent to αAla68 (*fig.* 5.11 A). In the crystal structure of the 8C composite NHase mutant, the same pattern of relative spacing of side-chains is shown; however the side-chain of αVal188 is pointing towards the cluster of hydrophobic side-chains. The absence of water molecules from this region within 5 Å of the cluster of hydrophobic side-chains in both the crystal structures of WT NHase and the 8C mutant (*fig.* 5.11) can be seen when the region is compared to the rest of the NHase structure. The side-chain of αLys195 swings towards αGlu192 by more than 3 Å and points into the surrounding solvent. The electron density around αMet188 in (*fig.* 5.11 C) shows the orientation the side-chain takes without much flexibility compared to the side-chain of αVal188 whose electron density is poorly defined (*fig.* 5.11 D). This suggests that the packing of the side-chains around the mutation position 188, results in a shift of the backbone of residues from αVal188 to αGlu192. This shift is by more than 0.5 Å and is coupled with the measured increase in thermal stability of the αM188V single mutant relative to the thermal stability of WT NHase would suggest that hydrophobic packing could be the cause of the enhanced thermal stability following the replacement of αMet at position 188 with αVal.

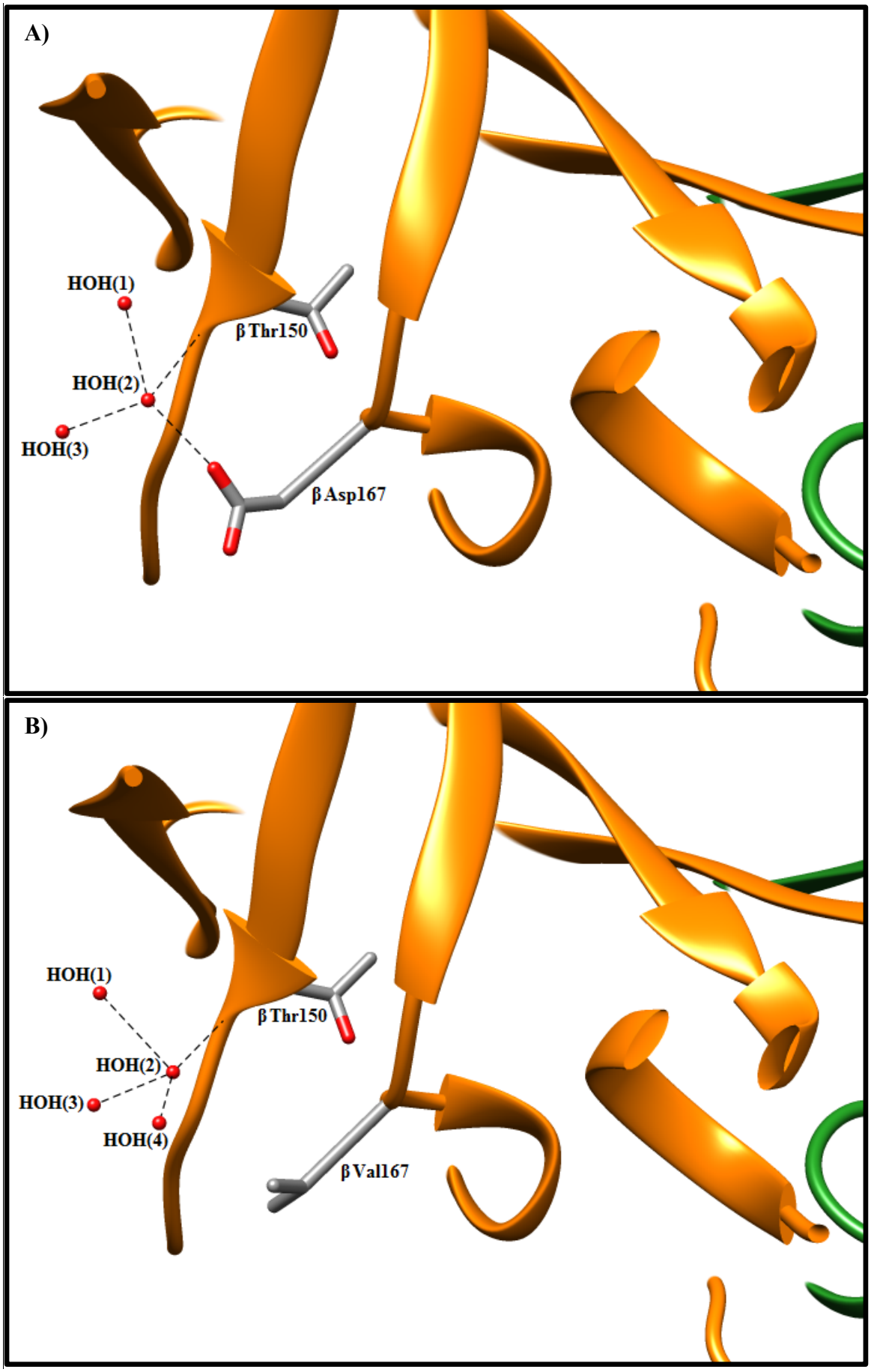
A)
HOH(1)
HOH(2)
HOH(3)
βThr150
βAsp167
B)
HOH(1)
HOH(2)
HOH(3)
HOH(4)
βThr150
βVal167

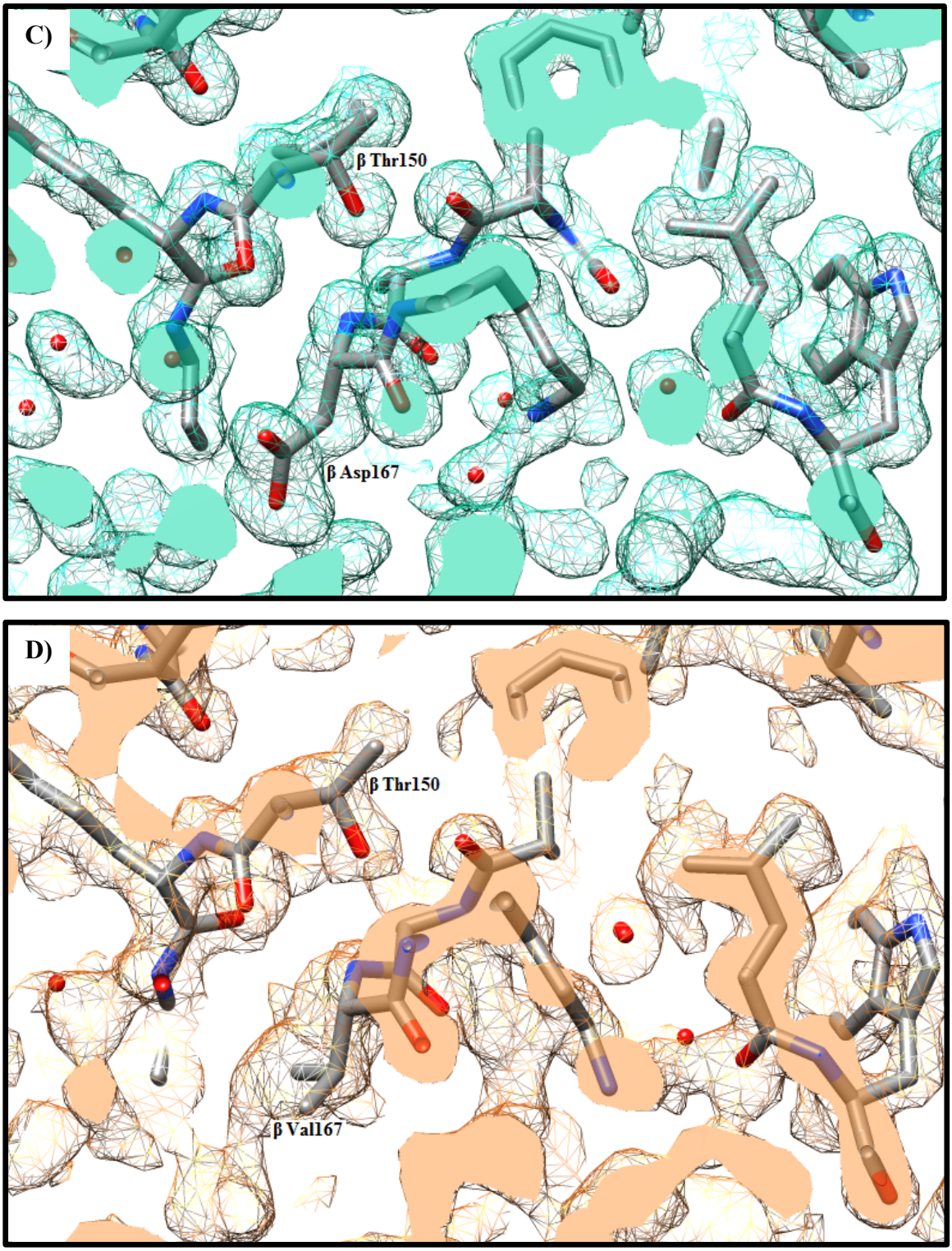

Figure 5.12: A) The WT NHase variant A) compared with the βD167V mutation in the 8C NHase variant B). Images C) and D) show the electron density maps and the protein mutation sites of the WT NHase and βD167V NHase mutant respectively. The water molecule, HOH(2), is hydrogen bonded to the backbone carbonyl of βThr150 in both the WT NHase and mutant NHase. The same water molecule is involved in a water-mediated hydrogen bond

in the WT NHase with the side-chain of βAsp167. The water molecule stays in place after mutation of βAsp to βVal at position 167 and does not form a water-mediated hydrogen bond in the mutant NHase.

The measured decrease in $\Delta\Delta G^*$ of the βD167V NHase mutant was 0.24 kJ/mol. This is in agreement with the observed decrease in energy of hydrogen bonds with increased distance compared to previous $\Delta\Delta G^*$ values of mutants utilising shorter hydrogen bonds that showed higher $\Delta\Delta G^*$ values (Table 4.3). The βD167V mutation is located in the β subunit of NHase (*fig.* 5.12 B). It is an intra-subunit mutation. The WT NHase has an Asp at position 167 in the β subunit which interacts via a water-mediated hydrogen bond with the backbone carbonyl of βThr150. The water molecule involved in the water-mediated hydrogen bond, HOH(2), is 2.7 Å from the Oδ1 of βAsp167 and 3 Å from the backbone carbonyl O of βThr150 (*fig.* 5.12 B). The same water molecule, HOH(2), is hydrogen bonded to other water molecules: HOH(1) and HOH(3), at distances of 2.9 Å and 3.4 Å, forming a network of hydrogen bonded water molecules (*fig.* 5.12 B). No hydrophobic side-chains were observed within 3.5 Å of the Asp at position 167 in the WT NHase crystal structure (*fig.* 5.12 A) or adjacent to the Val at position 167 in the 8C composite mutant NHase crystal structure (*fig.* 5.12 B). The presence of hydrophilic side-chains clustering around this position suggests that the WT NHase required hydrogen bonding to maintain the thermal stability for this region. The βD167V single mutant exhibited less thermal stability than the WT NHase. The electron density around βAsp176 in (*fig*. 5.12 C) is more precisely defined than the electron density around βVal167 (*fig*. 5.12 D). The location of this mutation is also towards the periphery of the enzyme structure and is thus more prone to be flexible and accessible to the solvent. The presence of the βVal167 side-chain at this position in the mutant disrupted the water-mediated hydrogen bond mediated between βAsp167 and βThr150 leading to a decrease in thermal stability of the βD167V single mutant NHase.

In summary, the positioning of additional interactions (hydrogen bonds and salt bridges) between subunits contributes to thermal stability of some of the single mutants such as: αS169R, βD96E and βY127N. The network of hydrogen bonds linking the interacting side-chains is also an important factor that facilitates the interaction of thermo-stabilising mutations particularly when situated between subunits.

Thermal Shift Assay Analysis

The thermal shift assay was conducted to determine the effects of thermal stability independent of catalysis. This was done due to the reported presence of an oxidisable Cys sulfenic side-chain in the active site of NHase which irreversibly reduces NHase catalysis. The oxidation of the Cys sulfenic side-chain was countered by inclusion of 5mM DTT in all protein solutions containing NHase while using the hydroxamic acid assay. For the thermal shift assay using Sypro Orange dye, the inclusion of DTT would be unnecessary.

The thermal shift assay gave melting temperatures that suggested that minor conformational effects influenced the thermal stabilities of the NHase samples (*fig.* 4.17) and (Table 4.4) compared to the thermal stabilities influenced by major conformational effects previously determined using the hydroxamic acid assay (*fig*. 4.14, 4.15, 4.16) and (Table 4.3). All the composite NHase mutants had lower melting temperatures than the WT NHase which suggests that the composite NHase mutants were less stable than the WT NHase in the thermal shift assay conditions. This could be attributed to the different buffer conditions in which the NHase was measured: in the hydroxamic acid assay, there was the nitrile substrate, hydroxylamine, hydroxamic acid and acetamide while in the thermal shift assay, the NHases under study were in 0.025 M potassium phosphate buffer pH 7.2 and the Sypro Orange dye. The presence of the substrate in the hydroxamic acid assay may have contributed to thermal stability of NHase by facilitating more interactions with the active site. The ionic strength of each reaction cocktail may also have influenced ionic interatomic interactions. In addition, the availability of hydrogen bond donors and acceptors surrounding the mutants that utilised water-mediated hydrogen bonding as a mechanism of thermal stability could also be influenced by the reaction cocktail of the Sypro Orange assay being different from the hydroxamic acid assay.

Some of the single mutants that were determined to be less thermostable when using the hydroxamic acid assay were also determined to be less thermostable when using the thermal shift assay. These are the βL103S and βT150A mutants (Table 4.3). In addition, some of the mutants that were determined to be more thermostable when using the hydroxamic acid assay were also determined to be more thermostable when using the thermal shift assay such as the αS169R, βY127N, βD96E, αM188V and βF36L (Table 4.3). The single mutants whose hydroxamic acid assay thermal stability results contradicted the thermal shift assay results are: βM43K and βD167V (Table 4.3). The difference in results between the two assay methods could be caused by the different buffer media in which the mutants were

tested in the two assays. The hydroxamic acid assay allowed the NHase to be measured by exploiting its catalytic function. The mechanisms of thermal stability of proteins which were shown by the hydroxamic acid assay have also been shown in other studies to contribute to thermal stability of proteins as described earlier. The thermal shift assay also showed some of the single mutants being more thermostable than the WT NHase however, the magnitudes of energy of thermal unfolding differed and could be attributed to the reaction cocktail in which the NHase was measured.

Structural Determinants of Thermal stability

The protein structure components that contributed to thermal stability of the *G. pallidus* RAPc8 NHase have also been observed in other proteins. These include mutations at the interface of different subunits, additional hydrogen bonds and salt bridges to enhance structural rigidity and the limiting of the degrees of freedom of ligands involved in interactions in the vicinity of hydrophobic side-chains. According to the hydroxamic acid assay, the βY127N mutation contributed the most to thermal stability while other mutations such as βT150A made NHase less thermostable.

The measured energies required for thermal unfolding of the single NHase mutants add up to within 0.1kJ/mol and 0.8 kJ/mol of the determined energy required for thermal unfolding for the 9C and 8C NHase mutants respectively. However, the determined energy of thermal unfolding for the 9E composite NHase mutant has a deficit of 2.6 kJ/mol relative to the sum of the energies required for unfolding of the single mutants. This could be attributed to the αD4G mutant which was not measured because it was not observed in the crystal structure and could not account for its thermostabilising mechanism. The nature of the mutation, an Asp to Gly mutation, could make the NHase more thermolabile by breaking an interaction facilitated by the Asp side-chain of the WT NHase.

Comparison with Thermal Stability Studies of Other Proteins

The phenomenon of thermal stability has been studied in different proteins across numerous studies as reviewed by (Buschner *et al*., 2011; Ferreon *et al*., 2011). Sadeghi *et al*., (2006) reviewed 60 different proteins from thermophiles and 42 from mesophiles together with their respective PDB structures and compared them with their homologues. Their study showed previous findings such as increases in the number of Glu and charged amino acids

did not necessarily lead to an increase in thermal stability. However, the same study suggested that thermophiles had increased hydrophobicity of their protein core, more interlinking hydrogen bonds and salt bridges when compared to their mesophilic homologs. Comparisons of protein crystal structures from thermophilic organisms with their mesophilic homologues may suggest the likely target amino acid residues for conferring thermal stability but, at present, would still require measurement of the effects of single amino acid substitutions and comparison to the WT form of the protein to rule out the effects of other mutations.

The active dimeric form of the super oxide dismutase from *Potentilla atrosanguinea* var. *argyrophylla* was mutated to impart thermal stability (Kumar *et al*., 2012). One of the single mutations, C95A, involved an intersubunit mutation that facilitated retention of activity in thermally denaturing temperatures with additional partial tolerance to autoclaving. However, the intersubunit mutation enhanced monomerization of the active enzyme which was also reported to result in higher activity than the dimeric form. In contrast, the dimeric super oxide dismutase from *Carica papaya* had higher activity than its monomeric form and was suggested to be more stable as a dimer (Lin *et al*., 1999).

Additional studies on thermostabilising intersubunit mutations have been reported by Bogin *et al*., (2002) by comparing the intersubunit interactions in the alcohol dehydrogenase (ADH) from mesophilic *Clostridium beijernickii* and thermophilic *Thermoanaerobacter brockii*. The ADH from *T. brockii* exhibited two more additional salt bridge interactions compared to the *C. beijernickii* ADH. Thus the enhancement of thermal stability by mutating intersubunit amino acid residues of multimeric enzymes impacts the stability of the multimer. This can be compared to the αS169R mutant and the βD96E mutant which formed intersubunit salt bridges.

Alignment, analysis and comparison of the sequences and crystal structures of the *G. pallidus* RAPc8 NHase WT and mutants (9E, 9C and 8C) with the industrial *R. rhodochrous* J1 NHase shows that several amino acid residues studied in the WT *G. pallidus* RAPc8 NHase are also present in the *R. rhodochrous* J1 NHase, such as, αSer169, βAsp96 and βMet43. These amino acid residues show their potential application into the *R. rhodochrous* J1 NHase. The sidechain of the αS169R mutation interacts with the sidechain of βArg218 in *G. pallidus* RAPc8 NHase. The *R. rhodochrous* J1 NHase possesses a Ser in the WT at position 169 in the α subunit and an Arg at position 214 in the β subunit which aligns with Arg 218 in the β subunit of *G. pallidus* RAPc8. The mutation βM43K interacts with a water molecule that is held in place via an intersubunit hydrogen bond network with the amino acid

residues αGlu99, αGln97 and αGlu172 which are also conserved in the *R. rhodochrous* J1 NHase at the same structural position. However, the adjacent hydrophobic side-chains βPhe52 and βLeu130 which are present in the *G. pallidus* RAPc8 NHase are replaced with the hydrophobic side-chains βLeu48 and βAla127 at the same structural position in the *R. rhodochrous* J1 NHase. If this mutation is designed into the latter NHase, the hydrophobic side-chains βLeu48 and βAla127 could influence the energy of the adjacent hydrogen bonds but not likely to influence the bonding pattern due to the absence of hydrogen bond donors or acceptors on the hydrophobic side-chains.

The mutant αM188V is located within a water shell as shown previously (*fig*. 5.11). The amino acid residues involved in the water shell are: αLeu193, αAla68, αThr185, αThr72, αGlu190 and αThr189. These amino acid residues are also conserved in the *R. rhodochrous* J1 NHase except αThr72 which is replaced with a Val. The addition of a more hydrophobic residue to the water shell would likely contribute to the hydrophobic exclusion of water molecules as depicted in *fig.* 5.11. The βD96E mutation interacts with αArg28 via hydrogen bonding. The *R. rhodochrous* J1 NHase also possesses an Asp at position 96 in the β subunit and the interacting Arg at position 28 in the α subunit. Thus these mutations drawn from the 8C composite NHase mutant could be designed into the *R. rhodochrous* J1 NHase to facilitate the enhancement of its thermal stability.

The 9E composite mutant βL103S interacts via a water-mediated hydrogen bond as previously shown. The βLeu is replaced with a βMet at position 99 while the target interacting amino acid residue for this mutation, αSer, is replaced with an α Glu at the same position. The βY127N mutation is replaced with a βThr at position 124 in the *R. rhodochrous* J1 NHase and the amino acid residues interacting with this mutation: αArg49, αGlu57, αHis53 and αTyr54 via the intersubunit hydrogen bond network are replaced with αHis49, αGlu57, αVal53 and αTyr54, respectively, in the *R. rhodochrous* J1 NHase. The remaining βPhe in the βF36L mutation possesses a βLeu in the *R. rhodochrous* J1 NHase at this structural position. The amino acid residues in the *G. pallidus* RAPc8 NHase interacting with the βF36L mutation through hydrophobic packing: βPhe27, αTyr54, βTyr26, βTrp76 and αLeu129, are replaced with βPhe27, αTyr54, βVal24, βTrp72 and αLeu129 in the *R. rhodochrous* J1 NHase respectively. For these mutations to be applied in the *R. rhodochrous* J1 NHase, additional studies would be required due to the apparent differences in the interacting amino acid residues at these structural positions.

In our studies, the αS169R, βM43K and βD96E intersubunit mutations facilitated interlinks between the α and β subunits of the *G. pallidus* RAPc8 NHase and showed

considerable similarities with regard to structural positions of amino acid residues when aligned with the *R. rhodochrous* J1 NHase homology model. In addition, since the active form of the enzyme is a tetramer and the measurement of thermal stability relies on the structural integrity of the tetramer remaining intact and active despite heat treatment it follows that a good region for targeting mutations that enhance thermal stability of multimeric enzymes would be the intersubunit region.

CONCLUSION

An assay for measurement of thermal stability of NHase has been refined from previous techniques to utilise purified NHase samples. The structural features required for thermal stability of NHase have been determined and are in agreement with other features reported in literature in NHases and also other proteins. The feature that contributes the most to thermal stability in the *G. pallidus* RAPc8 NHase involves increasing the number of inter-subunit links via hydrogen bonds and salt bridges. Hydrophobic packing was also been shown to contribute to thermal stability, by excluding water molecules from the water shell surrounding hydrophobic side-chains.

The thermal stability $\Delta\Delta G^*$ contributions by specific structural features in NHase have also added up to the wild-type value for one composite mutant and to within 0.8 kJ/mol of the wild-type for another composite mutant. Thus the effects of the individual mutations on the thermostability of *G. pallidus* RAPc8 NHase seem to be additive. Some of the *G. pallidus* RAPc8 NHase thermostabilising mutations have potential application in the current industrial NHase from *R. rhodochrous* J1 such as: αS169R, βD96E and M43K, in addition to the insight obtained from some of the other mutations: αM188V, βY127N and βM43K.

The influence of the hydrophobic effect and the intersubunit hydrogen bonds and salt bridges on thermal stability has been presented and potential application to current industrial NHase variant has been suggested. Further work on applying thermostabilising mechanisms of thermophilic NHases to the current mesophilic NHases used in industry could aid the development of thermotolerant NHase in industry with enhanced large scale production of industrially important amide products.

REFERENCES

Adams P. D., Afonine PV, Bunkoczi G., Chen V. B., Davis I. W., Echols N., Headd J. J., Hung L. W., Kapral G. J., Grosse-Kunstleve R. W., McCoy A. J., Moriarty N. W., Oeffner R., Read R. J., Richardson D. C., Richardson J. S., Terwilliger T. C., Zwart P. H., (2010). PHENIX: a comprehensive Python-based system for macromolecular structure solution. *ACTA CRYSTALLOGRAPHICA* D66:213-221.

Agarkar V. B., Kimani S. W., Cowan D. A., Sayed M. F-R. and Sewell B. T., (2007). The quarternary structure of amidase from *Geobacillus pallidus* RAPc8 is revealed by its crystal packing. *ACTA CRYSTALLOGRAPHICA*. F62,1174-1178.

Albeck S., Unger R. and Schreiber G., (2000). Evaluation of direct and cooperative contributions towards the strength of buried hydrogen bonds and salt bridges. *MOLECULAR BIOLOGY*. 298(**3**): 302-520.

Andrade J., Karmali A., Carrondo M. A. and Frazao C., (2007). Structure of amidase from *Pseudomonas aeruginosa* showing a trapped acyl transfer reaction intermediate state. *BIOLOGICAL CHEMISTRY*. 282(**27**) 19598-19605.

Andrieux F. P. L., Boxall C. and Taylor R. J., (2014). The hydrolysis of hydroxamic acid complexants in the presence of non-oxidising medal ions 1: ferric ions. Centre for Materials Science, University of Central Lancashire, Preston, UK.

Artimo P, Jonnalagedda M, Arnold K, Baratin D, Csardi G, de Castro E, Duvaud S, Flegel V, Fortier A, Gasteiger E, Grosdidier A, Hernandez C, Ioannidis V, Kuznetsov D, Liechti R, Moretti S, Mostaguir K, Redaschi N, Rossier G, Xenarios I, and Stockinger H., (2012). ExPASy: SIB bioinformatics resource portal**.** *NUCLEIC ACIDS RESEARCH*. 40(W1):W597-W603.

Asano Y., Tani., Y and Yamada H., (1980). A new enzyme "Nitrile Hydratase" which degrades acetonitrile in combination with amidase. *AGRICULTURAL BIOLOGICAL CHEMISTRY*. 44(**9**),2251-2252.

Asano Y., Fujishiro K., Tani Y. and Yamada H., (1982a). Aliphatic nitrile hydratase from *Arthrobacter* sp. J-1 purification and characterization. *AGRICULTURAL BIOLOGICAL CHEMISTRY*. 46(**5**):1165-1174.

Asano Y., Fujishiro K., Tani Y. and Yamada H., (1982b). Aliphatic nitrile hydratase from *Arthrobacter* sp. J-1 purification and characterization. *AGRICULTURAL BIOLOGICAL CHEMISTRY*. 46 (**5**): 1165-1174.

Atkins P. and DePaula J., (2006). Atkin's physical chemistry. Oxford University Press. Part 1: pages 92-135 and Part 3: pages 804-815.

Aymard C. and Belarbi A., (2000). Kinetics of thermal deactivation of enzymes: a simple three parameters phenomenological model can describe the decay of enzyme activity, irrespectively of the mechanism. *ENZYME AND MICROBIAL TECHNOLOGY*. 27(2000) 612-618.

Baldwin R. L., (1996). How Hofmeister ion interactions affect protein stability. *BIOPHYSICAL JOURNAL*. 71: 2056-2063.

Bauer R., Knackmuss H-J. and Stolz A., (1997). Enantioselective hydration of 2-arylpropionitriles by a nitrile hydratase from *Agrobacterium tumefaciens* strain d 3. *APPLIED MICROBIOLOGY BIOTECHNOLOGY*. **49**: 89-95.

Bischof J. C. and He X., (2005). Thermostability of proteins. *ANNALS NEW YORK ACADEMY OF SCIENCES*. 1066:12-33.

Black G. W., Gregson T., McPake C. B., Perry J. J. and Zhang M., (2010). Biotransformation of nitriles using the solvent-tolerant nitrile hydratase from *Rhodopseudomonas palustris*. *TETRAHEDERON LETTERS.* **51:** 1639-1641.

Bogin O., Levin I., hacham Y., Tel-Or S., peretz M., Frolow F. and Burstein Y., (2002). Structural basis for the enhanced thermal stability of alcohol dehydrogenase mutants from the mesophilic bacterium *Clostridium beijerinckii*: contribution of salt bridging. *PROTEIN SCIENCE*. (**11**): 2562-2574.

Bosshard H. R., Marti D. N. and Jelesarov I., (2004). Protein stabilization by salt bridges: concepts, experimental approaches and clarification of some misunderstandings. *MOLECULAR RECOGNITION*. **17**: 1-16.

Brammar W. J. and Clarke P. H., (1964). Induction and repression of *Pseudomonas aeruginosa* amidase. *GENERAL MICROBIOLOGY*. **37**, 807-819.

Buschner G. S., Murphy R. D., Buchete N-V. and Kubelka J., (2011). Dynamics of protein folding: probing the kinetic network of folding-unfolding transitions with experiment and theory. *BIOCHIMICA ET BIOPHYSICA ACTA*. 1814(2011)1001-1020.

Cameron R. A., Sayed M. and Cowan D. A., (2005). Molecular analysis of the nitrile catabolism operon of the thermophile *Bacillus pallidus* RAPc8. *BIOCHIM BIOPHYSICA ACTA*. 1725**(1)**: 35-46.

China Jilin, (2013). Annual output of 50,000 tons of polyacrylamide project of Jilin city.[online] Available at: English.jl.gov.cn/Investment/Opportunities/Industry/syhg/201208/t20120829_1265288.html

Chen J., Yu H., Liu C., Liu J. and Shen Z., (2012). Improving stability of nitrile hydratase by bridging the salt-bridges in specific thermal-sensitive regions. *BIOTECHNOLOGY*. 164:354-362.

Cowan D. A., Cameron R. A. and Tsekoa T. L., (2003). Comparative Biology of Mesophilic and Thermophilic Nitrile Hydratases. *ADVANCES IN APPLIED MICROBIOLOGY*. 52:123-153.

Deechongkit S., Nguyen H., Marcus J., Powers E. T., Gruebele M. and Kelly J. W., (2006). B-sheet folding mechanisms from perturbation energetics. *CURRENT OPINION IN STRUCTURAL BIOLOGY*. 16: 94-101.

Doran J. P., Duggan P., Materson M., Turner P. D. and O'Reilly C., (2005). Expression of a recombinant enantioselective amidase. *PROTEIN EXPRESSION AND PURIFICATION*. 40: 190-196.

Duran R., Nishiyama M., Horinouchi S and Beppu T., (1993). Characterization of nitrile hydratase genes cloned by DNA screening from *Rhodococcus erythropolis*. *BIOSCIENCE BIOTECHNOLOGY BIOCHEMISTRY*. 57(8): 1323-1328.

Emsley P., Lohkamp B., Scott W., Cowtan K, (2010). Features and Development of Coot *ACTA CRYSTALLOGRAPHICA* D66, 486-501, 2010.

Endo I., Nojiri M., Tsujimura M., Nakasako M., Nagashima S., Yohda M. and Odaka M., (2001). Fe-type nitrile hydratase. *INORGANIC BIOCHEMISTRY*. 83(**4**): 247-253.

Endo I., Odaka M. and Yohda M., (1999). An enzyme controlled by light: the molecular mechanism of photoreactivity in nitrile hydratase. *TIBTECH*. **17:** 244-248.

Fallon R. D., Stieglitz B. and Turner I. Jr., (1997). A *Pseudomonas putida* capable of stereoselective hydrolysis of nitriles. *APPLIED MICROBIOLOGY AND BIOTECHNOLOGY*. **47**: 156-161.

Farnaud S., Tata R., Sohi M., Wan T., Brown P. and Sutton B., (1999). Evidence that cysteine-166 is the active-site nucleophile of *Pseudomonas aeruginosa* amidase: crystallization and preliminary X-ray diffraction analysis of the enzyme. *BIOCHEMISTRY*. 340:711-714.

Ferreon A. C. M. and Deniz A. A., (2011). Protein folding at single-molecule resolution. *BIOCHIMICA ET BIOPHYSICA ACTA*. 1814:1021-1029.

Fields P. A., (2001). Review: Protein function at thermal extremes: balancing stability and flexibility. *COMPARATIVE BIOCHEMISTRY AND PHYSIOLOGY A*. 129, 417-431.

Fitter J., Herrmann R., Dencher N. A., Blume A. and Hauss T., (2001). Activity and stability of a thermostable α-amylase compared to its mesophilic homologue: mechanisms of thermal adaptation. *BIOCHEMISTRY*. 40: 10723-10731.

Fournand D. and Arnaud A., (2001). Aliphatic and enantioselective amidases: from hydrolysis to acyl transfer activity. *APPLIED MICROBIOLOGY*. **91**, 381-393.

Fournand D., Arnaud A. and Galzy P., (1998). Study of the acyl transfer activity of a recombinant amidase overproduced in an *Escherichia coli* strain. Application for short-chain hydroxamic acid and acid hydrazide synthesis. *MOLECULAR CATALYSIS B* (1998) 4:77-90.

Fournand D., Bigey F. and Arnaud A., (1998). Acyl transfer activity of an amidase from Rhodococcus sp. Strain R312: Formation of a wide range of hydroxamic acids. *APPLIED AND ENVIRONMENTAL MICROBIOLOGY*. 64 (**8**): 2844-2852.

Gao J., Bosco D. A., Powers E. T. and Kelly J. F., (2009). Localized thermodynamic coupling between hydrogen bonding and microenvironment polarity substantially stabilizes proteins. *NATURE STRUCTURAL AND MOLECULAR BIOLOGY*. 16 (7): 684-691.

Garrett R. H. and Grisham C. M., (2010). Biochemistry. CENGAGE LEARNING. 4th edition. Part 2: chapter 13 pages 382-415 and chapter 14 pages 419-448.

Gasteiger E., Gattiker A., Hoogland C., Ivanyi I., Appel R.D. and Bairoch A., (2003). ExPASy: the proteomics server for in-depth protein knowledge and analysis. *NUCLEIC ACIDS RESEARCH*. 31:3784-3788.

Gavagan J. E., DiCosimo R., Eisenberg A., Fager S. K., Folsom P. W., Hann E. C., Schneider K. J., Fallon R. D., (1999). A Gram-negative bacterium producing a heat-stable nitrilase highly active on aliphatic dinitriles. *APPLIED MICROBIOLOGY AND BIOTECHNOLOGY*. **52**: 654-659.

Ghisalba O., Meyer H-P. and Wohlgemuth R., (2010). Encyclopaedia of Industrial Biotechnology: bioprocess, bioseparation, and cell technology: Industrial Biotransformation. John Wiley & Sons, Inc. 1-19.

Gromiha M. M., Thomas S. and Santhosh C., (2006). Role of cation-π interactions to the stability of thermophilic proteins. *PREPARATIVE BIOCHEMISTRY AND BIOTECHNOLOGY*. 32(**4**):355-362.

Hann E. C., Eisenberg A., Fager S. K., Perkins N. E., Gallagher F. G., Cooper S. M., Gavagan J. E., Stieglitz B., Hennessey S. M. and Di Cosimo R., (1999). 5-cyanovaleramide production using immobilized *Pseudomonas chlororaphis* B23. *BIOORGANIC AND MEDICINAL CHEMISTRY*. 7: 2239-2245.

Hashimoto K., Suzuki H., Taniguchi K., Noguchi T., Yohda M. and Odaka M., (2008). catalytic mechanism of nitrile hydratase proposed by time-resolved x-ray crystallography using a novel substrate, *tert*-butylisonitrile. *BIOLOGICAL CHEMISTRY*. 283**(52)**36617-36623.

Hashimoto Y., Hosaka H., Oinuma K-I., Goda M., Higashibata H., and Kobayashi M., (2005). Nitrile pathway involving acetyl-CoA synthetase. *BIOLOGICAL CHEMISTRY*. 280 **(10):** 8660-8667.

Hashimoto Y., Sasaki S., Herai S., Oinuma K-I., Shimizu S. And Kobayashi M., (2002). Site-Directed Mutagenesis for cysteine residues of cobalt-containing nitrile hydratase. *JOURNAL OF INORGANIC BIOCHEMISTRY*. **91**: 70-77.

Hideaki Y., Nagasawa T., Beppu T., Horinouch S. and Nishiyama M., (1997). Gene encoding a polypeptide having nitrile hydratase activity, a transformant containing the gene and a process for the production of amides using the transformant. Patent number: US 5648256 A.

Hopmann K. H., (2014). Full reaction mechanism of nitrile hydratase: a cyclic intermediate and an unexpected disulphide switch. *INORGANIC CHEMISTRY*. **53**: 2760-2762.

Hourai S., Miki M., Takashima Y., Mitsuda S. and Yanagi K., (2003). Crystal structure of nitrile hydratase from a thermophilic *Bacillus smithii*. *BIOCHEMICAL AND BIOPHYSICAL RESEARCH COMMUNICATIONS*. 312(**2**):340-345.

Huang W., Jia J., Cummings J., Nelson M., Schneider G., and Lindqvist Y. (1997). Crystal structure of nitrile hydratase reveals a novel iron centre in a novel fold. *STRUCTURE.* **15**: 691–699.

Jaenicke R. and Bohm G., (1998). The stability of proteins in extreme environments. *CURRENT OPINION IN STRUCTURAL BIOLOGY*. 8: 738-748.

Jelesarov I. and Karshikoff A., (2009) Defining the role of salt bridges in protein stability. PROTEIN STRUCTURE, STABILITY AND INTERACTIONS. *METHODS IN MOLECULAR BIOLOGY*. HUMANA PRESS. Chapter 10:227-260.

Kato Y., Ooi R. and Asaon Y., (2000). Distribution of aldoxime dehydratase in microorganisms. *APPLIED ENVORONMENTAL MICROBIOLOGY*. 66(**6**):2290-2296.

Kato Y., Yoshida S., Xie S-X and Asano Y., (2004). Aldoxime Dehydratase co-existing with nitrile hydratase and amidase in the Iron-type nitrile hydratase producer *Rhodococcus* sp. N-771. *BIOSCIENCE AND BIOENGINEERING*. 97 (**4**):250-259.

Kimani S. W., Agarkar V. B., Cowan D. A., Sayed M. F-R. and Sewell B. T., (2007). Structure of an aliphatic amidase from *Geobacillus pallidus* RAPc8. *ACTA CRYSTALLOGRAPHICA D*. 63:1048-1058.

Kim S-H. and Oriel P., (2000). Cloning and expression of the nitrile hydratase and amidase genes from *Bacillus* sp. BR449 into Escherichia coli. *ENZYME AND MICROBIAL TECHNOLOGY*. 27:492-501.

Kim T. D., Ryu H. J., Cho H. I., Yang C-H. and Kim J., (2000). Thermal behaviour of proteins: heat-resistant proteins and their heat-induced secondary structural changes. 39, 14839-14846.

Klotz I. M., (1993). Solvent water and protein behaviour: view through a retroscope.*PROTEIN SCIENCE*. 2:1992-1999.

Kobayashi M., Komeda H., Nagasawa T., Nishiyama M., Horinouchi S., Beppu T., Yamada H. and Shimizu S., (1993). Amidase coupled with low-molecular-mass nitrile hydratase from *Rhodococcus rhodochrous* J1.*EUROPEAN JOURNAL OF BIOCHEMISTRY*. 217, 327-336.

Komeda H. and Asano Y., (2008). A novel D-stereoselctive amino acid amidase from *Brevibacterium iodinum*: gene cloning, expression and characterization. *ENZYME AND MICROBIAL TECHNOLOGY*. 43: 276-283.

Konrad U. F., Doerks T., Mueller J., Raes J. and Bork P., (2008). A nitrile hydratase in the eukaryote *Monosiga brevicollis*. *PLOS ONE*. 3 (**12**): 1-5.

Kuhn M. L., Martinez S., Gumataotao N., Bornscheuer U, Liu D. and Holz R. C., (2012). The Fe type nitrile hydratase from Comamonas testosteroni Ni1 does not require an activator accessory protein for expression in Escherichia coli. *BIOCHEMICAL AND BIOPHYSICAL RESEARCH COMMUNICATIONS*. 424: 365-370.

Kumar S. and Nussinov R., (1999). Salt bridge stability in monomeric proteins. *JOURNAL OF MOLECULAR BIOLOGY*. 293: 1241-1255.

Kumar S., Tsai C-J. and Nussinov R, (2000a). Factors enhancing thermostability. *PROTEIN ENGINEERING*. 13 (**3**):179-191.

Kumar S., Ma B., Tsai C-J and Nussinov R., (2000b). Electrostatic strengths of salt bridges in thermophilic and mesophilic glutamate dehydrogenase monomers. *PROTEINS: STRUCTURE, FUNCTION AND GENETICS*. 38:368-383.

Kumar A., Dutt S., bagler G., Singh P and Kumar S., (2012). Engineering a thermos-stable superoxide dismutase functional at sub-zero to >50 ^{o}C, which also tolerates autoclaving. *NATURE*. 2(**387**):1-8.

Kurenkov V. F., Hartan H-G. and Lobanov F. I., (2002). Application of polyacrylamide flocculants for water treatment. *BUTERLOV COMMUNICATIONS*. 3**(11)**:31-40.

Laemili U. K., (1970). Cleavage of structural proteins during the assembly of the head of bacteriophage T4. *NATURE*. 227:680-685: Abstract retrieved from www.nature.com

Lin C-T., Kuo T-J., Shaw J-F. and Kao M-C., (1999). Characterization of the dimer-monomer equilibrium of the papaya copper/zinc superoxide dismutase and its equilibrium shift by a single amino acid mutation. *AGRICULTURAL AND FOOD CHEMISTRY*. 47:2944-2949.

Liu J., Yu H. and Shen Z., (2008). Insights into thermal stability of thermophilic anitrile hydratases by molecular dynamics simulation. *MOLECULAR GRAPHICS AND MODELLING*. 27:529-535.

Lu J., Zheng Y., Yamagishi H., Odaka M., Tsujimura M., Maeda M. and Endo I., (2003). Motif CXCC in nitrile hydratase activator is critical for NHase biogenesis in vivo. *FEBS LETTERS*. 553:391-396.

Maestracci M., Thiery A., Arnaud A. and Galzy P., (1986). A study of the mechanism of the reaction catalysed by the amidase *Brevobacterium* sp. R312. *AGRICULTURAL AND BIOLOGICAL CHEMISTRY*. 50**(9)**: 2237-2241.

Makhongela H. S., Glowacka A. E., Agarkar V. B., Sewell B. T., Weber B., Cameron R. A., Cowan D. A. and Burton S. G., (2007). A novel thermostable nitrilase superfamily amidase from *Geobacillus pallidus* showing acyl transfer activity. *APPLIED MICROBIOLOGY AND BIOTECHNOLOGY*. 75:801-811.

Maron A. O., Akam M. and Walker G., (2012). Nitrile hydratase genes are present in multiple eukaryotic super groups. *PLOS ONE*. 7(**4**): 1-10.

Martinez S., Wu R., Sanishvili R., Liu D. and Holz R., (2014). The active site sulfenic acid ligand in nitrile hydratases can function as a nucleophile. *AMERICAN CHEMICAL SOCIETY*. 136:1186-1189.

Matsumura H., Yamamoto T., Leow T. C., Mori T., Salleh A. B., Basri M., Inoue T., Kai Y. and Rahman N. Z. R. A., (2007). Novel cation-π interaction revealed by crystal structure of thermoalkalophilic lipase. *PROTEINS*. 70(**2**):592-598.

Mitsubishi Chemical Corporation (MCC), (2001). Mitsubishi-Tokyo pharmaceuticals merger with Welfide Corporation. *NEWS LETTER*. MCC Public Relations Department, Marunouchi 2-chome, Chiyoda-ku, Tokyo 100-0005, Japan.

Miyanaga A., Fushinobu S., Ito K., and Wakagi T., (2001) Crystal structure of cobalt-containing nitrile hydratase. *BIOCHEMICAL AND BIOPHYSICAL RESEARCH COMMUNICATIONS*. **288**: 1169–1174.

Miyanaga A., Fushinobu S., Ito K., Shoun H. and Wakagi T., (2004). Mutational and structural analysis of cobalt-containing nitrile hydratase on substrate and metal binding. *EUROPEAN JOURNAL OR BIOCHEMISTRY*. 271,429-438.

Murakami T., Nojiri M., Nakayama H., Odaka M., Yohda M., Dohmae N., Takio K., Nagamune T. and Endo I., (2000). Post-translational modification is essential for catalytic activity of nitrile hydratase. *PROTEIN SCIENCE*. 9**(5)**:1024-1030.

Nagasawa T. and Yamada H., (1990). Application of nitrile converting enzyme for the production of useful compounds. *PURE AND APPLIED CHEMISTRY*. 62(**7**): 1441-1444.

Nagasawa T., Mathew C. D., Mauger J. and Yamada H., (1988). Nitrile hydratase-catalysed production of nicotinamide from 3-cyanopyridine in *Rhodococcus rhodochrous* J1. *APPLIED AND ENVIRONMENTAL MICROBIOLOGY*. 54**(7):**1766-1769.

Nagasawa T., Takeuchi K. and Yamada H., (1991). Characterization of a new cobalt-containing nitrile hydratase purified from urea-induced cells of *Rhodococcus rhodochrous* J1. *EUROPEAN JOURNAL OF BIOCHEMISTRY*. 196, 581-589.

Nagasawa T., Shimizu H. and Yamada H., (1993). The superiority of the third-generation catalyst, *Rhodococcus rhodochrous* J1 nitrile hydratase, for industrial production of

acrylamide. *APPLIED MICROBIOLOGY AND BIOTECHNOLOGY*. 40:189-195. Abstract retrieved from www.link.springer.com/article/10.1007%2FBF00170364#page-1

Nel A. J. M., Tuffin I. M., Sewell B. T. and Cowan D. A., (2011). Unique aliphatic amidase from a psychrotophic and haloalkalophilic Nesterenkonia isolate. *APPLIED AND ENVORNMENTAL MICROBIOLOGY*. 77**(11)**: 3696-3702.

Nishiyama M., Horinouchi S., Kobayashi M., Nagasawa T., Yamada H. and Beppu T., (1991). Cloning and characterization of genes responsible for metabolism of nitrile compounds from Pseudomonas chlororaphis B23. *BACTERIOLOGY*. 173(**8**):2465-2472.

Nojiri M., Nakayama H., Odaka M., Yohda M., Takio K. and Endo I., (2000). Cobalt substituted Fe-type nitrile hydratase of Rhodococcus sp. N-771. *FEBS LETTERS*. 465:173-177.

Novo C., Farnaud S., Tata R., Clemente A and Brown P., (2002). Support for a three-dimensional structure predicting a Cys-Glu-Lys catalytic triad for *Pseudomonas aeruginosa* amidase comes from site-directed mutagenesis and mutations altering substrate specificity. *BIOCHEMISTRY*. 365:731-738.

Odaka M., Tsujimura M. and Endo I., (2001). Post-translational modifications in nitrile hydratase family. *RIKEN*. 41:58-60.

Ohtaki A., Murata K., Sato Y., Noguchi K., Miyatake H., Dohmae N., Yamada K., Yohda M and Odaka M., (2010). Structure and characterization of amidase from Rhodococcus sp. N-771: Insight into the molecular mechanism of substrate recognition. *BIOCHIMICA ET BIOPHYSICA ACTA*. 1804:184-192.

Pace C. N., Horn G., Hebert E. J., Bechert J., Shaw K., Urbanikova L., Scholtz J. M. and Sevcik J., (2001). Tyrosine hydrogen Bonds Make a Large Contribution to Protein Stability. *JOURNAL OFMOLECULAR. BIOLOGY*. (2001) **312**: 393-404.

Pace H. C. and Brenner C., (2001). The nitrilase superfamily: classification, structure and function. *GENOME BIOLOGY*. 2**(1)**:reviews0001.1-0001.9

Pereira A. R., Graham D., Rainey F. A. and Cowan D. A., (1998). A novel thermostable nitrile hydratase. *EXTREMOPHILES*. 2:347-357.

Petrillo K. L., Wu S., Hann E. C., Cooling F. B., Ben-Bassat A., Gavagan J. E., Dicosimo R., and Payne M. S., (2005) Overexpression in Escherichia coli of a thermally stable and regioselective nitrile hydratase from Comamonas testosteroni 5-MGAM-4D. *APPLIED MICROBIOLOGY AND BIOTECHNOLOGY***. 67**: 664-670.

Pettersen E. F., Goddard T. D., Huang C. C., Couch G. S., Greenblatt D. M., Meng E. C. and Ferrin T. E., (2004). UCSF Chimera-a visualization system for exploratory research and analysis. *COMPUTATIONAL CHEMISTRY*. 25:1605-1612.

Piersma S. R., Nojiri M., Tsujimura M., Noguchi T., Odaka M., Yohda M., Inoue Y. and Endo I., (2000). Arginine 56 mutation in the β subunit of nitrile hydratase: importance of hydrogen bonding to the non-heme iron center. *INORGANIC BIOCHEMISTRY*. 80:283-288.

Prajapati R. S., Sirajuddin M., Durani V., Sreeramulu S. and Varadarajan R., (2006). Contribution of cation-π interactions to protein stability. *BIOCHEMISTRY*. 45:15000-15010.

Rajakumara E., Acharya P., Ahmad S., Sankaranaryanan R. and Rao N. M., (2007). Structural basis for the remarkable stability of Bacillus subtilis lipase (Lip A) at low pH. *BIOCHIMICA ET BIOPHYSICA ACTA*. 1784:302-311.

Ramakrishnan V., (2002). Ribosome structure and the mechanism of translation. *CELL*. 108:557-572.

Reed Business Information, ICIS, (2008). Chemical profile: acrylamide. **Date accessed: 29-06-2012** http://www.icis.com/resources/news/2008/07/21/9141553/chemical-profile-acrylamide.html

Sadeghi M., Naderi-manesh H., Zarrabi M. and Ranjbar B., (2006). Effective factors in thermostability of thermophilic proteins. *BIOPHYSICAL CHEMISTRY*. 119:256-270.

Santoro M. M., Liu Y., Khan S. M. A., Hou L. and Bolen D. W., (1992). Increased thermal stability of proteins in the presence of naturally occurring osmolytes. *BIOCHEMISTRY*. 31, 5278-5283.

Senmin, Dauberman R., (2016). Annual Amide Production [raymond.daubermann@senmin.co.za].

Scandurra R., Conslavi V., Chiaraluce R., Politi L. and Engel P. C., (1998). Protein thermostability in extremophiles. *BIOCHIMIE*. 80, 933-941.

Sharma M., Sarma N. N. and Bhalla T. C., (2012). Biotransformation of acetamide to acetohydroxamic acid at bench scale using acyl transferace activity of amidase of Geobacillus pallidus BTP-5x MTCC 9225. *INDIAN JOURNAL OF MICROBIOLOGY*. 52(1):76-82

Sheu S-Y., Yang D-Y., Selzle H. L. And Schlag E. W., (2003). Energetics of hydrogen bonds in peptides. *PNAS*. 100 **(22)**: 12683-12687.

Sikkink L. A. and Ramirez-Alvarado M., (2008). Salts both enhance both protein stability and amyloid formation of an immunoglobulin light chain. *BIOPHYSICAL CHEMISTRY*. 135: 25-31.

SNF Floerger, (2013). SNF Press Release January 2013. [online] Available at www.snf-group.com/en/library/publications.

Song L., Wang M., Shi J., Xue Z., Wang M-X. and Qian S., (2007). High resolution x-ray molecular structure of nitrile hydratase from Rhodococcus erythropolis AJ270 reveals posttranslational oxidation of two cysteines into sulfinic acids and a novel biocatalytic nitrile hydration mechanism. *BIOCHEMICAL AND BIOPHYSICAL RESEARCH COMMUNICATIONS*. 362:319-324.

Sterner R. and Liebel W., (2001). Thermophilic adaptation of proteins. *CRITICAL REVIEWS IN BIOCHEMISTRY AND MOLECULAR BIOLOGY*. 36**(1)**39-106.

Takarada H., Kawano Y., Hashimoto K., Nakayama H., Ueda S., Yohda M., Kamiya N., Dohmae N., Maeda M. and Odaka M., (2006). Mutational study on αGln90 of Fe-type nitrile hydratase from Rhodococcus sp. N771. *BIOSCIENCE BIOTECHNOLOGY BIOCHEMISTRY*. 70**(4)**:881-889.

Taylor R. J., May I., Wallwork A. L., Denniss I. S., Hill N. J., Galkin B. Y., Zilberman B. Y. and Fedorov Y. S., (1998). The applications of formo-and acetohydroxamic acids in nuclear fuel reprocessing. *ALLOYS AND COMPOUNDS*. 271-273:534-537.

Taylor S. C., Berkelman T., Yadav G. and Hammond M., (2013). A defined methodology for reliable quantification of western blot data. *MOLECULAR BIOTECHNOLOGY*. 55:217-226.

Van Wyk, J. C., (2008). The relationship between structure and thermostability of a nitrile hydratase from Geobacillus pallidus RAPc8. PhD. University of the Western Cape.

Vincent S. G., Cunningham P. R., Stephens N. L., Halayko A. J and Fisher J. T., (1997). Quantitative densitometry of proteins stained with coomassie blue using a Hewlett Packard Scanjet scanner and scanplot software. *ELECTROPHORESIS*. 18:67-71.

Vogt G. and Argos P., (1997). Protein thermal stability: hydrogen bonds or internal packing? *FOLDING AND DESIGN*. 2:S40-S46.

Vogt G., Woell S. and Argos P., (1997). Protein thermal stability, hydrogen bonds and ion pairs. *MOLECULAR BIOLOGY*. 269:631-643.

Watanabe F., Ujihara D., Sakai M, Yu F. and Nakamura T., (2010). Heat resistant nitrile hydratase. Patent number: US 7,645,605 B2

Weber B. W., Kimani S. W., Varsani A., Cowan D. A., Hunter R., Venter G. A., Gumbart J. C., and Sewell B. T., (2013). The mechanism of the amidases: mutating the glutamate adjacent to the catalytic triad inactivates the enzyme due to substrate mispositioning. *BIOLOGICAL CHEMISTRY*. 288:28514-28523.

Weiser M., Takeuchi K., Wada Y., Yamada H. and Nagasawa T., (1998). Low molecular mass nitrile hydrates from *Rhodococcus rhodochrous* J1: purififcation, substrate specificity and comparison with the analogous high-molecular-mass enzyme. 169: 17-22.

Williamson D. S., Dent K. C., Weber B. W., Varsani A., Frederick J., Thuku R. N., Cameron R. A., van Heerden J. H., Cowan D. A. and Sewell B. T., (2010). Structural and biochemical characterization of a nitrilase from thermophilic bacterium Geobacillus pallidus RAPc8. *APPLIED MICROBIOLOGY AND BIOTECHNOLOGY*. 88:143-153.

World Health Organisation, WHO (2012). Global Health Observatory (GHO): Data and statistics: water and sanitation**. Date accessed: 29-06-2012**. http://www.who.int/gho/mdg/environmental_sustainability/en/index.html

Yanenko A. S., Astaurova O. B., Voronin S. P., Gerasimova T. V., Kirsanov N. B., Paukov V. N., Polyakova N. I. and Debabov V. G., (1998). Strain of RHodococus rhodochrous as a producer of nitrile hydratase. Patent number: US 6827699 A

Yamada H. and Kobayashi M., 1996. Nitrile hydratase and its application to industrial production of acrylamide. *BIOSCIENCE BIOTECHNOLOGY AND BIOCHEMITRY*. **60:**1391–1400.

Yamaki T., Oikawa T., Ito K. And Nakamura T., (1997). Cloning and sequencing of a nitrile hydratase gene from Pseudonorcardia thermophila JCM3095. *FERMENTATION AND BIOENGINEERING*.83**(5)**:474-477.

Yamanaka Y., Hashimoto K., Ohtaki A., Noguchi K., Yohda M. and Odaka M., (2010). Kinetic and structural studies on roles of the serine ligand and a strictly conserved tyrosine residue in nitrile hydratase. *JOURNAL OF BIOLOGICAL CHEMISTRY*. 15: 655-665

Yamanaka Y., Kato Y., Hashimoto K., Iida K., Nagasawa K., Nakayama H., Dohmae N., Noguhi K., Noguchi T., Yohda M. and Odaka M., (2015). Time-resolved crystallography of the reaction intermediate of nitrile hydratase: revealing the role of cysteine sulfenic acid ligand as a catalytic nucleophile. *ANGEWANDTE CHEMIE*. 54:10763-10767.

Yogavel M., Mishra P. C., Gill J., Bharwaj P. K., Dutt S., Kumar S., Ahuja P. S. and Sharma A., (2008). Structure of a super oxide dismutase and implications for copper-ion chelation. *ACTA CTRYSTALLOGRAPHICA D*. 64:892-901.

Yonath A., Piefke J., Mussig J., Gewitz H-S., and Wittman H. G., (1983). A compact three-dimansional crystal form of the large ribosomal subuit from bacillus stearothermophilus. *FEBS*. 163(1):69-72.

Zhou Z., Yoshiteru H., kentaro S. and Kobayashi M. (2008). Discovery of posttratslational maturation by self-subunit swapping. *PNAS* (105) **39**: 14849-14854

APPENDICES

Appendix 1: Amino acid alignment of the α subunit of 8C, 9C composite, 9E composite and WT composite NHases created from superposition of the corresponding structures.

The aligned mutation sites are highlighted in yellow.

Appendix 2: Amino acid alignment of the β subunit of 8C, 9C composite, 9E composite and WT composite NHases created from superposition of the corresponding structures.

The aligned mutation sites are highlighted in yellow.

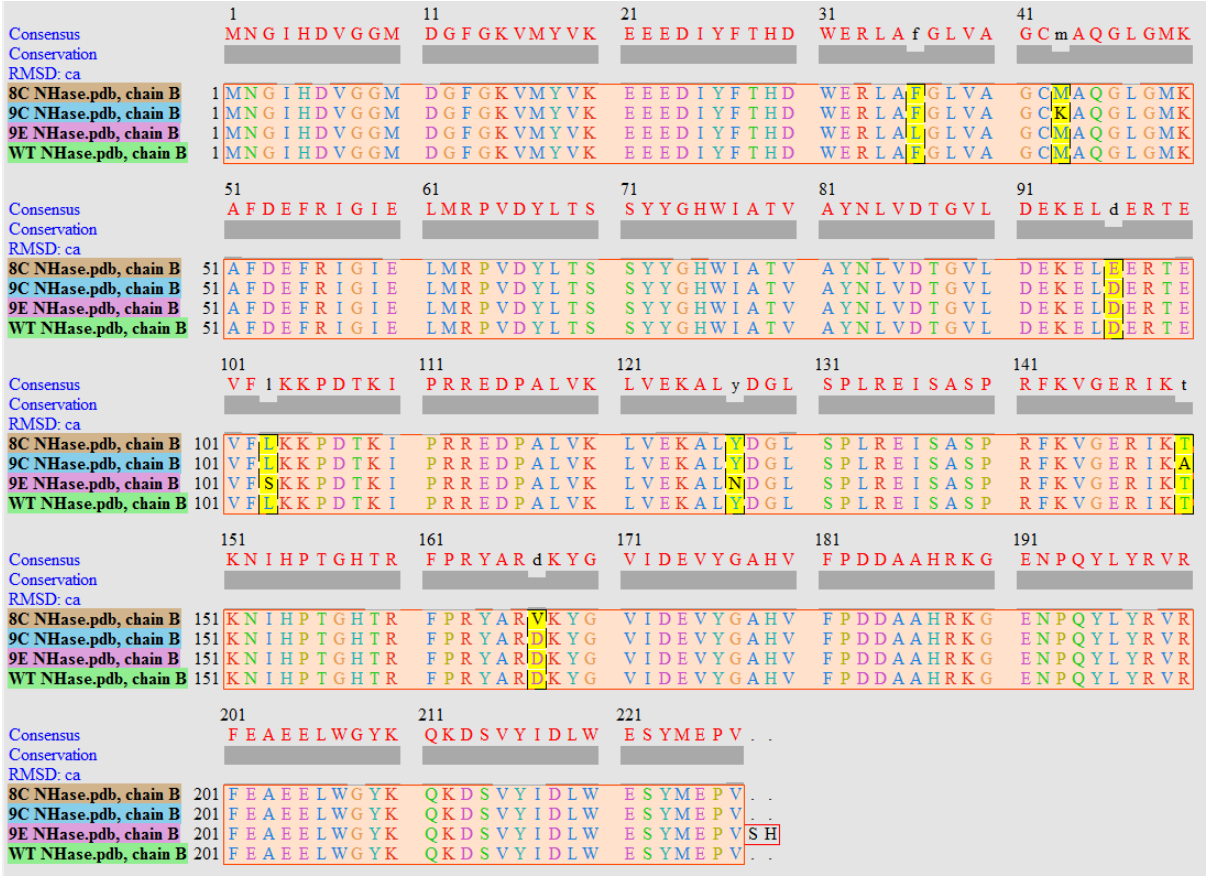

Appendix 3: Nucleotide alignment of the α subunit of WT NHase and all single mutants.

```
                                        10         20         30
40
                                ....|....|....|....|....|....|....|....|
WT NHase alpha subunit          ATGACGATTGATCAAAAAAATACTAATATAGATCCAAGAT
L103S NHase alpha subunit       ATGACGATTGATCAAAAAAATACTAATATAGATCCAAGAT
Y127N NHase alpha subunit       ATGACGATTGATCAAAAAAATACTAATATAGATCCAAGAT
F36L NHase alpha subunit        ATGACGATTGATCAAAAAAATACTAATATAGATCCAAGAT
M188V NHase alpha subunit       ATGACGATTGATCAAAAAAATACTAATATAGATCCAAGAT
D167V NHase alpha subunit       ATGACGATTGATCAAAAAAATACTAATATAGATCCAAGAT
D96E NHase alpha subunit        ATGACGATTGATCAAAAAAATACTAATATAGATCCAAGAT
S169R NHase alpha subunit       ATGACGATTGATCAAAAAAATACTAATATAGATCCAAGAT
M43K NHase alpha subunit        ATGACGATTGATCAAAAAAATACTAATATAGATCCAAGAT
T150A NHase alpha subunit       ATGACGATTGATCAAAAAAATACTAATATAGATCCAAGAT

                                     50         60         70         80
                                ....|....|....|....|....|....|....|....|
WT NHase alpha subunit          TTCCACATCATCATCCGCGTCCACAATCATTTTGGGAGGC
L103S NHase alpha subunit       TTCCACATCATCATCCGCGTCCACAATCATTTTGGGAGGC
Y127N NHase alpha subunit       TTCCACATCATCATCCGCGTCCACAATCATTTTGGGAGGC
F36L NHase alpha subunit        TTCCACATCATCATCCGCGTCCACAATCATTTTGGGAGGC
M188V NHase alpha subunit       TTCCACATCATCATCCGCGTCCACAATCATTTTGGGAGGC
D167V NHase alpha subunit       TTCCACATCATCATCCGCGTCCACAATCATTTTGGGAGGC
D96E NHase alpha subunit        TTCCACATCATCATCCGCGTCCACAATCATTTTGGGAGGC
S169R NHase alpha subunit       TTCCACATCATCATCCGCGTCCACAATCATTTTGGGAGGC
M43K NHase alpha subunit        TTCCACATCATCATCCGCGTCCACAATCATTTTGGGAGGC
T150A NHase alpha subunit       TTCCACATCATCATCCGCGTCCACAATCATTTTGGGAGGC

                                     90        100        110        120
                                ....|....|....|....|....|....|....|....|
WT NHase alpha subunit          ACGTGCAAAAGCTCTTGAATCCTTGTTGATTGAGAAAGGG
L103S NHase alpha subunit       ACGTGCAAAAGCTCTTGAATCCTTGTTGATTGAGAAAGGG
Y127N NHase alpha subunit       ACGTGCAAAAGCTCTTGAATCCTTGTTGATTGAGAAAGGG
F36L NHase alpha subunit        ACGTGCAAAAGCTCTTGAATCCTTGTTGATTGAGAAAGGG
M188V NHase alpha subunit       ACGTGCAAAAGCTCTTGAATCCTTGTTGATTGAGAAAGGG
D167V NHase alpha subunit       ACGTGCAAAAGCTCTTGAATCCTTGTTGATTGAGAAAGGG
D96E NHase alpha subunit        ACGTGCAAAAGCTCTTGAATCCTTGTTGATTGAGAAAGGG
S169R NHase alpha subunit       ACGTGCAAAAGCTCTTGAATCCTTGTTGATTGAGAAAGGG
M43K NHase alpha subunit        ACGTGCAAAAGCTCTTGAATCCTTGTTGATTGAGAAAGGG
T150A NHase alpha subunit       ACGTGCAAAAGCTCTTGAATCCTTGTTGATTGAGAAAGGG

                                    130        140        150        160
                                ....|....|....|....|....|....|....|....|
WT NHase alpha subunit          CATCTTTCCTCAGATGCTATTGAAAGGGTAATAAAACATT
L103S NHase alpha subunit       CATCTTTCCTCAGATGCTATTGAAAGGGTAATAAAACATT
Y127N NHase alpha subunit       CATCTTTCCTCAGATGCTATTGAAAGGGTAATAAAACATT
F36L NHase alpha subunit        CATCTTTCCTCAGATGCTATTGAAAGGGTAATAAAACATT
M188V NHase alpha subunit       CATCTTTCCTCAGATGCTATTGAAAGGGTAATAAAACATT
D167V NHase alpha subunit       CATCTTTCCTCAGATGCTATTGAAAGGGTAATAAAACATT
D96E NHase alpha subunit        CATCTTTCCTCAGATGCTATTGAAAGGGTAATAAAACATT
S169R NHase alpha subunit       CATCTTTCCTCAGATGCTATTGAAAGGGTAATAAAACATT
M43K NHase alpha subunit        CATCTTTCCTCAGATGCTATTGAAAGGGTAATAAAACATT
T150A NHase alpha subunit       CATCTTTCCTCAGATGCTATTGAAAGGGTAATAAAACATT

                                    170        180        190        200
                                ....|....|....|....|....|....|....|....|
WT NHase alpha subunit          ATGAGCATGAGCTGGGACCAATGAACGGAGCAAAGGTCGT
L103S NHase alpha subunit       ATGAGCATGAGCTGGGACCAATGAACGGAGCAAAGGTCGT
Y127N NHase alpha subunit       ATGAGCATGAGCTGGGACCAATGAACGGAGCAAAGGTCGT
F36L NHase alpha subunit        ATGAGCATGAGCTGGGACCAATGAACGGAGCAAAGGTCGT
```

```
M188V NHase alpha subunit  ATGAGCATGAGCTGGGACCAATGAACGGAGCAAAGGTCGT
D167V NHase alpha subunit  ATGAGCATGAGCTGGGACCAATGAACGGAGCAAAGGTCGT
D96E NHase alpha subunit   ATGAGCATGAGCTGGGACCAATGAACGGAGCAAAGGTCGT
S169R NHase alpha subunit  ATGAGCATGAGCTGGGACCAATGAACGGAGCAAAGGTCGT
M43K NHase alpha subunit   ATGAGCATGAGCTGGGACCAATGAACGGAGCAAAGGTCGT
T150A NHase alpha subunit  ATGAGCATGAGCTGGGACCAATGAACGGAGCAAAGGTCGT

                                    210       220       230       240
                           ....|....|....|....|....|....|....|....|
WT NHase alpha subunit     AGCGAAGGCTTGGACTGATCCTGCTTTTAAACAAAGATTG
L103S NHase alpha subunit  AGCGAAGGCTTGGACTGATCCTGCTTTTAAACAAAGATTG
Y127N NHase alpha subunit  AGCGAAGGCTTGGACTGATCCTGCTTTTAAACAAAGATTG
F36L NHase alpha subunit   AGCGAAGGCTTGGACTGATCCTGCTTTTAAACAAAGATTG
M188V NHase alpha subunit  AGCGAAGGCTTGGACTGATCCTGCTTTTAAACAAAGATTG
D167V NHase alpha subunit  AGCGAAGGCTTGGACTGATCCTGCTTTTAAACAAAGATTG
D96E NHase alpha subunit   AGCGAAGGCTTGGACTGATCCTGCTTTTAAACAAAGATTG
S169R NHase alpha subunit  AGCGAAGGCTTGGACTGATCCTGCTTTTAAACAAAGATTG
M43K NHase alpha subunit   AGCGAAGGCTTGGACTGATCCTGCTTTTAAACAAAGATTG
T150A NHase alpha subunit  AGCGAAGGCTTGGACTGATCCTGCTTTTAAACAAAGATTG

                                    250       260       270       280
                           ....|....|....|....|....|....|....|....|
WT NHase alpha subunit     CTAGAAGATTCAGAGACTGTATTAAGGGAGCTAGGATACT
L103S NHase alpha subunit  CTAGAAGATTCAGAGACTGTATTAAGGGAGCTAGGATACT
Y127N NHase alpha subunit  CTAGAAGATTCAGAGACTGTATTAAGGGAGCTAGGATACT
F36L NHase alpha subunit   CTAGAAGATTCAGAGACTGTATTAAGGGAGCTAGGATACT
M188V NHase alpha subunit  CTAGAAGATTCAGAGACTGTATTAAGGGAGCTAGGATACT
D167V NHase alpha subunit  CTAGAAGATTCAGAGACTGTATTAAGGGAGCTAGGATACT
D96E NHase alpha subunit   CTAGAAGATTCAGAGACTGTATTAAGGGAGCTAGGATACT
S169R NHase alpha subunit  CTAGAAGATTCAGAGACTGTATTAAGGGAGCTAGGATACT
M43K NHase alpha subunit   CTAGAAGATTCAGAGACTGTATTAAGGGAGCTAGGATACT
T150A NHase alpha subunit  CTAGAAGATTCAGAGACTGTATTAAGGGAGCTAGGATACT

                                    290       300       310       320
                           ....|....|....|....|....|....|....|....|
WT NHase alpha subunit     ATGGTTTACAGGGTGAGCATATCAGGGTAGTAGAAAATAC
L103S NHase alpha subunit  ATGGTTTACAGGGTGAGCATATCAGGGTAGTAGAAAATAC
Y127N NHase alpha subunit  ATGGTTTACAGGGTGAGCATATCAGGGTAGTAGAAAATAC
F36L NHase alpha subunit   ATGGTTTACAGGGTGAGCATATCAGGGTAGTAGAAAATAC
M188V NHase alpha subunit  ATGGTTTACAGGGTGAGCATATCAGGGTAGTAGAAAATAC
D167V NHase alpha subunit  ATGGTTTACAGGGTGAGCATATCAGGGTAGTAGAAAATAC
D96E NHase alpha subunit   ATGGTTTACAGGGTGAGCATATCAGGGTAGTAGAAAATAC
S169R NHase alpha subunit  ATGGTTTACAGGGTGAGCATATCAGGGTAGTAGAAAATAC
M43K NHase alpha subunit   ATGGTTTACAGGGTGAGCATATCAGGGTAGTAGAAAATAC
T150A NHase alpha subunit  ATGGTTTACAGGGTGAGCATATCAGGGTAGTAGAAAATAC

                                    330       340       350       360
                           ....|....|....|....|....|....|....|....|
WT NHase alpha subunit     GGATACGGTACACAATGTTGTAGTCTGCACTTTATGTTCA
L103S NHase alpha subunit  GGATACGGTACACAATGTTGTAGTCTGCACTTTATGTTCA
Y127N NHase alpha subunit  GGATACGGTACACAATGTTGTAGTCTGCACTTTATGTTCA
F36L NHase alpha subunit   GGATACGGTACACAATGTTGTAGTCTGCACTTTATGTTCA
M188V NHase alpha subunit  GGATACGGTACACAATGTTGTAGTCTGCACTTTATGTTCA
D167V NHase alpha subunit  GGATACGGTACACAATGTTGTAGTCTGCACTTTATGTTCA
D96E NHase alpha subunit   GGATACGGTACACAATGTTGTAGTCTGCACTTTATGTTCA
S169R NHase alpha subunit  GGATACGGTACACAATGTTGTAGTCTGCACTTTATGTTCA
M43K NHase alpha subunit   GGATACGGTACACAATGTTGTAGTCTGCACTTTATGTTCA
T150A NHase alpha subunit  GGATACGGTACACAATGTTGTAGTCTGCACTTTATGTTCA

                                    370       380       390       400
                           ....|....|....|....|....|....|....|....|
```

```
WT NHase alpha subunit      TGTTACCCTTGGCCATTGCTTGGTTTACCGCCTTCATGGT
L103S NHase alpha subunit   TGTTACCCTTGGCCATTGCTTGGTTTACCGCCTTCATGGT
Y127N NHase alpha subunit   TGTTACCCTTGGCCATTGCTTGGTTTACCGCCTTCATGGT
F36L NHase alpha subunit    TGTTACCCTTGGCCATTGCTTGGTTTACCGCCTTCATGGT
M188V NHase alpha subunit   TGTTACCCTTGGCCATTGCTTGGTTTACCGCCTTCATGGT
D167V NHase alpha subunit   TGTTACCCTTGGCCATTGCTTGGTTTACCGCCTTCATGGT
D96E NHase alpha subunit    TGTTACCCTTGGCCATTGCTTGGTTTACCGCCTTCATGGT
S169R NHase alpha subunit   TGTTACCCTTGGCCATTGCTTGGTTTACCGCCTTCATGGT
M43K NHase alpha subunit    TGTTACCCTTGGCCATTGCTTGGTTTACCGCCTTCATGGT
T150A NHase alpha subunit   TGTTACCCTTGGCCATTGCTTGGTTTACCGCCTTCATGGT

                                    410       420       430       440
                            ....|....|....|....|....|....|....|....|
WT NHase alpha subunit      ACAAAGAACCTGCTTATAGAGCTCGTGTCGTAAAAGAGCC
L103S NHase alpha subunit   ACAAAGAACCTGCTTATAGAGCTCGTGTCGTAAAAGAGCC
Y127N NHase alpha subunit   ACAAAGAACCTGCTTATAGAGCTCGTGTCGTAAAAGAGCC
F36L NHase alpha subunit    ACAAAGAACCTGCTTATAGAGCTCGTGTCGTAAAAGAGCC
M188V NHase alpha subunit   ACAAAGAACCTGCTTATAGAGCTCGTGTCGTAAAAGAGCC
D167V NHase alpha subunit   ACAAAGAACCTGCTTATAGAGCTCGTGTCGTAAAAGAGCC
D96E NHase alpha subunit    ACAAAGAACCTGCTTATAGAGCTCGTGTCGTAAAAGAGCC
S169R NHase alpha subunit   ACAAAGAACCTGCTTATAGAGCTCGTGTCGTAAAAGAGCC
M43K NHase alpha subunit    ACAAAGAACCTGCTTATAGAGCTCGTGTCGTAAAAGAGCC
T150A NHase alpha subunit   ACAAAGAACCTGCTTATAGAGCTCGTGTCGTAAAAGAGCC

                                    450       460       470       480
                            ....|....|....|....|....|....|....|....|
WT NHase alpha subunit      GAGACAAGTGTTGAAAGAATTCGGATTAGATCTTCCAGAT
L103S NHase alpha subunit   GAGACAAGTGTTGAAAGAATTCGGATTAGATCTTCCAGAT
Y127N NHase alpha subunit   GAGACAAGTGTTGAAAGAATTCGGATTAGATCTTCCAGAT
F36L NHase alpha subunit    GAGACAAGTGTTGAAAGAATTCGGATTAGATCTTCCAGAT
M188V NHase alpha subunit   GAGACAAGTGTTGAAAGAATTCGGATTAGATCTTCCAGAT
D167V NHase alpha subunit   GAGACAAGTGTTGAAAGAATTCGGATTAGATCTTCCAGAT
D96E NHase alpha subunit    GAGACAAGTGTTGAAAGAATTCGGATTAGATCTTCCAGAT
S169R NHase alpha subunit   GAGACAAGTGTTGAAAGAATTCGGATTAGATCTTCCAGAT
M43K NHase alpha subunit    GAGACAAGTGTTGAAAGAATTCGGATTAGATCTTCCAGAT
T150A NHase alpha subunit   GAGACAAGTGTTGAAAGAATTCGGATTAGATCTTCCAGAT

                                    490       500       510       520
                            ....|....|....|....|....|....|....|....|
WT NHase alpha subunit      TCAGTAGAAATCCGGGTATGGGACAGCAGTTCAGAAATTC
L103S NHase alpha subunit   TCAGTAGAAATCCGGGTATGGGACAGCAGTTCAGAAATTC
Y127N NHase alpha subunit   TCAGTAGAAATCCGGGTATGGGACAGCAGTTCAGAAATTC
F36L NHase alpha subunit    TCAGTAGAAATCCGGGTATGGGACAGCAGTTCAGAAATTC
M188V NHase alpha subunit   TCAGTAGAAATCCGGGTATGGGACAGCAGTTCAGAAATTC
D167V NHase alpha subunit   TCAGTAGAAATCCGGGTATGGGACAGCAGTTCAGAAATTC
D96E NHase alpha subunit    TCAGTAGAAATCCGGGTATGGGACAGCAGTTCAGAAATTC
S169R NHase alpha subunit   TCAGTAGAAATCCGGGTATGGGACCGCAGTTCAGAAATTC
M43K NHase alpha subunit    TCAGTAGAAATCCGGGTATGGGACAGCAGTTCAGAAATTC
T150A NHase alpha subunit   TCAGTAGAAATCCGGGTATGGGACAGCAGTTCAGAAATTC

                                    530       540       550       560
                            ....|....|....|....|....|....|....|....|
WT NHase alpha subunit      GCTTTATGGTATTGCCGCAAAGACCTGAAGGTACGGAAGG
L103S NHase alpha subunit   GCTTTATGGTATTGCCGCAAAGACCTGAAGGTACGGAAGG
Y127N NHase alpha subunit   GCTTTATGGTATTGCCGCAAAGACCTGAAGGTACGGAAGG
F36L NHase alpha subunit    GCTTTATGGTATTGCCGCAAAGACCTGAAGGTACGGAAGG
M188V NHase alpha subunit   GCTTTATGGTATTGCCGCAAAGACCTGAAGGTACGGAAGG
D167V NHase alpha subunit   GCTTTATGGTATTGCCGCAAAGACCTGAAGGTACGGAAGG
D96E NHase alpha subunit    GCTTTATGGTATTGCCGCAAAGACCTGAAGGTACGGAAGG
S169R NHase alpha subunit   GCTTTATGGTATTGCCGCAAAGACCTGAAGGTACGGAAGG
M43K NHase alpha subunit    GCTTTATGGTATTGCCGCAAAGACCTGAAGGTACGGAAGG
```

```
T150A NHase alpha subunit  GCTTTATGGTATTGCCGCAAAGACCTGAAGGTACGGAAGG

                                    570        580        590        600
                           ....|....|....|....|....|....|....|....|....|
WT NHase alpha subunit     AATGACGGAGGAGGAGCTTGCAAAACTTGTTACTCGAGAC
L103S NHase alpha subunit  AATGACGGAGGAGGAGCTTGCAAAACTTGTTACTCGAGAC
Y127N NHase alpha subunit  AATGACGGAGGAGGAGCTTGCAAAACTTGTTACTCGAGAC
F36L NHase alpha subunit   AATGACGGAGGAGGAGCTTGCAAAACTTGTTACTCGAGAC
M188V NHase alpha subunit  AGTGACGGAGGAGGAGCTTGCAAAACTTGTTACTCGAGAC
D167V NHase alpha subunit  AATGACGGAGGAGGAGCTTGCAAAACTTGTTACTCGAGAC
D96E NHase alpha subunit   AATGACGGAGGAGGAGCTTGCAAAACTTGTTACTCGAGAC
S169R NHase alpha subunit  AATGACGGAGGAGGAGCTTGCAAAACTTGTTACTCGAGAC
M43K NHase alpha subunit   AATGACGGAGGAGGAGCTTGCAAAACTTGTTACTCGAGAC
T150A NHase alpha subunit  AATGACGGAGGAGGAGCTTGCAAAACTTGTTACTCGAGAC

                                    610        620        630        640
                           ....|....|....|....|....|....|....|....|....|
WT NHase alpha subunit     TCCATGATTGGTGTCGCTAAAATAGAGCCGCCTAAAGTTA
L103S NHase alpha subunit  TCCATGATTGGTGTCGCTAAAATAGAGCCGCCTAAAGTTA
Y127N NHase alpha subunit  TCCATGATTGGTGTCGCTAAAATAGAGCCGCCTAAAGTTA
F36L NHase alpha subunit   TCCATGATTGGTGTCGCTAAAATAGAGCCGCCTAAAGTTA
M188V NHase alpha subunit  TCCATGATTGGTGTCGCTAAAATAGAGCCGCCTAAAGTTA
D167V NHase alpha subunit  TCCATGATTGGTGTCGCTAAAATAGAGCCGCCTAAAGTTA
D96E NHase alpha subunit   TCCATGATTGGTGTCGCTAAAATAGAGCCGCCTAAAGTTA
S169R NHase alpha subunit  TCCATGATTGGTGTCGCTAAAATAGAGCCGCCTAAAGTTA
M43K NHase alpha subunit   TCCATGATTGGTGTCGCTAAAATAGAGCCGCCTAAAGTTA
T150A NHase alpha subunit  TCCATGATTGGTGTCGCTAAAATAGAGCCGCCTAAAGTTA

                                    650
                           ....|....|.
WT NHase alpha subunit     CGGTAGGTTAG
L103S NHase alpha subunit  CGGTAGGTTAG
Y127N NHase alpha subunit  CGGTAGGTTAG
F36L NHase alpha subunit   CGGTAGGTTAG
M188V NHase alpha subunit  CGGTAGGTTAG
D167V NHase alpha subunit  CGGTAGGTTAG
D96E NHase alpha subunit   CGGTAGGTTAG
S169R NHase alpha subunit  CGGTAGGTTAG
M43K NHase alpha subunit   CGGTAGGTTAG
T150A NHase alpha subunit  CGGTAGGTTAG
```

Appendix 4: Nucleotide alignment of the β subunit of WT NHase and all single mutants.

```
                                10        20        30        40
                       ....|....|....|....|....|....|....|....|
WT NHase beta subunit  ATGAACGGTATTCATGATGTTGGAGGCATGGATGGATTTG
L103S NHase beta subunit ATGAACGGTATTCATGATGTTGGAGGCATGGATGGATTTG
Y127N NHase beta subunit ATGAACGGTATTCATGATGTTGGAGGCATGGATGGATTTG
F36L NHase beta subunit ATGAACGGTATTCATGATGTTGGAGGCATGGATGGATTTG
M188V NHase beta subunit ATGAACGGTATTCATGATGTTGGAGGCATGGATGGATTTG
D167V NHase beta subunit ATGAACGGTATTCATGATGTTGGAGGCATGGATGGATTTG
D96E NHase beta subunit ATGAACGGTATTCATGATGTTGGAGGCATGGATGGATTTG
S169R NHase beta subunit ATGAACGGTATTCATGATGTTGGAGGCATGGATGGATTTG
M43K NHase beta subunit ATGAACGGTATTCATGATGTTGGAGGCATGGATGGATTTG
T150A NHase beta subunit ATGAACGGTATTCATGATGTTGGAGGCATGGATGGATTTG

                                50        60        70        80
                       ....|....|....|....|....|....|....|....|
WT NHase beta subunit  GAAAAGTTATGTATGTAAAAGAAGAAGAGGACATTTATTT
L103S NHase beta subunit GAAAAGTTATGTATGTAAAAGAAGAAGAGGACATTTATTT
Y127N NHase beta subunit GAAAAGTTATGTATGTAAAAGAAGAAGAGGACATTTATTT
F36L NHase beta subunit GAAAAGTTATGTATGTAAAAGAAGAAGAGGACATTTATTT
M188V NHase beta subunit GAAAAGTTATGTATGTAAAAGAAGAAGAGGACATTTATTT
D167V NHase beta subunit GAAAAGTTATGTATGTAAAAGAAGAAGAGGACATTTATTT
D96E NHase beta subunit GAAAAGTTATGTATGTAAAAGAAGAAGAGGACATTTATTT
S169R NHase beta subunit GAAAAGTTATGTATGTAAAAGAAGAAGAGGACATTTATTT
M43K NHase beta subunit GAAAAGTTATGTATGTAAAAGAAGAAGAGGACATTTATTT
T150A NHase beta subunit GAAAAGTTATGTATGTAAAAGAAGAAGAGGACATTTATTT

                                90       100       110       120
                       ....|....|....|....|....|....|....|....|
WT NHase beta subunit  TACACATGATTGGGAAAGACTTGCGTTCGGACTTGTAGCT
L103S NHase beta subunit TACACATGATTGGGAAAGACTTGCGTTCGGACTTGTAGCT
Y127N NHase beta subunit TACACATGATTGGGAAAGACTTGCGTTCGGACTTGTAGCT
F36L NHase beta subunit TACACATGATTGGGAAAGACTTGCGCTCGGACTTGTAGCT
M188V NHase beta subunit TACACATGATTGGGAAAGACTTGCGTTCGGACTTGTAGCT
D167V NHase beta subunit TACACATGATTGGGAAAGACTTGCGTTCGGACTTGTAGCT
D96E NHase beta subunit TACACATGATTGGGAAAGACTTGCGTTCGGACTTGTAGCT
S169R NHase beta subunit TACACATGATTGGGAAAGACTTGCGTTCGGACTTGTAGCT
M43K NHase beta subunit TACACATGATTGGGAAAGACTTGCGTTCGGACTTGTAGCT
T150A NHase beta subunit TACACATGATTGGGAAAGACTTGCGTTCGGACTTGTAGCT

                               130       140       150       160
                       ....|....|....|....|....|....|....|....|
WT NHase beta subunit  GGTTGTATGGCACAAGGATTGGGGATGAAGGCTTTTGATG
L103S NHase beta subunit GGTTGTATGGCACAAGGATTGGGGATGAAGGCTTTTGATG
Y127N NHase beta subunit GGTTGTATGGCACAAGGATTGGGGATGAAGGCTTTTGATG
F36L NHase beta subunit GGTTGTATGGCACAAGGATTGGGGATGAAGGCTTTTGATG
M188V NHase beta subunit GGTTGTATGGCACAAGGATTGGGGATGAAGGCTTTTGATG
D167V NHase beta subunit GGTTGTATGGCACAAGGATTGGGGATGAAGGCTTTTGATG
D96E NHase beta subunit GGTTGTATGGCACAAGGATTGGGGATGAAGGCTTTTGATG
S169R NHase beta subunit GGTTGTATGGCACAAGGATTGGGGATGAAGGCTTTTGATG
M43K NHase beta subunit GGTTGTAAGGCACAAGGATTGGGGATGAAGGCTTTTGATG
T150A NHase beta subunit GGTTGTATGGCACAAGGATTGGGGATGAAGGCTTTTGATG

                               170       180       190       200
                       ....|....|....|....|....|....|....|....|
WT NHase beta subunit  AATTCAGGATCGGCATTGAGCTTATGCGTCCAGTGGATTA
L103S NHase beta subunit AATTCAGGATCGGCATTGAGCTTATGCGTCCAGTGGATTA
Y127N NHase beta subunit AATTCAGGATCGGCATTGAGCTTATGCGTCCAGTGGATTA
F36L NHase beta subunit AATTCAGGATCGGCATTGAGCTTATGCGTCCAGTGGATTA
M188V NHase beta subunit AATTCAGGATCGGCATTGAGCTTATGCGTCCAGTGGATTA
```

```
D167V NHase beta subunit    AATTCAGGATCGGCATTGAGCTTATGCGTCCAGTGGATTA
D96E NHase beta subunit     AATTCAGGATCGGCATTGAGCTTATGCGTCCAGTGGATTA
S169R NHase beta subunit    AATTCAGGATCGGCATTGAGCTTATGCGTCCAGTGGATTA
M43K NHase beta subunit     AATTCAGGATCGGCATTGAGCTTATGCGTCCAGTGGATTA
T150A NHase beta subunit    AATTCAGGATCGGCATTGAGCTTATGCGTCCAGTGGATTA

                                    210       220       230       240
                            ....|....|....|....|....|....|....|....|
WT NHase beta subunit       TTTGACGTCGTCGTATTATGGCCATTGGATTGCAACCGTT
L103S NHase beta subunit    TTTGACGTCGTCGTATTATGGCCATTGGATTGCAACCGTT
Y127N NHase beta subunit    TTTGACGTCGTCGTATTATGGCCATTGGATTGCAACCGTT
F36L NHase beta subunit     TTTGACGTCGTCGTATTATGGCCATTGGATTGCAACCGTT
M188V NHase beta subunit    TTTGACGTCGTCGTATTATGGCCATTGGATTGCAACCGTT
D167V NHase beta subunit    TTTGACGTCGTCGTATTATGGCCATTGGATTGCAACCGTT
D96E NHase beta subunit     TTTGACGTCGTCGTATTATGGCCATTGGATTGCAACCGTT
S169R NHase beta subunit    TTTGACGTCGTCGTATTATGGCCATTGGATTGCAACCGTT
M43K NHase beta subunit     TTTGACGTCGTCGTATTATGGCCATTGGATTGCAACCGTT
T150A NHase beta subunit    TTTGACGTCGTCGTATTATGGCCATTGGATTGCAACCGTT

                                    250       260       270       280
                            ....|....|....|....|....|....|....|....|
WT NHase beta subunit       GCATACAACTTAGTAGATACGGGAGTATTAGACGAAAAAG
L103S NHase beta subunit    GCATACAACTTAGTAGATACGGGAGTATTAGACGAAAAAG
Y127N NHase beta subunit    GCATACAACTTAGTAGATACGGGAGTATTAGACGAAAAAG
F36L NHase beta subunit     GCATACAACTTAGTAGATACGGGAGTATTAGACGAAAAAG
M188V NHase beta subunit    GCATACAACTTAGTAGATACGGGAGTATTAGACGAAAAAG
D167V NHase beta subunit    GCATACAACTTAGTAGATACGGGAGTATTAGACGAAAAAG
D96E NHase beta subunit     GCATACAACTTAGTAGATACGGGAGTATTAGACGAAAAAG
S169R NHase beta subunit    GCATACAACTTAGTAGATACGGGAGTATTAGACGAAAAAG
M43K NHase beta subunit     GCATACAACTTAGTAGATACGGGAGTATTAGACGAAAAAG
T150A NHase beta subunit    GCATACAACTTAGTAGATACGGGAGTATTAGACGAAAAAG

                                    290       300       310       320
                            ....|....|....|....|....|....|....|....|
WT NHase beta subunit       AACTAGATGAACGAACGGAGGTTTTCTTGAAGAAACCTGA
L103S NHase beta subunit    AACTAGATGAACGAACGGAGGTTTTCTCGAAGAAACCTGA
Y127N NHase beta subunit    AACTAGATGAACGAACGGAGGTTTTCTTGAAGAAACCTGA
F36L NHase beta subunit     AACTAGATGAACGAACGGAGGTTTTCTTGAAGAAACCTGA
M188V NHase beta subunit    AACTAGATGAACGAACGGAGGTTTTCTTGAAGAAACCTGA
D167V NHase beta subunit    AACTAGATGAACGAACGGAGGTTTTCTTGAAGAAACCTGA
D96E NHase beta subunit     AACTAGAAGAACGAACGGAGGTTTTCTTGAAGAAACCTGA
S169R NHase beta subunit    AACTAGATGAACGAACGGAGGTTTTCTTGAAGAAACCTGA
M43K NHase beta subunit     AACTAGATGAACGAACGGAGGTTTTCTTGAAGAAACCTGA
T150A NHase beta subunit    AACTAGATGAACGAACGGAGGTTTTCTTGAAGAAACCTGA

                                    330       340       350       360
                            ....|....|....|....|....|....|....|....|
WT NHase beta subunit       TACCAAAATACCACGAAGAGAGGATCCGGCATTAGTGAAG
L103S NHase beta subunit    TACCAAAATACCACGAAGAGAGGATCCGGCATTAGTGAAG
Y127N NHase beta subunit    TACCAAAATACCACGAAGAGAGGATCCGGCATTAGTGAAG
F36L NHase beta subunit     TACCAAAATACCACGAAGAGAGGATCCGGCATTAGTGAAG
M188V NHase beta subunit    TACCAAAATACCACGAAGAGAGGATCCGGCATTAGTGAAG
D167V NHase beta subunit    TACCAAAATACCACGAAGAGAGGATCCGGCATTAGTGAAG
D96E NHase beta subunit     TACCAAAATACCACGAAGAGAGGATCCGGCATTAGTGAAG
S169R NHase beta subunit    TACCAAAATACCACGAAGAGAGGATCCGGCATTAGTGAAG
M43K NHase beta subunit     TACCAAAATACCACGAAGAGAGGATCCGGCATTAGTGAAG
T150A NHase beta subunit    TACCAAAATACCACGAAGAGAGGATCCGGCATTAGTGAAG

                                    370       380       390       400
                            ....|....|....|....|....|....|....|....|
WT NHase beta subunit       CTTGTAGAAAAGGCACTGTATGATGGCTTATCTCCGCTCC
```

```
L103S NHase beta subunit    CTTGTAGAAAAGGCACTGTATGATGGCTTATCTCCGCTCC
Y127N NHase beta subunit    CTTGTAGAAAAGGCACTGAATGATGGCTTATCTCCGCTCC
F36L NHase beta subunit     CTTGTAGAAAAGGCACTGTATGATGGCTTATCTCCGCTCC
M188V NHase beta subunit    CTTGTAGAAAAGGCACTGTATGATGGCTTATCTCCGCTCC
D167V NHase beta subunit    CTTGTAGAAAAGGCACTGTATGATGGCTTATCTCCGCTCC
D96E NHase beta subunit     CTTGTAGAAAAGGCACTGTATGATGGCTTATCTCCGCTCC
S169R NHase beta subunit    CTTGTAGAAAAGGCACTGTATGATGGCTTATCTCCGCTCC
M43K NHase beta subunit     CTTGTAGAAAAGGCACTGTATGATGGCTTATCTCCGCTCC
T150A NHase beta subunit    CTTGTAGAAAAGGCACTGTATGATGGCTTATCTCCGCTCC

                                    410       420       430       440
                            ....|....|....|....|....|....|....|....|
WT NHase beta subunit       GTGAAATTTCAGCTTCTCCTCGGTTTAAGGTAGGAGAGAG
L103S NHase beta subunit    GTGAAATTTCAGCTTCTCCTCGGTTTAAGGTAGGAGAGAG
Y127N NHase beta subunit    GTGAAATTTCAGCTTCTCCTCGGTTTAAGGTAGGAGAGAG
F36L NHase beta subunit     GTGAAATTTCAGCTTCTCCTCGGTTTAAGGTAGGAGAGAG
M188V NHase beta subunit    GTGAAATTTCAGCTTCTCCTCGGTTTAAGGTAGGAGAGAG
D167V NHase beta subunit    GTGAAATTTCAGCTTCTCCTCGGTTTAAGGTAGGAGAGAG
D96E NHase beta subunit     GTGAAATTTCAGCTTCTCCTCGGTTTAAGGTAGGAGAGAG
S169R NHase beta subunit    GTGAAATTTCAGCTTCTCCTCGGTTTAAGGTAGGAGAGAG
M43K NHase beta subunit     GTGAAATTTCAGCTTCTCCTCGGTTTAAGGTAGGAGAGAG
T150A NHase beta subunit    GTGAAATTTCAGCTTCTCCTCGGTTTAAGGTAGGAGAGAG

                                    450       460       470       480
                            ....|....|....|....|....|....|....|....|
WT NHase beta subunit       AATCAAGACGAAAAACATTCATCCAACTGGTCATACGAGA
L103S NHase beta subunit    AATCAAGACGAAAAACATTCATCCAACTGGTCATACGAGA
Y127N NHase beta subunit    AATCAAGACGAAAAACATTCATCCAACTGGTCATACGAGA
F36L NHase beta subunit     AATCAAGACGAAAAACATTCATCCAACTGGTCATACGAGA
M188V NHase beta subunit    AATCAAGACGAAAAACATTCATCCAACTGGTCATACGAGA
D167V NHase beta subunit    AATCAAGACGAAAAACATTCATCCAACTGGTCATACGAGA
D96E NHase beta subunit     AATCAAGACGAAAAACATTCATCCAACTGGTCATACGAGA
S169R NHase beta subunit    AATCAAGACGAAAAACATTCATCCAACTGGTCATACGAGA
M43K NHase beta subunit     AATCAAGACGAAAAACATTCATCCAACTGGTCATACGAGA
T150A NHase beta subunit    AATCAAGGCGAAAAACATTCATCCAACTGGTCATACGAGA

                                    490       500       510       520
                            ....|....|....|....|....|....|....|....|
WT NHase beta subunit       TTCCCTCGATATGCCCGTGACAAATATGGTGTCATTGATG
L103S NHase beta subunit    TTCCCTCGATATGCCCGTGACAAATATGGTGTCATTGATG
Y127N NHase beta subunit    TTCCCTCGATATGCCCGTGACAAATATGGTGTCATTGATG
F36L NHase beta subunit     TTCCCTCGATATGCCCGTGACAAATATGGTGTCATTGATG
M188V NHase beta subunit    TTCCCTCGATATGCCCGTGACAAATATGGTGTCATTGATG
D167V NHase beta subunit    TTCCCTCGATATGCCCGTGTCAAATATGGTGTCATTGATG
D96E NHase beta subunit     TTCCCTCGATATGCCCGTGACAAATATGGTGTCATTGATG
S169R NHase beta subunit    TTCCCTCGATATGCCCGTGACAAATATGGTGTCATTGATG
M43K NHase beta subunit     TTCCCTCGATATGCCCGTGACAAATATGGTGTCATTGATG
T150A NHase beta subunit    TTCCCTCGATATGCCCGTGACAAATATGGTGTCATTGATG

                                    530       540       550       560
                            ....|....|....|....|....|....|....|....|
WT NHase beta subunit       AGGTATATGGAGCTCATGTTTTCCCTGATGATGCTGCTCA
L103S NHase beta subunit    AGGTATATGGAGCTCATGTTTTCCCTGATGATGCTGCTCA
Y127N NHase beta subunit    AGGTATATGGAGCTCATGTTTTCCCTGATGATGCTGCTCA
F36L NHase beta subunit     AGGTATATGGAGCTCATGTTTTCCCTGATGATGCTGCTCA
M188V NHase beta subunit    AGGTATATGGAGCTCATGTTTTCCCTGATGATGCTGCTCA
D167V NHase beta subunit    AGGTATATGGAGCTCATGTTTTCCCTGATGATGCTGCTCA
D96E NHase beta subunit     AGGTATATGGAGCTCATGTTTTCCCTGATGATGCTGCTCA
S169R NHase beta subunit    AGGTATATGGAGCTCATGTTTTCCCTGATGATGCTGCTCA
M43K NHase beta subunit     AGGTATATGGAGCTCATGTTTTCCCTGATGATGCTGCTCA
T150A NHase beta subunit    AGGTATATGGAGCTCATGTTTTCCCTGATGATGCTGCTCA
```

```
                                570       580       590       600
                               ....|....|....|....|....|....|....|....|
WT NHase beta subunit          TAGAAAAGGAGAAAACCCGCAATATCTTTACCGGGTACGT
L103S NHase beta subunit       TAGAAAAGGAGAAAACCCGCAATATCTTTACCGGGTACGT
Y127N NHase beta subunit       TAGAAAAGGAGAAAACCCGCAATATCTTTACCGGGTACGT
F36L NHase beta subunit        TAGAAAAGGAGAAAACCCGCAATATCTTTACCGGGTACGT
M188V NHase beta subunit       TAGAAAAGGAGAAAACCCGCAATATCTTTACCGGGTACGT
D167V NHase beta subunit       TAGAAAAGGAGAAAACCCGCAATATCTTTACCGGGTACGT
D96E NHase beta subunit        TAGAAAAGGAGAAAACCCGCAATATCTTTACCGGGTACGT
S169R NHase beta subunit       TAGAAAAGGAGAAAACCCGCAATATCTTTACCGGGTACGT
M43K NHase beta subunit        TAGAAAAGGAGAAAACCCGCAATATCTTTACCGGGTACGT
T150A NHase beta subunit       TAGAAAAGGAGAAAACCCGCAATATCTTTACCGGGTACGT

                                610       620       630       640
                               ....|....|....|....|....|....|....|....|
WT NHase beta subunit          TTTGAGGCTGAAGAATTATGGGGATATAAACAGAAAGATT
L103S NHase beta subunit       TTTGAGGCTGAAGAATTATGGGGATATAAACAGAAAGATT
Y127N NHase beta subunit       TTTGAGGCTGAAGAATTATGGGGATATAAACAGAAAGATT
F36L NHase beta subunit        TTTGAGGCTGAAGAATTATGGGGATATAAACAGAAAGATT
M188V NHase beta subunit       TTTGAGGCTGAAGAATTATGGGGATATAAACAGAAAGATT
D167V NHase beta subunit       TTTGAGGCTGAAGAATTATGGGGATATAAACAGAAAGATT
D96E NHase beta subunit        TTTGAGGCTGAAGAATTATGGGGATATAAACAGAAAGATT
S169R NHase beta subunit       TTTGAGGCTGAAGAATTATGGGGATATAAACAGAAAGATT
M43K NHase beta subunit        TTTGAGGCTGAAGAATTATGGGGATATAAACAGAAAGATT
T150A NHase beta subunit       TTTGAGGCTGAAGAATTATGGGGATATAAACAGAAAGATT

                                650       660       670       680
                               ....|....|....|....|....|....|....|....|
WT NHase beta subunit          CCGTTTATATAGATCTATGGGAAAGTTATATGGAGCCTGT
L103S NHase beta subunit       CCGTTTATATAGATCTATGGGAAAGTTATATGGAGCCTGT
Y127N NHase beta subunit       CCGTTTATATAGATCTATGGGAAAGTTATATGGAGCCTGT
F36L NHase beta subunit        CCGTTTATATAGATCTATGGGAAAGTTATATGGAGCCTGT
M188V NHase beta subunit       CCGTTTATATAGATCTATGGGAAAGTTATATGGAGCCTGT
D167V NHase beta subunit       CCGTTTATATAGATCTATGGGAAAGTTATATGGAGCCTGT
D96E NHase beta subunit        CCGTTTATATAGATCTATGGGAAAGTTATATGGAGCCTGT
S169R NHase beta subunit       CCGTTTATATAGATCTATGGGAAAGTTATATGGAGCCTGT
M43K NHase beta subunit        CCGTTTATATAGATCTATGGGAAAGTTATATGGAGCCTGT
T150A NHase beta subunit       CCGTTTATATAGATCTATGGGAAAGTTATATGGAGCCTGT

                                690
                               ....|....|
WT NHase beta subunit          TTCACATTAA
L103S NHase beta subunit       TTCACATTAA
Y127N NHase beta subunit       TTCACATTAA
F36L NHase beta subunit        TTCACATTAA
M188V NHase beta subunit       TTCACATTAA
D167V NHase beta subunit       TTCACATTAA
D96E NHase beta subunit        TTCACATTAA
S169R NHase beta subunit       TTCACATTAA
M43K NHase beta subunit        TTCACATTAA
T150A NHase beta subunit       TTCACATTAA
```